Optimisation of a 3D living skin equivalent model for studying drug metabolism

Hatem Ali H Sallem

A thesis submitted in partial fulfilment of the requirements of

Sheffield Hallam University

for the Degree of Doctor of Philosophy

July 2022

Candidate's declaration

I hereby declare that:

1- This Work covers a wider field of study than work previously submitted for a degree or comparable award, at SHU or any other institution, and I have clearly indicated which work has been so incorporated in the thesis.
2- This submission is my own work and to the best of my knowledge it contains no materials previously published or written by another person, or substantial proportions of material which have been accepted for the award of any other degree at SHU or any other educational institution.
3- None of material in this PhD thesis has been previously submitted for a degree or any other qualification at this university or another institution.
4- I understand the University's policy on plagiarism and declare that the intellectual content of this thesis is the product of my own work, except to the extent that assistance from others in the project's design and conception or in style, and presentation.
5- Any contribution made to the research by others, with whom I have worked at SHU or elsewhere, is explicitly acknowledged in the thesis.
6- The work of the thesis has been performed in accordance with the SHU Principles of Integrity in Research and the SHU Research Ethics Policy.
7- The PhD thesis word count: 58,200

Student Name:	***Hatem Ali H Sallem***
Student Number:	***24045324***
Faculty:	***Health and Wellbeing***
Intended Award:	***Doctor of philosophy (PhD)***
Supervisor:	***Professor Malcolm R Clench***
Co-Supervisor:	***Doctor Catherine J Duckett***
Co-Supervisor:	***Doctor Vikki A Carolan***
Date of Submission:	***July 2022***

Acknowledgments

After an intensive period of 4 years, today is the day: writing this note of thanks is the finishing touch on my PhD thesis. At the end of this long and tortuous journey, thanks are due to everyone who was close to me, supporting and bearing with me in these years.

I would like to reflect on the people who have supported and helped me so much throughout my PhD degree. Special thanks go to my parents for their wise counsel and sympathetic ear. To my father and mother for encouraging and teaching me and my first supporter whenever I needed. To my friends, I am extremely glad for all your support. You have been more than just a friend, sharing with me the happiest moments.

I would like to thank my supervisor Professor Malcolm Clench (Head of Biomedical Research Centre, Sheffield Hallam University) for giving me the opportunity of being part of his research group. I am truly grateful for all your support, your guidance and especially for your faith in me. I learnt from you what it means to carry out real research, one without linguistic and geographic barriers. In addition, I heartily thank the rest of my supervisory team Dr. Catherine Duckett and Dr. Vikki Carolan for the excellent help and advice throughout my PhD.

Also, I would like to thank Prof. Simona Francese and mass spectrometry group for help and support me in the laboratory throughout all my PhD. Special thanks go to all BMRC colleagues, Dr. Daniel Kingsman and Michael Cox. You were supportive during the period of my PhD. A huge thanks to Tanya Klymenko for help me druring the research period.

Finally, I respect and thank my country (Libya) to give me the opportunity in successfully completing my PhD degree.

Thank you very much, everyone

Hatem Sallem

July 2022

Abstract

Skin is the largest organ in the human body and is used as a defence against foreign chemicals “xenobiotics”. The human skin has the capacity to metabolise foreign chemicals “xenobiotics” that pass through the stratum corneum, but knowledge of the enzymes involved is incomplete. There is an important need for validated 3D skin models, which can be utilised in the safety assessment of chemicals. An important component of the validation of these Labskin model is characterising the levels of xenobiotic metabolising enzymes (XME), particularly those that have been reported as important in the skin, Phase I XME (*e.g*. cytochrome P450s and flavin containing monooxygenase FMOs) and Phase II XME (*e.g*. glutathione S-transferase) isoforms. RT-qPCR and proteomics approach such as LC-MS/MS, nano-LC-MS/MS and DESI-MSI techniques were used to describe the profile of XME present in human skin and *in vitro* Labskin model that has been developed for the purpose of safety assessment. Overall, the general aims of this study were to measure the levels of Phase I and Phase II XMEs in a commercial 3D living skin equivalent model “Labskin” to determine if it is possible to recover drug response by induced genes and proteins expression and provide a 3D skin model for future drug development.

The results showed that about 84 genes expression by RT-qPCR and 327 function protein by LC-MS/MS and nano-LC-MS/MS of phase I and Phase II levels were measured in the 3D Labskin model compared with native human skin. Though the expression of Phase I and Phase II level were low in the 3D Labskin model as supplied, significant induction of cytochrome P450-dependent monooxygenase (CYP1A1, CYP3A5, CYP1B1) and non-CYPs (FMO1/3) were observed after treatment with β-naphthoflavone, *all-trans* retinoic acid and phenobarbital which yielded a upregulated of fold change in the induced 3D Labskin model compared with 3D labskin model control. Of the enzymes indicated as present, only CYP3A5 protein was confirmed to be expressed in the 3D skin model and human skin by Western blotting. These findings suggest that the XMEs of Labskin model appears to be representative of native human skin for metabolism studies of cutaneous exposures to xenobiotics.

The biotransformation of benzydamine in *in vitro* skin model was investigated. DESI-MS on Synapt XS and MRT was applied to evaluate the metabolic activity of FMO1/3 and

CYP P450 gene/protein in 3D Labskin model using benzydamine substrate-based mass spectrometry imaging. DESI-MS detected benzydamine-*N*-oxide and nor-benzydamine to induced with β-naphthoflavone by FMO1/3 and P450 activity in the epidermal layer of Labskin.

i. Contents

ii. List of figures

Chapter 1: Introduction

Chapter 2: Gene expression (RT-qPCR)

iii. List of Tables

Chapter 1: Introduction

iv. Abbreviations

µg: microgram

µm: micrometer

3D: three dimensional

3-MC: 3-methylcholanthrene

AC: acetyl carnitine

ACAT: acetyl-coa acetyltransferase

ACN: acetonitrile

ADH: alcohol dehydrogenase

AHR: aryl hydrocarbon receptor

ALDH: aldehyde dehydrogenase

BCA: bichinchonic acid

BZD: Benzydamine

CDNB: 1-chloro-2, 4-dinitrobenzene

CEM: chain ejection model

CES: carboxylesterase

CPEs: chemical penetration enhancer

CRM: charge reduction model

CRM: charged residue model

CYPs: cytochrome P450

DC: direct current

dH_2O: deionised water

Desmethyl-BZD: nor-benzydamine

DMSO: dimethyl Sulfoxide

DTT: dithiothreitol

EPHX: epoxide hydrolase

EROD: 7-ethoxyresorufin O-deethylase

ESI: electrospray ionisation

ESI-MS: electrospray ionization mass spectrometry

EU: European Union

Ex vivo: *ex vivo* human skin

FA: formic acid

FHS: fesh human Skin

FMOs: flavin containing monooxygenases

FT-ICR: Fourier transform-ion cyclotron resonance

G: gram

GO: protein ontology

GST: glutathione-S-transferase

GSTO1: glutathione S-transferase omega-1

GSTP1: glutathione S-transferase P1

HCl: hydrochloride

HGDC: human genomic DNA contamination

HRP: horseradish peroxidase

HS: native human skin

HSEs: human skin equivalents

IA: iodoacetamide

IEM: ion evaporation Model

K: coefficient of partition

Labskin: 3D living skin equivalent model (Innovenn-UK)

LC: liquid chromatography

LCD: liquor carbonis detergents

LC-MS/MS: liquid Chromatography-tandem mass spectrometry

LCs: langerhans culture

LES_PB: 3D living skin equivalent model (3D Labskin) induced with Phenbarbital

LES_RA: 3D living skin equivalent Model (3D Labskin) induced with *all-trans* retinoic acid

LES_βNF: 3D living Skin equivalent model (3D Labskin) induced with β-naphthoflavone

LIT: Linear ion trap

LS: Labskin

LS_BZD: Labskin treated with benzydamine

Lses: Full Thickness Living Skin Equivalents

M/z: mass to charge ratio

m/z: mass-to-charge ratio

M: molar

MALDI: Matrix assisted laser desorption ionisation

MeOH: methanol

Mg: milligram

mL: milliliter

mm: millimiter

mM: millimolar

MS/MS: tandem mass spectrometry

MS: mass spectrometry

MSI: mass spectrometry imaging

Nano-LC-MS/MS: nano-liquid chromatography-tandem mass spectrometry

NAT: N-acetyltransferase

ng: nanogram

NHEK: normal human keratinocytes

NHS: normal human skin

N-oxid-BZD: benzydamine-N-oxide

NVP: nevirapine

ORS-RHE: 3D human skin equivalent model

PAH: polycyclic aromatic hydrocarbons

PAH: polycyclic aromatic hydrocarbons

PB: Phenobarbital

PBS: phosphate buffered saline

PCR: Polymerase Chain Reaction

PRDX: peroxiredoxin

Q: quadrupole

QIT: quadrupole ion trap

QTOF: quadrupole time of flight

RA: *all-trans* retinoic acid

RHEs: reconstructed human epidermis

RT-qPCR: real time-quantitative polymerase Chain Reaction

SC: stratum corneum

SDS-PAGE: sodium dodecyl sulphate polyacrylamide Gels

SIMS: secondary ion mass spectrometry

TBST: tris buffered saline with tween-20

TCDF: tetrachlorodibenzofuran

TFA: trifluoroacetic acid

TOF/TOF: tandem time-of-flight

TOF: time of flight

U: direct current

UDP-GT: UDP-glucuronosyltransferase

v/v: volume to volume

WB: western blot

XMEs: xenobiotic metabolising enzymes

α CHCA: alpha-cyano-4-hydroxycinnamic acid

βNF: β-naphthoflavone

Ml: microliter

Chapter 1

Introduction

1.1 European Legislation

Animal testing using, rat and pig skin and excised human skin have been used as historical standards to confirm the effects of therapeutics and toxicants that occur in the skin as a result of drug and other chemical metabolism. On 27th February 2003, the European Union (EU) amending Council Directive 76/768/EEC "The Cosmetics Directive" was introduced as new legislation. The 7th amendment to this directive imposed a testing and marketing ban on cosmetic products tested on animals from 2004 and cosmetic ingredients tested on animals from 2013. A deadline of 11 March 2013 depending on the availability of alternative non-animal tests was proposed (Pauwels & Rogiers, 2007). This legislation was a major impetus in the development of 3D skin models. Luu-The *et al*., (2009) emphasised that understanding the 3D skin models as an alternative method is important to inform risk of foreign chemicals compounds, such as drugs, cosmetics and their ingredients (Madison, 2003; Wickett & Visscher, 2006).

The work described in this thesis is concerned with the optimisation and validation of a human *in vitro* 3D living skin equivalent model for metabolism studies of topically applied xenobiotics.

1.2. Skin – Structure and Function

1.2.1 Native Human Skin

Human skin is largest organ in the body with functions, such as protection, metabolism, excretion, sensation and immunity (Bonifant & Holloway, 2019). It has a surface area of about 1.5-2 m^2 in adults and weighs about 15 % total body weight. Skin consists of three layers, subcutis, epidermis and the dermis each with distinct function. The subcutis is comprised (adipose and epithelial cell). The human skin contains blood vessels, vater-pacini-mechanosensors, sweat glands, hair follicles and neurites of peripheral neurons that are connected to skin (Bonifant & Holloway, 2019). The dermis supplies the epidermis with mechanical support and nutrients. It is attached to subcutaneous layer (underlying hypodermis of adipose tissue and areolar connective tissue) (See Figure 1.1). The epidermis is an epithelium (outermost layer) of the skin (100-150 µm thick) where cells are established through mitosis at the basale layer (Bonifant & Holloway, 2019).

The main cells of epidermis include maerkel, keratinocytes, melanocytes and langerhans cells which are constantly generated in basal lamina as they migrate to the skin surface (Sandilands *et al*., 2009; Honari *et al*., 2017). About 95 % of the cells of the epidermis are keratinocytes. The epidermis is further divided into the following sublayers including (stratum corneum, stratum lucidum, stratum granulosum, stratum spinosum, stratum basale). All have a significant role in the anatomy and function as seen in Figure 1.2. Among epidermis and the dermis of human skin is a thin sheet called basement membrane. The function of this membrane is to attach the dermis and epidermis (Honari *et al*., 2017).

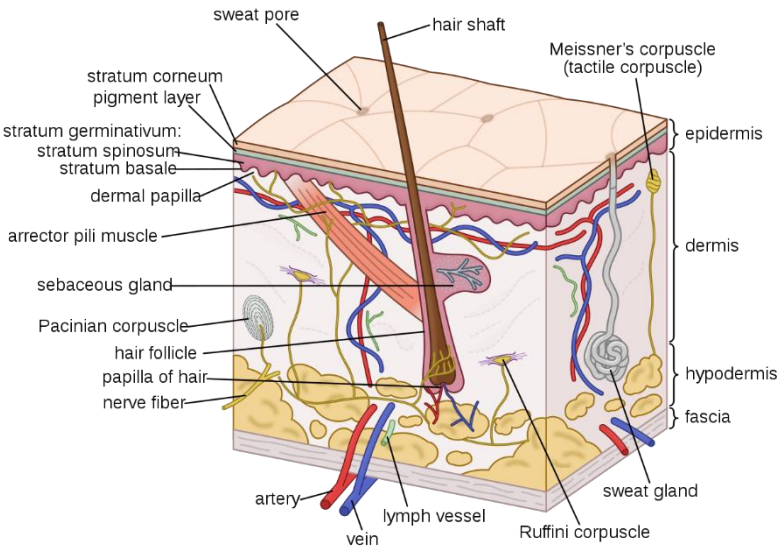

Figure 1.1: Illustration the structure of the skin. A copy from Bonifant & Holloway (2019)

The epidermis is made up of five layers as shown in Figure 1.2:

- The stratum lucidum layer composes of keratinocytes that are clear, flat, dead cells that are densely packed with eleiden, clear protein rich in lipids, derived from keratohyalin which makes these cells transparent. This layer is about 2-3 cell layers, normally found in the thick skin of the palm and soles (Yousef *et al*., 2017).
- The stratum spinosum layer (known as prickle-cell layer) is about 8-10 layers of keratinocytes cells which are between stratum granulosum and stratum basale. These cells prickle cell layer accumulate many desmosomes that attach a cell to its neighbour providing ‘prickles’ or 'spines'. Langerhans cells and melanocytes are also present in this layer (Tortora & Nielsen, 1995; Yousef *et al*., 2017).

- The stratum granulosum has about 3-5 cell layers of keratinocyte cells that comprises diamond-shaped cells with keratohyalin and lamellar granules. Keratohyalin granules comprise a protein that is responsible for binding keratin intermediate filaments into keratin. The lamellar granules contain the glycolipids that get secreted to the surface of the cells and function as a glue to keep cells stuck together.

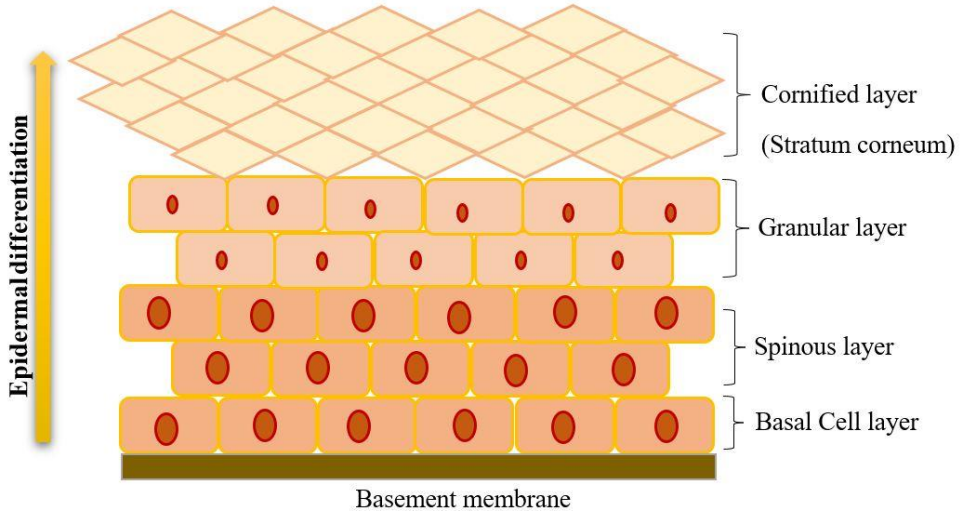

Figure 1.2: Representation of the structure of the epidermis. Beginning from the basal layer, the keratinocytes which transmit into layers: spinous, granular, lucidum and corneum.

- The stratum corneum; about 20-30 cell layers made up of keratin and non viable keyatinocytes cells (known as corneocytes) that have lost their nucleus, which are shed from the skin via desquamation (Sandilands *et al*., 2009; Yousef *et al*., 2017). Their function is to act a protective barrier to protect the body from chemicals, infection and the external environment.

  The dermis is much thicker than the epidermis (1-5 mm). The dermis is attached to the epidermis at the level of the basement membrane. Structurally, the layers of the dermis are typically sub-divided into two zones, the papillary layer, which includes (loose connective tissue containing capillaries, elastic fibres and collagen) and the reticular layer which includs (larger blood vessels, closely interlaced elastic fibres and thicker bundles of collagen). This layer provides strength and elasticity to the skin (Butcher & White, 2005). Additionally, it contains fibroblasts, mast cells, nerve endings, lymphatics and appendages and sebaceous glands, sweat glands, hair follicles, smooth muscle cells, and capillary beds (Butcher & White, 2005). The principal cells making up the dermis are fibroblasts, macrophages and adipocytes.

The papillary layer is characterized by relatively loose connective tissue immune cells (particularly mast cells and dendritic cells) which are patrolling in the papillary layer. Finally, dermal fibroblasts secrete extracellular matrix (ECM). The functions of the dermis are to support the epidermis, provide thermal insulation and to support the vascular network to supply the avascular epidermis with nutrients (Yousef *et al*., 2017). The hypodermis layer also known as "subcutaneous fascia" is the deepest and thicknest layer of skin that lies underneath the dermis (Tortora & Nielsen, 1995).

1.2.2 The Skin as a Barrier

The barrier function of skin is due to the outermost of skin layer: the stratum corneum (SC). Michaels and colleagues first introduced the "brick and mortar" model in 1979 to decribe the structure of the SC (Michaels *et al*., 1975). The SC is made up of about 10 to 25 terminally differentiated keratinocytes (layers of corneocytes) as the "bricks" embedded in lipid matrix and lipid envelope which surrounds the cells as the "mortar" as shown in Figure 1.3 (Prausnitz & Langer, 2008; Mitragotri *et al*., 2011). Extensive studies have shown that in the SC corneocytes are filled with water and microfibrillar keratin is surrounded via an envelope which is comprised of a cross-linked layer of proteins, such as filaggrin, loricrin and involucrin (Lazo *et al*., 1995) and a monolayer of non-polar lipids described as "lipid envelope".

This monolayer of non-polar lipids is esterified to the cornified envelope, mainly to glutamate residues of involucrin, to produce a template of the intercellular structure (Downing, 1992; Meguro *et al*., 2000). The cornified envelope, together with the lipid envelope, prevents most substances from entering corneocytes and it allows for optimal lipid matrix production (Downing, 1992; Meguro *et al*., 2000).

This envelope of the lipids represents 20 % of the stratum corneum volume and involves mostly ceramides, cholesterol, cholesterol esters, fatty acids, and cholesterol sulphate (Bouwstra *et al*., 2003). However, intercellular lipid matrix is lacking in a few places of the stratum corneum, allowing lipid envelopes of nearby corneocytes to contact, enhancing stratum corneum cohesion (Wertz *et al*., 1989). Both skin layers (epidermis and dermis) have been developed to provide a high effective barrier function for the penetration of xenobiotics (Scheuplein & Blank, 1971).

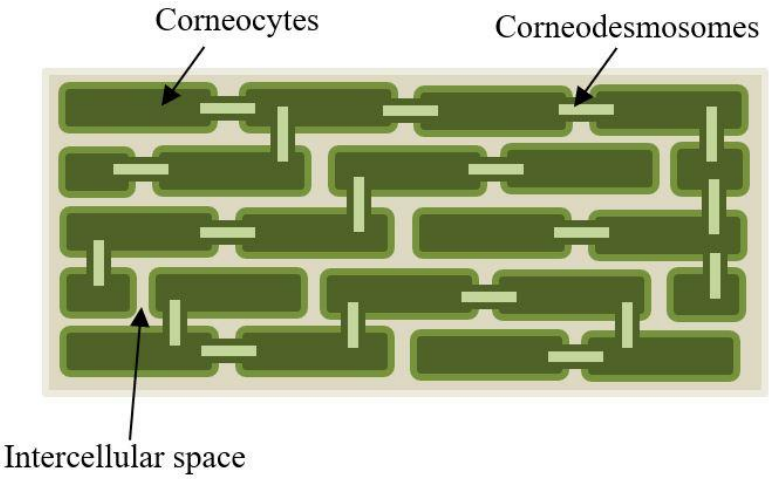

Figure 1.3: Schematic representation of the stratum corneum as the "bricks" embedded in lipid matrix and lipid envelope surrounding the cells as "mortar" model. Figure amended from (Michaels *et al*., 1975).

1.3 Cutaneous absorption "percutaneous"

Cutaneous absorption phenomena are useful for evaluate toxicity, and understand safety as well as therapeutic aspects of xenobiotics, chemicals, and cosmetics. Percutaneous absorption is the transport of a topically applied compound from the surface as it penetrates the skin, before reaching the blood stream (Carpentieri-Rodrigues *et al*., 2007). Several studies showed that the stratum corneum is the principle penetration barrier for the majority of the pharmacueticals through the various layers of the skin (epidermis and dermis) into into the systemic or blood circulation for a therapeutic effect (Brown *et al*., 2006; Murthy & Shivakumar, 2010). Currently, percutaneous delivery is an important route for the systemic administration of drugs as an alternative route for drug delivery, overcoming some of the drawbacks of conventional oral administration, such as the hepatic "first-pass effect" (Brown *et al*., 2006; Pathan & Setty, 2009). In addition, transdermal drug delivery can be controlled for a longer period of time compared to the normal gastrointestinal transfer of oral dose form (Pathan & Setty, 2009).

The epidermis is comprised of mosaic of proteins and lipids. The permeation of drug through the stratum corneum occurs by three transport pathways as shown in Figure 1.4 (Pathan & Setty, 2009):

- Intercellular diffusion through the lipid matrix.
- Intracellular diffusion through both the corneocytes and the lipid matrix.
- Transappendageal diffusion along the sweat pores and follicles.

A transcellular route is responsible for drug delivery across cells of the stratum corneum. In constrast, intercellular route refers to as drug absorption among cells, and anexial route through hair follicles, sweat glands, and sebaceous glands (Carpentieri-Rodrigues *et al*., 2007).

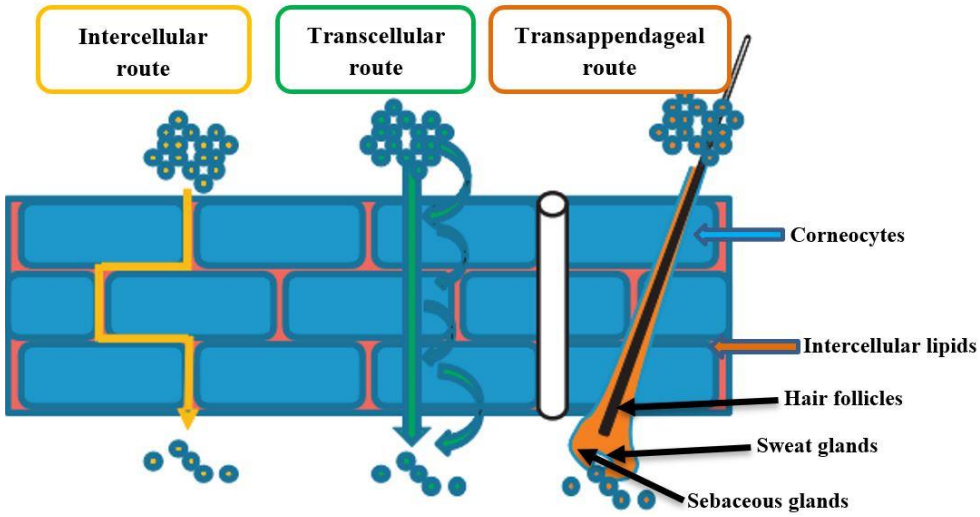

Figure 1.4: Schematic illustrattion of the process of drug transport through the stratum corneum. Figure adapted from Lane (2013).

Hair follicles and sweat glands are visible pores beneath the skin's surface, which provides a pathway for drug to enter through skin layers (Carpentieri-Rodrigues *et al*., 2007). The biomembranes contain of a lipophilic membrane with a hydrophilic portion.

According to Lane, (2013), useful way to consider drug penetration through stratum corneum can be described by Fick's first law equation which is shown below for steady state flux1:

$$Jss = \frac{ADKCv}{h} \qquad (1)$$

Jss is steady state flux

A is the surface region

D is the diffusion coefficient and *h* is thickness of membrane

K is the is the partition coefficient of the drug between vehicle/membrane

Cv is the the constant concentration of drug in solution

From the equation 1 that shown above, it can be observed that steady state flux is directly proportional to the concentration, by contrast inversely proportional to the stratum

corneum thickness (Lane, 2013). Percutaneous drug absorption through stratum corneum can be enhanced by chemical penetration enhancer (CPEs). Also, the enzymatic activity of the skin can be affected by different factors as seen in Table 1.1 (Leite-Silva *et al*., 2012; Pyo & Maibach, 2019). In addition, the enzymatic activity in skin can also effect the delivery of therapeutic agents.

Table 1.1: A different factors affecting on the enzymatic activity of the skin.

Skin	1. Age 2. Anatomical Site 3. Gender 4. Environmental Factors (Temperature)
Drug	1. Drug Solubility 2. Drug concentration 3. Molecular dimension 4. Effect of time
Vehicle	1. Distrubution of drug in stratum corneum 2. Absorption enhancer 3. Volatility

1.3.1 Chemical penetration enhancers (CPEs)

CPEs are commonly used in a variety of transdermal, dermatological and cosmetic products to aid delivery of drugs through the skin. Several chemical compounds can enhance transdermal drug delivery, in particular improving delivery across the stratum corneum (Pathan & Setty, 2009; Polat *et al*., 2012). These include alcohols, glycols, non ionic surfactants, sulfoxides, azone, derivatives, fatty acids, derivatives, pyrrolidones, cyclodextrins and also lectroporation and ultrasound (Carpentieri-Rodrigues *et al*., 2007; Sindhu *et al*., 2017). CPEs help in drug penetration through the outlayer of skin by disruption of the stratum corenum. They interact with the hydrophobic tails of lipids in the SC to leading increased disordering of their lamellar and lateral packing. They may also denature stratum corneum (SC) proteins causing swelling and increasing hydration improving partition of the drug into SC (Pathan & Setty, 2009).

1.4 Models for analysis

Animal models have been used in cosmetic skin research since the 1980s (Bronaugh *et al*., 1982). Animals skin including rat, pig, and guinea pig have been explored to replace human skin in order to generate representative information for determining or estimating the permeabilities of drugs, cosmetics, skin care products, and and metabolism of. Many reports have discussed the relative merits of different animal (Bronaugh *et al*., 1982; Leite-Silva *et al*., 2012). Pig and rat skin are considered to represent the most suitable alternative to human skin for testing permeation of topically applied chemicals, but the differences in thickness of the stratum corneum compared to human skin does affect permeability (Lademann *et al*., 2010; Netzlaff *et al*., 2006; Leite-Silva *et al*., 2012; Mead *et al*., 2016). The relative proportion of the principal lipid classes: fatty acids, triglycerides cholesterol, cholesterol ester and ceramides were found to be different in the skin of these species (Shanks *et al*., 2009). According to these findings, the variation in lipid composition seems to be major factor accounting for the differences in skin barrier function across the species (Shanks *et al*., 2009).

Perel and his colleagues has made signifcant contribution to understanding why animal models could not predict human reactions (Bracken, 2009). They conducted reviews of research using animal models and compared the findings in humans in six areas. The results of the animal research were in substantial disagreement with the human data. This is a concern for drug development and evaluation (Bracken, 2009; Lademann *et al*., 2010). A second major issue for the use of animal skin in research is the European Cosmetics Directive of March 2009 and Authorization and Restriction of Chemicals (REACH) Legislation of June 2007. These prohibited using animal skin for testing of cosmetics and ingredients including skin irritation, corrosion, and genotoxicity testing (Pauwels & Rogiers, 2007). Therefore as Luu-The *et al*., (2009) concluded an in-depth understanding of the properties of tissue engineered 3D cellular models of human skin is important so that they can be used in testing to inform risk assessments of topically applied xenobiotics.

1.4.1 3D skin models

In vitro models of skin are desirable as tools for studying absorption, detoxification and metabolism of topically applied xenobiotics as an alternative to experiments using, hard to obtain, *ex vivo* human skin or live animals (Madison, 2003; Wickett & Visscher, 2006).

The major cell types present in skin: keratinocytes and fibroblasts, when cultured in a scaffold develop into a highly discriminated 3D skin equivalent model containing both dermal and epidermal layers (Hu *et al*., 2010). The scaffolds most generally used are collagen or fibrin gel to produce a dermal fibroblast equivalent model (dermis) which is seeded onto nylon mesh and grown for ~ 4 weeks until a physiologic dermal-like matrix is formed (El-Ghalbzouri *et al*., 2002). This is then seeded with keratinocytes which are cultured for 14 days at an air liquid interface form an epidermis (which contains distinct basal, spinous, granular, and stratum corneum layers). This epidermal layer closely resembles the structure of the *in vivo* skin epidermis (Niehues *et al*., 2018). These models have been called human skin equivalents (HSEs) and are divided into two major types: reconstructed human epidermis (RHEs) differentiated epidermis cultures derived from human keratinocytes and full thickness living skin equivalents (LSEs), comprised of epidermis and dermis as shown in Figure 1.5 (Mathes *et al*., 2014).

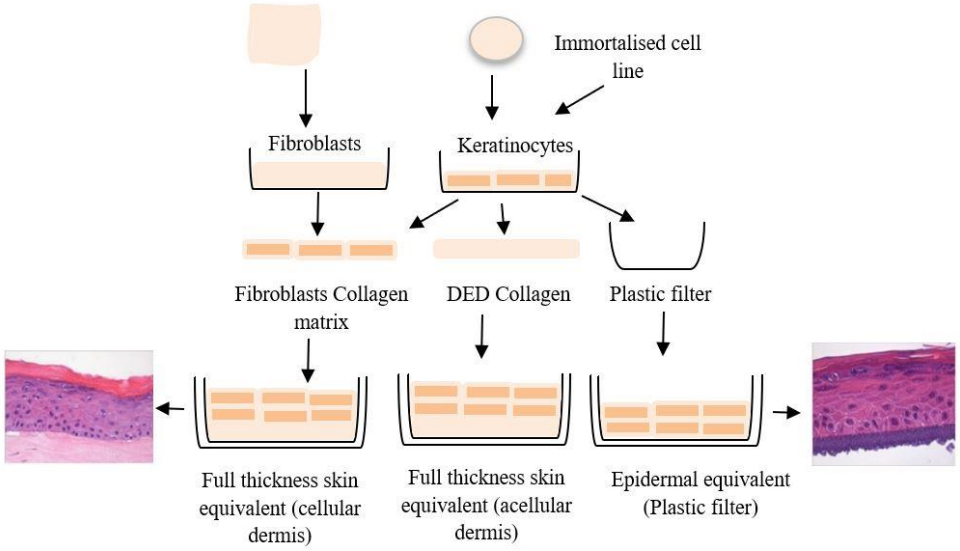

Figure 1.5: Diagram representation of 3D skin model (reconstructed human epidermis (RHEs) and and full thickness living skin equivalents (LSEs). To generate 3D skin model: the keratinocyte can be grown-up on a cellular matrix (fibroblast-collagen matrix), an acellular matrix (inert plastic filter or de-epidermised dermis, DED). Additionally, keratinocytes are seeded and grown in submerged cell culture at the air-liquid interface. After 14 days, a multilayered stratified epithelium (epidermis and dermis) is full grown to created 3D skin model which is comparable to *in vivo* skin (Niehues *et al*., 2018).

LSEs can be further refined by adding further cell types, such as melanocytes, stem cells, langerhans cells and others or by their use in combination with other organotypic models in organ-on-a-chip systems (Mathes *et al*., 2014). In addition organ-on-a-chip can mimic

the dynamic interactions of microenvironments that exist in *in vivo* tissues (Wang & Guengerich, 2013). Several 3D tissue skin models have been constructed utilizing and used this approach to incorporate vascularization into their model (Lee et *al.*, 2017).

3D skin equivalent models, such as LSE and RHE have a weak barrier function compared to normal human skin due to the lack of mechanical forces and dynamic flow system that provide continuous supply of nutrients and metabolites. Despite advances in the use of 3D skin models, the skin permeability issue *in vitro* remains unresolved. It has been found that LSE and RHE exhibit different permeability to native human skin. The permeability is mainly in the stratum corneum (SC) of the epidermis layer, providing a barrier for lipophilic chemicals. It is clear that of the variability in the thickness, composition and cells of are involved in the process. A concern that has been expressed in the use of 3D models permeability is mainly due to the deviations in lipid composition within skin models (Bell *et al*., 1991; Mathes *et al*., 2014). The most abundant in the SC are cholesterol, free fatty acids (FFAs) and ceramides. These lipid matrix create the continuous pathway through the SC, and contributes significantly to the barrier functions of the skin.

LSE have not been extensively studied in terms of characterising their Phase I and Phase II metabolic capability (Gibbs *et al*., 2007). Studies that have been conducted have been reviewed in a number of papers (See Table 1.2) (Oesch *et al*., 2007; Oesch *et al*., 2014; Oesch *et al*., 2018; Kazem *et al*., 2019). Other reviews which covered absorption, distribution, metabolism and excretion for topical and systemic chemical exposure have been published (Luu-The *et al*., 2009; Hu *et al*., 2010).

The main purpose of developing of skin models is to obtain models able to mimic the structure and function of human skin. One important aspect of this is as gene and protein expression of Phase I and Phase II xenobiotic metabolising enzymes (XMEs) (Kazem *et al*., 2019).

Table 1.2: Overview of different type of commercial 3D reconstructed human skin models used for studying Phase I and Phase II XMEs. Adapted from: Jäckh *et al*., (2012) and Oesch *et al*., (2018).

Skin model	Cell origin	Company	Type	References
Phenion® FT (PFT)	Male foreskin	Henkel, Düsseldorf, Germany	Full thickness (collagen matrix)	Mewes *et al*., (2007)
Episkin™ FTM	Adult breast skin	SkinEthic™ laboratories	Full thickness (polycarbonate and collagen matrix)	Eilstein *et al*., (2015)
EpiDermFT™ (EFT)	Male foreskin	MatTek, MA, USA	Full thickness (collagen matrix**)**	Hu *et al*., (2010)
SkinEthik™ RHE	Adult abdomen Male foreskin	SkinEthic™ laboratories, Nice, France	Epidermal	Netzlaff *et al*., (2006) Eilstein *et al*., (2010)
EST-1000 (EST)	Male foreskin	Cell Systems, Troisdorf, Germany	Epidermal	Hoffmann *et al*., (2005)
EpiDerm™ (EPI-200)	Male foreskin	MatTek, MA, USA	Epidermal	Hayden *et al*., (2006)
StrataTest®	NIKS® human keratinocyte cell line	StrataTech, MA, USA	Epidermal	Slavik *et al*., (2007)
ORS-RHE	Outer root sheath	PierreFabreDermo cosmétique	Epidermal	Guiraud *et al.*, (2014)
EPI-MODEL	-	LabCyte, Aichi, Japan	Epidermal	Katoh *et al*., (2009)
Episkin™	Adult breast skin	SkinEthic™ laboratories, Nice, France	Epidermal	Tinois *et al*., (1991)

Studies as shown in Table 1.2 by (Oesch *et al*., 2007; Oesch *et al*., 2014; Kazem *et al*., 2019), compared XME in reconstructed human skin and reconstructed human epidermis models to native human skin. It has been found that Phase I and Phase II enzymes are expressed (mRNA, protein expression and enzyme activity) at low levels compared to human skin. In one study by Wiegand *et al*., (2014), *in vitro* human skin test systems (2D and 3D) from a different donors were investigated and compared with liver and native human skin. This group suggested that overall, XMEs basal and induced levels of Phase I and Phase II enzymes (gene/protein expression) in 3D models of skin reflected the *in vivo* situation more realistically than 2D system.

Almost all XMEs in human skin are also detected in liver (Wiegand *et al*., 2014). However, the levels have been reported to be lower than those that present in liver and fewer enzymes are reported in skin and in studies of commercial skin models (Oesch *et al*., 2018; Kazem *et al*., 2019). There is therefore, a need to understand drug metabolism (in respect of mRNA and protein expression levels) in all commercially available skin models and to examine whether enzyme activity equivalent to native human skin can be induced (Wiegand *et al*., 2014). Such studies have been reported by Luu-The *et al*., (2009) and Eilstein *et al*., (2015) using the commerical 3D models Episkin™ and Episkin™ FTM who characterised the mRNA expression of XMEs level following exposure to cosmetic ingredients and chemical compounds using Real Time qPCR quantification.

1.4.2 Labskin model

Labskin is a commercially available 3D skin model (produced by Innovenn, York, UK, https://www.labskin.co.uk/skin-model). It is a full skin structure model including an epidermis, dermis and a complete basement membrane as shown in Figure 1.6.

This model is produced using primary dermal fibroblasts cells embedded in a fibrin gel scaffold and incubated for 6 days within Labskin media to form the dermis. Once cells are settled in dermal compartment, keratinocytes derived from human skin, cultured in a fibrin scaffold are grown submerged on top of the dermal component and cultured in media (6 days). The keratinocyte cells are then grown and maintained for 14 days at an air-liquid-interface, which is critical to allow differentiation into the different layers of the epidermis including the stratum spinosum, stratum granulosum and stratum lucidum.

At the day 12 air-liquid interface, the SC becomes thicker therefore, mimicking mature skin. This skin model culture is a unique full thickness model with a fully differentiated epidermis supported by dermal compartment consisting of fibroblasts in a fibrin scaffold. The use of fibrin, instead of the more usual collagen-based scaffolds, yields unique physical properties making this model is viable for further 2 weeks and hence very suitable for xenobiotic/drug testing experiments including metabolism studies. However, xenobiotics metabolism is not yet well characterised in this skin model.

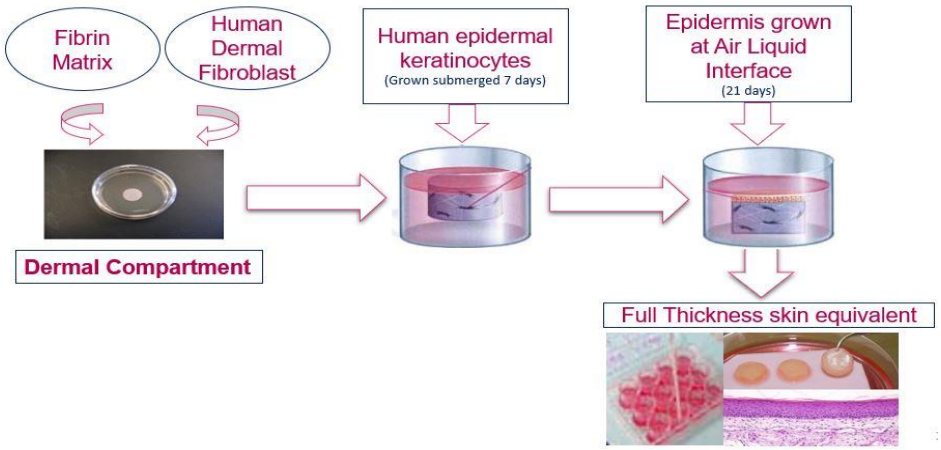

Figure 1.6: Schematic of commercial avaliable 3D skin equivalent model represents the structural of human skin consists of a full thickness epidermis and dermis layers which shows a similar function as native human skin.

A further advantage of this model compared with others is that it the only available model able to host micro-organisms on the surface. It could therefore be used to produce a model that mimics the endogenous micoflora of native human skin. This is owing to the surface properties, which are relatively dry in comparison to other skin models and have protective functions similar to the native skin. Due to these considerations this 3D skin model was selected for the XME studies carried out in this thesis.

1.5 Skin Xenobiotics Metabolising Enzymes

Xenobiotic metabolism takes place in two phases: Phase I biotransformation reactions (*e.g.* oxidation, reduction, and hydrolysis) included formation of new or modified functional groups (oxidation, reduction, hydrolysis) and Phase II conjugation reactions with endogenous substances (*e.g.* glucuronic acid, sulfate, and glycine). These processes have the overall aim to make the xenobiotic more water soluble, "polar" and thus more readily excreted from the body. Understanding xenobiotic metabolism (XMEs) in 3D skin

models and its relationship to human skin metabolism is important to improve and develop the transfer of drugs from the *in vitro* to *in vivo* situation. Luu-The *et al*., (2009) pointed out that this information could be used to inform risk assessments of topcally applied drugs. In contrast to the human liver (which is the main a first pass organ responsible for drug metabolism), less is known about the xenobiotic metabolising enzymes of the skin. These XMEs are known to be located mainly in keratinocytes within the epidermis, even though levels are lower than those discovered in liver (van Eijl *et al*., 2012).

Despite the key role of these processes in the absorption of xenobiotics (and in the ultimate toxicology of compounds absorbed through the skin), the levels of distributon of Phase I and Phase II enzymes have not been widely studied in either skin or 3D models of skin (Hu *et al*., 2010; Oesch *et al*., 2007). However, it has been reported that due to the variety of cell types present (*e.g.* fibroblast, lymphocytes and monocytes), human skin contains higher levels of xenobiotic metabolising enzymes than keratinocytes (Oesch *et al*., 2014) and additionally that Phase II enzymes are expressed in higher levels in human skin and the Epi-Derm^{TM} 3D cell model than Phase I enzymes (Wiegand *et al*., 2014).

A recent publication in this field by Bacqueville *et al*., (2017) compared metabolism in the 3D human skin equivalent model (ORS-RHE) to those that in native human skin. This study found that Phase II enzymes were present in higher amounts compared to the Phase I in the ORS-RHE model. This was especially true for glutathione-S-transferase (GST) and N-acetyltransferase (NAT) enzymes. However, since levels of cytochrome P450 (CYPs) enzymes are consistently reported to be very low in whole skin and it is not easy to confidently identify them. This was also found to be the case in both *in vivo* human skin and in the ORS-RHE model used in this study (Bacqueville *et al*., 2017). Observable in this model are alcohol and aldehyde dehydrogenases, and esterases (Bacqueville *et al*., 2017). The presence of functional Phase I and Phase II xenobiotic metabolism enzymes (XME) were confirmed by incubating the skin models within several substrates and some inducers such as, testosterone inducer, 3-methylcholanthrene (3-MC), 7-ethoxycoumarin, β-naphthoflavone (βNF) which metabolised after topical application (Bacqueville *et al*., 2017).

Only very few publications have attempted to investigate the full range of XMEs present in whole skin (Oesch *et al*., 2007; Oesch *et al*., 2014; Oesch *et al*., 2018). In the initial

work of Oesch and colleagues (2007) Phase I (*e.g.* cytochrome P450s, alcohol dehydrogenase, flavin-dependent monooxgenase, aldehyde dehydrogenase, epoxide hydrolase, esterases and amidases and NAD (P) H: quinone) and Phase II (*e.g.* glutathione S-transferase, sulfotransferase, N-acetyltransferase and UDP-glucuronosyltransferase) were characterised in skin, more specifically in the epidermis (which is in agreement with the higher levels found to occur in keratinocytes rather than fibroblasts) (Wiegand *et al*., 2014; Pyo & Maibach, 2019).

Reconstructed commercial models of human skin, including, the full-thickness skin equivalent EpiDermFT ™, full-thickness skin model Phenion®, AST-2000 full-thickness skin model and EpiSkin® and 3-dimensional reconstructed human skin models (3D skin model) have been used as an alternative to animals in the study of XMEs (Table 1.2). However, xenobiotic metabolism is not well characterised in 3D skin models nor it's relationship to xenobiotic metabolism in human skin established. Cytochrome P450 dependent metabolism of xenobiotics has however been suggested to be similar in human skin and 3D skin models. Studies by Hu *et al*., (2010), Luu-The *et al.,* (2009), Neis *et al*., (2010), van Eijl *et al*., (2012), and Pyo & Maibach (2019) were carried out using various techniques to measure levels of expressed XMEs in skin models and native human skin.

A major focus of this project is to to investigate if Labskin has levels of XME comparable to *in vivo* human skin. In order to achive this, we set out to determine the number and levels of the Phase I and Phase II XMEs in Labskin compared with the native human skin at the levels of gene/protein expression as well as by studying enzymatic activity.

1.6 Polymerase Chain Reaction (PCR)

The PCR technique was first introduced in 1985 by the American Biochemist Kary Mullis (Saiki *et al*., 1985; Mullis *et al*., 1986). Mullis won the Nobel Prize for the discovery of PCR in 1993 (Bartlett & Stirling, 2003). The PCR technique based on the polymerase chain reaction (PCR) allows quantitation and amplification of nucleic acids sequences (Saiki *et al*., 1985). Because it is sensitive, specific and reproducible method for the quantitation of nucleic acids, PCR has become one of the successful applications in molecular biology and medical research. It is used to amplify a single or double copies of a piece of DNA to generate of copies of a specific DNA sequence (Joshi & Deshpande, 2010).

The main principle of the polymerase chain reaction is the amplification of segments of DNA to create more than one million specific DNA sequences between the priming sites. Primers are small DNA fragments that function by linking the building blocks to form templates for building the new strand (Joshi & Deshpande, 2010). The key steps involved in PCR are: denaturation, annealing, and extension (Joshi & Deshpande, 2010). In denaturing, the DNA is first heated and denatured at the denaturing temperature of typically 95 °C to be amplified single strands. In the annealing step, primers are annealed to oligonucleotide primers to prime the extension step at a low temperature approaching 50-60 °C. This enables the primers to form hybrids with their complementary template strands. In the extension step of the PCR cycle, polymerase extension is repeated several times at the end of the annealed primers, resulting in an exponential increase in the copy strand of DNA sequence between the priming sites. In this stage, the extension of the primers can be monitored by the incorporation of dyes (*e.g.* SYBR® Green or TaqMan®). Cycles are repeated 20-40 times to generate multiple copies and amplify the target DNA as seen Figure 1.7.

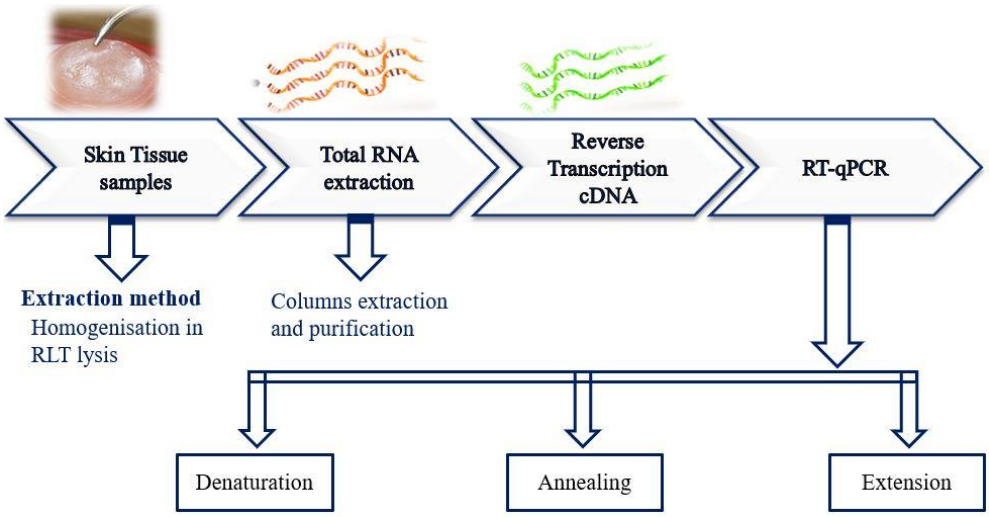

Figure 1.7: The principle of PCR: Denaturation, annealing, and extension (PCR depended on the high denaturing temperatures includes heating the double stranded target DNA molecule and seperated by breaking bonds among A-T and G-C. In annealing stage, the two strands allows binding and reverse primers of particular sections of the separated strands in the target DNA. Extension stage occurs by adding complimentary the dyes *e.g.*, TaqMan® to the new strands.

1.6.1 Real time-quantitative PCR (RT-qPCR)

The development of real-time quantitative (q-) PCR represents significant progress in a variety of molecular techniques, including nucleic acid analysis (Konermann *et al.*, 2013).

Higuchi developed qPCR in 1992 (Higuchi *et al*., 1992). qPCR method works by the detection of fluorescent DNA stains, such as SYBR® Green which can be bound to double-stranded DNA. Such stains generate fluorescence which is used to quantify the amplification of the target DNA at each cycle of PCR process (Singh *et al*., 2014). Hence, the qPCR data are collected during the PCR process (*i.e*. monitoring of the cycle of PCR amplifcation as they are accumulate in a "Real Time Detection" by using fuorescence not only at the end of reaction). During the log-linear phase of amplification, the fluorescence rises to the measurable level which is known as the threshold cycle (CT) (Rodríguez-Lázaro *et al*., 2013; Singh *et al*., 2014).

qPCR outputs include amplification; standard curves log concentration vs CT, which are plotted via using serial dilutions of a known magnitude of standard DNA and Ct value, which the complementry DNA (cDNA) can be used to quantify the amount of DNA molecules as CT value using standard curve as shown in Figure 1.8 (Singh *et al*., 2014). In RT-qPCR, the comparative Ct ($2^{-\Delta\Delta Ct}$) method is a statistical model that evaluates changes in gene expression as a relative fold change among an experimental and calibrator sample (Singh *et al*., 2014). Due to the increased sensitivity and the dynamic range of amplification, many of housekeeping genes have been used for normalization results (Singh *et al*., 2014).

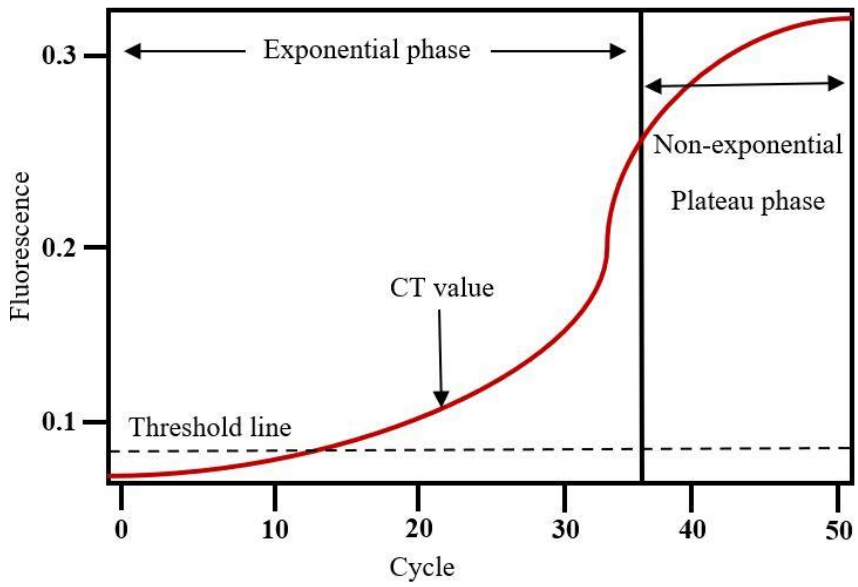

Figure 1.8: Amplification plot. Fluorescence Vs Cycle. Adapted from: Rodríguez-Lázaro *et al*., (2013)

qPCR can be applied for many functions, it is particularly used for quantifying nucleic acids and genotyping in a similar manner to conventional PCR. Its main advantage is that the amplifcation and detection methods have combined into one stage, thus removing any requirement for post-amplification processing of targeted DNA (Mackay, 2004). It also has a low level of contamination caused by PCR products like cDNA and RNA. However, qPCR has some shortcoming including high cost of the reagents.

In comparison to the conventional PCR process, qPCR is preferred for several reasons, including the ability to amplify short DNA fragments, the ability of fluorescent detection to detect minor amounts of amplified products, and an enhanced tolerance to inhibiting materials interfering with DNA purification compared to conventional PCR processes.

1.6.2 Reverse Transcription-PCR (RT- PCR)

Reverse Transcriptase PCR, enables measurement of the levels of RNA by creating complementary DNA (cDNA) from RNA, which is produced by reverse transcribing of the RNA templates, followed by amplification of cDNA using standard PCR (Singh *et al*., 2014). This approach is applied to evaluate gene expression, and combined with real-time PCR (qPCR) to measure RNA levels (Singh *et al*., 2014).

1.6.3 RT-PCR/qPCR combined

RT-PCR/qPCR combined known as RT-qPCR technique has enabled the successful completion of the 'human genome project: the determination of expression levels of target genes by enabling the amplification and sequencing of the human genes in human tissue (Singh *et al*., 2014). This technique used in our study to measure the quantitative detection expression of RNA by converting the RNA template to cDNA in human skin and 3D skin model (Labskin).

1.7 The application of RT-qPCR in Human Skin and 3D Skin Models (Gene expression)

1.7.1 Cytochrome P450 (*CYP*) gene expression

The cytochrome P450 (*CYPs P450*) family of enzymes are responsible for numerous oxidative reactions and metabolise a wide range of xenobiotics. *CYP* enzymes metabolise a wide range of endogenous and exogenous substrates by mono-oxygenation reaction (including epoxidation, dealkylation, hydroxylation, decarboxylation and isomerisation), but *CYPs* of Phase I also have the ability to act as peroxidases or reductases. Lipophilic

xenobiotic compound metabolism is often catalysed by *CYP* as a means of conversion into more hydrophilic compounds as an aid to excretion (Vondracek *et al*., 2001). Several researchers have investigated the role of *CYPs* in Phase I drug metabolism in the skin (Oesch *et al*., 2007; Oesch *et al*., 2014; Oesch *et al*., 2018; Kazem *et al*., 2019). In an early study by immunohistochemical staining, RT-PCR and HPLC analysis showed *CYPs* were predominantly expressed in the epidermal layer of skin, hair follicles and sebaceous glands. However, levels were found to be much lower than in the liver.

Whilst *CYP* levels have been shown to be very low in the skin by using RT-PCR, many compounds to which the skin is exposed, such as cosmetics (and their ingredients) and health care products, are substrates of *CYPs* such as *CYP1A1, 1A2, 2C9, 2D6, 2E1* and *3A4*. Additionally, therapeutic drugs used in dermatology, *i.e.* 7-ethoxyresorufin-O-dethylase, para-nitrophenol, diclofenac hydroxylase, 7-pentoxyresorufin-O-depentylase, 7-methoxyresorufin-O-demethylase, dextromethorphan, chlorzoxazone, hydroxylation, testosterone and erythromycin-N-demethylase are inducers, substrates and inhibitors for several CYPs (Vondracek *et al*., 2001).

In native human skin, transcripts coding for CYPs have been found to be present in many studies. Yengi *et al*., (2003) detected that about 13 CYP P450 subfamilies of enzymes were found using RT-qPCR to be present in whole skin collected directly from human donors. Levels of *CYP 1A2, 2A6* and *2C8* were below the limits of detection. Moreover, Baron *et al*., (2008) reported about 36 CYP genes experssion were expressed in whole human skin namely*: CYP1A1, 1A2, 2A6, 2A7, 3A4, 3A7, 3A5, 1B1, 2B6, 2B7, 2C9, 2C18, 2C19, 2D6, 2E1 and 2S1*. Thus, Smith *et al*., (2006) showed that *all trans* retinoic acids (RA) was a powerful inducers for *CYP1A1, 1A2, 1B1. CYP2C18, CYP3A5 and CYP1A2*. These were also shown to be induced by clobetasol-17-propionate in full thickness adult human skin in the same study.

Hu *et al*., (2010) compared the expression of 139 xenobiotic metabolizing enzymes in EpiDerm™ model and full thickness human bottom skin tissues using RT-PCR and Microarray analysis. Approximately 87 percent of the genes were expressed in detectable levels in both the EpiDermis™ model and human skin. Five *CYP* mRNA (*1A1, 2E1, 1B1, 4F8, 4X1*) were found to have much lower expression in the reconstructed skin models (EpiDerm™) compared to full thickness bottom skin (FTHBS). *CYPs* were also present at low levels in EpiDerm™ but CYP1A1/1B1expression was induced following exposure

to 3-methylcholanthrene (3MC). On the other hand, the *CYP* isoforms such as *2C9*, *2C18*, *4B1, 2J2* were detected at higher levels in EpiDerm™ than FTHBS. It has been reported that many of the *CYPs* found in FTHBS and EpiDerm™ can be induced (Wiegand *et al*., 2014). Hayden *et al*., (2006) and Rassmussen *et al*., (2011) demonstrated that 3-MC and βNF were induced both *CYP1A1* and *CYP1B1* in EpiDerm™ model. These studies have confirmed *CYP1A1* and *CYP1B1* activity is increased in EpiDerm™ by ethoxyresorufine induction.

A study by Neis *et al*., (2010) reported real time quantitative PCR (RT-qPCR) analysis CYPs expression (*1A1, 1B1, 2E1, 2J2*, *3A4*, *4B1*) in several full thickness skin models. mRNAs coding for CYP 2C18 and 3A4 were found in low abundance in all organotypic skin models, EpiDermFT ™, Phenion®, EpiSkin®, while *CYP2B6* was not identified in any. *CYP1B1, 2E1, 2J2, 3A4* and *4B1* (expect *CYP1A1* was slightly induced in Phenion®) by liquor carbonis detergents (LCD). On the other hand, Luu-The *et al*., (2009) reported the presence of various Phase I enzymes in Episkin ™ and EpiSkin™ FTM and the human epidermis. *CYP1A, 2B, 2E* and *3A* were induced in the models by treatment with dexamethasone. In addition, arachidonic acid was used to induce *CYP2J2*, prostaglandins and leukotrienes *4F8* and *4F12* and eicosatrienoic acids *2C8*. In more recent studies by Eilstein *et al*., (2015) and Bacqueville *et al*., (2017), the identification of XMEs in a reconstructed human epidermal model derived from adult hair follicles (ORS-RHE) has been reported at low level of the gene compared with human skin.

Some Phase I and II XMEs identified by RNA and protein expression will be discussed in more detail, including detection and localisation in native human skin and the *in vitro* skin models.

1.7.2 Phase I drug metabolising enzymes

1.7.2.1 CYP1 family

Several publications have investigated the levels of and changes in the levels of *CYP 1A* in skin by treatment of keratinocytes with known inducers. A range of fold change increases in *CYP1A1* mRNA and protein have been reported. Approximately 60 % of the genes of the *CYP1* family were detected and reported to be higher in keratinocytes isolated from the epidermal layer compared with those of the dermal layer of skin (Wiegand *et al*., 2014; Kazem *et al*., 2019).

CYP1A1 subfamily: mRNA was reported to expressed at different levels in keratinocytes, fibroblasts, cultured langerhans cells and melanocytes. It was found to be expressed higher in the sebaceous glands, epidermis, and high in hair follicles. *CYP1A1* expression was reported to not be consistent across subjects *i.e.* it exhibits genetic polymorphism. *CYP1A1* and *CYP1A2* mRNA were expressed in the three donors used to construct the reconstructed model (OS-Rep), but was not detectable in a commercial 3D skin full skin model Phenion FT Skin (Wiegand *et al*., 2014).

Baron *et al*., (2008) found that dexamethasone and benzanthracene lead to transcriptional induction of *CYP1A1* and localised mostly to the suprabasal layer of keratinocytes. In contrast, Berghard *et al*., (1990) reported that 2, 3, 7, 8-tetrachlorodibenzofuran (TCDF) treatment did not increase the levels of *CYP1A1* mRNA in normal human keratinocytes. However, exposure of normal human keratinocytes (NHK) cultured in serum-free and extracellular Ca^{2+} to the TCDF lead to transcriptional induction of CYPs expression, a 3.0-fold induction compared with control cultures. Saeki *et al*., (2002) showed *CYP1A* mRNA is expressed in langerhans culture (LCs), melanocytes and keratinocytes. Götz *et al*., (2012) detected *CYP1A1* and *CYP1A2* activity in EPI-200 models following EROD induction, otherwise it was below the limit of detection in 3D skin models.

CYP1A2 subfamily: *CYP1A2* has been reported to play an important role in xenobiotics metabolism in human skin (Vondracek *et al*., 2001). More recently, Oesch *et al*., (2007) have shown that several substrates, such as, polycyclic aromatic hydrocarbons, 7-methoxyresorufin-O-demethylase, acetaminophen, aflatoxin B1, phenacetin, phenacetin, aromatic amines, theophylline, warfarin, imipramine and theophylline are metabolised by *CYP1A2* in human skin and other tissues. It has been shown to be only weakly induced compared with *CYP1A1* by dibenzo [a, l] pyrene (Schober *et al*., 2006).

CYP1B1 subfamily: CYPlBl mRNA was observed in 15 different normal human skin samples (Sutter *et al*., 1994). It is expressed and localized in the epidermis (in contrast to *CYP1A1* which is observed in epidermis specifically in the basal cells (Oesch *et al*., 2007; Kazem *et al*., 2019). Oesch *et al*., (2007) observed that the biotransformation of dibenzo [a, l] pyrene via *CYP1B1* was less efficient compared to CYP1A. CYP1B1 can be induced by 2, 3, 7, 8-tetrachlorodibenzo-p-dioxin treatment 10 ng treatment for 24 h gave a 100-fold increase in *CYP1B1* in primary human keratinocytes (Akintobi *et al*., 2007). In the

primary keratinocytes and HaCaT cell cultures exposure to ultraviolet-B enhanced induction of *CYP1B1* by polycyclic aromatic hydrocarbons (PAH) (Katiyar *et al*., 2000).

Villard *et al*., (2002) reported that *CYP1B1* was present at higher catalytic activities compared to other *CYPs, e.g. CYP1A1,* in a study of the biotransformation of many PAH. This has been confirmed by similar results for levels of *CYP1B1* mRNA in human keratinocytes following exposure to UV-B irradiation (Villard *et al*., 2002). In addition, they also reported *CYP1B1* gene induction in HaCaT cells by N-acetylcysteine (*NAT*). *CYP1B1* can be induced by liquor carbonis detergents (LCD) (Neis *et al*., 2010). RT-PCR analysis showed that 24 h after drug treatment of 3D skin models with LCD inducer inducer, *CYP1B1* gene expression was induced in all skin models.

Wiegand *et al*., (2014) reported the expression of *CYP1B1* in native human skin, the three-dimensional full skin model Phenion FT and an epidermal model OSREp. *CYP1B1* gene expression was higher in the dermis (Wiegand *et al*., 2014). In the most recently reported study by Bacqueville *et al*., (2017) it was shown that *CYP1B1* expression in ORSRHE models could be induced by topical application of βNF and 3-MC for 24 h (13.9-fold increase for treatment with βNF and 11.9-fold for 3-MC). The induction of *CYP1B1* gene expression level was confirmed in ORS-RHE tissues by using changes in flouresence to demonstrate the biotransformation of ethoxyresorufin, 24 h after the induction with 3-MC or βNF.

1.7.2.2 CYP2 family

The *CYP2* family is mainly observed in the human dermis and in differentiated keratinocytes rather than the epidermis outer cell layers and skin appendages. Du *et al*., (2004) reported that only the 13 CYP2 XME genes (*CYP2A6*, *2A7*, *2B6, 2C9, 2C18, 2C19, 2D6, 2E1*, *2J2*, *2R1*, *2S1*, *2U1*, and *2W1*) were expressed in whole human skin.

CYP2A subfamily: CYP2A is mostly observed in the human dermis. Only the *CYP2A6* and *CYP2A7* expression have been reported in skin. In contrast, 2A13 is not observed in skin (although it is found in other epithelial skin tissues) (Ding & Kaminsky, 2003). Ding *et al*., (1995) demonstrated expression of *CYP2A7* mRNA in the human skin fibroblasts while finding no evidence in keratinocytes. Interestingly, transcripts of *CYP2A6* also appeared in the dermis. In contrast, levels of *CYP2A6* and *CYP2A7* genes were reported to be below the detection limit in another study (Saeki *et al*., 2002). Yengi *et al*., (2003)

also reported *CYP2A6* abundance was below both limits of detection and quantification in a study of 27 individual human skin biopsies. Using a quantitative ribonuclease protection assay, Janmohamed *et al*., (2001) detected CYP2A6 RNA in five out of nine human skin samples, *CYP2A6* transcript has shown to be expressed in different samples of human skin in proliferating keratinocyte cultures derived from the HaCaT cell line.

Wiegand *et al*., (2014) reported *CYP2A6* mRNA to be present in the epidermis of two out of three donor samples of human skin. In addition, Wiegand *et al*., (2014) also studied mRNA *CYP2A6* in a 3D skin model derived from the same donors and found it to be weakly expressed in the commercial Phenion FT Skin model.

CYP2B subfamily: Only *CYP2B6* transcripts have been reported to be expressed in the normal human skin (Hoffman *et al*., 2001; Hu *et al*., 2010; Janmohamed *et al*., 2001), in HaCaT cells and proliferating cultures of human keratinocytes (Baron *et al*., 2001). *CYP2B6* was induced by PB (Baron *et al*., 2001) in proliferating skin keratinocyte cultures. Yengi *et al*., (2003) suggested that the variability of the *CYP2B6* gene was the same as that found in the human liver.

Wiegand *et al*., (2014) found that there is also variation in levels of mRNA between human individuals. Some individuals have no *CYP2B6* mRNA expression and other individuals had high levels of total RNA.

CYP2B6 was not however detected in human skin; fibroblasts, melanocytes, Langerhans cells or keratinocytes (Saeki *et al*., 2002). Rolsted *et al*., (2008) and Rassmussen *et al*., (2011) have studied *CYPs* in the commercial 3D models EpiDerm™ and StrataTestR respectively and *CYP2B6* was also not found to be present.

CYP2C subfamily: CYP2C18, CYP2C19, CYP2C19, CYP2C8, and CYP2C9)

CYP2C8, CYP2C18 and *CYP2C19* gene expression has been detected in human epidermis (EpiSkin™, EpiDerm, ORS-RHE, SkinEthic™), full thickness reconstructed human skin models (Skin™ FTM, Phenion FTM) and cultured keratinocytes by using RT-PCR studies (Zaphiropoulos, 1999; Finta & Zaphiropoulos, 2000). Yengi *et al*., (2003) observed that *CYP2C9* and *CYP2C19* expression of the *CYP2C* family was detected at low levels whilst CYP2C8 was found to be below the limits of detection in full thickness skin biopsy samples (epidermis and dermis layers) taken from 27 individuals. *CYP2C18* was detected at higher levels in the dermal tissue compared with others of the *CYP2C*

subfamily. These results confirmed previous data from a RT-PCR study that found them in 5 individuals of keratinocytes (Saeki *et al*., 2002). In contrast, Gonzalez *et al*., (2001) reported that mRNA of *CYP2C19* was expressed and induced by clofibrate inducer in proliferating human keratinocyte, but no *CYP2C19* was detected in monolayer cultures using RT-PCR.

Several physiological substrates, drugs and xenobiotics are metabolised by *CYP2C* in skin:

- Physiological substrates, for example *all-trans* retinoic acid, arachidonic and linoleic acid were metabolised by *CYP2C9, all-trans* retinoic acid and progesterone were also inducers for *CYP2C18*. In addition, *CYP2C19* was expressed by many treatments such as 9-cis-retinal, arachidonic, testosterone, linoleic acids as well as progesterone (Du *et al*., 2004; Oesch *et al*., 2007).
- Capsaicin, limonene, nicotine, diallyldisulfide, galangin, genistein 4'-methyl ether, kaempferide, ochratoxin A and tamarixetin were metabolised by *CYP2C9* whilst limonene was also an inducer for *CYP2C18*. Furthermore, diallyldisulfide, limonene, genistein 4'-methyl ether, capsaicin, nicotine, ochratoxin A and tetrahydrocannabinol were inducers for the *CYP2C* family especially for the *CYP2C19* enzyme (Du *et al*., 2004; Oesch *et al*., 2007).
- Pharmaceutical drugs such as diclofenac, (S)-warfarin, indomethacin, tolbutamide, ibuprofen and phenytoin, have been used for *CYP2C9* induction and mephenytoin, diazepam, amitryptiline, omeprazole, lansoprazole, pantoprazole and (R)-warfarin) were turned over by *CYP2C19* (Du *et al*., 2004).

CYP2D subfamily: CYP2D6 transcripts of the *CYP2D* subfamily were reported to be expressed in full human skin biopsies in a study of samples taken from 27 individuals. *CYP2D6* mRNA was detected at the highest levels in skin compared to the 10 other *CYP* genes studied with a level 10-fold greater (Yengi *et al*., 2003). Whilst Saeki *et al*., (2002) reported that the *CYP2D6* could be detected in dermal fibroblasts. *CYP2D6* transcripts were undetected in native human skin (microsomes) and in both 3D skin models PFT and EpiDerm™ 3D models in this study. Wiegand *et al*., (2014) showed that levels of *CYP2D6* mRNA were below the detection limit in both layers (dermis and epidermis) of normal human skin, the dermis of the Phenion FT skin model and in monolayer fibroblasts derived from the same donors. In contrast, low expression of *CYP2D6* was found in an

OS-REp model of three different donors, two of three donors in keratinocytes, only 1 donor of 3 donors in the Phenion FT skin model and in the NHEK derived from 2 donors.

- Pharmaceuticals, such as bufuralol, fluoxetin, propranolol, debrisoquine and dextromethorphan were specific for *CYP2D6*.
- Xenobiotic compounds such as 4-methyl ether, aflatoxin *CYP1B1*, capsaicin, curcumin, emetine, genisteine ibogaine, ochratoxin A, nicotine, as well as sparteine.

CYP2E subfamily (2E1 transcripts) is one of the *CYP2* families that has been found in the supra-basal cell layers of human foreskin epidermis skin biopsies as well as in langerhans cells, in freshly isolated epidermal cells and proliferation keratinocyte cultures (Baron *et al*., 2001; Gonzalez *et al*., 2001; Saeki *et al*., 2002). In the study of *CYP2E1*, mRNA was found in native human (both epidermis layer and dermis layer), in fibroblasts, and the monolayer epidermal cells (NHEK) (Wiegand *et al*., 2014). Moreover, it was found to be expressed in reconstructed skin models, such as the Phenion FT and Skin^{TM} FTM as well as in the OS-REp model (Wiegand *et al*., 2014; Du *et al*., 2004; Luu-The *et al*., 2009).

- Substrates such as 17 ß-estradiol, *all-trans* retinoic acid, estrone, phosphatidylcholine, uroporphyrinogen, aflatoxin B1 were metabolised via *CYP2E1* enzyme. In addition to that capsaicin, curcumin, genisteine, diallyl disulfide, nicotine, and methyl eugenol are also other substrates that were metabolized by *CYP2E1* in the human skin.
- Many substrates for *CYP2E1* in both skin (human skin and 3D skin models) include ethanol, benzene and dimethylnitrosamine (Du *et al*., 2004).

CYP2J, CYP2R, CYP2U1 and CYP2W subfamilies

Du *et al*., (2004) reported that other members of the *CYP2* family (*CYP2J*, *CYP2R*, *CYP2U1* and *CYP2W*) are expressed in human skin cultured keratinocytes and in the epidermis. CYP2J2 mRNA of the *CYP2J* family was observable in cultured human epidermal keratinocytes. In contrast, *CYP2R1* mRNA was found in this study. This gene has 25-hydroxylase activity toward vitamin D in the human epidermis (Bikle & Pillai, 1993; Cheng *et al*., 2003). *CYP2U1* is active toward arachidonic acid 19- and 20-hydroxyeicosatetraenoic acids and *CYP2W1* is active toward benzphetamine and indole. In studies of reconstructed models of the epidermis, these *CYP2* enzymes were expressed in EpiDerm, while only *CYP2U1* and *CYP2W1* were detected in ORS-RHE. However,

CYP2J2 has been detected in a full thickness skin model (Phenion FTM). Keratinocytes cultured such as primary were a good representative model for these *CYP* expression (Hu *et al*., 2010).

CYP2S subfamily: The CYP2S subfamily like many *CYP2* subfamily has been studied in the human skin. CYP2S1 transcripts were observed in the skin model (full-thickness skin punch biopsies comprising epidermis and dermis) from 26 psoriasis patients after systematic induction with ultraviolet or topical drug. However, in this experiment discrimination among the dermal or epidermal compartments of skin was not attempted (Smith *et al*., 2006). *CY2S1* was detected in the differentiated cells of epidermal skin by using immunocytochemistry with specific antibodies (Smith *et al*., 2006). Saarikoski *et al*., (2005) reported CYP2S1 is able to metabolise many endogenous substrates. Ultraviolet radiation, PUVA, *all trans* retinoic acid and coal tar detergents induce *CYP2S1* expression and this has been shown to have a greater impact on levels in lesional psoriatic skin compared to non-lesional skin. However, it was observed that *CYP2S1* was not induced by coal tar in the seven of 13 individuals studied (Smith *et al*., 2006). *CYP2S1* expression was reported to be similar in HaCaT cells compared to human skin. HaCaT exposure to acetretin increased abundance of both CYP2S1 and CYP1B1 (McNeilly *et al*., 2012). Most studies of the *CYP2S* subfamily conducted to date have investigated *CYP2S1* induction by retinoic acid, UV light and coal tar. Wiegand *et al*., (2014) studied *CYP2S1* in native skin, NHEK, and in skin model Phenion FT Skin (in the epidermis, dermis as well as in fibroblasts).

CYP2S1 has also been reported to be inducible by dioxin, which implies mediation via aryl hydrocarbon nuclear translocator (ARNT) and aryl hydrocarbon receptor (AHR) (Saarikoski *et al*., 2005). In summary for *CYP2* genes (*CYP2A6*, *2A7*, *2B6*, *2C9*, *2C18*, *2C19*, *2D6*, *2E1*, *2J2*, *2R1*, *2S1*, *2U1*, and *2W1*) have been shown to be involved in drug biotransformation in the normal skin and 3D skin models (mostly in epidermis or cultured keratinocytes).

1.7.2.3 CYP3 family (*CYP3A4* and *CYP3A5*)

***CYP3A subfamily*:** The *CYP3A* subfamily has been proposed as responsible in native human skin for the metabolism of many drugs and substrates particularly *CYP3A4* and *CYP3A5* (Götz *et al*., 2012). A variety of researchers have reported that *CYP3A5* appears to be the most important enzyme of the *CYP3* family at the basal level when no inducers

are present (Kazem *et al*., 2019). Rolsted *et al*., (2008) showed that *CYP3A* activity is similar (*i.e.* low basal *CYP3A* activity) in both EPI-200 models and human skin but lacking in NHEKs which is in agreement with (Götz *et al*., 2012).

Gibbs *et al*., (2007) showed that the *CYP3A* subfamily are responsible for the metabolism of testosterone to 6-β-hydroxytestosterone in fresh full-thickness human skin (*ex vivo* abdominal human skin). They also reported that *CYP3A4* metabolised midazolam and dexamethasone following induction in HaCaT cells. Yengi *et al*., (2003) also studied *CYP3A4* and *CYP3A5* expression in full thickness skin. This was found to express both, with CYP3A4 being more abundant than *CYP3A5*. In contrast, *CYP3A5* was observed in the proliferating human skin keratinocytes cultured by reverse PCR, while *CYP3A4* mRNA could be induced markedly by dexamethasone (Baron *et al*., 2001). However, *CYP3A4* levels were not affected by rifampicin and dexamethasone (Wiegand *et al*., 2014). In this study, *CYP3A4* mRNA was expressed in different human skin samples, but it was difficult to distinguish from *CYP3A5*. Both *CYP3A5* were very variable between donors (present in some donor but absent in others). Wiegand *et al*., (2014) also observed that *CYP3A4* was prominently expressed in the epidermis, while it was below the detection limit in NHEKs.

Examples of *CYP3A4* and *CYP3A5* substrates include acetaminophen, benzphetamine, Aflatoxin B1, nifedipine and midazolam, dexamethasone, ethinylestradiol, levonorgestrel and steroid hormones including cortisol, testosterone, dehydroepiandrosterone and17ß-estradiol (Oesch *et al*., 2007).

1.7.2.4 Other cytochrome P450 enzyme expression including the CYP4 family

Many other cytochrome P450 enzymes such as *CYP4B1*, *CYP27B*, and *CYP26B1*genes have been observed in whole human skin. Studies have shown CYP4B1 to be present in human skin samples (Baron *et al*., 2008), confirming early work by Saeki *et al*., (2002) in epidermal keratinocyte cultures and supported by Luu-The *et al*., (2009) who studied the reconstructed human skin model EpiSkin™. *CYP4B1* was found in Episkin™ and the human epidermis while *CYP26B1* is found in lower abundance in Episkin™ compared with human epidermis. However in Epiderm™, levels of this enzyme are similar to that found in the human epidermis (Luu-The *et al*., 2009). Also, *CYP27B1* was detected in the Epiderm™ and epidermis only skin models Episkin™.

1.7.3 Non-Cytochrome P450 Phase I enzymes

1.7.3.1 Flavin containing monooxygenases (*FMOs*)

Flavin containing monooxygenases (*FMOs*) play an important role in the detoxification of a wide number of xenobiotics. *FMO1/5* mRNAs vary in their expression in human skin similarly to *CYP* mRNA. FMO include *FMO1, FMO2*, *FMO3, FMO4* and *FMO5* and their genes are expressed in many human tissues. Previous studies have shown that in skin, the *FMO* mRNA is much lower compared to the high expression levels in the kidney and the liver. There is a lack of consensus concerning expression of *FMO* in human skin. However, the immortalised keratinocyte cell line, HaCaT and primary keratinocyte cultures express *FMOs* levels which appear to be close to those detected in human skin. Approximately 90 % *FMO5* mRNA and half contained *FMO 1*, *FMO3* and *FMO4* was observed in epidermis layer, hair follicles and sebaceous gland (Janmohamed *et al*., 2001; Kazem *et al*., 2019).

Janmohamed *et al*., (2001) also reported that skin models, such as in PhenionR FT (PFT) full-thickness, the native skin (epidermis and dermis) and EpiDermFT™ (EFT) full-thickness reconstructed skin models exhibited *FMO1* activity. However, HaCaT, an immortalised human keratinocyte cell line appeared to mirror *FMO3* and *FMO5* mRNAs compared with whole skin. *FMO1* mRNA was intensively expressed in the skin five of nine individuals while mRNAs for *FMO1* were undetected in the HaCaT cells. In contrast, levels of *FMO3, FMO5* were found in this cell line to be similar to levels in human skin, but they were different to those in keratinocyte cultures. In HaCaT cells, *FMO4* mRNA was 3-fold greater than in the human skin samples (Luu-The *et al*., 2009). These studies confirmed in three-dimensional reconstructed human skin models (Jäckh *et al*., 2011). In contrast, *FMO2* and *FMO3* expression has been reported to be higher predominantly in the dermis than the epidermis of normal human while *FMO4* and *FMO5* in skin model were reported to absent and *FMO4* at a low level in in Episkin^{TM} (Luu-The *et al*., 2009).

Hu *et al*., (2010) found that in the three-dimensional human skin model EpiDerm™, *FMO1-5* transcripts did not mirror those expressed in native human skin. (Luu-The *et al*., 2009) found that in Episkin^{TM} and Episkin^{FTM} *FMO1, 3* and *5* were present in different levels. These levels were found to be of low abundance in the Episkin^{TM} while the *FMO2* identified at higher abundance compared with FMO4 level which was low in Episkin^{TM} and EpiskinFTM. In addition, *FMO5* was more highly expressed in the epidermis while

FMO3 expression could not be detected in reconstructed human skin model EpiDerm™ (Luu-The *et al*., 2009).

Induction of *FMO* has been studied. *All trans* retinoic acids, at a concentration of 10 μM, induced *FMO3* in native human skin after 24 h, and this induction was sustained up to 72 h. It also induced *FMO3* at the mRNA level after 24 h in both compartments of the Phenion FT skin model, OS-REp model and fibroblast monolayers. *FMO3* was not expressed or induced, however by *all trans* retinoic acid in NHEK cultures from any of the three skin donors studied. In contrast to native skin and the *in vitro* dermal models. *FMO3* mRNA expression was below the limit of detection in HepG2 cells cultured as spheroids or monolayers (Wiegand *et al*., 2014). In general, there was a lower basal gene expression of ten (out of 13) enzymes in fibroblast and keratinocyte monolayer cultures compared to native human skin. *FMO1* was not found in keratinocyte cultures from all different donors. The dermis and epidermis of native human skin had distinct gene expression profiles. *FMO3*, for example- another Phase I enzyme was detected in the dermal compartments of both native human skin and Phenion FT skin model, as well as in fibroblasts. Conversely, the OSREp models and the keratinocytes from which they were derived lacked *FMO3*. This rather profound difference in *FMO3* distribution is in accordance with the findings by (Luu-The *et al*., 2009). *FMO1* reported as being selectively expressed in the epidermis was detected in the dermis of two of the three native skin donors in this study, as well as in the dermis of the Phenion FT skin model (Hu *et al*., 2010). Notably, *FMO1* was absent from keratinocytes, but re-expressed if the keratinocytes were cultured as the 3D OS-REp model, suggesting this enzyme is strongly affected by the culture conditions (Wickett & Visscher, 2006).

Other studies comparing native human skin and 3D skin models showed that the 3D models were good models of *FMO* mRNA expression (Janmohamed *et al*., 2001; Luu-The *et al*., 2009; Hu *et al*., 2010; Wiegand *et al*., 2014; Bacqueville *et al*., 2017). *FMO5* expression has been found to be high in native skin (epidermis layer) and in OS-REp while it was moderate in native skin (dermis) and in the epidermis of the full thickness skin model Phenion FT Skin. In contrast, *FMO5* was weakly expressed in fibroblasts, in the epidermal NHEK and the dermis of the full skin model Phenion FT Skin (Wiegand *et al.*, 2014). Nevertheless, in the most recent study by Bacqueville *et al*., (2017) the ORS-RHE model was show to express *FMO4* mRNA. *FMO3* mRNA was observed by Western

blot analysis in the native human skin after *all trans*-retinoic acid induction (24 h). *FMO3* was not detected in NHEK cultures of three donors after attempted induction with *all trans* retinoic acid, in the epidermis of the full-thickness skin model Phenion FT skin, in the epidermis of the native skin or in epidermal three-dimensional skin model OSREp. *FMO1* was identified in the dermis of the Phenion FT skin model and the dermis of native human skin (Wiegand *et al*., 2014).

1.7.3.2 Carboxylesterase (CE1, CE2 and CE3)

These enzymes have been reported to be highly active in normal human skin (Pillai *et al*., 2004). Carboxylesterase enzymes are also one of the main Phase I enzyme responsible for detoxification reactions in skin for of a number of xenobiotics (Prusakiewicz *et al*., 2006; Oesch *et al*., 2007). A few studies have reported that *CE1* and *CE2* are lower in human skin compared to rat tissue (Prusakiewicz *et al*., 2006), but these enzymes have been found to be expressed in human keratinocyte cultures. Interestingly, the *CE1/2* (*CE1* most significantly than *CE2*) is expressed in the liver tissue (Casey Laizure *et al*., 2013). However, Zhu *et al*., (2007) reported that only *CE2* mRNA was expressed in the human keratinocyte cell line (HaCaT). Furthermore, these enzymes also have greater activity in human epidermis-derived keratinocyte monolayers and human dermis-derived fibroblast monolayers (Gysler *et al*., 1997; Sugibayashi *et al*., 2004). In contrast, *CEs* activity in the human keratinocyte cell line NCTC 2544 was observed to be higher in comparison to a skin homogenate (Lamb *et al*., 1994).

In the most recent study of carboxylesterase in skin (Bacqueville *et al*., 2017), using the ORS-RHE model, *CES1/2* gene expression had a key role in the hydrolysis of many drugs. *CES1/2* activity was observed in ORS-RHE models and native human skin but CES3 is lacking in ORS-RHE models. In summary, the authors found out that both reconstructed human full-thickness skin and reconstructed human epidermis exhibited esterase activity.

1.7.3.3 Alcohol Dehydrogenase (ADH)

ADH mRNA has also been detected in full-thickness human bottom skin FTHBS and the reconstructed human skin model EpiDerm™ (Hu *et al*., 2010). *ADH1B1* was only expressed in FTHBS tissue even though it was not found in EpiDerm™ tissue. This indicates some difference in the human skin expression of *ADH* genes.

1.7.4 Phase II enzymes (Conjugating enzymes)

1.7.4.1 Glutathione-S-transferase (GST)

The GST family are distributed widely in human skin. *GST* activity was first reported to be present in human neonatal foreskin keratinocytes and whole human skin without describing if it was in epidermal or dermal layers. *GST* protein (*GST* alpha, *GST Mu* and *GSTP1*) were expressed at high level in human skin cytosol and normal human skin (in sebaceous glands and epidermis) (Pendlington *et al*., 1994). The *GSTP1* had the highest levels of glutathione-dependent enzymes which could be induced by UV irradiation in native human skin. The induction was increased about 3.7-fold in sample of psoriatic plaques (Smith *et al*., 2006). The enzyme was constitutively expressed showing activity towards 1-chloro-2, 4-dinitrobenzene in normal skin and in the keratinocytes cell line NCTC2544. It showed similar abundance in reconstructed epidermal models and cultured keratinocytes when induced by 3 MC and βNF (Gelardi *et al*., 2001; Harris *et al*., 2002). However, only *GSTP1* expression was induced (at a level 4-fold higher in cultured human keratinocytes than in primary cultured keratinocytes) whilst *GSTM5* was expressed in cultured keratinocytes, and EpiDerm™, but it was found at low level in EpiSkin, SkinEthic and fresh epidermis (Hirel *et al*., 1996; Harris *et al*., 2002). Götz *et al*., (2012) found GSTs as protein in the all monolayer cells that has been investigated in NHEK, HaCaT and NCTC2544.

Luu-The *et al*., (2009) reported that *GSTP1* could be detected at much higher levels in skin than other Phase I metabolism enzymes. This suggests that glutathione conjugation is a key elimination process for exogenous and endogenous hydrophobic electrophiles in human skin and skin models. Both *GSTT1* and *GSTM5* transcripts were also seen at higher levels in the dermis (*GSTM5* expressed in dermis) but not in the FTM and EpiSkin™ skin model. In contrast, *GST* expression was shown to be relatively greater in normal skin and the EpiDerm™ model. This *GST* activity was observed by 1-chloro- 2, 4-nitrobenzene.

Hu *et al*., (2010) investigated mRNA of *GSTA1*, *A4*, *M1*, *M2*, *M3*, *M4*, *M5*, *P1*, *Z1*) and found them to be selectively expressed in the all EpiDerm™ skin samples and in the FTHBS skin but *GSTM5* mRNA, only appeared in 2 of 4 EpiDerm™ samples. Moreover, glutathione S-transferase mRNA was significantly increased (3 to 10-fold) in primary skin fibroblasts in response to sulphoraphane treatment (Warwick *et al*., 2012). On the other hand, *GST* activity was also studied by Wiegand *et al*., (2014) in *in vitro* skin models

and compared to human skin as well as HepG2 cells. *GST* activity toward CDNB were detected overall in the human skin biopsies, the epidermis and the dermis. In the dermis and the epidermis of Phenion FT model, *GST* activity was similar to native skin but in the NHEKs, it was greater than in fibroblast monolayers. The OS-REp model possessed the highest *GST* activity. Fibroblasts exhibited the lowest expression *GST* activity (Wiegand *et al.,* 2014).

1.7.4.2 N acetyltransferase (NAT)

NAT (*NAT1* and *NAT2*) have been detected in human skin and in reconstructed human epidermis models. They have been proposed to be a significant contributor to the direct detoxification in skin of aromatic amines (Nohynek *et al*., 2005). The major enzymes that catalyse acetylation of arylamines are the N-acetyltransferases (*NAT1/2*). *NAT2* is mainly expressed in the human liver cells (Grant *et al*., 1997), while *NAT1* was also found in the epidermis layer and many other tissues (Hein *et al*., 1993). In addition, dermal fibroblasts and cultures of human keratinocytes were showed to be good tissues for *NAT1* mRNA expression. However, *NAT2* was not seen to be expressed in cultured human keratinocytes. In contrast, *NAT1* was clearly observed in both neonatal and adult human epidermal keratinocytes (Reilly *et al*., 2000).

In studies of commercial skin models, mRNA expression of *NAT1* was identified at very low levels in FTM and EpiSkin™. *NAT2* expression in FTM and EpiSkin™ models weremeasured but not compared to total normal human skin tissue, skin epidermis or skin dermis by (Luu-The *et al*., 2009). Hu *et al*., (2010) reported that only *NAT1* was observed at high level in the four reconstructed model and in full-thickness human skin, however the level of *NAT2* appeared very low in the full-thickness human and reconstructed model. Therefore, there does appear to be a consensus (Bronaugh *et al*., 1982). Many drugs such as para-toluidine, benzocaine, and para-aminobenzoic acid are known to be acetylated in human skin (Bronaugh *et al*., 1982). *NAT* activity has been demonstrated by Götz *et al*., (2012) in *in vitro* skin models and human skin using para-toluidine as substrate.

Moreover, N-acetyltransferase activity could be induced by p-aminophenol and 4-amino-2-hydroxytoluene in HaCaTcells (Goebel *et al*., 2009). Only *NAT1* activity was induced in human skin and primary keratinocytes (NHEK) by exposure to para-aminobenzoic acid and para-phenylenediamine as substrate (Hein *et al*., 1993). More recently, Eilstein *et al*.,

(2015) also reported para-aminobenzoic acid as substrate was metabolised by *NAT1* activity in tissues SkinEthik™ RHE, Episkin™ FTM, Episkin™, and human skin.

1.8 Western blot (WB)

Western blotting has become an important technique in cell and molecular biology, which has been used not only to identify the presence or absence of proteins, to quantify and determine the size of the proteins based on molecular weight by gelelectrophoresis. The use of WS was first reported by Towbin in 1979 to measure the size of specific protein isolated from cells or tissues. Later in 1981, Burnette used sodium dodecyl sulphate polyacrylamide gels (SDS-PAGE), which is basically separated or denatured proteins by using polyacryl-amide gels and then transferred onto nitrocellulose membrane yielding a band for each protein (Burnette, 1981; Gürtler *et al*., 2013; Kurien & Scofield, 2006; Mahmood & Yang, 2012). The membrane result then incubated with specific antibodies.

The basis principles of western blotting (See Figure 1.9) can be stated in five steps:

1. Diffusion of target proteins based on their sizes by applying polyacrylamide gel electrophoresis (SDS-PAGE).
2. Transfer of the protein of interest from the SDS-gel to the nitrocellulose or polyvinylidene difluoride PVDF membranes.
3. Use of a particular primary antibody to bind the membrane-bound protein of interest.
4. Use of the specific enzyme conjugate secondary antibody, such as horseradish peroxidase (HRP) to bind the protein primary antibody complex.
5. Imaging of protein bands by LI-COR-western blot detection (Jensen, 2012).

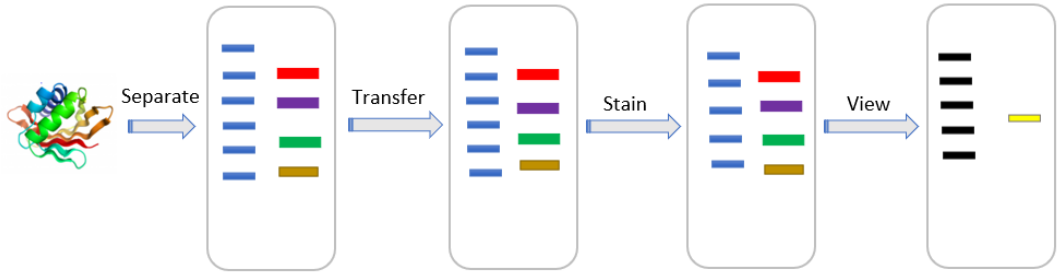

Figure 1.9: Summary of the western blot process. Beginning with proteins mixture, then separated in a gel, transferred to nitrocellulose membrane, after that it is stained with primary ans secondary antibodies, and visualized using by LI-COR-western blot detection.

The band density of the protein of interest is proportional to protein concentration (Mahmood & Yang, 2012). WB also has the capacity to detect the existence of a protein by size or antibody binding, which increases the potential of the WB approach to follow protein fractions during the protein purification (Westermeier & Marouga, 2005). This study allows observing protein expression from cells or the response reaction of certain proteins after treatment by a specific drug.

1.8.1 The application of Western blot in Human Skin and 3D Skin Models (Protein expression)

The use of PCR to identify mRNA species is extremely sensitive however the relationship of low mRNA levels to protein levels is uncertain. The WB technique has been recently developed and introduced to detect the protein expression of the Phase I and II XMEs in 3D skin model, human skin and liver (Wiegand *et al*., 2014; Oesch *et al*., 2018). In the human epidermal keratinocytes, AhR protein has been observed to be at the highest levels in the granular layer while it appears that the lowest amounts are present in the spinous layer and basal layer. This indicates the Ah receptor (AhR) is the most important receptor for the CYP1A family (Wiegand *et al*., 2014). Likewise, CYP2D6 protein expression was also observed in human skin and the Phenion FT skin model, although no protein was induced in either tissue. After 24 h, CYP3A4 protein only was induced at low level in human skin by 2 mM phenobarbital as drug inducer (using Western blotting) (Wiegand *et al*., 2014). This level of CYP3A4 induction has no further increased among 24 and 72 h. Wiegand *et al*., (2014) reported that only FMO3 of non-CYPs in human skin was induced after incubated for 24 h and 72 h by *all trans*-retinoic acid using WS compared with Vehicle controls (ethanol).

In addition, using western blot analysis it appeared that CYP1A1 and CYP1B1 protein could detected in the epidermal layer by non-ultraviolet-B (UVB) induction approximate 3-fold change, even though most CYPs of other drug biotransformation enzymes exist mostly in basal cells. CYP1A1 exhibited a fold change induction in UVB exposed skin compared to non-UVB-exposed skin (Katiyar *et al*., 2000).

On the other hand, van Eijl *et al*., (2012) studied levels of CYP protein expression in 3D skin model and normal human skin compared to liver by using immunoblotting. CYP1A1, CYP2E1 and CYP3A4 could not be detected in skin under immunoblotting while they readily showed their presence in human liver. CYP1A1 could not be observed in either

skin or liver. The limit of detection of these proteins is 2.5 pmol/mg microsomal protein by immunoblotting. Additional attempts were made to detect CYP2B6, CYP2C8, CYP2C9, CYP2C19, CYP2D6 and CYP3A5 expression in skin model using western blotting, but no specific immunoreactive bands were detected (van Eijl *et al*., 2012). CYP proteins expression in 3D skin model was studied further by estimating the limit of detection of CYP proteins. Overall, Phase I and Phase II XMEs protein expression was detected in liver but not detected in whole skin (van Eijl *et al*., 2012).

Baron *et al*., (2001) studied levels of CYP1A1, CYP1B1, CYP2B6, CYP2E1, CYP3A4 and CYP3A5 proteins in microsomal of proliferating human skin keratinocytes. In this study, proteins was induced with benzanthracene and dexamethasone. The obtained data demonstrated CYP3A4 and CYP3A5 induction by dexamethasone.

1.9 Mass spectrometry (MS)

Mass spectrometry (MS) is a powerful analytical technique for both quantitative and qualitative applications. MS analysis can be applied to provide important information about the analytes, including their composition, purity, and structure of different molecules separates according to their specific mass-to-charge ratio (*m/z*) of one or more molecules and relative abundances within sample (De Hoffmann & Stroobant, 2007).

A schematic of a mass spectrometer as shown in Figure 1.10:

- Ionisation source:

  The molecule in the sample is ionised.
- Mass analyser:

  Sperate these ions according to their *m/z* ratio by mass analyser.
- Detector:

  To detect the ions and measure their abundance that that converts the ions into electrical signals.

  Data output mass spectrometry (*m/z* Vs Intensity): Including computer and software that are processing the data of MS (De Hoffmann & Stroobant, 2007).

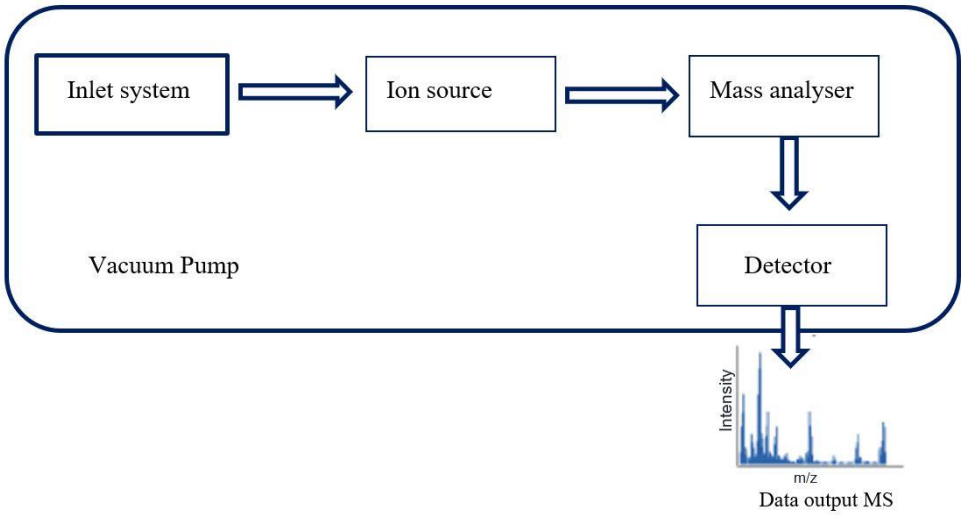

Figure 1.10: Basic diagram of the main parts of an ESI-mass spectrometry.

A variety of ionisation source are used for mass spectrometry. Some ionisation techniques are very energetic and cause fragmentation. Others are softer and produce ions only the molecular species. In this study, electrospray ionisation (ESI) and matrix assisted laser desorption ionisation (MALDI) are used as "soft" ionisation techniques to study the peptides and proteins.

1.9.1 Electrospray Ionisation (ESI)

The ESI source is used widely in the analysis of peptides and proteins (proteomics) through mass spectrometry. The advantages of ESI are that it is requires very little sample preparation and is able to generate multiply charged ions. Multiply charge ions allow the identification of large molecules. The first ESI source was designed in 1960 Professor Dole, a physical chemist at North Western University, focused on the polymerization chemistry (Gieniec *et al*., 1984). The Fenn group combined ESI with MS in the mid 1980 (Fenn *et al*., 1989). The main theory of ESI is as seen in Figure 1.11.

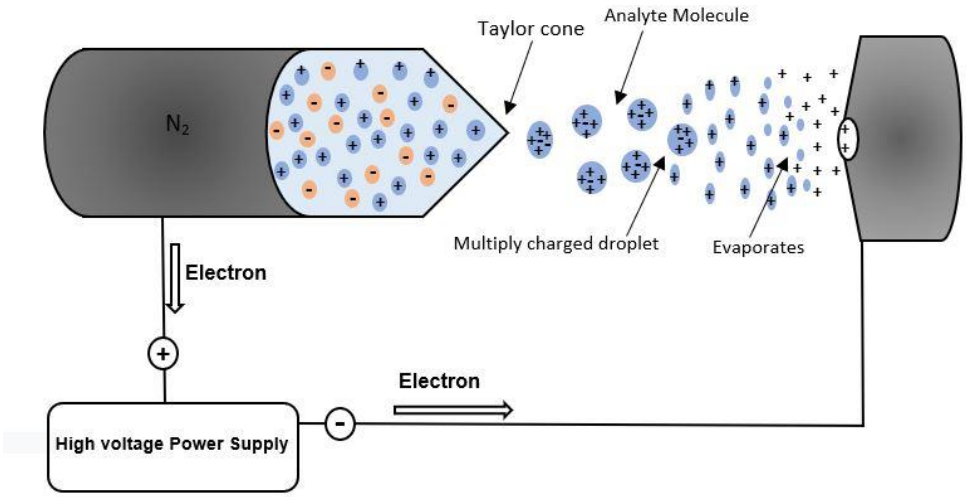

Figure 1.11: Diagram of ESI ion source. The Taylor cone emits liquid drops under high voltage. Liquid evaporates from the charged droplets and leaving them more charged. After the charge exceeds the Rayleigh limit the droplet explosively dissociates, leaving a stream of charged positive ions. Adapted from: Ho *et al*., (2003).

The analyte solution is pumped through a hypodermic needle (~0.2 mm o.d and ~0.1 mm i.d) at low flow rate e.g 20 µL/min) via HPLC, direct injection. A very high voltage between (2–6 kV) is applied to the tip of the metal capillary and it is located 1–3 cm relative to the surrounding source-sampling cone. The strong electric field generated causes dispersion of the sample (droplets) to an aerosol of highly charged electrospray (ES) droplets (See Figure 1.11) (El-Aneed *et al*., 2009; De Hoffmann & Stroobant, 2007). In the chamber, the droplet size reduces due to the evaporation of the solvent under a stream of drying gas/heat. Droplets become unstable upon reaching the Rayleigh instability limit. Then, the droplets goes through coulomb explosion, where the original droplet explodes forming more small and stable droplets. At this point, the formation of gaseous phase analyte ions occurs (Figure 1.11). The main explanations of gas-phase ion formation are the ion evaporation model (IEM), charge residue model (CRM) and the chain ejection model (CEM). These are the three-principal mechanisms for the formation of gas-phase ions. Protein ions are released into the gas phase from "charged droplets" through ESI (Aliyari & Konermann, 2020; Banerjee & Mazumdar, 2012). Several routes have been proposed as presented in Figure 1.12:

- The Ion Evaporation Model (IEM) was proposed via Iribarne and Thomson (1976). When solvent evaporation is repeated, the charged droplets reduce to a given size ions undergoes electrostatically driven desorption from the droplet surface (Konermann *et*

al., 2013) as shown in Fgure 1.12 a. The IEM supported for small precharged species such as Na^+.

- The Charged Residue Model (CRM) mechanism was hypothesized by Dole (Gieniec *et al*., 1984). This model is a result of solvent evaporation where a small charged droplet is formed which includes a single analyte molecule (Banerjee & Mazumdar, 2012). The droplets dissolve and cause charges on the surface to land on the analyte molecules. At the last phase of the solvent evaporation in the ES, the droplets charge is retained by the analyte molecule in the gas phase as illustrated in Figure 1.12 b (Konermann *et al*., 2013).

- The Chain Ejection Model (CEM) was firstly defined by Ahadi and co-worker to occur during analysis of unfolded and disordered proteins (Konermann *et al*., 2013). In this model the protein is unfolding in solution and therefore immediately migrates to the droplet surface due to the exposure of hydrophobic residues. One chain terminus then gets expelled into the gas phase which results in highly charged ions (Konermann *et al*., 2013). Overall, the CRM, CEM, and IEM represent viable pathways for generating gaseous protein ions during ESI in Figure 1.12 c (Konermann *et al.*, 2013; Metwally *et al*., 2018).

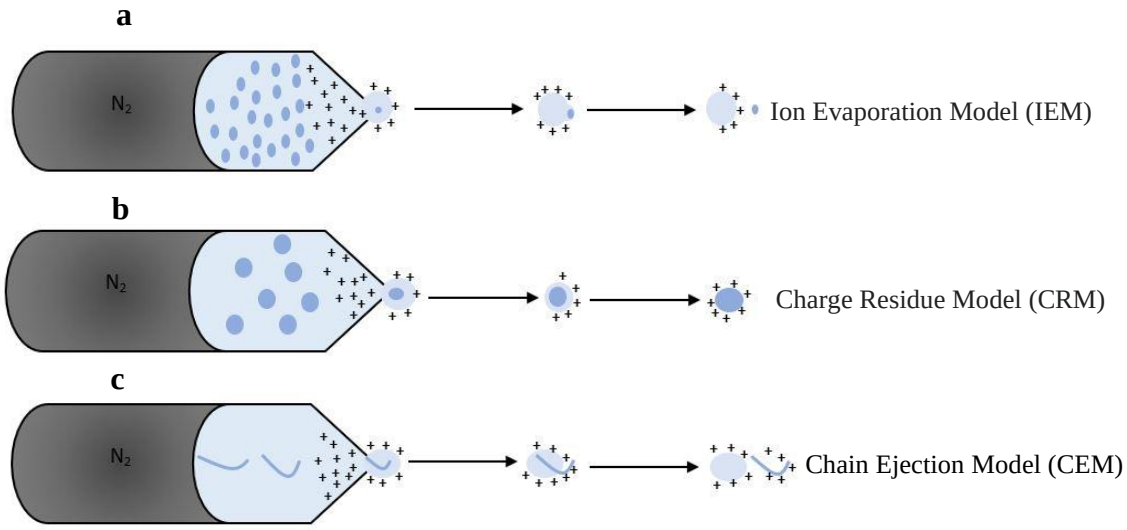

Figure 1.12: Illustration of the three-principal mechanism of ion formation through the ESI process. **(a)** IEM: Small ion ejection from a charged droplet. **(b)** CRM: Release of a globular protein into the gas phase. **(c)** CEM: Ejection of an unfolded protein. Adapted from De Hoffmann & Stroobant, (2007).

1.9.2 The application of LC-MS/MS in skin Proteomics

Proteomics, using mass spectrometry (MS) is a method that has been used to analyse a large-number of proteins include peptides in a single experiment (Alsagaby, 2019). This is in contrast to antibody-based techniques, such as western blotting, enzyme-linked immunosorbent assay (ELISA), and fluorescence microscopy, which are used to detect single proteins.

Several investigators have used LC-MS/MS to study skin proteomics. It can be used to identify differences in the relative abundance of Phase I and Phase II XME (van Eijl *et al*., 2012; Lundberg *et al*., 2015). Different studies of protein expression have been shown the inductibility of CYP1A1 in skin following to the exposure to β-naphthoflavone (βNF), and gluco-corticoid, and 3-methylcholanthrene (3-MC) (Harris *et al*., 2002; Ahmad & Mukhtar, 2004). However, only very few proteomic studies of XME induction have been reported (Hansell *et al*., 2008; van Eijl *et al*., 2012).

In these studies, the use of PCR to identify mRNA species is extremely sensitive however the relationship of low mRNA levels to CYP protein levels is uncertain. van Eijl *et al*., (2012) studied levels of CYP protein expression in 3D skin model and normal human skin compared to liver by using a proteomic approach. CYP1A2, CYP2E1 and CYP3A4 could not be detected in skin by immunoblotting while they readily showed their presence in human liver. Also, CYP1A1 could not be observed in either skin or liver. The limit of detection of these CYP proteins is 2.5 pmol/mg microsomal protein by immunoblotting. Additional attempts were also made to detect CYP2B6, CYP2C8, CYP2C9, CYP2C19, CYP2D6 and CYP3A5 in skin model by western blotting, but no specific immunoreactive bands were identified (van Eijl *et al*., 2012). CYP proteins expression in 3D skin model was studied further by estimating the limit of detection of CYP proteins. LC-MS/MS was more sensitive method about 25-times than immunoblotting. Overall, Phase I and Phase II XMEs protein expression was detected in liver but not detected in whole skin (van Eijl *et al*., 2012).

CYP1A1 has been induced by the AhR ligand 6-formylindolo 3, 2 -b carbazole in HaCaT cells at 10 pmol/min/mg (Jäckh *et al*., 2011). Bonifas *et al*., (2010) observed CYP activity in three different skin models, such as HaCaT cells and normal human keratinocytes (NHEK) by using 7-ethoxyresorufin (EROD) treatment. In keratinocyte cell lines CYP levels are close to the detection limit (0.047 pmol/mg/min), for primary keratinocytes

levels were 0.76 pmol/mg/min but HaCaT showed B[a]P induced EROD activities of 19.0 ± 0.9 pmol/mg/min and 5.8 ± 0.5 pmol/mg/min were found in NHEK. The CYP2D6 gene has been reported to be below the limit of detection in different skin cell types and in proliferating sub-confluent cultures of epidermal keratinocytes (Jäckh *et al*., 2011).

In the most recent study, Couto *et al*., (2021) reported the label-free quantification of XME, transporters, redox enzymes, proteases, and nucleases in human skin and the commercial 3D skin "LabSkin". The aim of this work was to evaluate the appropriateness of Labskin as an alternative to animal testing for topical drugs and cosmetics. In this study more than 2000 proteins were found in Labskin. Alcohol dehydrogenase 1C Phase I XME and glutathione S-transferase P1 were the most abundant of Phase II XME in Labskin compred to human skin. By contrast, no P450 were found in native human skin (Couto *et al*., 2021).

This systematic determination of functional XMEs level among human skin and Labskin is a significant step to the construction of a representative *in vitro* skin model as replacment model for chemical safety and topical treatments (Couto *et al*., 2021).

Even though the exact expression levels of the cytochrome P450s and glutathione S-transferases (GSTs) in skin is not known, the relatively low activity of these enzymes has been studied indirectly using the metbolism of nevirapine (NVP) (Chen *et al*., 2008; Dekker *et al*., 2016). NVP is metabolized by P450s to produce hydroxy-metabolites at positions 2, 3, 8, and 12. 12-sulfoxyl-NVP is further metabolised by GSHs to form NVP-12-GSH. This was the first instance in which a substrate was used to determine the metabolic pathway in rat skin (Chen *et al*., 2008). Jewell *et al*., (2007) demonstrated that parabens are selective substrates for human carboxylesterase in skin. The data they obtained shows that parabens penetrate the stratum corneum of the human and minipig skin, where they are metabolised to 4-hydroxybenzoic acid by carboxylesterases of Phase I enzyme. Jäckh *et al*., (2011) has been investigated activities of biotransforming enzymes of CYPs, FMO1, NAT1 and UDP-GT1 using benzydamine and p-aminobenzoic acid testing in the EpiDerm™ and PhenionFT (PFT). While CYPs were expressed as expression profiling, no CYP activity was identified in either skin model even though expression and their activity of FMO1, UDP-GT1and NAT1 were validated in both. Russo *et al*., (2018) identified and validated the presence of esterases of full thickness 3D skin model (Labskin) with methylparaben and confirmed this by LC-MS/MS.

No studies have investigated the levels of CYPs and GSTs enzymes in induced 3D skin model (Labskin) and the effect of inducers.

1.10 Matrix assisted laser desorption ionisation (MALDI)

MALDI is one of the most successful "soft" ionization technique in mass spectrometry and enables the analysis of a broad range of molecules, including lipids, proteins and oligonucleatides. MALDI was introduced in 1980's by Karas, Hillenkamp and co-workers (Karas *et al*., 1990). It was applied in 1988 to detect molecules of molecular mass up to 300,000 Daltons (Karas *et al*., 1990). A number of lasers have been used, which operate at varying wavelengths and emit differing levels of energy (De Hoffmann & Stroobant, 2007). Initially, MALDI MS was used for the analysis of liquids spotted on target plate and air-dried. The principle (See Figure 1.13) is proceeds in two steps: Step 1: Ions are desorbed from the solid phase. A sample (include the compound to be analysed) is dissolved in an appropriate solvent and mixed with matrix (small UV absorbing organic molecules such as alpha-cyanohydroxy cinnamic acid (CHCA). The components of the mixture are carried into the gas phase as matrix ions formed by a laser are desorbed (Pomerantz *et al*., 2008). When the laser beam hits an analyte-matrix crystal, this leads to absorption of the laser energy by the matrix and subsequent desorption and ionization of the analytes in the sample (Pomerantz *et al*., 2008). The second step occurs in vacuum conditions within the source of MALDI where the charge transfer from the matrix ions to the molecules occur which are mostly performed by the gas phase cation (H^+, Na^+, K^+) (Beine *et al*., 2016). Nevertheless, ions are produced in MALDI is not fully understood (Pomerantz *et al*., 2008; Fremout, 2014; Beine *et al*., 2016; Allen & McWhinney, 2019).

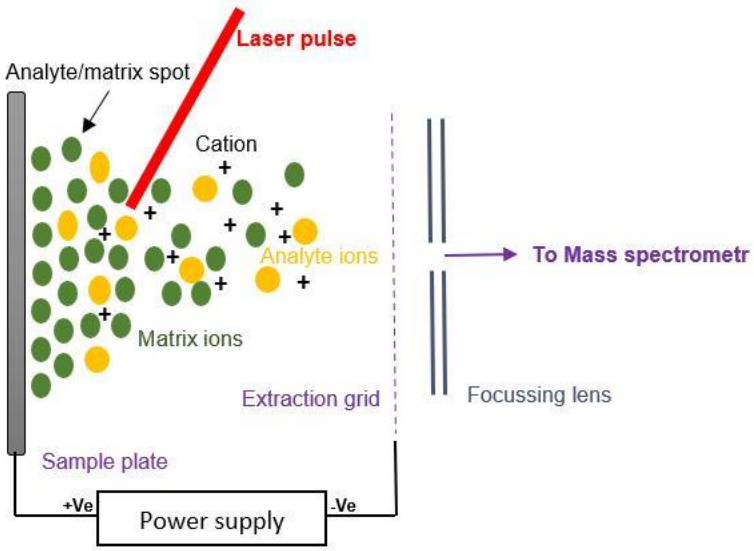

Figure 1.13: Schematic of MALDI-MSI imaging, from tissue sectioning to matrix. Amended from: Fremout (2014).

1.10.1 MALDI mass spectrometry imaging (MALDI-MSI)

MALDI mass spectrometry imaging (MALDI-MSI) is powerful bioanalytical technique for identifying and quantifying molecules with high sensitivity and high mass accuracy in tissue samples MALDI-MSI imaging was first described in study of biological tissue by Spengler and co-worker, 1994 (Spengler *et al*., 1994).

In the last few years, significant progress has been established by MALDI MSI to study skin absorption in pharmaceutical analysis by Clench and co-worker (Bunch *et al*., 2004). In this work, the authors described the development of the MALDI-MSI technique to localise ketoconazole in both skin model and native human skin (Anderson *et al*., 2010; Francese & Clench, 2010; Solon *et al*., 2010; Ryan *et al*., 2019). In a typical MALDI-MSI experiment, the essential steps for sample preparation are required including, section and matrix application (Shimma & Sugiura, 2014). Several matrix applications techniques has been used such as manual spotting, automated sprayers and sublimation In this thesis, sublimation application was used exclusively and is the technique that will be described in more detail.

1.10.2 Matrix application "Sublimation Process "

Sublimation was developed as method of matrix application for the detection of lipids across brain tissue sections by Hankin and co-workers (Hankin *et al*., 2007). Sublimation is direct solid to gas-phase transition: α-cyano-4-hydroxycinnamic acid, 3, 5-dimethoxy-4-hydroxycinnamic acid and 2, 5-dihydroxybenzoic acid are the most commonly organic matrices that have been discovered to undergo sublimation without decomposition under conditions of high temperature and reduced pressure (Hankin *et al*., 2007).

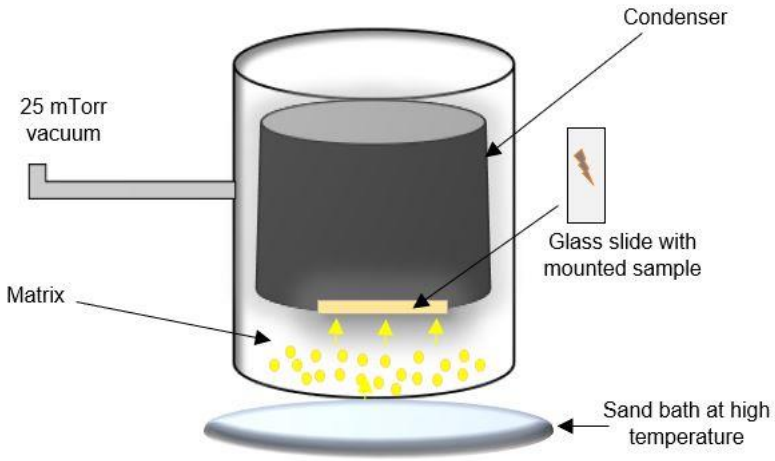

Figure 1.14: Schematic of MALDI matrix typical sublimation process.

Sublimation produces a layer of small crystals onto tissue samples and is a solvent-free matrix application method for MALDI-MSI imaging (See Figure 1.14) (Hansen & Janfelt, 2016). Deposition is readily controllable using time, temperature, and pressure settings and is highly reproducible from one sample to the next.

1.11 Mass analysers

The mass analyser is the part of a mass spectrometer that is responsible for separating ions depending on their mass to charge ratio (*m/z*). Commercially available mass analysers include time of flight (TOF), quadrupole (Q), linear ion trap (LIT), quadrupole ion trap (QIT), fourier transform-ion cyclotron resonance (FT-ICR) and orbitrap that are differentiated by their of mass accuracy, mass resolution, and transmission of ions (De Hoffmann & Stroobant, 2007).

1.11.1 Time of flight (TOF)

The concept of the TOF mass analyser was first presented by William Stephens in 1946. The TOF was by Russian scientist, Boris Mamyrin in 1974, by the incorporation of a reflector to reduce the impact of the kinetic energy distribution of the ions on mass resolution (De Hoffmann & Stroobant, 2007).

In a TOF analyser, a bundle of ions is expelled from the source and introduced in the chamber known as “drift tube” by a high voltage. All ions of the same charge acquire the "same" kinetic energy and hence their velocities are proportional to their mass. The ion leave the source with an acceleration region and enters field free region where they are separated according to their velocities and hence the time that ions take to move through the tube before getting to detector is a function of their *m/z*. The ions with lower *m/z* will reach faster to the detector compared with those that has higher *m/z*. The TOF analyser is illustrated in Figure 1.15 (Medhe, 2018).

Equation:

$$t^2 = \frac{m}{z}\left(\frac{L^2}{2eVs}\right) \qquad (2)$$

The equation shows the m/z calculation: where is:

t is the time required to cover the distance.

L before reaching the detector.

m = mass of ions.

z = number of charges.

e = charge of an electron.

Vs = acceleration potential.

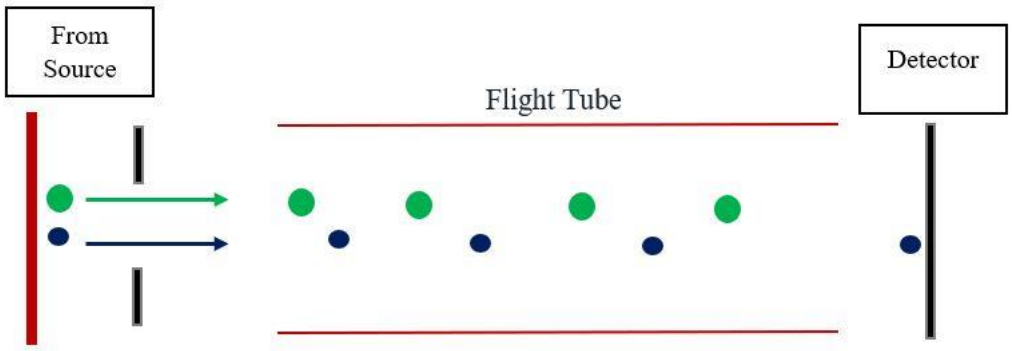

Figure 1.15: Representation of Time of flight (TOF) mass analyser. Amended from: Medhe (2018).

The main advantage of the linear time of flight instruments is that it is suitable for soft ionisation and has a high transmission efficiency and hence high sensitivity (Medhe, 2018). However, the most important limitation of a simple TOF analyser is the poor mass resolution. Mass resolution is affected by time distribution (the distribution in flight times between ions that have same *m/z*), space distribution (the size of the volume where ions is formed) and kinetic energy distribution (the spread kinetic energy of the ions by the laser-based ion sources) (Medhe, 2018).

One attempt to improve the resolution is to use reflection or ion mirror (See Figure 1.16) (Mamyrin *et al*., 1973). A single stage reflector comprise of a series of even spaced grids or ring electrodes. When ions leaving the source and enter the electrical field, they are deflected back along the flight tube.

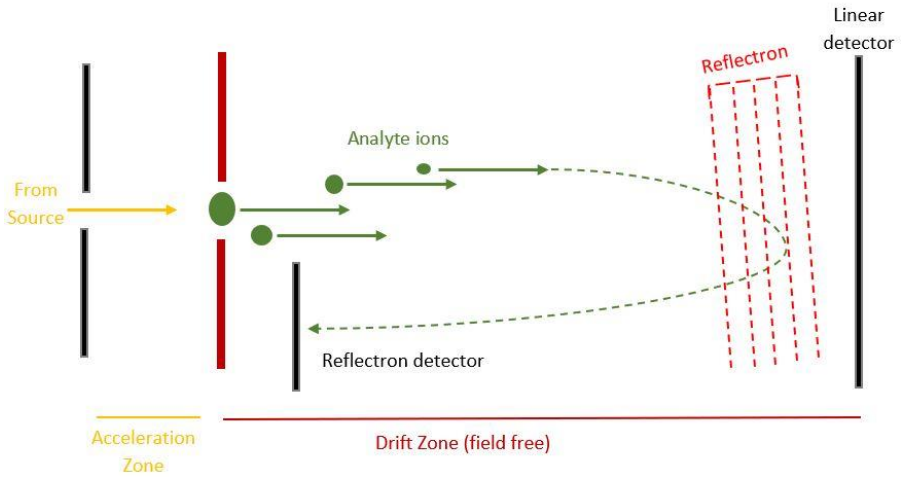

Figure 1.16: Schematic represent of the reflectron mode of time of flight mass spectrometer. Amended from: Fremout (2014).

Therefore, ions with high kinetic energy will penetrate more deeply in the reflection than ions with low kinetic energy. As result, the faster ions will spend more time in the reflection tube and arrive to the detector at the same time as slower ions with same *m/z* ratio (De Hoffmann & Stroobant, 2007).

TOF can be coupled with various an ionisation sources (*i.e.* coupling of an ESI source) because ESI source yield a continuous ion beam the TOF in this system works on pulse process. Figure 1.17 shows a schematic diagram of an orthogonal reflection time of flight analyser. In this process, the TOF analyser is set orthogonally to the axial path of ions that derived from the source. Ions are accelerated in a 'pusher' region into the orthogonal TOF by a pulsed voltage. The insertion of an orthogonal reflectron TOF analyser after a horizontal path of ion confers a V-geometry of the ion trajectory as shown in Figure 1.16 (De Hoffmann & Stroobant, 2007; Greaves & Roboz, 2014).

Further reflectron TOF can be introduced into the analyser as shown in Figure 1.17 giving "W" geometry for the ion trajectory. Introducing the the additional reflectron has some limitations. One of these is the affect on the sensitivity. When increasing the length path of the TOF analyser, it is possible to achieve high resolution, but this can increase the ion loss and reduce sensitivity (Fliegel *et al*., 2006; Greaves & Roboz, 2014; Chernushevich et al., 2017).

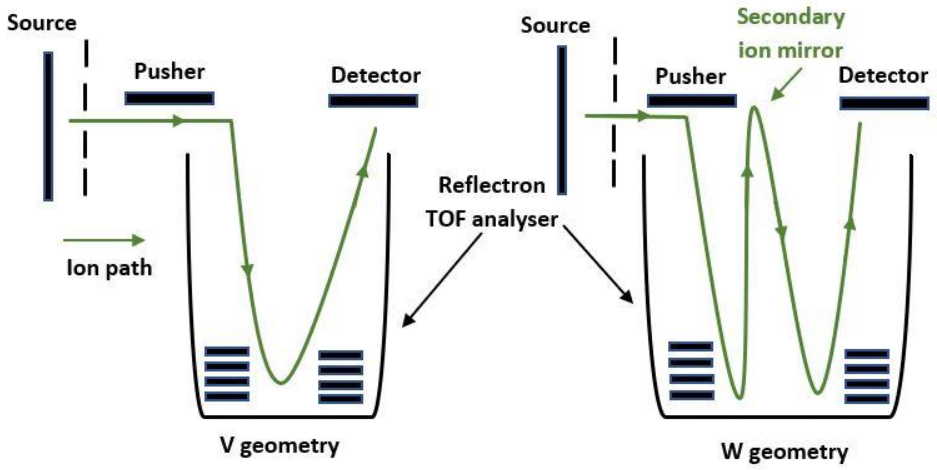

Figure 1.17: Representation of an orthogonal reflectron TOF analyser. A comparison of reflectron TOF analyser (V-geometry and W-geometry).

1.11.2 Quadrupole Mass Filter

The principles of a quadrupole mass filter were described and instruments developed in 1956s. This analyser consists of four electrical rods set parallel to each other as shown in Figure 1.18. A direct current (U) is applied to one pair of rods, and the other two rods are connected to an alternating radio-frequency (Chernushevich *et al*., 2017) potential (the potential is termed V, and the frequency is termed ω). Electric fields are used to separate of the sample ions based on their mass to charge ratio (*m/z*). Ion separation is based on the stability of their trajectories in the oscillating electric field that are applied to the rods. Ions with bounded oscillation (stable trajectory) will travel along the central axis of parallel rods and reach the detector. However, ions with unbounded oscillation (unstable trajectory) will strike the rods (Figure 1.18).

The quadrupole analyser MS system can operate in two modes (Full Scan and Selected Ion Monitoring) (Garcia, 2016). In scan mode, voltages is configured to the quadrupoles that the entire mass range specified is scanned sequentially of ions with different mass to charge ratios. In selected ion monitoring, the quadrupole is performed at a particular voltage to allow only ions with a specific *m/z* to reach the detector. The main advantages of quadrupole analysers are low cost, robustness, relatively small size, and ease of maintenance.

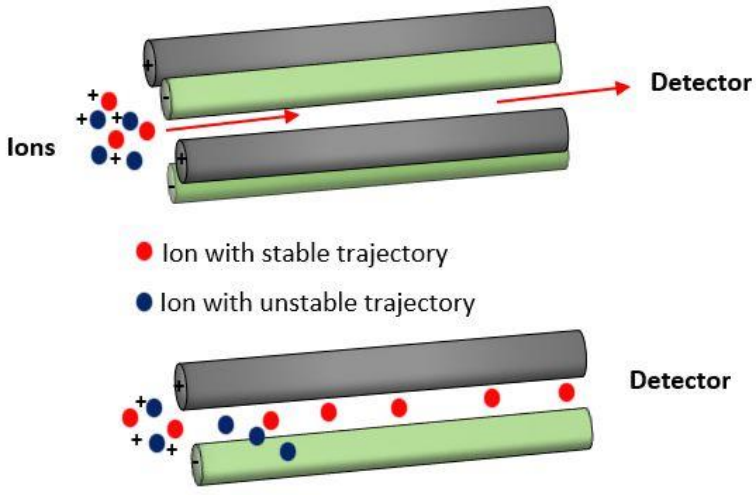

Figure 1.18: Schematic of the applied voltage for quadrupole mass analysing system: (four parallel electrical rods with alternating radio frequency and direct current potentials. Only *m/z* value (red dots) will possess trajectory to reach the detector (red dots). The rest (blue dots) will hit with rods to be removed.

1.11.3 Quadrupole time of flight (Q-TOF) Mass Analysers used in this study

QTOF mass analysers have been combined with various ion sources, including MALDI and ESI. Q-TOF-MS has found widespread use in biological and pharmaceutical research including metabolite identification peptides and drug discovery (De Hoffmann & Stroobant, 2007). Q-TOF-MS is similar to a triple MS, but the third quadrupole is replaced by time-of-flight. In normal acquisition mode, the quadrupole function as a transmission mode, while the TOF mass analyser records spectra (Chernushevich et al., 2017; Allen & McWhinney, 2019).

In Q-TOF for MS/MS acquisition, the first quadrupole is used in "transmission" made to select a specific mass or range of masses for transmission to the collision cell. The second is used as a "collision cell". The TOF analyser is used for the recording of the ions (accurate mass measurement as shown in Figure 1.19. Ions detection is achieved by detector system which converts the flight time of the ion into a mass signal. QTOF has been evaluated for analysis and imaging on skin in Chapters 3.

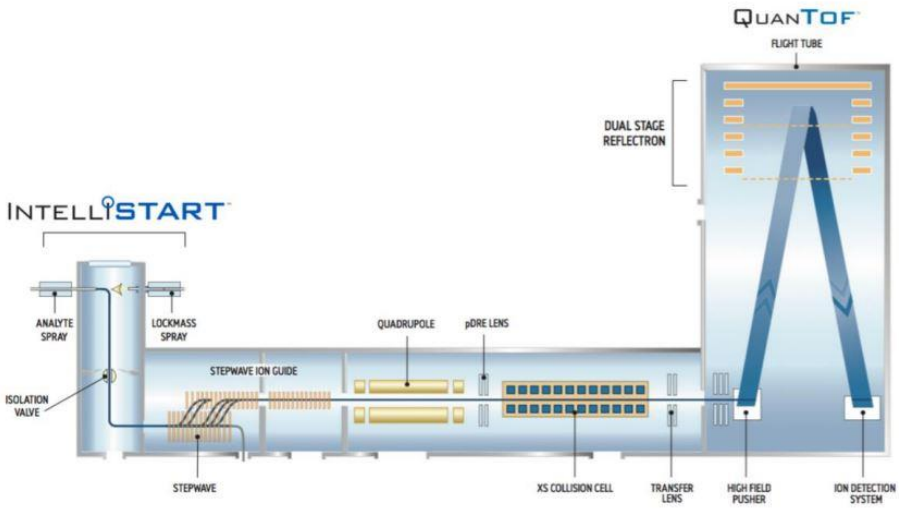

Figure 1.19: Schematic of the the Xevo G2-XS QTof system (Copy from Garcia, 2016).

1.11.4 Multi-analyser systems (Tandem time-of-flight)

Tandem time-of-flight (TOF/TOF) is a tandem MS system introduced 1993 and uses TOF/TOF as the method of choice for characterizing proteins. In this system (Figure 1.20), peptide mixtures are introduced into the MS either as a continuous flow of a liquid solution, such as in ESI, or as MALDI-MSI.

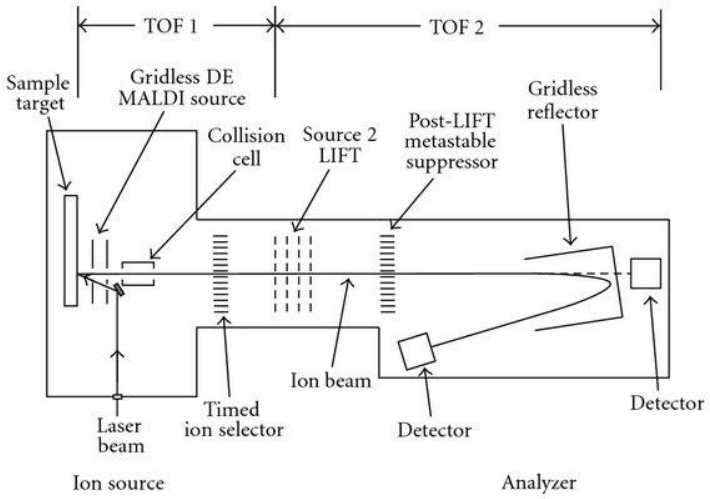

Figure 1.20: A diagram representation of a tandem time of flight mass analyser (Bergquist *et al*., 2012).

The most approach used for MS is combination of a linear TOF "first analyser" with a reflectron TOF "second analyser" (Garcia, 2016). Ions produced in the source at the timed- ion-selector allows ion separated from the first TOF, and go into a collision chamber, where the parent ion will undergo dissociation by induced collision with nitrogen or argon gas (TIS in Figure 1.20) separated from the first TOF to pass through a collision chamber to collide with a collision gas (usually argon) in the collision cell, to activate the precursor ions by collision and undergo further fragmentation as collision-induced dissociation (Ho *et al*., 2003). This tandem system is commonly used in this project.

1.11.5 Quadrupole-Orbitrap mass spectrometery

Orbitrap mass spectrometery is the most recent addition to the high-resolution mass spectrometry analysers. It combines high speed with excellent quantification properties in various analytical applications and mainly contains an nanoESI ion source, a stacked-ring ion guide (S-lens), a quadrupole mass filter, a curved linear trap (C-trap), a higher energy collisional Dissociation cell, and an orbitrap mass analyzer (Perry *et al*., 2008). Samples introduced into the ion source by HPLC methods and transmits ions from the nanoESI source to the quadrupole. The quadrupole works as ion transmission with the possibility to filter the transmitted ion according to *m/z* ratios (Perry *et al*., 2008). Then, ions are moved into the C-Trap and injected into the Orbitrap mass analyzer as shown in Figure 1.21.

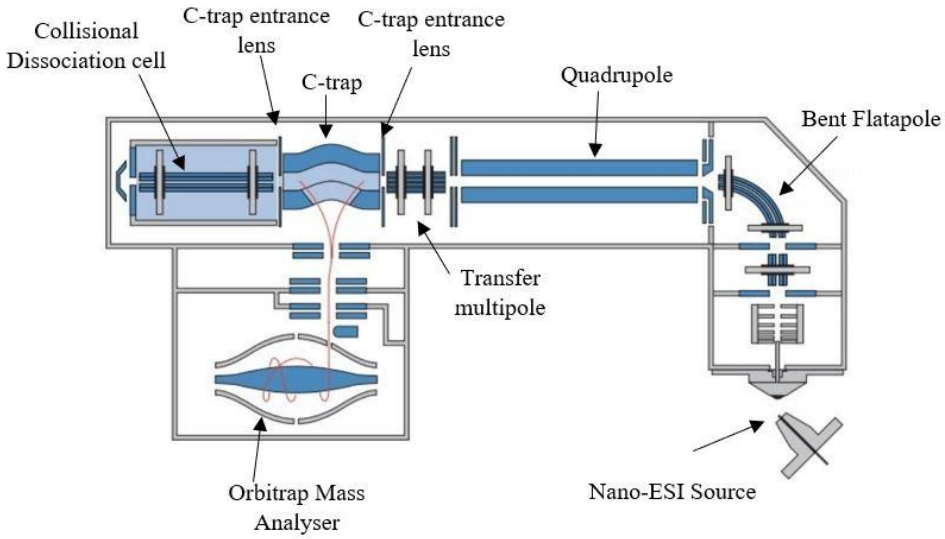

Figure 1.21: A Schematic of Orbitrap as ions circulate through the trap (Perry *et al*., 2008).

The Orbitrap mass analyser comprises essentially of four electrodes as indicated in Figure 1.21. The electrodes have the structure as cups facing each other and electrically isolated via hair thin gap secured by a central ring made of a dielectric. The central electrode holds the trap together. Once voltage is applied among the outer and the central electrodes, the resulting electric field is accurately linear along the axis and hence oscillations along this direction. At the time progresses, the radial electric field strongly attract the ion trajectory to the central electrode. By oscillating ion trajectory in cylindrical electrode with tapered ends, the identifies signals for *m/z* based on Fourier transforms into the frequency (Perry *et al*., 2008).

1.11.6 Desorption electrospray ionization mass spectrometry (DESI-MS)

DESI was introduced in 2004 as a novel method by Cooks' group at Purdue (Takats *et al*., 2004). DESI-MS coupled with mass spectrometry is an ambient ionization that carried out by directing electrosprayed charged droplets and ions of solvent onto the surface to be analysed with no sample preparation (Takats *et al*., 2004). It is directly ionizing analytes in a "flying" liquid jet. The effect of the charged particles on the surface creates gaseous ions of material originally appear on the surface. The droplets/ions are then mass analysed as shown in Figure 1.21.

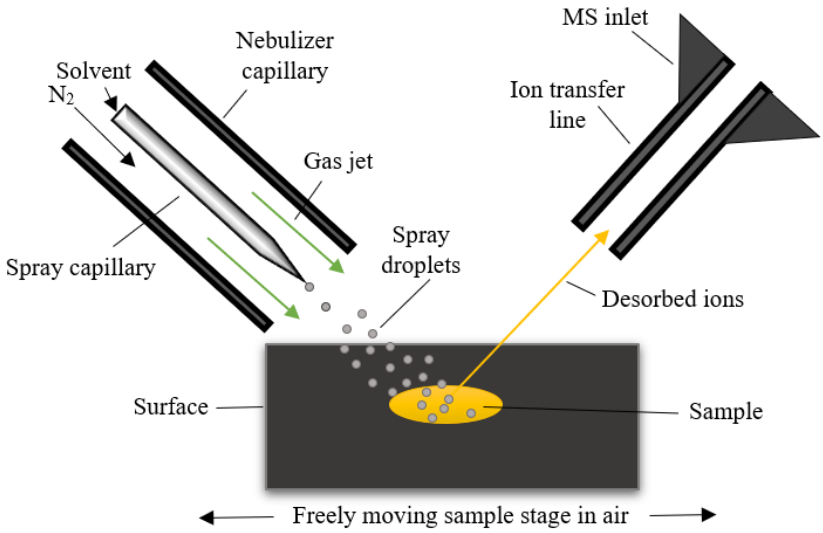

Figure 1.22: An illustrates the idea of a typical DESI-MS system.

The resulting mass spectra is similar to the normal electrospray ionization mass spectra that they show mainly singly or multiply charged molecular ions of the analytes. These ions travel across air into the atmospheric pressure interface which is linked to MS. By scanning the charged-droplet beam through the surface of tissue, molecular images are constructed by mapping the intensity of one or more of the ion signals derived from the tissue surface. In DESI-MS imaging experiment, the charged droplets created by the electrospray are directed at high velocities toward the surface (Wiseman et al., 2008).

DESI is related to other spray ionization techniques, such as electrospray ionization (ESI) and desorption ionization techniques, including laser desorption and secondary ion mass spectrometry (SIMS). No matrix such as α CHCA matrix is needed to carry out the experiment. Figure 1.21 shows the idea of a typical DESI-MS system which comprises of solvent delivery line, nebulizing gas (N_2), high voltage power supply (v), and x, y, z-moving stages with z-axis applied only for initial position. The setup also involves x, y

axis, which enable sample position throughout the analysis and provide the independent control of the sample position as well as the position of the ion source in relation to the mass spectrometry inlet.

Several DESI-MS applications have been reported for drug detection to tissue imaging, the latest DESI-MS such as DESI-MS on Synapt XS or MRT has more efficient ion transfer with the heated transfer line and further enhancing the sensitivity and precision using the high resolution to visualize compounds at previously unobtainable. In addition, it was developed for the improvements in sprayer and reproducibility to allow higher quality data acquisition. The application has been reported in the analysis of biological tissues and fluids (*i.e.* skin, liver, fingerprints, urine, and blood) for detection of drug discovery and development for metabolite identification (Wiseman *et al*., 2008; Wójtowicz & Wietecha-Posłuszny, 2019).

1.11.7 The application of MALDI-MSI Image in skin research

Matrix assisted laser desorption ionization (MALDI) imaging mass spectrometry (MSI) is one of the best commonly used MS methods to study skin. This may be due to the ease of direct analysis of biological molecules, such as chemical elements, metabolites, and drugs from skin sections (eliminates the requirement for stains or antibodies) (de Macedo *et al*., 2017). In brief, sample preparation for MALDI-MSI workflow consists of tissue sectioning by cryosectioning technique and placing sections onto (generally) a conductive slide. Then, CHCA matrix is applied to the section of skin tissue by sublimation method. MALDI-MSI has been applied to address the questions on the identification and localisation of absorption and distribution of drug compounds in the skin tissue (epiderms and dermis) (de Macedo *et al*., 2017; Sørensen *et al*., 2017). The combination of skin models with MALDI-MSI has been extensively used to assist in the prediction of drug response in skin layers. Despite the fact that a wide range of applications have been demonstrated, some data remained inconclusive. Thus, additional studies are required to determine metabolism of drug (Spencer *et al*., 2020). A variety of 3D skin models have been developed for drug analysis. Rheinwald and Green reported the first organoid structure in 1975, when they created a living skin replacement from epidermal keratinocytes that was utilised to treat burn patients (Rheinwatd & Green, 1975).

The earliest work on skin models with MALDI-MSI was an investigation of the distribution of imipramine by Avery *et al*., (2011) who analysed the pentration of imipramine and its metabolizing properties into Straticell-RHE-EP-001. A significant change in imipramine intensities after 2 h and 8 h with greater drug signals in the epidermis at 8 h. This clearly showed the potential capabilities of MALDI-MSI to study the penetration (Avery *et al*., 2011). However, no evidence of the metabolism of imipramine was detected in Straticell-RHE-EP-001, although some small ions are detectable, such as the hydroxyimipramine image in the *m/z* 267.4.

It is clear from the literature that the combination of LSE with MALDI-MSI can provide significant result for drug absorption/penetration, Francese *et al*., (2013), studied the effects of curcumin as a matrix compared with CHCA to acheive the efficient detection of acitretin in the epidermis in LSE. A successful penetration of acitretin after 4 h was observed within the epidermis by MALDI-MSI at *m/z* 326.4 (Francese *et al*., 2013). The following study demonstrated by Harvey *et al*., (2016) MALDI-MSI was examined the absorption of the same drug (acitretin) at longer time trough the epidermis at 24 h then additional permeated into the derms of the skin after 48 h. This meant MALDI-MSI successfully identifying the localisation of drug of skin equivalent model.

Quantitative MSI in combination with LSE model 'Labskin' was developed to study the absorption of terbinafine hydrochloride by Russo *et al*., (2018). The study used an optimised micro-spotting technology to produce exact and consistent analytical and internal standards at nanolitre volumes applied solely to the epidermal layer. MALDI-MSI effectively detected increasing analyte. Furthermore, the study evaluated the effect of the penetration enhancer dimethyl isosorbide (DMI) added to drug formulation on delivery through the LSE (Russo *et al*., 2018). Additionally a study conducted also by Russo, *et al.*, (2018) which combine MSI with 3D skin model has shown that MSI could detect the presence of esterases in the commercial full thickness 3D skin model (Russo *et al*., 2018).

MALDI-MSI has also been used with fresh human skin. *Ex-vivo* human skin was treated with tofacitinib and ruxolitinib (Sørensen *et al*., 2017). These drugs were shown to be present in the epidermis by MALDI-MSI.

1.12 Aims and Objectives

This thesis is concerned with the optimisation and validation of a human *in vitro* 3D living skin equivalent model for metabolism studies of topically applied xenobiotics. The general aims of this study are to measure the levels of Phase I and Phase II XMEs in a commercial 3D living skin equivalent model "labskin" and to determine if it is possible to recover drug response by induced genes and proteins expression and provide a 3D skin model for future drug development.

The specific aims of the thesis are as follows:

- Comparison of levels of Phase I and II XME in the 3D skin model "Labskin" (UK Limited, York) compared with *ex vivo* human skin.
- Induction of the XME activity in the commercial 3D skin model by using β-naphto-flavon (βNF), *all trans* retinoic acid (RA), and phenobarbital (PB)
- Detection and localisation of the induced metabolising enzyme activity in skin layers by using benzydamine (BZD) as substrate based on mass spectrometry.

The objectives of the thesis are:

- Detection of Metabolising Enzymes in Commercial 3D Skin Model and *ex-vivo* human skin by Real time qPCR and Western blotting techniques, nanoLC-MS/MS and LC-MS/MS techniques.

- Investigation of the Induction of Xenobiotic Metabolising Enzymes in a 3D Skin Model compared with native human skin by RT-qPCR, Western blotting, LC-MS/MS and nano-LC-MS/MS.

- Detection and Localisation of Benzydamine Metabolism in Commercial 3D Skin Model using LC-MS/MS and MALDI-MSI and DESI XS-MS.

Table 1.3: Detection of expression of gene, protein, and activity of Phase I XMEs in commercial 3D human skin models, native human skin keratinocytes skin model (cells culture). Adapted from: Kazem *et al*., (2019).

Phase I enzymes	3D epidermis skin models	Commercial human skin models	Keratinocytes skin model (cells culture)	Human skin	References
CYP1A1	**mRNA** (EpiSkin™ , EpiDerm) **Activity** (EpiSkin™ , SkinEthic™ RHE, ORS-RHE)	**mRNA** (Skin™ FTM, Phenion FTM) **Activity** (Skin™ FTM)	**mRNA** (primary Keratinocytes, HaCaT, NHEK) **Protein** (primary Keratinocytes)	**mRNA / activity**	Eilstein *et al*., (2015) Hu *et al*., (2010) Wiegand *et al*., (2014) Luu-The *et al*., 2009) Neis *et a*l., (2010) Jäckh *et al*., (2012) Bacqueville *et al*., (2017) Swanson (2004) Delescluse *et al*., (1997)
CYP1A2	**mRNA** (EpiSkin™ , EpiDerm, ORS-RHE) **Activity** (EpiSkin™ , SkinEthic™**,** EpiDerm)	**mRNA** (Skin™ FTM) **Activity** (Skin™ FTM)	**mRNA** (primary Keratinocytes) **Activity** (primary Keratinocytes, NCTC, HaCaT)	**mRNA / activity**	Hu *et al*., (2010) Luu-The *et al*., (2009) Götz *et al*., (2012) Eilstein *et al*., (2015) Jäckh *et al*., (2011)
CYP2A6	-	**mRNA** (Phenion FTM) **Activity** (SkinTM FTM)	**mRNA** (primary Keratinocytes)	-	Hu *et al*., (2010) Swanson (2004) Janmohamed *et al*., (2001) Eilstein *et al*., 2015) Wiegand *et al*., 2014)
CYP1B1	**mRNA** (EpiSkin™ , EpiDerm, ORS-RHE) **Activity** (EpiSkin™ , SkinEthic™ RHE)	**mRNA** (Skin™ FTM, Phenion FTM) **Activity** (Skin™ FTM)	**mRNA** (primary Keratinocytes, HaCaT)	**mRNA / activity**	Eilstein *et al*., (2015) Hu *et al*., (2010) Götz *et al*., (2012) Swanson (2004) Wiegand *et al*., (2014) Luu-The *et al*., (2009) Neis *et al*., (2010) Bacqueville *et al*., (2017)

Table 1.4: Detection of expression of gene, protein, and activity of Phase I XMEs in commercial 3D human skin models, native human skin keratinocytes skin model (cells culture). Adapted from: Kazem *et al*., (2019).

Phase I enzymes	3D epidermis skin models	Commercial human skin models	Keratinocytes skin model (cells culture)	Human skin	References
CYP2B6	**mRNA** (EpiSkin™**)** **Activity** (EpiSkin™, SkinEthic™ RHE)	**mRNA** (Skin™ FTM) **Activity** (Skin™ FTM)	**mRNA** (primary Keratinocytes, HaCaT) **Protein** (primary Keratinocytes)	**mRNA/ No activity**	Janmohamed *et al*., (2001) Eilstein *et al*., (2015) Baron *et al*., (2008) Götz *et al*., (2012) Swanson (2004) Luu-The *et al*., (2009)
CYP2C8	**mRNA** (EpiSkin™**)**	**mRNA** (Skin™ FTM)	**mRNA** (primary Keratinocytes)	–	Hu *et al*., (2010) Swanson (2004) Luu-The *et al*., (2009)
CYP2C9	**mRNA** (EpiSkin™ , EpiDerm)	**mRNA** (Skin™ FTM)	**mRNA** (primary Keratinocytes)	**mRNA/ No activity**	Luu-The *et al*., (2009) Hu *et al*., (2010) Du *et al*., (2004)
CYP2C18	**mRNA** (EpiSkin™ , EpiDerm, ORS-RHE, SkinEthic™) **Activity** (EpiSkin™ , SkinEthic™ RHE)	**mRNA** (Skin™ FTM, Phenion FTM) **Activity** (Skin™ FTM)	**mRNA** (primary Keratinocytes)	**mRNA** **No activity**	Luu-The *et al*., (2009) Du *et al*., (2004) Neis *et al*., (2010) Bacqueville *et al*., (2017)
CYP2C19	**mRNA** (EpiDerm)	-	**mRNA** (primary Keratinocytes)	-	Neis *et al*., (2010) Du *et al*., (2004)
CYP2D6	**mRNA** (EpiSkin™ , EpiDerm, ORS-RHE)	**mRNA** (Skin™ FTM, Phenion FTM)	**mRNA** (primary Keratinocytes)	**mRNA** **No activity**	Luu-The *et al*., (2009) Wiegand *et al*., (2014) Du *et al*., (2004)
CYP2E1	**mRNA** (EpiSkin™ , EpiDerm) **Activity** (EpiSkin™ , SkinEthic™ RHE)	**mRNA** (Skin™ FTM, Phenion FTM) **Activity** (Skin™ FTM)	**mRNA** (primary Keratinocytes) **Protein** (primary Keratinocytes) **Activity** (primary Keratinocytes)	**mRNA** **No activity**	Luu-The *et al*., (2009) Wiegand *et al*., (2014) Du *et al*., (2004) Hu *et al*., (2010) Saeki *et al*., (2002)

Table 1.5: Detection of expression of gene, protein, and activity of Phase I XMEs in commercial 3D human skin models, native human skin keratinocytes skin model (cells culture). Adapted from: Kazem *et al*., (2019).

Phase I enzymes	3D epidermis skin models	Commercial human skin models	Keratinocytes skin model (cells culture)	Human skin	References
CYP2F1	**mRNA** (EpiSkin™**)**	**mRNA** (Skin™ FTM)	-	**mRNA**	Luu-The *et al*., (2009)
CYP2J2	**mRNA** (EpiSkin™ , EpiDerm)	**mRNA** (Skin™ FTM, Phenion FTM)	**mRNA** (primary Keratinocytes)	**mRNA**	Hu *et al*., (2010) Luu-The *et al*., (2009) Neis *et al*., (2010) Du *et al*., (2004)
CYP2R1	**mRNA** (ORS-RHE, EpiDerm)	-	**mRNA** (primary Keratinocytes)	**mRNA**	Hu *et al*., (2010) Neis *et al*., (2010) Du *et al*., (2006) Bacqueville *et al*., (2017)
CYP2S1	**mRNA** (ORS-RHE, EpiDerm)	**mRNA** (Phenion FTM)	**mRNA** (primary Keratinocytes, HaCaT)	**mRNA**	Hu *et al*., (2010) Wang & Guengerich (2013) Wiegand *et al*., (2014) Du *et al*., (2006) McNeilly *et al*., (2012) Bacqueville *et al*., (2017)
CYP2U1	**mRNA** (EpiDerm)	-	**mRNA** (primary Keratinocytes)	**mRNA**	Hu *et al*., (2010) Du *et al*., (2006)
CYP2W1	**mRNA** (EpiDerm)	-	**mRNA** (primary Keratinocytes)	**mRNA**	Hu *et al*., (2010) Du *et al*., (2006)
CYP3A1	**Activity** (EpiDerm)	**Activity (**Phenion FTM)	**Protein** (primary Keratinocytes) **Activity** (primary Keratinocytes)	**mRNA** **No activity**	Götz *et al*., (2012) Jäckh *et al*., (2012) Baron *et al*., (2008) Wiegand *et al*., (2014)

Table 1.6: Detection of expression of gene, protein, and activity of Phase I XMEs in commercial 3D human skin models, native human skin keratinocytes skin model (cells culture). Adapted from: Kazem *et al*., (2019).

Phase I enzymes	3D epidermis skin models	Commercial human skin models	Keratinocytes skin model (cells culture)	Human skin	References
CYP3A4	**mRNA** (EpiSkin™**)** **Activity** (EpiSkin™ , EpiDerm)	**mRNA (**Phenion FTM) **Activity** (Skin™ FTM)	**mRNA** (primary Keratinocytes) **Protein** (primary Keratinocytes) **Activity** (primary Keratinocytes) **Activity** (NCTC, HaCaT)	**mRNA** **Activity**	Eilstein *et al*., (2015) Götz *et al*., (2012) Wiegand *et al*., (2014) Neis *et al*., (2010) Swanson (2004) Du *et al*., (2006) Baron *et al*., (2008)
CYP3A5	**mRNA** (EpiSkin™ , EpiDerm, ORS-RHE) **Activity** (EpiSkin™ , SkinEthic™ RHE)	**mRNA** (Skin™ FTM, Phenion FTM) **Activity** (Skin™ FTM)	**mRNA** and **Activity** (primary Keratinocytes)	**mRNA** **Activity**	Eilstein *et al*., (2015) Götz *et al*., (2012) Luu-The *et al*., (2009) Neis *et al*., (2010) Baron *et al*., (2008) Bacqueville *et al*., (2017)
CYP4B1	**mRNA** (EpiSkin™, EpiDerm, ORS-RHE)	**mRNA** (Skin™ FTM, Phenion FTM)	**mRNA** (primary Keratinocytes)	**mRNA** **Activity**	Luu-The *et al*., (2009) Hu *et al*., (2010) Neis *et al*., (2010) Du *et al*., (2006)
CYP26B1	**mRNA** (EpiSkin™, EpiDerm, ORS-RHE)	**mRNA** (Skin™ FTM**)**	-	**mRNA**	Luu-The *et al*., (2009) Hu *et al*., (2010) Bacqueville *et al*., (2017)
CYP27B1	**mRNA** (EpiSkin™**)**	**mRNA** (Skin™ FTM**)**	-	**mRNA**	Luu-The *et al*., (2009)
CYP4F3	**mRNA** (EpiSkin™, EpiDerm, ORS-RHE)	**mRNA** (Skin™ FTM**)**	-	**mRNA**	Luu-The *et al*., (2009) Hu *et al*., (2010) Bacqueville *et al*., (2017)

Table 1.7: Detection expression of gene, protein, and activity of non-cytochrome P450 Phase I XMEs in commercial 3D human skin models, native human skin keratinocytes skin model (cells culture). Adapted from: Kazem *et al*., (2019).

Phase I enzymes	3D epidermis skin models	Commercial human skin models	Keratinocytes skin model (cells culture)	Human skin	References
FMO1	**Activity** (EpiDerm)	**Activity (**Phenion FTM)	-	-	Jäckh *et al*., (2012)
FMO2	**mRNA** (EpiSkin™ , EpiDerm)	**mRNA** (Skin™ FTM)	-	**mRNA**	Hu *et al*., (2010) Wiegand *et al*., (2014) Luu-The *et al*., 2009)
FMO3	**Activity** (EpiDerm)	**Activity (**Phenion FTM)	**Protein** (primary Keratinocytes)	**mRNA** **Protein**	Hu *et al*., (2010) Wiegand *et al*., (2014) Luu-The *et al*., (2009) Jäckh *et al*., (2011)
FMO4	**mRNA** (EpiSkin™, EpiDerm, ORS-RHE)	**mRNA** (Skin™ FTM**)**	-	**mRNA**	Hu *et al*., (2010) Wiegand *et al*., (2014) Luu-The *et al*., (2009) Bacqueville *et al*., (2017)
FMO5	**mRNA** (EpiSkin™, EpiDerm)	**mRNA** (Skin™ FTM, Phenion FTM)	**mRNA** (primary Keratinocytes)	**mRNA**	Hu *et al*., (2010) Wiegand *et al*., (2014) Luu-The *et al*., (2009)
CES1	-	-	-	**Protein**	van Eijl *et al*., (2012)
CES2	**mRNA** (ORS-RHE, EpiDerm)	-	**mRNA** (HaCaT)	**mRNA**	Hu *et al*., (2010) Bacqueville *et al*., (2017) Zhu *et al*., (2007)

Table 1.8: Detection expression of gene, protein, and activity of non-cytochrome P450 Phase I XMEs in commercial 3D human skin models, native human skin keratinocytes skin model (cells culture). Adapted from: Kazem *et al*., (2019).

Phase I enzymes	3D epidermis skin models	Commercial human skin models	Keratinocytes skin model (cells culture)	Human skin	References
CES3	**mRNA** (EpiDerm)	-	-	-	Hu *et al*., (2010)
CES5	**mRNA** (ORS-RHE)	-	-	-	Bacqueville *et al*., (2017)
ADH1	-	-	-	**Protein**	van Eijl *et al*., (2012)
ADH3	**mRNA** (EpiSkin™, EpiDerm, SkinEthic™ RHE)	-	-	**Protein**	van Eijl *et al*., (2012)
ADH4	-	-	-	**Protein**	Luu-The *et al*., (2009)

Table 1.9: Detection of expression of gene, protein, and activity of Phase II XMEs in commercial 3D human skin models, native human skin keratinocytes skin model (cells culture). Adapted from: Kazem *et al*., (2019).

Phase II enzymes	3D epidermis skin models	Commercial human skin models	Keratinocytes skin model (cells culture)	Human skin	References
GST	**Activity** (EpiSkin™, EpiDerm,)	**Activity (**Phenion FTM, Skin™ FTM)	**mRNA** (NCTC) **Activity (**primary Keratinocytes, HaCaT)	**Activity**	Wiegand *et al*., (2014) Eilstein *et al*., (2015) Götz *et al*., (2012) Hirel *et al*., (1996)
GST A1	**mRNA** (EpiDerm, ORS-RHE)	-	-	**mRNA** **Protein**	Hu et al., (2010) Wiegand *et al*., (2014) van Eijl *et al*., (2012) Bacqueville *et al*., (2017)
GST A3	-	-	-	**mRNA**	Wiegand *et al*., (2014)
GST A4	**mRNA** (EpiDerm, ORS-RHE)	-	-	-	Hu *et al*., (2010) Bacqueville *et al*., (2017)
GST M1	**mRNA** (ORS-RHE) **Protein (**EpiSkin™, EpiDerm, SkinEthic™)	-	-	**mRNA** **Protein**	Hu *et al*., (2010) Bacqueville *et al*., (2017) van Eijl *et al*., (2012)
GST M2	**mRNA** (ORS-RHE, EpiDerm)	-	-	**Protein**	Hu *et al*., (2010) Bacqueville *et al*., (2017)
GST M3	**mRNA** (ORS-RHE, EpiDerm)	-	-	**mRNA**	Hu *et al*., (2010) Bacqueville *et al*., (2017)

Table 1.10: Detection of expression of gene, protein, and activity of Phase II XMEs in commercial 3D human skin models, native human skin keratinocytes skin model (cells culture). Adapted from: Kazem *et al*., (2019).

Phase I enzymes	3D epidermis skin models	Commercial human skin models	Keratinocytes skin model (cells culture)	Human skin	References
GST M4	**mRNA** (ORS-RHE, EpiDerm)	-	-	**mRNA**	Hu *et al*., (2010) Bacqueville *et al*., (2017)
GST M5	**mRNA** (EpiSkin™ , EpiDerm)	-	-	**mRNA**	Hu *et al*., (2010) Bacqueville *et al*., (2017)
GST P1	**mRNA (**EpiSkin™, (ORS-RHE, EpiDerm,) **Protein (**EpiSkin™, EpiDerm, SkinEthic™)	**mRNA (**Phenion FTM, Skin™ FTM)	**mRNA** (primary Keratinocytes) **Protein (**HaCaT)	**mRNA** **Protein**	Hu *et al*., (2010) Wiegand *et al*., (2014) Luu-The *et al*., (2009) van Eijl *et al*., (2012) Hirel *et al*., (1996)
GST Z1	**mRNA** (EpiDerm)	-	-	**mRNA**	Hu *et al*., (2010)
NAT 1	**Activity** (EpiSkin™, SkinEthic™ RHE)	**Activity** (Skin™ FTM, Phenion FTM)	(primary Keratinocytes, HaCaT, NCTC)	**Activity**	Eilstein *et al*., (2015) Götz *et al*., (2012) Jäckh *et al*., (2011) Bonifas *et al*., (2010) Eilstein *et al*., (2015)
NAST 2	**mRNA** (EpiSkin™)	-	-	**mRNA**	Hu *et al*., (2010) Bacqueville *et al*., (2017) Zhu *et al*., (2007) Eilstein *et al*., (2015)

Table 1.11: Summary of the analysis of 3D models and human skin in combination with MALDI-MSI. Adapted from: Spencer *et al*., (2020)

Skin Tissues	Disease	MSI Method	Spatial Resolution	Refernces	Summary
3D Skin Innovenn "Labskin"	Healthy living skin equivalent (LSE)	MALDI	60 µm	Russo et al., (2018)	Quantitation terbinafine hydrochloride in the epidermis of a full thickness living skin equivalent model by MALDI-MSI and confermed by LC-MS/MS
Human normal skin	Healthy norml human Skin	MALDI	20 µm	de Macedo *et al*., (2017)	Identification and localization of skin absorption and distribution of drug compounds in the skin layer (epiderms and dermis)
Fresh human skin	Healthy human skin	MALDI	20µm	Sørensen *et al*., (2017)	The former tofacitinib and of ruxolitinib mainly localized in the layers of fresh human skin
3D Skin Model Innovenn "Labskin"	Healthy living skin equivalent (LSE)	MALDI	60 µm	Russo *et al*., (2018)	The combination of fullthickness 3D skin model treated methylparaben. with MALDI-MSI for the study of the presence of esterases.
3D Skin Model Innovenn "Labskin"	Healthy and psoriatic LSE	MALDI	100 µm	Harvey *et al*., (2016)	The penetration of acitretin within psoriatic LSE compared with healthy LSE by MALDI-MSI.
3D Skin Model Evocutis "LabSkin"	Healthy living skin equivalent (LSE)	MALDI	50 µm	Francese *et al*., (2013)	Detection of acitretin distribution within epidermis and dermis layer in the LSE.

1.13 References

Ahmad, N., & Mukhtar, H. (2004). Cytochrome p450: a target for drug development for skin diseases. *Journal of Investigative Dermatology*, ***123***(3), 417-425.

Akintobi, A. M., Villano, C. M., & White, L. A. (2007). 2, 3, 7, 8-Tetrachlorodibenzo-p-dioxin (TCDD) exposure of normal human dermal fibroblasts results in AhR-dependent and-independent changes in gene expression. *Toxicology and Applied Pharmacology*, ***220***(1), 9-17.

Aliyari, E., & Konermann, L. (2020). Formation of Gaseous Proteins via the Ion Evaporation Model (IEM) in Electrospray Mass Spectrometry. *Analytical Chemistry*, ***92***(15), 10807-10814.

Allen, D. R., & McWhinney, B. C. (2019). Quadrupole time-of-flight mass spectrometry: a paradigm shift in toxicology screening applications. *The Clinical Biochemist Reviews*, ***40***(3), 135.

Alsagaby, S. A. (2019). Understanding the fundamentals of proteomics. *Curr.Top.Pept.Protein Res*, ***20***(3), 25.

Anderson, D. M., Carolan, V. A., Crosland, S., Sharples, K. R., & Clench, M. R. (2010). Examination of the translocation of sulfonylurea herbicides in sunflower plants by matrix-assisted laser desorption/ionisation mass spectrometry imaging. *Rapid Communications in Mass Spectrometry*, ***24***(22), 3309-3319.

Avery, J. L., McEwen, A., Flinders, B., Francese, S., & Clench, M. R. (2011). Matrix-assisted laser desorption mass spectrometry imaging for the examination of imipramine absorption by Straticell-RHE-EPI/001 an artificial model of the human epidermis. *Xenobiotica*, ***41***(8), 735-742.

Bacqueville, D., Jacques, C., Duprat, L., Jamin, E. L., Guiraud, B., Perdu, E., Bessou-Touya, S., Zalko, D., & Duplan, H. (2017). Characterization of xenobiotic metabolizing enzymes of a reconstructed human epidermal model from adult hair follicles. *Toxicology and Applied Pharmacology*, *329*, 190-201.

Banerjee, S., & Mazumdar, S. (2012). Electrospray ionization mass spectrometry: a technique to access the information beyond the molecular weight of the analyte. *International Journal of Analytical Chemistry, 2012*

Baron, J. M., Wiederholt, T., Heise, R., Merk, H. F., & Bickers, D. R. (2008). Expression and function of cytochrome p450-dependent enzymes in human skin cells. *Current Medicinal Chemistry, **15***(22), 2258-2264.

Baron, J. M., HoÈller, D., Schiffer, R., Frankenberg, S., Neis, M., Merk, H. F., & Jugert, F. K. (2001). Expression of multiple cytochrome p450 enzymes and multidrug resistance-associated transport proteins in human skin keratinocytes. *Journal of Investigative Dermatology, **116***(4), 541-548.

Bartlett, J. M., & Stirling, D. (2003). A short history of the polymerase chain reaction. *PCR protocols* (pp. 3-6). Springer.

Beine, B., Diehl, H. C., Meyer, H. E., & Henkel, C. (2016). Tissue MALDI mass spectrometry imaging (MALDI MSI) of peptides. *Proteomics in Systems Biology* (pp. 129-150). Springer.

Bell, E., Parenteau, N., Gay, R., Nolte, C., Kemp, P., Bilbo, P., Ekstein, B., & Johnson, E. (1991). The living skin equivalent: its manufacture, its organotypic properties and its responses to irritants. *Toxicology in Vitro, **5***(5-6), 591-596.

Berghard, A., Gradin, K., & Toftgård, R. (1990). Serum and extracellular calcium modulate induction of cytochrome P-450IA1 in human keratinocytes. *Journal of Biological Chemistry, **265***(34), 21086-21090.

Bergquist, J., Baykut, G., Bergquist, M., Witt, M., Mayer, F., & Baykut, D. (2012). Human myocardial protein pattern reveals cardiac diseases. *International Journal of Proteomics*, 2012.

Bikle, D. D., & Pillai, S. (1993). Vitamin D, calcium, and epidermal differentiation. *Endocrine Reviews, **14***(1), 3-19.

Bonifant, H., & Holloway, S. (2019). A review of the effects of ageing on skin integrity and wound healing. *British Journal of Community Nursing, **24***(Sup3), S28-S33.

Bonifas, J., Hennen, J., Dierolf, D., Kalmes, M., & Blömeke, B. (2010). Evaluation of cytochrome P450 1 (CYP1) and N-acetyltransferase 1 (NAT1) activities in HaCaT cells: implications for the development of in vitro techniques for predictive testing of contact sensitizers. *Toxicology in Vitro, **24***(3), 973-980.

Bouwstra, J. A., Honeywell-Nguyen, P. L., Gooris, G. S., & Ponec, M. (2003). Structure of the skin barrier and its modulation by vesicular formulations. *Progress in Lipid Research, **42***(1), 1-36.

Bracken, M. B. (2009). Why animal studies are often poor predictors of human reactions to exposure. *Journal of the Royal Society of Medicine, **102***(3), 120-122.

Bronaugh, R. L., Stewart, R. F., & Congdon, E. R. (1982). Methods for in vitro percutaneous absorption studies II. Animal models for human skin. *Toxicology and Applied Pharmacology, **62***(3), 481-488.

Brown, M. B., Martin, G. P., Jones, S. A., & Akomeah, F. K. (2006). Dermal and transdermal drug delivery systems: current and future prospects. *Drug Delivery, **13***(3), 175-187.

Bunch, J., Clench, M. R., & Richards, D. S. (2004). Determination of pharmaceutical compounds in skin by imaging matrix-assisted laser desorption/ionisation mass spectrometry. *Rapid Communications in Mass Spectrometry, **18***(24), 3051-3060.

Burnette, W. N. (1981). “Western blotting”: electrophoretic transfer of proteins from sodium dodecyl sulfate-polyacrylamide gels to unmodified nitrocellulose and radiographic detection with antibody and radioiodinated protein A. *Analytical Biochemistry, **112***(2), 195-203.

Butcher, M., & White, R. (2005). The structure and functions of the skin. *Skin Care in Wound Management: Assessment, Prevention and Treatment.Wounds UK, Aberdeen, *, 1-16.

Carpentieri-Rodrigues, L. N., Zanluchi, J. M., & Grebogi, I. H. (2007). Percutaneous absorption enhancers: Mechanisms and potential. *Brazilian Archives of Biology and Technology, **50***, 949-961.

Casey Laizure, S., Herring, V., Hu, Z., Witbrodt, K., & Parker, R. B. (2013). The role of human carboxylesterases in drug metabolism: have we overlooked their importance? *Pharmacotherapy: The Journal of Human Pharmacology and Drug Therapy, **33***(2), 210-222.

Chen, J., Mannargudi, B. M., Xu, L., & Uetrecht, J. (2008). Demonstration of the metabolic pathway responsible for nevirapine-induced skin rash. *Chemical Research in Toxicology, **21***(9), 1862-1870.

Cheng, J. B., Motola, D. L., Mangelsdorf, D. J., & Russell, D. W. (2003). De-orphanization of Cytochrome P450 2R1 a microsomal vitamin D 25-hydroxylase. *Journal of Biological Chemistry, **278***(39), 38084-38093.

Chernushevich, I. V., Merenbloom, S. I., Liu, S., & Bloomfield, N. (2017). A W-geometry ortho-TOF MS with high resolution and up to 100% duty cycle for MS/MS. *Journal of the American Society for Mass Spectrometry, **28***(10), 2143-2150.

Couto, N., Newton, J. R., Russo, C., Karunakaran, E., Achour, B., Al-Majdoub, Z. M., Sidaway, J., Rostami-Hodjegan, A., Clench, M. R., & Barber, J. (2021). Label-free quantitative proteomics and substrate-based mass spectrometry imaging of xenobiotic metabolizing enzymes in ex vivo human skin and a human living skin equivalent model. *Drug Metabolism and Disposition, **49***(1), 39-52.

De Hoffmann, E., & Stroobant, V. (2007). *Mass spectrometry: principles and applications*. John Wiley & Sons.

de Macedo, C. S., Anderson, D. M., & Schey, K. L. (2017). MALDI (matrix assisted laser desorption ionization) imaging mass spectrometry (IMS) of skin: aspects of sample preparation. *Talanta, 174*, 325-335.

Dekker, S. J., Zhang, Y., Vos, J. C., Vermeulen, N. P., & Commandeur, J. N. (2016). Different reactive metabolites of nevirapine require distinct glutathione S-transferase isoforms for bioinactivation. *Chemical Research in Toxicology, **29***(12), 2136-2144.

Delescluse, C., Ledirac, N., de Sousa, G., Pralavorio, M., Botta-Fridlund, D., Letreut, Y., & Rahmani, R. (1997). Comparative study of CYP1A1 induction by 3-

methylcholanthrene in various human hepatic and epidermal cell types. *Toxicology in Vitro, **11***(5), 443-450.

Ding, S., Lake, B. G., Friedberg, T., & Wolf, C. R. (1995). Expression and alternative splicing of the cytochrome P-450 CYP2A7. *Biochemical Journal, **306***(1), 161-166.

Ding, X., & Kaminsky, L. S. (2003). Human extrahepatic cytochromes P450: function in xenobiotic metabolism and tissue-selective chemical toxicity in the respiratory and gastrointestinal tracts. *Annual Review of Pharmacology and Toxicology, **43***(1), 149-173.

Downing, D. T. (1992). Lipid and protein structures in the permeability barrier of mammalian epidermis. *Journal of Lipid Research, **33***(3), 301-313.

Du, L., Hoffman, S. M., & Keeney, D. S. (2004). Epidermal CYP2 family cytochromes P450. *Toxicology and Applied Pharmacology, **195***(3), 278-287.

Du, L., Neis, M. M., Ladd, P. A., & Keeney, D. S. (2006). Differentiation-specific factors modulate epidermal CYP1–4 gene expression in human skin in response to retinoic acid and classic aryl hydrocarbon receptor ligands. *Journal of Pharmacology and Experimental Therapeutics, **319***(3), 1162-1171.

Eilstein, J., Léreaux, G., Arbey, E., Daronnat, E., Wilkinson, S., & Duché, D. (2015). Xenobiotic metabolizing enzymes in human skin and SkinEthic reconstructed human skin models. *Experimental Dermatology, **24***(7), 547-549.

Eilstein, J., Lereaux, G., Daronnat, E., Meunier, J., Leclaire, J., & Duche, D. (2010). Characterization of N-Acetyl and Glutathione S-Transferase Activities in Skin and Reconstructed Human Skin Models. Paper presented at the *Drug Metabolism Reviews, , 42* 150.

El-Ghalbzouri, A., Gibbs, S., Lamme, E., Van Blitterswijk, C. A., & Ponec, M. (2002). Effect of fibroblasts on epidermal regeneration. *British Journal of Dermatology, **147***(2), 230-243.

El-Aneed, A., Cohen, A., & Banoub, J. (2009). Mass spectrometry, review of the basics: electrospray, MALDI, and commonly used mass analyzers. *Applied Spectroscopy Reviews, **44***(3), 210-230.

Fenn, J. B., Mann, M., Meng, C. K., Wong, S. F., & Whitehouse, C. M. (1989). Electrospray ionization for mass spectrometry of large biomolecules. *Science, **246***(4926), 64-71.

Finta, C., & Zaphiropoulos, P. G. (2000). The human CYP2C locus: a prototype for intergenic and exon repetition splicing events. *Genomics, **63***(3), 433-438.

Fliegel, D., Fuhrer, K., Gonin, M., & Günther, D. (2006). Evaluation of a pulsed glow discharge time-of-flight mass spectrometer as a detector for gas chromatography and the influence of the glow discharge source parameters on the information volume in chemical speciation analysis. *Analytical and Bioanalytical Chemistry*, ***386***(1), 169-179.

Francese, S., Bradshaw, R., Flinders, B., Mitchell, C., Bleay, S., Cicero, L., & Clench, M. R. (2013). Curcumin: a multipurpose matrix for MALDI mass spectrometry imaging applications. *Analytical Chemistry, **85***(10), 5240-5248.

Francese, S., & Clench, M. R. (2010). MALDI mass spectrometry imaging, a new frontier in biostructural techniques: applications in biomedicine. *Mass Spectrometry for Microbial Proteomics, ,* 91-116.

Fremout, W. (2014). No title. *Tryptic Cleavage of Proteinaceous Paint: A High-Performance Protein Binder Analytical Technique,*

Garcia, A. G. (2016). No title. *Characterisation of a Bacterial P450 System using Surface Mass Spectrometry,*

Gelardi, A., Morini, F., Dusatti, F., Penco, S., & Ferro, M. (2001). Induction by xenobiotics of phase I and phase II enzyme activities in the human keratinocyte cell line NCTC 2544. *Toxicology in Vitro, **15***(6), 701-711.

Gibbs, S., van de Sandt, Johannes JM, Merk, H. F., Lockley, D. J., Pendlington, R. U., & Pease, C. K. (2007). Xenobiotic metabolism in human skin and 3D human skin reconstructs: a review. *Current Drug Metabolism, **8***(8), 758-772.

Gieniec, J., Mack, L. L., Nakamae, K., Gupta, C., Kumar, V., & Dole, M. (1984). Electrospray mass spectroscopy of macromolecules: Application of an ion-drift spectrometer. *Biomedical Mass Spectrometry, **11***(6), 259-268.

Goebel, C., Hewitt, N. J., Kunze, G., Wenker, M., Hein, D. W., Beck, H., & Skare, J. (2009). Skin metabolism of aminophenols: human keratinocytes as a suitable in vitro model to qualitatively predict the dermal transformation of 4-amino-2-hydroxytoluene in vivo. *Toxicology and Applied Pharmacology, **235***(1), 114-123.

Gonzalez, M., Marteau, C., Franchi, J., & Migliore-Samour, D. (2001). Cytochrome P450 4A11 expression in human keratinocytes: effects of ultraviolet irradiation. *British Journal of Dermatology, **145***(5), 749-757.

Götz, C., Pfeiffer, R., Tigges, J., Blatz, V., Jäckh, C., Freytag, E., Fabian, E., Landsiedel, R., Merk, H. F., & Krutmann, J. (2012). Xenobiotic metabolism capacities of human skin in comparison with a 3D epidermis model and keratinocyte-based cell culture as in vitro alternatives for chemical testing: activating enzymes (Phase I). *Experimental Dermatology*, ***21***(5), 358-363.

Grant, D. M., Hughes, N. C., Janezic, S. A., Goodfellow, G. H., Chen, H. J., Gaedigk, A., Violeta, L. Y., & Grewal, R. (1997). Human acetyltransferase polymorphisms. *Mutation Research/Fundamental and Molecular Mechanisms of Mutagenesis, **376***(1-2), 61-70.

Greaves, J., & Roboz, J. (2014). *Mass spectrometry for the novice*. CRC Press Boca Raton, FL.

Guiraud, B., Hernandez-Pigeon, H., Ceruti, I., Mas, S., Palvadeau, Y., Saint-Martory, C., Castex-Rizzi, N., Duplan, H., & Bessou-Touya, S. (2014). Characterization of a human epidermis model reconstructed from hair follicle keratinocytes and comparison with two commercially models and native skin. *International Journal of Cosmetic Science*, ***36***(5), 485-493.

Gürtler, A., Kunz, N., Gomolka, M., Hornhardt, S., Friedl, A. A., McDonald, K., Kohn, J. E., & Posch, A. (2013). Stain-Free technology as a normalization tool in Western blot analysis. *Analytical Biochemistry, **433***(2), 105-111.

Gysler, A., Lange, K., Korting, H. C., & Schäfer-Korting, M. (1997). Prednicarbate biotransformation in human foreskin keratinocytes and fibroblasts. *Pharmaceutical Research, **14***(6), 793-797.

Hankin, J. A., Barkley, R. M., & Murphy, R. C. (2007). Sublimation as a method of matrix application for mass spectrometric imaging. *Journal of the American Society for Mass Spectrometry, **18***(9), 1646-1652.

Hansell, E., Braschi, S., Medzihradszky, K. F., Sajid, M., Debnath, M., Ingram, J., Lim, K. C., & McKerrow, J. H. (2008). Proteomic analysis of skin invasion by blood fluke larvae. *PLoS Neglected Tropical Diseases, **2***(7), e262.

Hansen, H. T., & Janfelt, C. (2016). Aspects of quantitation in mass spectrometry imaging investigated on cryo-sections of spiked tissue homogenates. *Analytical Chemistry, **88***(23), 11513-11520.

Harris, I. R., Siefken, W., Beck-Oldach, K., Brandt, M., Wittern, K., & Pollet, D. (2002). Comparison of activities dependent on glutathione S-transferase and cytochrome P-450 IA1 in cultured keratinocytes and reconstructed epidermal models. *Skin Pharmacology and Physiology, **15***(Suppl. 1), 59-67.

Harvey, A., Cole, L. M., Day, R., Bartlett, M., Warwick, J., Bojar, R., Smith, D., Cross, N., & Clench, M. R. (2016). MALDI-MSI for the analysis of a 3D tissue-engineered psoriatic skin model. *Proteomics, **16***(11-12), 1718-1725.

Hayden, P., Bolmarcich, J., Stolper, G., Hu, T., Aardema, M., Curren, R., & Klausner, M. (2006). Xenobiotic metabolizing capabilities of the EpiDerm in vitro human skin equivalent: utility for assessing dermal biotransformation of pharmaceuticals and environmental chemicals. *Toxicology Letters,* (164), S225-S226.

Hein, D. W., Doll, M. A., Rustan, T. D., Gray, K., Feng, Y., Ferguson, R. J., & Grant, D. M. (1993). Metabolic activation and deactivation of arylamine carcinogens by

recombinant human NAT1 and polymorphic NAT2 acetyltransferases. *Carcinogenesis, **14***(8), 1633-1638.

Higuchi, R., Dollinger, G., Walsh, P. S., & Griffith, R. (1992). Simultaneous amplification and detection of specific DNA sequences. *Bio/Technology, **10***(4), 413-417.

Hirel, B., Watier, E., Chesne, C., Patoux-Pibouin, M., & guillodzo, A. (1996). Culture and drug biotransformation capacity of adult human keratinocytes from post-mortem skin. *British Journal of Dermatology, 134*(5), 831-836.

Ho, C. S., Lam, C., Chan, M., Cheung, R., Law, L. K., Lit, L., Ng, K. F., Suen, M., & Tai, H. (2003). Electrospray ionisation mass spectrometry: principles and clinical applications. *The Clinical Biochemist Reviews, **24***(1), 3.

Hoffman, S. M., Nelson, D. R., & Keeney, D. S. (2001). Organization, structure and evolution of the CYP2 gene cluster on human chromosome 19. *Pharmacogenetics and Genomics, **11***(8), 687-698.

Hoffmann, J., Heisler, E., Karpinski, S., Losse, J., Thomas, D., Siefken, W., Ahr, H., Vohr, H., & Fuchs, H. W. (2005). Epidermal-skin-test 1000 (EST-1000)—A new reconstructed epidermis for in vitro skin corrosivity testing. *Toxicology in Vitro, **19***(7), 925-929.

Honari, G., Andersen, R., & Maibach, H. L. (2017). *Sensitive skin syndrome*. CRC Press.

Hu, T., Khambatta, Z. S., Hayden, P. J., Bolmarcich, J., Binder, R. L., Robinson, M. K., Carr, G. J., Tiesman, J. P., Jarrold, B. B., & Osborne, R. (2010). Xenobiotic metabolism gene expression in the EpiDerm™ in vitro 3D human epidermis model compared to human skin. *Toxicology in Vitro, **24***(5), 1450-1463.

Jäckh, C., Blatz, V., Fabian, E., Guth, K., van Ravenzwaay, B., Reisinger, K., & Landsiedel, R. (2011). Characterization of enzyme activities of Cytochrome P450 enzymes, Flavin-dependent monooxygenases, N-acetyltransferases and UDP-glucuronyltransferases in human reconstructed epidermis and full-thickness skin models. *Toxicology in Vitro, **25***(6), 1209-1214.

Jäckh, C., Fabian, E., van Ravenzwaay, B., & Landsiedel, R. (2012). Relevance of xenobiotic enzymes in human skin in vitro models to activate pro-sensitizers. *Journal of Immunotoxicology, **9***(4), 426-438.

Janmohamed, A., Dolphin, C. T., Phillips, I. R., & Shephard, E. A. (2001). Quantification and cellular localization of expression in human skin of genes encoding flavin-containing monooxygenases and cytochromes P4502. *Biochemical Pharmacology, **62***(6), 777-786.

Jensen, E. C. (2012). The basics of western blotting. *The Anatomical Record: Advances in Integrative Anatomy and Evolutionary Biology, **295***(3), 369-371.

Jewell, C., Prusakiewicz, J. J., Ackermann, C., Payne, N. A., Fate, G., Voorman, R., & Williams, F. M. (2007). Hydrolysis of a series of parabens by skin microsomes and cytosol from human and minipigs and in whole skin in short-term culture. *Toxicology and Applied Pharmacology, **225***(2), 221-228.

Joshi, M., & Deshpande, J. D. (2010). Polymerase chain reaction: methods, principles and application. *International Journal of Biomedical Research, **2***(1), 81-97.

Karas, M., Bahr, U., Ingendoh, A., Nordhoff, E., Stahl, B., Strupat, K., & Hillenkamp, F. (1990). Principles and applications of matrix-assisted UV-laser desorption/ionization mass spectrometry. *Analytica Chimica Acta, **241***(2), 175-185.

Katiyar, S. K., Mukhtar, H., & Matsui, M. S. (2000). Ultraviolet-B exposure of human skin induces cytochromes P450 1A1 and 1B1. *Journal of Investigative Dermatology, **114***(2), 328-333.

Katoh, M., Hamajima, F., Ogasawara, T., & Hata, K. (2009). Assessment of human epidermal model LabCyte EPI-MODEL for in vitro skin irritation testing according to European Centre for the Validation of Alternative Methods (ECVAM)-validated protocol. *The Journal of Toxicological Sciences, **34***(3), 327-334.

Kazem, S., Linssen, E. C., & Gibbs, S. (2019). Skin metabolism phase I and phase II enzymes in native and reconstructed human skin: a short review. *Drug Discovery Today,*

Konermann, L., Ahadi, E., Rodriguez, A. D., & Vahidi, S. (2013). No title. *Unraveling the Mechanism of Electrospray Ionization,*

Kurien, B. T., & Scofield, R. H. (2006). Western blotting. *Methods*, ***38***(4), 283-293.

Lademann, J., Richter, H., Meinke, M., Sterry, W., & Patzelt, A. (2010). Which skin model is the most appropriate for the investigation of topically applied substances into the hair follicles? *Skin Pharmacology and Physiology*, ***23***(1), 47-52.

Lamb, K., Denyer, S. P., Sanderson, F. D., & Shaw, P. N. (1994). The metabolism of a series of ester pro-drugs by NCTC 2544 cells, skin homogenate and LDE testskin. *Journal of Pharmacy and Pharmacology*, ***46***(12), 965-973.

Lane, M. E. (2013). Skin penetration enhancers. *International Journal of Pharmaceutics*, ***447***(1-2), 12-21.

Lazo, N. D., Meine, J. G., & Downing, D. T. (1995). Lipids are covalently attached to rigid corneocyte protein envelopes existing predominantly as β-sheets: a solid-state nuclear magnetic resonance study. *Journal of Investigative Dermatology*, ***105***(2), 296-300.

Lee, S., Jin, S., Kim, Y. K., Sung, G. Y., Chung, J. H., & Sung, J. H. (2017). Construction of 3D multicellular microfluidic chip for an in vitro skin model. *Biomedical Microdevices*, ***19***(2), 22.

Leite-Silva, V. R., De Almeida, M. M., Fradin, A., Grice, J. E., & Roberts, M. S. (2012). Delivery of drugs applied topically to the skin. *Expert Review of Dermatology*, ***7***(4), 383-397.

Lundberg, K. C., Fritz, Y., Johnston, A., Foster, A. M., Baliwag, J., Gudjonsson, J. E., Schlatzer, D., Gokulrangan, G., McCormick, T. S., & Chance, M. R. (2015). Proteomics of skin proteins in psoriasis: from discovery and verification in a mouse model to confirmation in humans. *Molecular & Cellular Proteomics*, ***14***(1), 109-119.

Luu-The, V., Duche, D., Ferraris, C., Meunier, J., Leclaire, J., & Labrie, F. (2009). Expression profiles of phases 1 and 2 metabolizing enzymes in human skin and the

reconstructed skin models Episkin™ and full thickness model from Episkin™. *The Journal of Steroid Biochemistry and Molecular Biology, **116***(3-5), 178-186.

Mackay, I. M. (2004). Real-time PCR in the microbiology laboratory. *Clinical Microbiology and Infection, **10***(3), 190-212.

Madison, K. C. (2003). Barrier function of the skin:“la raison d'etre” of the epidermis. *Journal of Investigative Dermatology, **121***(2), 231-241.

Mahmood, T., & Yang, P. (2012). Western blot: technique, theory, and trouble shooting. *North American Journal of Medical Sciences, **4***(9), 429.

Mamyrin, B. A., Karataev, V. I., Shmikk, D. V., & Zagulin, V. A. (1973). The mass-reflectron, a new nonmagnetic time-of-flight mass spectrometer with high resolution. *Zh.Eksp.Teor.Fiz, **64***(1), 82-89.

Mathes, S. H., Ruffner, H., & Graf-Hausner, U. (2014). The use of skin models in drug development. *Advanced Drug Delivery Reviews, **69***, 81-102.

McNeilly, A. D., Woods, J. A., Ibbotson, S. H., Wolf, C. R., & Smith, G. (2012). Characterization of a human keratinocyte HaCaT cell line model to study the regulation of CYP2S1. *Drug Metabolism and Disposition, **40***(2), 283-289.

Mead, A. N., Amouzadeh, H. R., Chapman, K., Ewart, L., Giarola, A., Jackson, S. J., Jarvis, P., Jordaan, P., Redfern, W., & Traebert, M. (2016). Assessing the predictive value of the rodent neurofunctional assessment for commonly reported adverse events in phase I clinical trials. *Regulatory Toxicology and Pharmacology*, ***80***, 348-357.

Medhe, S. (2018). Mass Spectrometry: Analysers an Important Tool. *International Journal of Chemical Sciences, **16***, 1-8.

Meguro, S., Arai, Y., Masukawa, Y., Uie, K., & Tokimitsu, I. (2000). Relationship between covalently bound ceramides and transepidermal water loss (TEWL). *Archives of Dermatological Research, **292***(9), 463-468.

Metwally, H., Duez, Q., & Konermann, L. (2018). Chain ejection model for electrospray ionization of unfolded proteins: evidence from atomistic simulations and ion mobility spectrometry. *Analytical Chemistry, **90***(16), 10069-10077.

Mewes, K. R., Raus, M., Bernd, A., Zöller, N. N., Sättler, A., & Graf, R. (2007). Elastin expression in a newly developed full-thickness skin equivalent. *Skin Pharmacology and Physiology, **20***(2), 85-95.

Michaels, A. S., Chandrasekaran, S. K., & Shaw, J. E. (1975). Drug permeation through human skin: theory and in vitro experimental measurement. *AIChE Journal, **21***(5), 985-996.

Mitragotri, S., Anissimov, Y. G., Bunge, A. L., Frasch, H. F., Guy, R. H., Hadgraft, J., Kasting, G. B., Lane, M. E., & Roberts, M. S. (2011). Mathematical models of skin permeability: an overview. *International Journal of Pharmaceutics, **418***(1), 115-129.

Mullis, K., Faloona, F., Scharf, S., Saiki, R., Horn, G., & Erlich, H. (1986). Specific enzymatic amplification of DNA in vitro: the polymerase chain reaction. Paper presented at the *Cold Spring Harbor Symposia on Quantitative Biology, **51***, 263-273.

Murthy, S. N., & Shivakumar, H. N. (2010). Topical and transdermal drug delivery. *Handbook of non-invasive drug delivery systems* (pp. 1-36). Elsevier.

Neis, M. M., Wendel, A., Wiederholt, T., Marquardt, Y., Joussen, S., Baron, J. M., & Merk, H. F. (2010). Expression and induction of cytochrome p450 isoenzymes in human skin equivalents. *Skin Pharmacology and Physiology, **23***(1), 29-39.

Netzlaff, F., Schaefer, U. F., Lehr, C., Meiers, P., Stahl, J., Kietzmann, M., & Niedorf, F. (2006). Comparison of bovine udder skin with human and porcine skin in percutaneous permeation experiments. *Alternatives to Laboratory Animals: ATLA, **34***(5), 499-513.

Niehues, H., Bouwstra, J. A., El Ghalbzouri, A., Brandner, J. M., Zeeuwen, P. L., & van den Bogaard, Ellen H. (2018). 3D skin models for 3R research: The potential of 3D

reconstructed skin models to study skin barrier function. *Experimental Dermatology, **27***(5), 501-511.

Nohynek, G. J., Duche, D., Garrigues, A., Meunier, P., Toutain, H., & Leclaire, J. (2005). Under the skin: biotransformation of para-aminophenol and para-phenylenediamine in reconstructed human epidermis and human hepatocytes. *Toxicology Letters, **158***(3), 196-212.

Oesch, F., Fabian, E., Guth, K., & Landsiedel, R. (2014). Xenobiotic-metabolizing enzymes in the skin of rat, mouse, pig, guinea pig, man, and in human skin models. *Archives of Toxicology, **88***(12), 2135-2190.

Oesch, F., Fabian, E., & Landsiedel, R. (2018). Xenobiotica-metabolizing enzymes in the skin of rat, mouse, pig, guinea pig, man, and in human skin models. *Archives of Toxicology, **92***(8), 2411-2456.

Oesch, F., Fabian, E., Oesch-Bartlomowicz, B., Werner, C., & Landsiedel, R. (2007). Drug-metabolizing enzymes in the skin of man, rat, and pig. *Drug Metabolism Reviews, **39***(4), 659-698.

Pathan, I. B., & Setty, C. M. (2009). Chemical penetration enhancers for transdermal drug delivery systems. *Tropical Journal of Pharmaceutical Research, **8***(2)

Pauwels, M., & Rogiers, V. (2007). EU legislations affecting safety data availability of cosmetic ingredients. *Regulatory Toxicology and Pharmacology, **49***(3), 308-315.

Pendlington, R. U., Williams, D. L., Naik, J. T., & Sharma, R. K. (1994). Distribution of xenobiotic metabolizing enzymes in skin. *Toxicology in Vitro, **8***(4), 525-527.

Perry, R. H., Cooks, R. G., & Noll, R. J. (2008). Orbitrap mass spectrometry: instrumentation, ion motion and applications. Mass Spectrometry Reviews, ***27***(6), 661-699.

Pillai, O., Hamad, M. O., Crooks, P. A., & Stinchcomb, A. L. (2004). Physicochemical evaluation, in vitro human skin diffusion, and concurrent biotransformation of 3-O-alkyl carbonate prodrugs of naltrexone. *Pharmaceutical Research, **21***(7), 1146-1152.

Polat, B. E., Deen, W. M., Langer, R., & Blankschtein, D. (2012). A physical mechanism to explain the delivery of chemical penetration enhancers into skin during transdermal sonophoresis—Insight into the observed synergism. *Journal of Controlled Release, **158***(2), 250-260.

Pomerantz, A. E., Hammond, M. R., Morrow, A. L., Mullins, O. C., & Zare, R. N. (2008). Two-step laser mass spectrometry of asphaltenes. *Journal of the American Chemical Society, **130***(23), 7216-7217.

Prausnitz, M. R., & Langer, R. (2008). Transdermal drug delivery. *Nature Biotechnology, **26***(11), 1261-1268.

Prusakiewicz, J. J., Ackermann, C., & Voorman, R. (2006). Comparison of skin esterase activities from different species. *Pharmaceutical Research, **23***(7), 1517-1524.

Pyo, S. M., & Maibach, H. I. (2019). Skin metabolism: relevance of skin enzymes for rational drug design. *Skin Pharmacology and Physiology, **4***(5), 283-294.

Rassmussen, C., Gratz, N., Simon, N., Van der Zanden, C., Johnston, C., & Allen-Hoffmann, B. L. (2011). Expression and induction of xenobiotic metabolism genes in the Strata Test human skin model. *The Toxicologist (Toxicol.Sci, **120***(Suppl 2), 139.

Reilly, T. P., Lash, L. H., Doll, M. A., Hein, D. W., Woster, P. M., & Svensson, C. K. (2000). A role for bioactivation and covalent binding within epidermal keratinocytes in sulfonamide-induced cutaneous drug reactions. *Journal of Investigative Dermatology, **114***(6), 1164-1173.

Rheinwatd, J. G., & Green, H. (1975). Seria cultivation of strains of human epidemal keratinocytes: the formation keratinizin colonies from single cell is. *Cell, **6***(3), 331-343.

Rodríguez-Lázaro, D., Cook, N., & Hernández, M. (2013). Real-time PCR in food science: PCR diagnostics. *Current Issues in Molecular Biology, **15***(2), 39-44.

Rolsted, K., Kissmeyer, A., Rist, G. M., & Hansen, S. H. (2008). Evaluation of cytochrome P450 activity in vitro, using dermal and hepatic microsomes from four

species and two keratinocyte cell lines in culture. *Archives of Dermatological Research, **300***(1), 11-18.

Russo, C., Lewis, E. E., Flint, L., & Clench, M. R. (2018). Mass spectrometry imaging of 3D tissue models. *Proteomics, **18***(14), 1700462.

Ryan, D. J., Spraggins, J. M., & Caprioli, R. M. (2019). Protein identification strategies in MALDI imaging mass spectrometry: a brief review. *Current Opinion in Chemical Biology, **48***, 64-72.

Saarikoski, S. T., Rivera, S. P., Hankinson, O., & Husgafvel-Pursiainen, K. (2005). CYP2S1: a short review. *Toxicology and Applied Pharmacology, **207***(2), 62-69.

Saeki, M., Saito, Y., Nagano, M., Teshima, R., Ozawa, S., & Sawada, J. (2002). mRNA expression of multiple cytochrome p450 isozymes in four types of cultured skin cells. *International Archives of Allergy and Immunology, **127***(4), 333-336.

Saiki, R. K., Scharf, S., Faloona, F., Mullis, K. B., Horn, G. T., Erlich, H. A., & Arnheim, N. (1985). Enzymatic amplification of beta-globin genomic sequences and restriction site analysis for diagnosis of sickle cell anemia. *Science, **230***(4732), 1350-1354.

Sandilands, A., Sutherland, C., Irvine, A. D., & McLean, W. I. (2009). Filaggrin in the frontline: role in skin barrier function and disease. *Journal of Cell Science, **122***(9), 1285-1294.

Scheuplein, R. J., & Blank, I. H. (1971). Permeability of the skin. *Physiological Reviews, **51***(4), 702-747.

Schober, W., Luch, A., Soballa, V. J., Raab, G., Stegeman, J. J., Doehmer, J., Jacob, J., & Seidel, A. (2006). On the species-specific biotransformation of dibenzo [a, l] pyrene. *Chemico-Biological Interactions, **161***(1), 37-48.

Shanks, N., Greek, R., & Greek, J. (2009). Philosophy, ethics, and humanities in medicine. *Philosophy, Ethics, and Humanities in Medicine, **4***(2)

Shimma, S., & Sugiura, Y. (2014). Effective sample preparations in imaging mass spectrometry. *Mass Spectrometry, **3***(Special_Issue), S0029.

Sindhu, R. K., Chitkara, M., Kaur, G., Jaiswal, P., Kalra, A., Singh, I., & Sriamornsak, P. (2017). Skin penetration enhancer's in transdermal drug delivery systems. *Research Journal of Pharmacy and Technology, **10***(6), 1809-1815.

Singh, J., Birbian, N., Sinha, S., & Goswami, A. (2014). A critical review on PCR, its types and applications. *Int J Adv Res Biol Sci, **1***(7), 65-80.

Slavik, M. A., Allen-Hoffmann, B. L., Liu, B. Y., & Alexander, C. M. (2007). Wnt signaling induces differentiation of progenitor cells in organotypic keratinocyte cultures. *BMC Developmental Biology, **7***(1), 1-8.

Smith, G., Ibbotson, S. H., Comrie, M. M., Dawe, R. S., Bryden, A., Ferguson, J., & Wolf, C. R. (2006). Regulation of cutaneous drug-metabolizing enzymes and cytoprotective gene expression by topical drugs in human skin in vivo. *British Journal of Dermatology, **155***(2), 275-281.

Solon, E. G., Schweitzer, A., Stoeckli, M., & Prideaux, B. (2010). Autoradiography, MALDI-MS, and SIMS-MS imaging in pharmaceutical discovery and development. *The AAPS Journal, **12***(1), 11-26.

Sørensen, I. S., Janfelt, C., Nielsen, M. M. B., Mortensen, R. W., Knudsen, N. Ø, Eriksson, A. H., Pedersen, A. J., & Nielsen, K. T. (2017). Combination of MALDI-MSI and cassette dosing for evaluation of drug distribution in human skin explant. *Analytical and Bioanalytical Chemistry, **409***(21), 4993-5005.

Spencer, C. E., Flint, L. E., Duckett, C. J., Cole, L. M., Cross, N., Smith, D. P., & Clench, M. R. (2020). Role of MALDI-MSI in combination with 3D tissue models for early stage efficacy and safety testing of drugs and toxicants. *Expert Review of Proteomics, **17***(11-12), 827-841.

Spengler, B., Hubert, M., & Kaufmann, R. (1994). MALDI ion imaging and biological ion imaging with a new scanning UV-laser microprobe. Paper presented at the

Proceedings of the 42nd Annual Conference on Mass Spectrometry and Allied Topics, , 1041 1041.

Sugibayashi, K., Hayashi, T., Matsumoto, K., & Hasegawa, T. (2004). Utility of a three-dimensional cultured human skin model as a tool to evaluate the simultaneous diffusion and metabolism of ethyl nicotinate in skin. *Drug Metabolism and Pharmacokinetics, **19***(5), 352-362.

Sutter, T. R., Tang, Y. M., Hayes, C. L., Wo, Y., Jabs, E. W., Li, X., Yin, H., Cody, C. W., & Greenlee, W. F. (1994). Complete cDNA sequence of a human dioxin-inducible mRNA identifies a new gene subfamily of cytochrome P450 that maps to chromosome 2. *Journal of Biological Chemistry, **269***(18), 13092-13099.

Swanson, H. I. (2004). Cytochrome P450 expression in human keratinocytes: an aryl hydrocarbon receptor perspective. *Chemico-Biological Interactions, **149***(2-3), 69-79.

Takats, Z., Wiseman, J. M., Gologan, B., & Cooks, R. G. (2004). Mass spectrometry sampling under ambient conditions with desorption electrospray ionization. *Science, **306***(5695), 471-473.

Tinois, E., Tiollier, J., Gaucherand, M., Dumas, H., Tardy, M., & Thivolet, J. (1991). In vitro and post-transplantation differentiation of human keratinocytes grown on the human type IV collagen film of a bilayered dermal substitute. *Experimental Cell Research, **193***(2), 310-319.

Tortora, G. J., & Nielsen, M. T. (1995). *Human Anatomy*. Harper Collins College Pub.

van Eijl, S., Zhu, Z., Cupitt, J., Gierula, M., Götz, C., Fritsche, E., & Edwards, R. J. (2012). Elucidation of xenobiotic metabolism pathways in human skin and human skin models by proteomic profiling. *PloS One, **7***(7), e41721.

Villard, P. H., Sampol, E., Elkaim, J. L., Puyoou, F., Casanova, D., Sérée, E., Durand, A., & Lacarelle, B. (2002). Increase of CYP1B1 transcription in human keratinocytes and HaCaT cells after UV-B exposure. *Toxicology and Applied Pharmacology, **178***(3), 137-143.

Vondracek, M., Xi, Z., Larsson, P., Baker, V., Mace, K., Pfeifer, A., Tjälve, H., Donato, M. T., Gomez-Lechon, M. J., & Grafström, R. C. (2001). Cytochrome P450 expression and related metabolism in human buccal mucosa. *Carcinogenesis, **22***(3), 481-488.

Wang, K., & Guengerich, F. P. (2013). Reduction of aromatic and heterocyclic aromatic N-hydroxylamines by human cytochrome P450 2S1. *Chemical Research in Toxicology, **26***(6), 993-1004.

Warwick, E., Cassidy, A., Hanley, B., Jouni, Z. E., & Bao, Y. (2012). Effect of phytochemicals on phase II enzyme expression in infant human primary skin fibroblast cells. *British Journal of Nutrition, **108***(12), 2158-2165.

Wertz, P. W., Madison, K. C., & Downing, D. T. (1989). Covalently bound lipids of human stratum corneum. *Journal of Investigative Dermatology, **92***(1), 109-111.

Westermeier, R., & Marouga, R. (2005). Protein detection methods in proteomics research. *Bioscience Reports, **25***(1-2), 19-32.

Wickett, R. R., & Visscher, M. O. (2006). Structure and function of the epidermal barrier. *American Journal of Infection Control, **34***(10), S98-S110.

Wiegand, C., Hewitt, N. J., Merk, H. F., & Reisinger, K. (2014). Dermal xenobiotic metabolism: a comparison between native human skin, four in vitro skin test systems and a liver system. *Skin Pharmacology and Physiology, **27***(5), 263-275.

Wiseman, J. M., Ifa, D. R., Zhu, Y., Kissinger, C. B., Manicke, N. E., Kissinger, P. T., & Cooks, R. G. (2008). Desorption electrospray ionization mass spectrometry: Imaging drugs and metabolites in tissues. *Proceedings of the National Academy of Sciences, **105***(47), 18120-18125.

Wójtowicz, A., & Wietecha-Posłuszny, R. (2019). DESI-MS analysis of human fluids and tissues for forensic applications. *Applied Physics A, **125***(5), 1-9.

Yengi, L. G., Xiang, Q., Pan, J., Scatina, J., Kao, J., Ball, S. E., Fruncillo, R., Ferron, G., & Wolf, C. R. (2003). Quantitation of cytochrome P450 mRNA levels in human skin. *Analytical Biochemistry, **316***(1), 103-110.

Yousef, H., Alhajj, M., & Sharma, S. (2017). Anatomy, skin (integument), epidermis.

Zaphiropoulos, P. G. (1999). RNA molecules containing exons originating from different members of the cytochrome P450 2C gene subfamily (CYP2C) in human epidermis and liver. *Nucleic Acids Research, **27***(13), 2585-2590.

Zhu, Q., Hu, J., Liu, J., Lu, S., Liu, Y., & Wang, J. (2007). Stereoselective characteristics and mechanisms of epidermal carboxylesterase metabolism observed in HaCaT keratinocytes. *Biological and Pharmaceutical Bulletin, **30***(3), 532-536.

Chapter 2

Investigation of the Induction of Xenobiotic Metabolising Enzymes in a 3D Skin Model by RT-qPCR and Western blotting.

2.1 Introduction

Skin is the largest organ of the body, it is used as a defence against xenobiotics, such as drugs, environmental pollutants and cosmetics (Du *et al*., 2004*;* Luu-The *et al*., 2005). Samples of either *ex-vivo* human or animal skin or suitable skin models are required for the study of the absorption, and metabolism of topically applied xenobiotics (Warwick *et al*., 2012). The 7th Amendment to EU cosmetic directive of March 2009 banned the use of animals for both cosmetic testing and testing of their individual ingredients (Götz *et al*., 2012). As a consequence of this and the difficulties in obtaining *ex*-vivo human skin, the use of 3D skin model is of increasing interest in the study of xenobiotic metabolism (Jäckh *et al*., 2012). However, whilst a number of studies on Phase I xenobiotic metabolising enzymes (XMEs) gene/protein expression have been carried out previously, they are not well characterised in all commercially available skin models.

Luu and colleagues (Luu-The *et al*., 2009) described the mechanisms present in 3D skin models and native human skin that are involved in metabolism of endogenous and exogenous substrates of Phase I enzymes that involve both cytochrome P450 (*CYP*) processes and those that are not dependent on the presence of CYP. It has been suggested that although skin is an extrahepatic metabolizing organ, a limitiation of skin models are that the majority of Phase I and Phase II XMEs are not present in them (Saeki *et al*., 2002; van Eijl *et al*., 2012). Whilst, XMEs are less well studied in skin compared with other organs such as liver, kidney and lung (van Eijl *et al*., 2012) it has been demonstrated that their expression levels are lower when compared to human liver tissue and microsomes. In other studies, the major enzymes of Phase I and II biotransformation were also found to be at far higher levels in the liver compared to skin, making their detection challenging (Nebert *et al*., 2004; Oesch *et al*., 2014). Some Phase I enzymes have also been detected in cultured keratinocytes and up regulation has been induced (Gelardi *et al*., 2001).

Levels of cytochrome P450-dependent monooxygenase (*CYPs*) and flavin containing monooxygenase (*FMOs*) enzymes have been reported to be present at very low levels or non-existent in both human skin and 3D skin models (van Eijl *et al*., 2012). In contrast, *CYPs* and *FMOs* genes were clearly observed in human skin keratinocytes (Gelardi *et al*., 2001) and in different skin models (Wiegand *et al*., 2014). *CYPs* activity/genes have been reported to be up-regulated after exposure to drug inducers such as 3-methylcholanthrene (MC), β-naphthoflavone (βNF) and phenobarbital (PB). A recent proteomics study found that, overall, the Phase II XME levels were generally expressed at higher level than Phase I XMEs, especially *GSTs* and *NAT1* (van Eijl *et al*., 2012). The literature shows that

whilst, the cytochrome P450 (*CYPs*) gene such as, *CYP1B1*and *CYP3A5* have been observed at low levels in human skin and skin models, they are consistently reported to be not easy to measure accurately at a gene level in *in vivo* human skin and in 3D models because of the low concentrations (Luu-The *et al*., 2009).

Therefore to date, only a few publications have reported levels of gene expression of Phase I XMEs in 3D skin models. An excellent study by Wiegand *et al*., (2014) showed that the expression of genes for Phase I XME (including the cytochrome P450-dependent monooxygenase isoforms (*CYP1A1/1B1*, *2B6/2C18/2C8/2E1* and *3A4/3A5*), esterases (*CES1/2/3*) and Flavin containing monooxgenase (FMO1/2/3) and Phase II including N-acetyl transferases (*NAT1/*5), glutathione-S-transferases (*GSTA, GSTM, GSTP, GSTT*), sulfotransferases (*SULT*, *1A1*, *1E1* and *2B1*) and UDP-glucuronosyl transferase) level were detectable in native human skin and a range of skin models such as EpiDermFT™, PhenionR FT, AST-2000, the epidermal model EpiDerm™ and full-thickness models (Wiegand *et al*., 2014). These expression of Phase II enzymes was found to be to be more pronounced than those of the Phase I enzymes in human skin and Epo-Derm^{TM} model and these were predominantly expressed in the keratinocytes of epidermis layer (Wiegand *et al*., 2014).

2.2 Aims of the Chapter

There is an urgent need to examine the induction of the major Phase I metabolising enzymes including cytochrome P450-dependent monooxygenase, and flavin containing monooxygenase in a commercially available *in vitro* 3D skin model and compare levels that can be induced with native human skin to ascertain if the model can be made suitable for drug biotransformation studies. The present study addresses this need by employing Real Time qPCR and Western blot techniques.

2.3 Material and Methods

2.3.1 Ethical Statement

Native human skin was obtained from from University of Bradford Ethical Tissue REC reference17/YH/0086 (Bradford, UK). The protocols used in this work has been approved by Ethical Tissue Bradford as being covered by the ethics approval giving to Biomolecular Sciences Research Centre (Sheffield Hallam University) for the use of fresh human skin for drug metabolism studies.

2.3.2 Chemicals and Methods

RT-qPCR chemicals were purchased from Qiagen (Manchester, UK). RNease-Free DNase set, RNeasey® Mini Kit (50) include Wash Buffer RPE, Wash Buffer RWT, RNease free water and RNease Mini Spin Column and RTL lysis buffer and RT2 SYBR Green/ROXTM PCR master mix, RT2 First Strand Kit were obtained from Qiagen (Manchester, UK). β-naphthoflavone, phenobarbital and *all trans* retinoic acid, phosphate buffered saline and pure ethanol were purchased from Sigma-aldrich (Gillingham, UK). Nitrocellulose membrane, 4 –15 % Mini-PROTEAN® TGX™ Precast Protein Gels, Tris Buffered Saline with Tween-20 (TBST) were purchased from Bio-Rad (Bio-Rad, Germany). Anti-Cytochrome P450 1A1 antibody (ab3568), Rabbit Anti-FMO2 antibody (ab95977), and Rabbit Anti-CYP3A5 antibody (ab108624) obtained from Abcam (Bio-Rad, Germany).

The commercial 3D skin model "Labskin product" labskin1.1 lot 190926 was obtained from Innoven (U.K.) Ltd. (York, England). "Labskin" model is produced from primary fibroblasts and keratinocytes derived from human skin seeded 14 days at the air-liquid interface and cultured in a fibrin scaffold as illustrated in Chapter 1.4.2.

2.3.3 3D skin model and native human skin sample preparation

The 3D skin model tissue was cultured in 12-well plate with 4.5 mL of ready Labskin kit maintenance medium from Innoven company as secret information of culture medium for each well for 48 h as Labskin be viable for 14 days described in Chapter 1.4.2. Following this time the 3D skin model was removed from the well plate insert with a scalpel. If not used immediately, it was snap-frozen in liquid nitrogen cooled isopentane. The dermal and epidermal layers from the human skin and the 3D skin models (both epidermis and epiderms layers) were separated in PBS at 60 ºC for 2 minutes, prior to careful seperation using tweezers prior to total RNA extraction (described in section 2.3.5).

Native human skin was obtained from volunteers with their informed consent from University of Bradford Ethical Tissue REC reference17/YH/0086 (Bradford, UK). After surgery in the hospital, skin was kept in PBS and delivered to BMRC. The procedures have been approved by Ethical Tissue Bradford as being covered by the ethics approval given to the Biomolecular Science Research Centre (BMRC, Sheffield Hallam University). The methods for samples prepration were applied the same in 3D Labskin model sampes.

2.3.4 Enzyme induction

After delivery of the 3D skin model, the Phase I and II enzymes were activated a (cultured the 3D Labskin model in Labskin medium (4.5 mL per well) for 24 h at 37 °C and 5% CO_2 before the induction experiments. Induction experiments were conducted in 3D skin model medium by systematic treatment. The medium was replaced every 24 h. Induction was performed through the addition of inducers dissolved in dimethyl sulfoxide "DMSO" (Sigma-aldrich, Gillingham, UK). (Note: the maximum concentration of DMSO in the medium did not exceed 0.2%). The concentrations of 25 and 50 µM β-naphthoflavone (βNF), 2 mM phenobarbital (PB) and 20 µM *all-trans* retinoic acid (RA) were selected on the basis of previously described methodology (Wiegand *et al*., 2014). The incubation time used for induction was 72 h as systematic treatment. After incubation, the skin model samples were taken, snap-frozen with liquid nitrogen cooled isopentane for 2 min and then stored at −80 °C for total RNA extraction.

2.3.5 Total RNA extraction and cDNA synthesis

Total RNA was extracted from native human skin and 3D skin model according to "in-house" modification of the RNeasy mini kit protocol from Qiagen. About170 mg of 3D skin model (Labskin) and human skin tissues were homogenized in RLT buffer using a manual homogeniser (Ultra-Turrax, Germany). Pipetted and transfered 600 µL of homogenised sample to a QIA shredder mini spin column in a 2 mL collection tube and centrifuged sample for 4 seconds to transfer the lysis solution from the column to the collection tube and transfer into new 2 mL eppendorf tube. Add equal volume of 70% pure ethanol (~ 600 µL) to the 2 mL eppendorf for each sample. Then, mix thoroughly by pipetting up and down. Subsequently, the total RNA was loaded in RNease spin column (Qiagen Ltd, UK). DNase working solution (80 µL) was added of DNase working solution to each sample column and incubate for 20 minutes at room temperature. RW1 buffer 350 µL added and centrifuged at 10 000 rpm for 15 seconds at room temperature. Next, 500 µL buffer RPE to each column and centrifuged at 10000 rpm for 15 seconds at room temperature.

The total RNA was isolated in two separated elutions by RNease spin column (Qiagen Ltd, UK). Added 30 µL RNase free water to column and at 10 000 rpm for 1 minute at room temperature. Then, the total RNA concentration of each skin sample was measured by the Nanodrop system (Nanodrop Technologies, Rockland, Del., UK). Total RNA

volume was chosen to give 2 µg per 110 µL cDNA synthesis reaction in each preparation and stored at -80 ^{O}C until cDNA synthesis (Luu-The *et al*., 2009).

The total RNA (2 µg) was reverse transcribed into cDNA using RT First Strand kit (12) including genomic DNA elimination mix, incubated at (42 °C for 15 min and immediately at 95 °C for 5 min to stop the reaction) according to the supplier's instructions (Qiagen, UK). Then, cDNA synthesis of each preparation was stored at -20 °C before RT-qPCR assay analysis.

2.3.6 Quantitative real-time PCR analysis

Quantification of RNA was performed on a QuantStudio Real time PCR system (Thermofisher) using SYBR Green (RT2 SYBER® Green ROX ™, Qiagen) following the protocol from Qiagen. In brief, 25 µL of total RNA were analysed on fluorescent based Real time PCR. The thermocycler program of RT-qPCR was as follows: for denaturation 1 cycle at 50 °C for 2 min, annealing at 95 °C for 10 min, 40 cycles of 92 °C for 15 s and extending at 60 °C for 60 s. Template-negative reaction human genomic DNA contamination (HGDC) was used as HGDC control for PCR amplifications and PCR (PPC) as positive. Profiler PCR arrays have primers for the Phase I and Phase II genes expression. Assay for five reference genes (housekeeping genes) were used for human drug metabolism of Phase I and Phase II enzymes RT2 profiler ™ PCR Array (Biosciences/Qiagen) to normalise data (Hu *et al.*, 2010). The results were analysed according to the $2^{-\text{Delta delta CT}}$ method by using web-based RT2 Profiler™ PCR Array Data Analysis Software. The run was set for 40 cycles however, there was no enzymes expression after 33 cycles for Labskin and 35 cycles for human skin.

2.3.7 Immunoblotting

Treated and control 3D skin models were isolated in a similar manner to RNA extraction with PBS at 65 °C, then homogenized using a manual homogeniser (Ultra-Turrax, Germany) in potassium phosphate buffer (pH 7.25 contain 250 mM K_2HPO_4, 150 mM KCl and 1 mM EDTA) (van Eijl *et al*., 2012). Human skin, both treated and untreated 3D skin model and liver as control (microsomal and cytosol fractions) were separated by differential centrifugation as described previously (Gibbs *et al*., 2007), then stored at -80 °C until further analysis.

The protein concentrations of the supernatant and pellet were measured by using the BCA protein assay according to the manufacturer's protocol (van Eijl *et al*., 2012). Samples of microsomal fraction (60 µg) were separated by SDS-PAGE (120 V for 1 h)

and transferred onto nitrocellulose filters (70 V for 1 h). Membranes were blocked by blocking solution (5 % milk in TBS with 0.1 % Tween-20 TBST) for 1 h on a shaker at room temperature with milk powder (5 g) in TBST. Each protein was blocked by exposing the membranes to specific primary antibodies overnight at 4 °C. Antibodies were diluted at 1:1000 for Rabbit Anti-Cytochrome P450 1A1 antibody (ab3568), 1:250 for Rabbit Anti-FMO2 antibody (ab95977), and 1:1000 for Rabbit Anti-CYP3A5 antibody (ab108624). After proteind blocked with primry antibodies, these membranes washed with tris-buffered saline. Following that, the membranes were incubated with secondary antibody IRDye® 680RD Goat anti-Rabbit IgG (H + L). The bands of interest were determined using Li-COR imaging technique.

2.4 Results

2.4.1 Comparison of gene expression in *in vitro* 3D living skin equivalent model control (DMSO treated) with that in human skin

The expression of xenobiotic metabolism enzymes (XMEs) in a commercial 3D skin model (Labskin, UK) Ltd) has been compared with that following treatment with the XME inducers β-naphthoflavone (βNF), *all trans* retionic acid (RA) and phenobarbital (PB). RT-qPCR was performed on the total RNA from the commercial *in vitro* 3D living skin equivalent model (both control and induced) and native fresh human skin. The relative expression levels of the 84 genes of the Phase I (*CYP1A1, 3A5* and *1B1* and non-*CYP: FMO2*) and Phase II (*GST*) XMEs studied were all lower in the untreated 3D skin model compared to human skin (Figure 2.1 a and b).

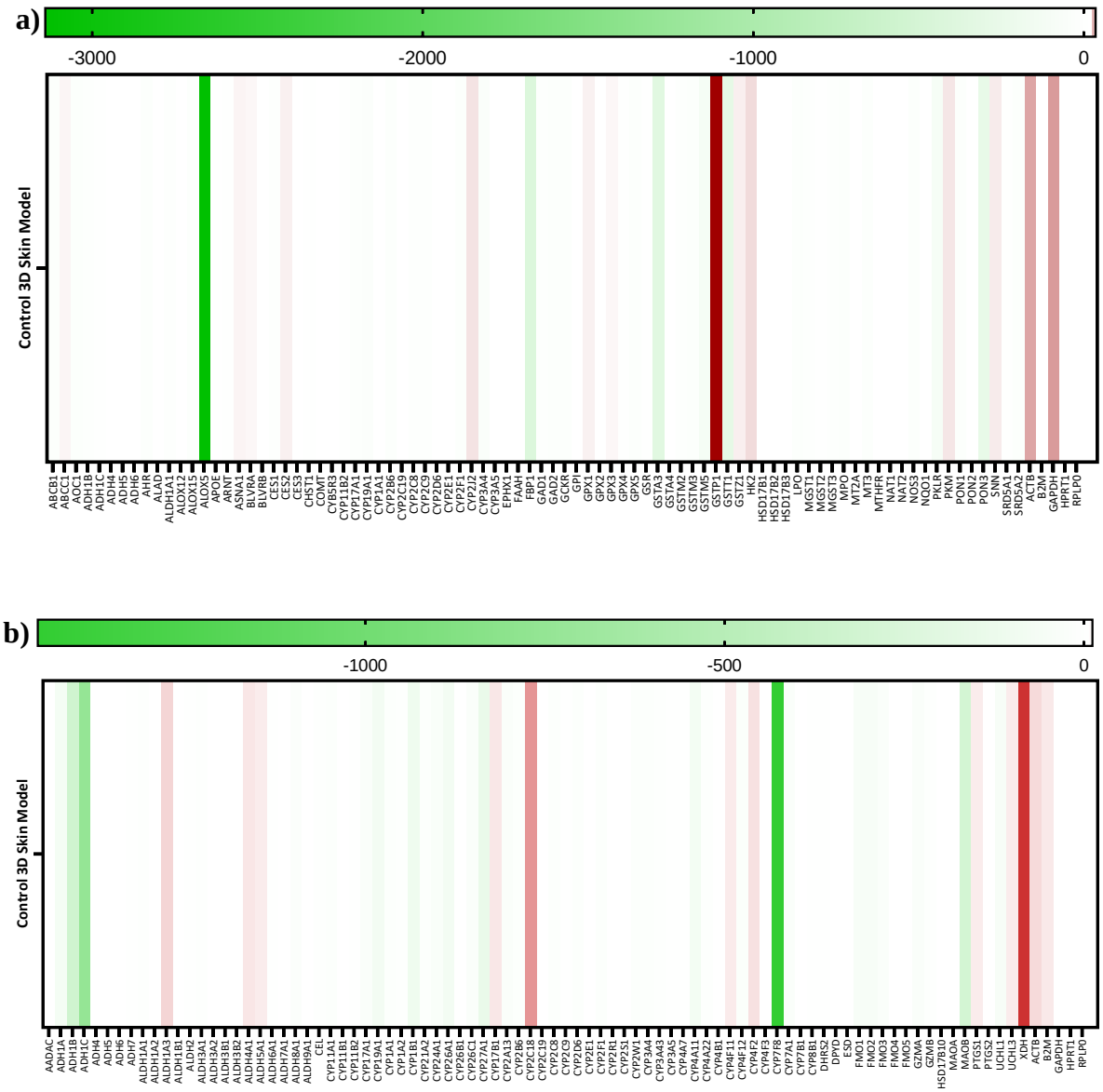

Figure 2.1 (a): Heatmap of 84 relative expression levels of the Phase I and Phase II basal genes corresponding to the xenobiotic metabolizing enzymes XMEs in *in vitro* control 3D skin model vs native human skin n=2 as duplicate. The signal intensity values are shown on a logarithmic scale. Lower signal intensity level of phase I and II genes are expresssed in green as downregulated (< 1 to white color, higher signal intensity level of phase I and II genes (>1) in white to red color as up-regulated. (b) Heatmap of 84 relative expression levels of the Phase I basal genes (*CYP1B1* and *FMO2*) corresponding to the xenobiotic metabolising enzymes XMEs *in vitro* control 3D skin model vs native human skin.

The levels of gene expression were expressed according to the fold change; while "no expression" was expressed to genes for which the Ct was below detectable limit up to 33 for 3D skin model. Ct value of 35 or more was considered to be absent in human skin.

All results are based on two biological repeats. The fold-change of the expression which is greater than one indicates an up-regulation while fold-change less than one indicate

down-regulation. All levels of XME were lower in the 3D skin model compared to the native human skin. The expression of the significant skin Phase I XME (*CYP1A1*, *CYP3A5*, *CYP1B1* and *FMO2*) were down-regulation with fold change (-10.26, -8.45, -115.56 and -18.76 respectively) compared with that those present in the native skin (Table 2.1).

Table 2.1: The expression level of *CYP1A1*, *CYP3A5*, *CYP1B1* and *FMO2* "down regulation" in the control "untreated" 3D Labskin model compared to human skin shows that the levels are significantly lower.

Enzyme	2 Δ Ct Human Skin	2 Δ Ct Untreated 3D skin model	Fold-Change
CYP1A1	6.80	10.16	-10.26
CYP3A5	2.06	5.14	-8.45
CYP1B1	4.41	11.26	-115.56
FMO2	5.58	9.81	-18.76

2.4.2 Comparison of gene expression in the control 3D living skin equivalent model (DMSO treated) with that following chemical induction of XME

The commercial skin model was treated with a series of known XME inducers, β-naphthoflavone (βNF), *all trans* retinoic acid (RA) and phenobarbital (PB). *CYP1A1* and *CYP3A5* genes were significantly ($P \leq 0.05$) upregulated in the 3D model treated with both βNF and PB compared with the control (Figure 2.2 a, b). *CYP1A1* expression was readily induced after exposure to 25 μM (4.65-fold) and with 50 μM βNF a 21.85-fold increase was observed (Table 2.2).

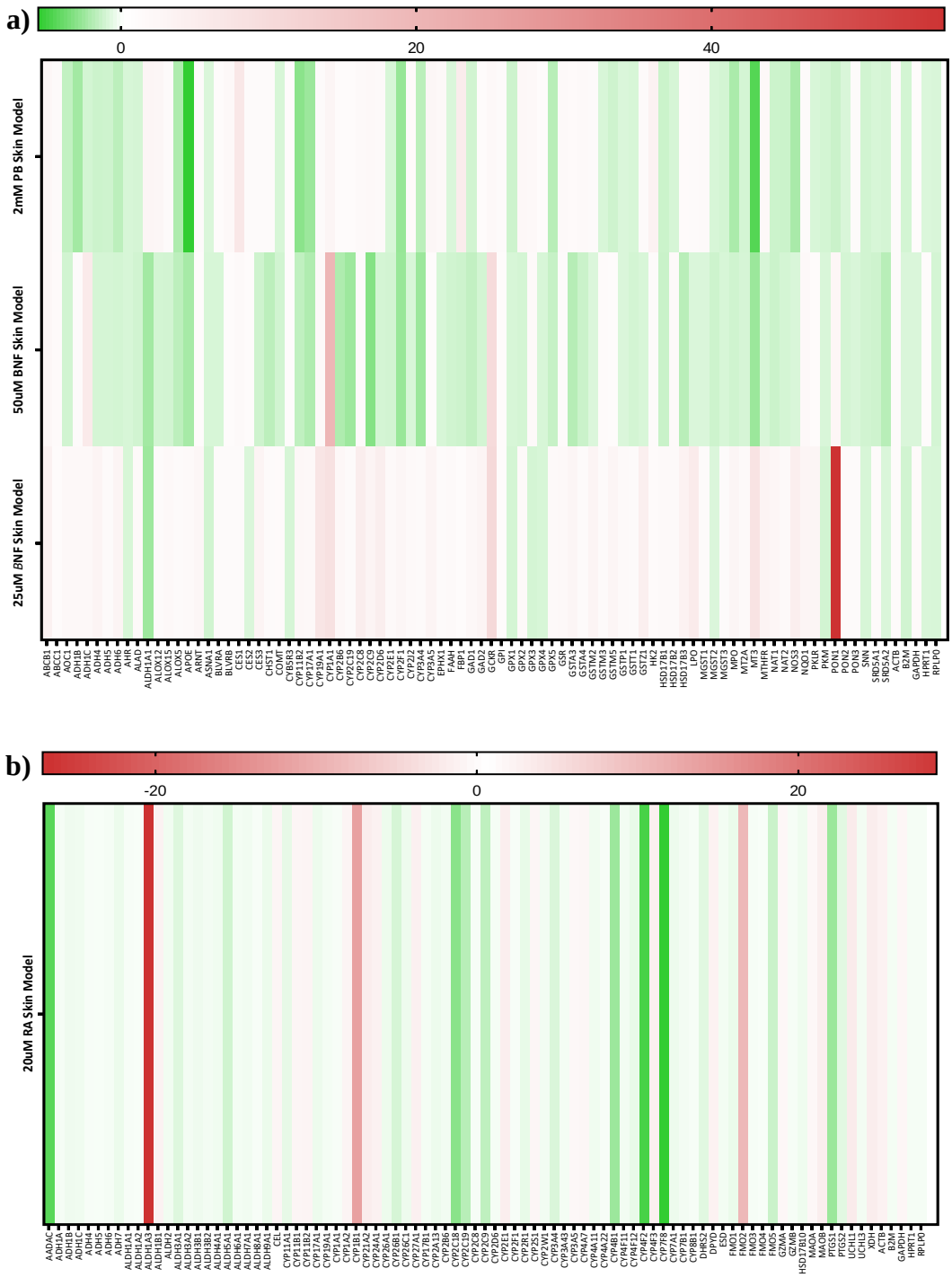

Figure 2.2 ***(a):*** Heatmap of 84 relative expression levels of the Phase I of the basal genes corresponding to the xenobiotic metabolising enzymes XMEs in *in vitro* control 3D skin model vs βNF (25 µM and 50 µM), and PB (2 mM) induced 3D skin mode. The signal intensity values are shown on a logarithmic scale. Lower level signal intensity genes are expresssed in green as down-regulation (< 1 to white color, higher level signal intensity (>1) in white to red color as up-regulation. Phase I of *CYPs*: *CYP1A1, CYP3A5* in red. ***(b)*** Heatmap of 84 relative expression levels of the Phase I the basal genes of *CYP1B1* and *FMO2* corresponding to the xenobiotic metabolising enzymes XMEs in *in vitro* control 3D skin model vs RA (20 µM) induced 3D skin model. The signal intensity values are shown on a logarithmic scale. Lower level signal intensity genes are expresssed in green (< 1) to white color, higher level signal intensity genes (>1) in white to red color. Phase I of *CYP1B1* and non-*CYPs* of *FMO2* in red**.**

CYP3A5 induction was also demonstrated following incubation with PB as shown in Figure 2.2 a. This resulted in a ~2.15-fold up-regulation compared with 3D Labskin control. The data showed in Figure 2.2 b, the intensity "level" genes of *CYP1B1* was induced with RA in red as up-regulated in 3D skin model at ~12.99-fold change compared with the control 3D model. Additionally, Non-*CYPs* of *FMO2* levels were significantly up-regulated in treated skin as following incubation with RA (Figure 2.2 b).

Table 2.2: The expression level for selected Phase I XMEs, *CYP1A1*, *CYP3A5*, *CYP1B1* and *FMO2* genes demonstrates up regulation in the induced 3D skin model compared to the control.

Enzyme	2 Δ Ct Untreated 3D Skin model	2 Δ Ct Treated 3D Skin model	Fold-Change	Inducers
CYP1A1	11.15	8.93	4.65	25 µM *B*NF
CYP1A1	12.61	8.16	21.85	50 µM *B*NF
CYP3A5	6.13	5.02	2.15	2 mM PB
CYP1B1	11.26	7.56	12.99	20 µM RA
FMO2	12.57	9.81	6.77	20 µM RA

Although this gene was present at low level -18.76-fold in the skin model control compared to human skin, RA induction led to a ~ 6.77-fold increase after 72 h systematic incubation (Table 2.2).

2.4.3 Comparison of the induced genes/protein level in the 3D skin model with that in native human skin

When comparing the findings for the induced 3D skin model with those present in the human skin, there was a clear variability, particularly with regards gene expression, of both the *CYP* and non-*CYP* of Phase I XMEs (Figure 2.3 a and Figure 2.3 b).

CYPs and *FMOs* are the main enzymes of Phase I drug metabolism in the liver, where they are expressed at much higher levels than in the 3D skin model and native skin. Phase I XMEs including *CYP1A1*, *CYP3A5*, *CYP1B1* and *FMO2* were expressed in human skin, but their expression levels were in both the control and induced skin models (Table 2.3).

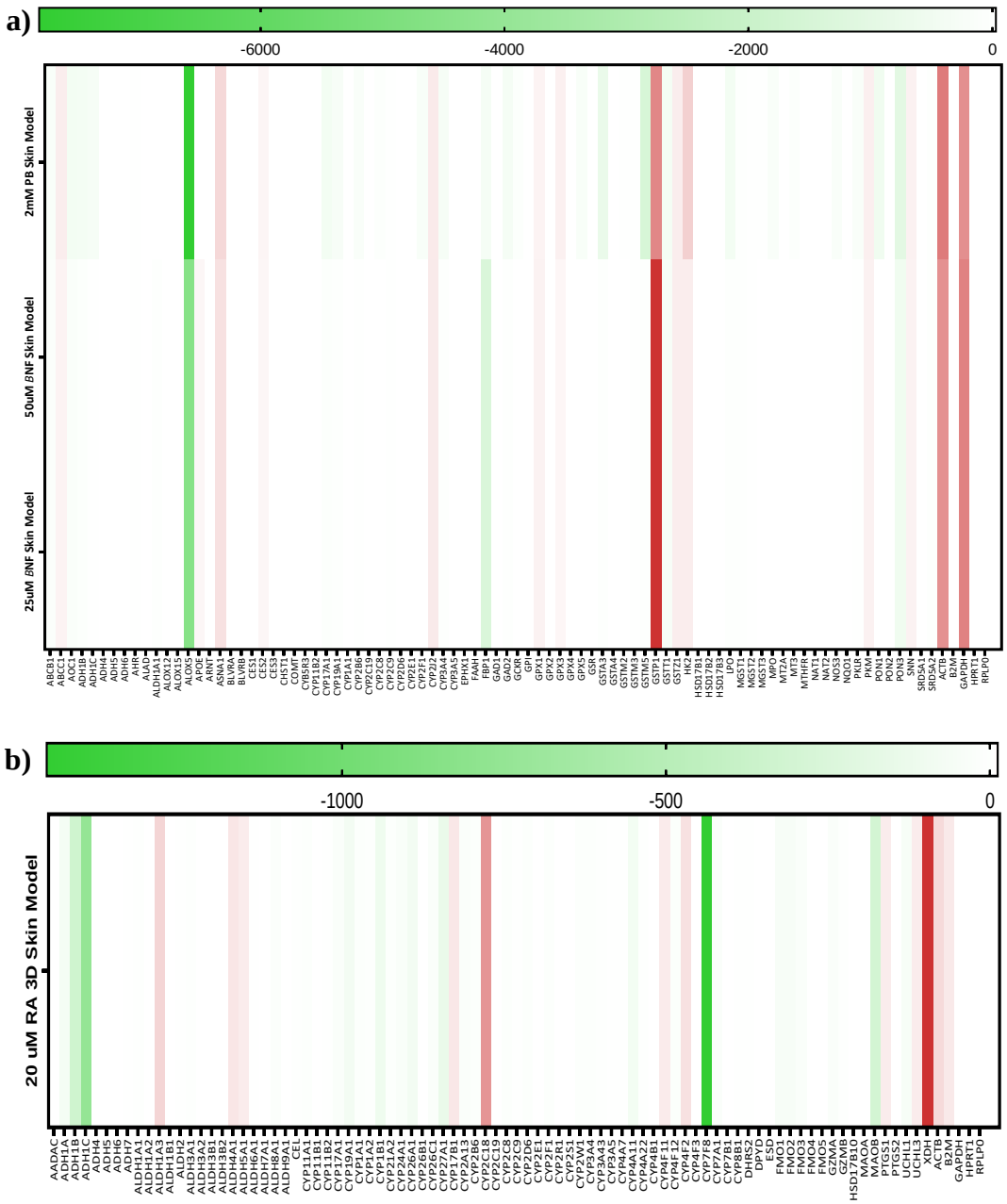

Figure 2.3 (a): Heatmap of 84 relative expression levels of the Phase I of the basal genes corresponding to the xenobiotic metabolising enzymes XMEs in βNF (25 µM and 50 µM), and PB (2 mM) induced 3D skin mode vs native human skin. The signal intensity values are shown on a logarithmic scale. Lower level signal intensity genes are expresssed in green (< 1) to white color, higher level signal intensity red (>1) in white to red color as up-regulation. Phase I of *CYPs*: *CYP1A1* and *CYP3A5* in green as dwon-regulation. **(b)** Heatmap of 84 relative expression levels of the Phase I of the basal genes corresponding to the xenobiotic metabolising enzymes XMEs in RA (20 µM) induced 3D skin mode vs native human skin. The signal intensity values are shown on a logarithmic scale. Lower level signal intensity genes are expresssed in green (< 1 to white color, higher level signal intensity genes (>1) in white to red color. Phase I of *CYP1B1*and non-*CYPs* of *FMO2* in green.

CYP1A1 and *CYP3A5* genes expressions were induced to a measurable level by βNF and RA induction in the Labskin model, but were still down-regulated compared with levels in human skin as shown in Figure 2. 3 a and Figure 2.3 b. The *CYP1A1* gene was induced

by systemic application of βNF in the 3D model by ~21.85-fold with no further increase after 72 h. The expression of *CYP3A5* was induced in the skin model by PB however, this was still down-regulated about -7.78-fold compared with those that present in human skin. *CYP1B1* was induced with RA about ~12.99-fold change in the induced 3D skin model, but still down-regulated -8.89-fold change in the induced 3D model comapred with native human skin as shown in Table 2.3. The induction of Phase I XME (FMO2) have shown significant increase by RA ~6.77-fold in this model but this was still -18.76-fold lower compared with human skin (Table 2.2 and 2.3).

Table 2.3: The expression level of *CYP1A1*, *CYP3A5*, *CYP1B1* and *FMO2* in induced 3D Labskin model compared to native human skin shows that the levels are still significantly lower even after induction.

Enzymes	2 Δ Ct Human Skin	2 Δ Ct Treated 3D model	Fold-Change	Inducers
CYP1A1	6.80	8.93	-4.37	25 µM *B*NF
CYP1A1	6.80	8.16	-2.54	50 µM *B*NF
CYP3A5	2.06	5.02	-7.78	2mM PB
CYP1B1	4.41	7.56	-8.89	20 µM RA
FMO2	5.58	9.81	-18.76	20 µM RA

Using Western blotting, *CYP1A1*, *CYP3A5* and *FMO2* protein were investigated in this study in skin model and native human skin. *CYP1A1* and *FMO2* protein expression could not be detected in either human skin or 3D skin model, while it was found to be expressed in liver as control Figure 2.4. In contrast, *CYP3A5* protein expression was detected in all induced 3D skin models and control. As shown in Figure 2. 4, the induced 3D skin model was shown to express more of *CYP3A5* than both the control and human skin.

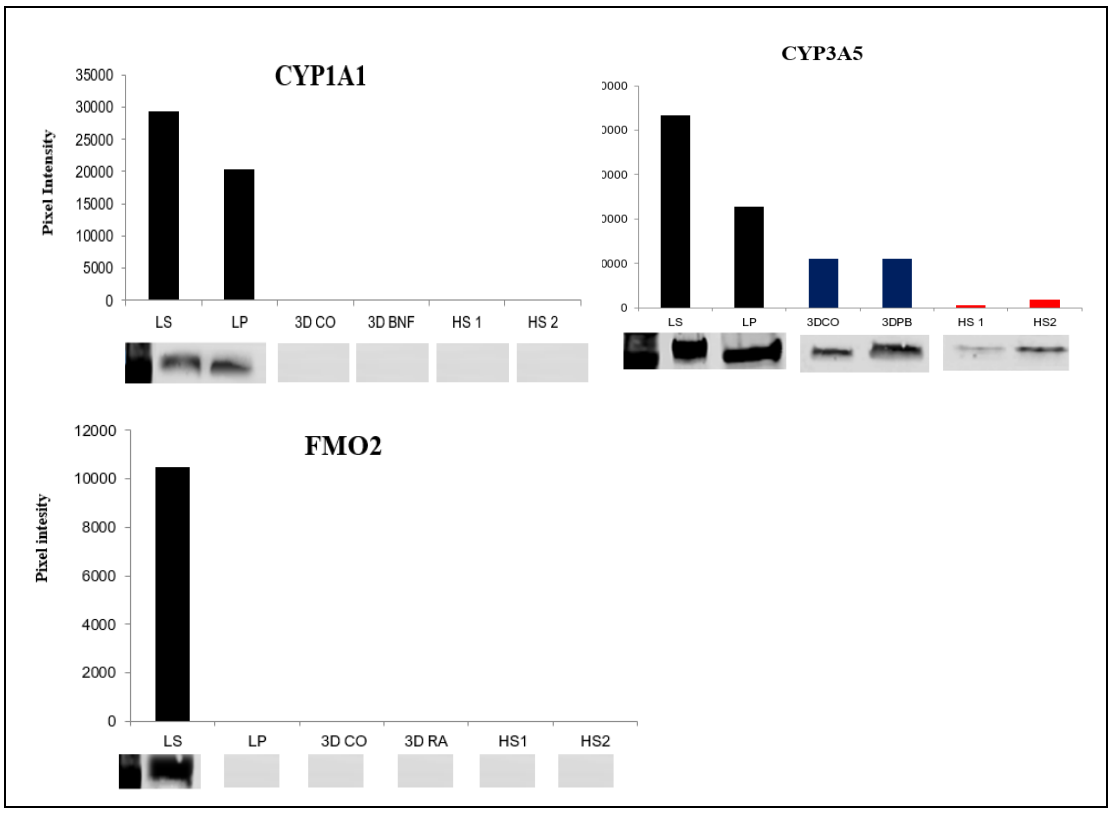

Figure 2.4: CYP1A1, CYP3A5 and FOM2 protein expression intensity in all skin by Western blot. The intensity of CYP1A1, CYP3A5 and FMO2 protein expression for several XMEs expressed in the induced 3D skin model and native human skin compared with liver as "control". "LS and LP" representative as liver tissue as control CYPs 1A1 and 3A5 proteins expression. The three proteins of phase I were detected as band and column intensity in 3D CO, 3D βNF, 3D RA and 3D PB representative as 3D skin model induced with βNF, RA and PB. In addition, thes proteins were detected in HS1 and HS2 representative as native (fresh) human skin tissues. (For full western blot shown in the appendix III).

2.5 Discussion

The aim of the study presented here was to compare the Phase I XME expression include cytochrome P450-dependent and flavin monooxygenase that are present in *in vitro* 3D skin model compared with human skin for drug biotransformation studies. The level of Phase I XMEs and their gene expression in 3D skin tissue model were measured after 72 h induction with a series of chemical inducers, β-naphthoflavone (βNF), *all trans* retinoic acid (RA) and phenobarbital (PB). RT-qPCR was performed on the total RNA from the commercial *in vitro* 3D living skin equivalent model "Labskin" (both untreated and treated) and native human skin. It has been demonstrated that the Phase I enzymes: *CYP1A1*, *CYP3A5* and *FMO2* were expressed in 3D Labskin model control albeit at a low level compared to that in human skin. Most enzymes detected in native skin, were also expressed in the Labskin model, however at greatly reduced levels.

There are a number of papers reporting the presence of non-*CYPs* and *CYPs* reviewed by Oesch *et al*., (2014), Oesch *et al*., (2018), Eilstein *et al*., (2015) and Delescluse *et al*., 1997) in skin. These enzymes were evident in our study including *CYP1A1*, *CYP3A5* and *FMO2* in Labskin model.

A variety of researchers have studied Phase I (*CYP* and non-*CYP*) XMEs gene, protein and activity in a range of epidermal skin models (EpiDerm, EpiSkin™, SkinEthic™ RHE, ORS-RHE), full thickness skin models (Skin™ FTM, Phenion FTM, Skin™ FTM) and Keratinocytes cells cultures (primary Keratinocytes, human keratinocyte cell line HCaT, NHEK) and native human skin (Jäckh *et al*., 2012; Luu-The *et al*., 2009; Wiegand *et al*., 2014; Bacqueville *et al*., 2017; Neis *et al*., 2010; Hu *et al*., 2010; Eilstein *et al*., 2015; Swanson, 2004; Ahmad & Mukhtar, 2004; Gibbs *et al*., 2007; Rolsted *et al*., 2008; Katiyar *et al*., 2000). Interestingly, the expression of Phase I XMEs (*CYP1A1*, *CYP3A5*, CYP1B1 and FMO2) of the 84 targetted genes Phase I (*CYP* and non-*CYP*) XMEs were overall relatively low level in 3D model compared to human skin. This shows a similar pattern to that previously reported for different skin models such as Phenion FT Skin Model, OS-REp and Monolayers (Baron *et al*., 2001; Wiegand *et al*., 2014). The *CYP1A1* gene were markedly down-regulated in 3D skin model control (untreated) compared to human skin. These observations support previous studies where the level of *CYP1A1* mRNA was below the limit of detection (Wiegand *et al*., 2014) in the dermis and epidermis compartments of the Phenion FT skin model. Treatment of Labksin for 72 h with a series of different inducers, such as β-naphthoflavone (βNF), *all trans* retinoic acid (RA) and phenobarbital (PB) up-regulated the expression of several XME. Interestingly, the increase in *CYP1A1* gene was significant in 3D model treated with βNF compared with untreated skin model. However, it was still markedly down-regulated compared to native human skin, *CYP1A1* expression was readily induced after exposure to 25 µM and 50 µM βNF. The induction response to 50 µM βNF after 72 h for *CYP1A1* was much higher than that induced by 25 µM βNF. This was found to be easily inducible in OS-REp model by βNF after 72 h systemic application (Bacqueville *et al*., 2017). CYP3A5 and FMO2 were markedly down-regulated in the 3D skin control (untreated) compared to human skin. The level of *CYP3A5* was extremely low in the Labskin model studied here and this has been previously reported in the ORS-RHE model (Neis *et al*., 2010).

CYP3A5 gene expression was also upregulated after exposure to PB in 3D skin model compared with the control. This induction resulted up-regulation in the induced Labskin.

Only Kazem *et al*., (2019). has studied that the levels phase I enzyme (CYP3A5 mRNA) in EpiSkinTM , EpiDerm, ORS-RHE using RT-qPCR.
In addition, *CYP1B1* was also up regulated, induced in our model by RA compared with the control Labskin. Although *CYP1B1* was increased in the RA induced 3D Labskin model, it was still low compared with native human skin. This was in agreement with the data in ORS-RHE model (Oesch *et al*., 2014).

Our skin model was used to understand the comparative levels of XMEs in respect of RNA level as well as their inducibility of enzymes in 3D skin compared with human skin. Using western blotting, *CYP1A1* and *FMO2* protein expression could not be detected in either human skin or 3D skin model whereas it was found to be expressed in liver as control to devloped WS method. This is in agreement with previous work where *CYP1A1* protein was not detected in whole human skin (comprising both epidermis and dermis) and in four *in vitro* epidermal skin models (van Eijl *et al*., 2012; Ahmad & Mukhtar, 2004). In contrast, CYP3A5 protein expression was observed in both the induced 3D skin model and control (DMSO). *FMO2* monooxygenase enzyme was induced by RA as gene expression but not observed as protein expression. This expression was significantly up-regulated in treated skin and in agreement with in human skin (Wiegand *et al*., 2014). Although this gene was at very low level in this skin model control compared to human skin, *all trans* retinoic acid induction gave an increase after 72 h systematic incubation. Phase I XME levels in the 3D skin model were mostly lower than that found in human liver (Wiegand *et al*., 2014).

Comparing gene expression in the control 3D the induced 3D skin equivalent model with the human skin, the expression of Phase I XMEs including *CYP1A1, CYP3A5, CYP1B1* and *FMO2* were expressed high level in human skin. A clear evidence of these CYPs in the 3D Labskin models were detected earlier (Oesch *et al*., 2018). The expression of these *CYPs* and non-*CYPs* investigated XMEs were still lower after induction in the Labskin skin model compared with those in native human skin. Notably, *CYP1A1* and *CYP3A5* genes were induced to measurable level by βNF and PB in this model but still down-regulated compared with levels in human skin. The *CYP1A1* gene was induced by systemic application of βNF in 3D model with no further increased upon 72 h. This induced level of *CYP1A1* did not get to the levels expressed in the native human skin. Using Western blotting of CYP1A1 protein was investigated that there was no protein

expressed in any skin tissue studied as showed by van Eijl *et al*., (20212). In contrast, normal human skin was shown to be expressed at high level of *CYP3A5* than both that presented in the control and induced 3D skin model. This expression was expressed and induced in the Labskin model by PB. However, this was still down-regulated compared with that present in human skin.

The induction of Phase I XME CYP1B1 and FMO2 protein have shown significant increase by induction with RA in this model compared with 3D skin conrol. While the phenobarbital inducer activated for CYP3A5 protein expression, levels of CYP3A5 protein were at a lower level in the human skin and 3D skin model than that shown in liver. FMO2 protein expression could not be detected at the the protein level in this model.

The RT-qPCR raw data of this chapter has been attached in the appendix I link page (220).

2.6 Conclusion

The overall aims of the current study was to make comprehensive characterization of the expression level of Phase I XMEs in the commericially available 3D Labskin model and to characterize them so that it could be used as a suitable surrogate for native human skin for metabolism assays. Overall, the *in vitro* 3D skin models showed distinctive profiles at the levels of CYP1A1, CYP3A5, CYP1B1 and FMO2 expression and enzymatic activity with regard to xenobiotic metabolism. A comparison of the expression in the Labskin skin model control, the induced model and the human skin, showed that the level of gene expression of Phase I XMEs including CYP1A1, CYP3A5, CYP1B1 and FMO2 level were lower in the 3D skin model compared with that presented in human skin. Chemical induction increased these levels but still not to those in native human skin. Understanding the relationship between the levels of XME in 3D skin models and human skin could potentially be used to develop computer models that would be able to predict human skin data from that obtained from 3D models. The data of phase I and II indicate that the Labskin model appears to be a valuable, robust *in vitro* tool improved non-animal models as an alternative methods for metabolism of cutaneous exposures.

2.7 References

Ahmad, N., & Mukhtar, H. (2004). Cytochrome p450: a target for drug development for skin diseases. *Journal of Investigative Dermatology, **123***(3), 417-425.

Bacqueville, D., Jacques, C., Duprat, L., Jamin, E. L., Guiraud, B., Perdu, E., Bessou-Touya, S., Zalko, D., & Duplan, H. (2017). Characterization of xenobiotic metabolizing enzymes of a reconstructed human epidermal model from adult hair follicles. *Toxicology and Applied Pharmacology, **329***, 190-201.

Baron, J. M., HoÈller, D., Schiffer, R., Frankenberg, S., Neis, M., Merk, H. F., & Jugert, F. K. (2001). Expression of multiple cytochrome p450 enzymes and multidrug resistance-associated transport proteins in human skin keratinocytes. *Journal of Investigative Dermatology, **116***(4), 541-548.

Delescluse, C., Ledirac, N., de Sousa, G., Pralavorio, M., Botta-Fridlund, D., Letreut, Y., & Rahmani, R. (1997). Comparative study of CYP1A1 induction by 3-methylcholanthrene in various human hepatic and epidermal cell types. *Toxicology in Vitro, **11***(5), 443-450.

Eilstein, J., Léreaux, G., Arbey, E., Daronnat, E., Wilkinson, S., & Duché, D. (2015). Xenobiotic metabolizing enzymes in human skin and SkinEthic reconstructed human skin models. *Experimental Dermatology, **24***(7), 547-549.

Gelardi, A., Morini, F., Dusatti, F., Penco, S., & Ferro, M. (2001). Induction by xenobiotics of phase I and phase II enzyme activities in the human keratinocyte cell line NCTC 2544. *Toxicology in Vitro, **15***(6), 701-711.

Gibbs, S., van de Sandt, Johannes JM, Merk, H. F., Lockley, D. J., Pendlington, R. U., & Pease, C. K. (2007). Xenobiotic metabolism in human skin and 3D human skin reconstructs: a review. *Current Drug Metabolism, **8***(8), 758-772.

Götz, C., Pfeiffer, R., Tigges, J., Blatz, V., Jäckh, C., Freytag, E., Fabian, E., Landsiedel, R., Merk, H. F., & Krutmann, J. (2012). Xenobiotic metabolism capacities of human skin in comparison with a 3D epidermis model and keratinocyte-based cell culture

as in vitro alternatives for chemical testing: activating enzymes (Phase I). *Experimental Dermatology*, ***21***(5), 358-363.

Hewitt, N. J., Edwards, R. J., Fritsche, E., Goebel, C., Aeby, P., Scheel, J., Reisinger, K., Ouédraogo, G., Duche, D., & Eilstein, J. (2013). Use of human in vitro skin models for accurate and ethical risk assessment: metabolic considerations. *Toxicological Sciences*, ***133***(2), 209-217.

Hu, T., Khambatta, Z. S., Hayden, P. J., Bolmarcich, J., Binder, R. L., Robinson, M. K., Carr, G. J., Tiesman, J. P., Jarrold, B. B., & Osborne, R. (2010). Xenobiotic metabolism gene expression in the EpiDerm™ in vitro 3D human epidermis model compared to human skin. *Toxicology in Vitro*, ***24***(5), 1450-1463.

Jäckh, C., Fabian, E., van Ravenzwaay, B., & Landsiedel, R. (2012). Relevance of xenobiotic enzymes in human skin in vitro models to activate pro-sensitizers. *Journal of Immunotoxicology*, ***9***(4), 426-438.

Katiyar, S. K., Mukhtar, H., & Matsui, M. S. (2000). Ultraviolet-B exposure of human skin induces cytochromes P450 1A1 and 1B1. *Journal of Investigative Dermatology*, ***114***(2), 328-333.

Kazem, S., Linssen, E. C., & Gibbs, S. (2019). Skin metabolism phase I and phase II enzymes in native and reconstructed human skin: A short review. *Drug Discovery Today*, ***24***(9), 1899-1910.

Luu-The, V., Duche, D., Ferraris, C., Meunier, J., Leclaire, J., & Labrie, F. (2009). Expression profiles of phases 1 and 2 metabolizing enzymes in human skin and the reconstructed skin models Episkin™ and full thickness model from Episkin™. *The Journal of Steroid Biochemistry and Molecular Biology*, ***116***(3-5), 178-186.

Luu-The, V., Paquet, N., Calvo, E., & Cumps, J. (2005). Improved real-time RT-PCR method for high-throughput measurements using second derivative calculation and double correction. *BioTechniques*, ***38***(2), 287-293.

Nebert, D. W., Dalton, T. P., Okey, A. B., & Gonzalez, F. J. (2004). Role of aryl hydrocarbon receptor-mediated induction of the CYP1 enzymes in environmental toxicity and cancer. *Journal of Biological Chemistry, **279(***23), 23847-23850.

Neis, M. M., Wendel, A., Wiederholt, T., Marquardt, Y., Joussen, S., Baron, J. M., & Merk, H. F. (2010). Expression and induction of cytochrome p450 isoenzymes in human skin equivalents. *Skin Pharmacology and Physiology, **23***(1), 29-39.

Oesch, F., Fabian, E., Guth, K., & Landsiedel, R. (2014a). Xenobiotic-metabolizing enzymes in the skin of rat, mouse, pig, guinea pig, man, and in human skin models. *Archives of Toxicology, **88***(12), 2135-2190.

Oesch, F., Fabian, E., Guth, K., & Landsiedel, R. (2014b). Xenobiotic-metabolizing enzymes in the skin of rat, mouse, pig, guinea pig, man, and in human skin models. *Archives of Toxicology, **88***(12), 2135-2190.

Oesch, F., Fabian, E., & Landsiedel, R. (2018). Xenobiotica-metabolizing enzymes in the skin of rat, mouse, pig, guinea pig, man, and in human skin models. *Archives of Toxicology, **92***(8), 2411-2456.

Rolsted, K., Kissmeyer, A., Rist, G. M., & Hansen, S. H. (2008). Evaluation of cytochrome P450 activity in vitro, using dermal and hepatic microsomes from four species and two keratinocyte cell lines in culture. *Archives of Dermatological Research, **300***(1), 11-18.

Saeki, M., Saito, Y., Nagano, M., Teshima, R., Ozawa, S., & Sawada, J. (2002). mRNA expression of multiple cytochrome p450 isozymes in four types of cultured skin cells. *International Archives of Allergy and Immunology, **127***(4), 333-336.

Swanson, H. I. (2004). Cytochrome P450 expression in human keratinocytes: an aryl hydrocarbon receptor perspective. *Chemico-Biological Interactions, **149***(2-3), 69-79.

van Eijl, S., Zhu, Z., Cupitt, J., Gierula, M., Götz, C., Fritsche, E., & Edwards, R. J. (2012). Elucidation of xenobiotic metabolism pathways in human skin and human skin models by proteomic profiling. *PloS One, **7***(7), e41721.

Warwick, E., Cassidy, A., Hanley, B., Jouni, Z. E., & Bao, Y. (2012). Effect of phytochemicals on phase II enzyme expression in infant human primary skin fibroblast cells. *British Journal of Nutrition*, ***108***(12), 2158-2165.

Wiegand, C., Hewitt, N. J., Merk, H. F., & Reisinger, K. (2014). Dermal xenobiotic metabolism: a comparison between native human skin, four in vitro skin test systems and a liver system. *Skin Pharmacology and Physiology*, ***27***(5), 263-275.

Chapter 3

Expression and Induction of Xenobiotic Metabolising Enzymes in a 3D Skin Model studied by using LC-MS/MS.

3.1 Introduction

Living skin equivalent models (LSE) have the capacity to metabolise xenobiotics, however, knowledge of xenobiotic metabolising enzymes (XME) in human skin and skin models and their role in detoxification metabolism studies of the topically applied drugs compounds is incomplete (Hu *et al*., 2010). There is increasing evidence indicating that epidermal XMEs and transport proteins play significant roles in the function of skin (Jugert *et al*., 1994; Du, *etal*., 2006) in addition to its barrier function. These XMEs including Phase I (*e.g*. cytochrome P450s) and Phase II (*e.g.* glutathione S-transferase) enzymes are mostely located in epidermis (in keratinocytes), levels are lower than those detected in human liver and are thus more difficult to detect (Gibbs *et al*., 2007; Oesch *et al*., 2014; Luu-The *et al*., 2009). There is increasing realization of the importance of CYPs and GST in extra-hepatic metabolism. However, knowledge of these expression of specific Phase I and Phase II XMEs in 3D skin models and human skin are limited and no systematic study of the model used in this work, Labskin a LSE produced by Labskin UK Ltd has been conducted.

As discussed in Chapter 1, only a few studies have been investigated at the expression of Phase I and Phase II XMEs proteins and their levels in human skin, 3D skin models and human skin (Gelardi *et al*., 2001; van Eijl *et al*., 2012; Wiegand *et al*., 2014).

However, induction of CYPs and GSTs in skin following exposure to β-naphthoflavone (βNF), phenobarbital (PB), and methylcholanthrene (MC) (Gelardi *et al*., 2001; Harris *et al*., 2002) has been demonstrated. Human keratinocyte cell line such as NCTC cell line (Gelardi, *et al*., 2001) and reconstructed epidermal models (Harris *et al*., 2002; Ahmad & Mukhtar, 2004), have been incubated with βNF, 3-MC and PB, basal and induced levels of mainly CYPs and GST activities that were detected and significant increase over those expressed in human skin.

LC-MS/MS has been used to study Phase I and II XME protein expression in skin (van Eijl *et al*., 2012; Couto *et al*., 2021). Both Phase II and II XMEs in whole *ex vivo* human skin (about 10 donors) and commericial *in vitro* epidermal models, such as Episkin, RHE, and Labskin have been studied (van Eijl *et al*., 2012; Couto *et al*., 2021). Phase II XME levels were reported to be generally expressed at a higher level than Phase I XMEs, especially GSTs (van Eijl *et al*., 2012). This was confirmed by Couto *et al*., (2021). In the

work of Couto the Phase II XME glutathione S-transferase was reported to be the most abundant XME in Labskin compared to human skin.

However, cytochrome P450 (CYPs) have only been observed at low levels in human skin and 3D skin models. In addition, CYPs enzymes also reported no or a low expression for the substrates tested in *ex-vivo* human skin and the *in vitro* 3D skin model "LabSkin" (Hewitt *et al*., 2013; Couto *et al*., 2021). It is, however, consistently reported that they are not easy to measure accurately at the gene or protein level in *in vivo* human skin and in 3D models because of the low levels abundance present (Luu-The *et al*., 2009). These data suggested that there is a need to further characterise the inducibility of Phase I and Phase II XMEs pathways in Labskin and to compare native and induced levels with those in human skin using more advanced MS techniques than those used in previous studies in chapter 2 of the thesis up-regulation of XME gene expression in a 3D Living skin equavelent model following chemical induction was demonstrated. In this chapter the expression of corosponding protein is studied using a LC-MS/MS.

3.2 Aims of the Chapter

In this Chapter, we set out to determine and the induction of Phase I and Phase II XMEs (including CYPs and GSTs) at the protein level in the commericial 3D skin model (LabSkin) and compare these with native human skin using LC-MS/MS.

3.3 Material and methods

3.3.1 Ethical statement

Native human skin was obtained and descriped in Chapter 2.3.1.

3.3.2 Chemicals and Materials

Trifluoroacetic acid (TFA), 1, 4-Dithiothreitol (DTT), iodoacetamide (IA) and copper II were purchased from Sigma-aldrich (Gillingham, UK). Trypsin was purchased from Promega (Chilworth, UK). LC-H_2O, LC-grade acetonitrile and 0.1% formic acid were obtained from Fisher Scientific (Loughborough, UK). The other chemicals and materials used were given in Chapter 2.3.2.

3.3.3 Enzyme induction

The commercial 3D skin model "Labskin product" labskin 1.3 lot 190573 was obtained from Innoven (York, UK). "Labskin" samples were generated and cultured as previously reported in Chapter 1.4.2. Induction experiments were conducted in 3D skin model

medium via systematic treatment as described in Chapter 2.4. The concentrations of β-naphthoflavone (βNF), phenobarbital (PB) and *all trans* retinoic acid (RA) were selected in Chapter 2.3.4.

3.3.4 3D skin model and native human skin sample preparation

Following induction, the dermal and epidermal layers from about 200 mg of the treated and control (untreated) 3D skin models and fresh native human skin were isolated as previously described for RNA extraction *i.e.* PBS at 65 °C for 2 min, then homogenization with a manual homogeniser (Ultra-Turrax, Germany) in potassium phosphate buffer (250 mM K_2HPO_4, 150 mM KCl and 1 mM EDTA, pH 7.25) (van Eijl *et al*., 2012).

Following homogenization, the microsomal and cytosolic fractions were separated by the differential centrifugation as described previously (van Eijl *et al*., 2012) The skin lysates were initially centrifuged at 14000 g at 4 °C for 10 min (Centrifugation, Micro Star17R Microcentrifuge, Germany). The supernatant was collected and high centrifuged at 105,000 g for 1 h at 4 °C (Optima^{TM} Ultracentrifuge, Beckman Coulter, Germany) as decribed previously (Boobis *et al*., 1980), then stored at -80 °C for further analysis.

The protein concentrations of the supernatant and pellet were determined in triplicate by bichinchonic acid (BCA) protein assay according to the manufacturer's protocol (Smith *et al*., 1985). The assay was performed as follows: 0.4 g of copper II was dissolved in total 10 mL of distilled water (ddH_2O). About 1mL of this copper II solution was transferred to 49 mL of bicinchoninic acid as solution for protein detection. A BCA solution was made of 0.1 g of albumin in 10 mL of ddH_2O and used to prepare protein concentration standards between 0.1-2.0 mg/mL. In the 96 well plate, 10 µL of each protein concentration was pipetted in triplicate. To each well of 96 well plate, 10 µL of BCA soulution was added to each well protein detection, and left for 30 min. The 96 ready well plate was read at 570 nm absorbance by Multiskan EX Absorbance Reader (Fisher Scientific, Loughborough, UK).

3.3.5 Enzymatic digestion (peptides extraction)

Samples of protein were performed according to the manufacturer's instructions (In-Solution Tryptic Digestion) protocol. Briefly, 30 µg of protein in digestion buffer (50 mM ammonium bicarbonate) was denatured and reduced according to in-solution tryptic digestion protocol. Reduction and alkylation were performed by incubation with 100 mM DTT at 95 °C for 5 min and 100 mM iodoacetamide in the dark for 30 min, respectively.

Trypsin digestion (20 ng/µL) was performed in 50 mM ammonium bicarbonate overnight. Before Zip Tip processing, the trypsin reaction was stopped by adding 10 µL formic acid to each sample, and then storage at -20 °C for further analysis.

Milipore ZipTip C18 (Size P10; Zip Tips) was preformed to clean-up peptides according to Sigma Zip tips protocol (Sigmaaldrich, Gillingham, UK).

- Stock solution: 100% ACN aq. (1000 µL ACN)
- Washing solution : 0.1% TFA aq. (100 µL 1% TFA, 900 µL dd H2O)
- Mixed Elution bufer : 50% ACN in 0.1% TFA (500 µL Acetonitrile, 500 µL 0.1% TFA)

3.3.6 Instrumentation

3.3.6.1 LC-MS/MS analysis.

LC-MS/MS analyses were carried out using a Xevo G2- XS QTof mass spectrometry (Waters Coorporation, Manchester, UK.) set to ESI^+ ionization mode. The spectra were acquired in positive mode. Peptide mixtures were obtained from in-solution trypsin digest extracted from untreated and treated 3D skin model and human skin samples (12 extracts: 6 microsomal and 6 pellets, as described above) were injected separately under the same experimental conditions.

The separation was performed on an Acquity UPLC® peptide GSH^{TM}-C18 (Waters^{TM}, UK) microbore column (2.1 mm x 100 mm, 1.7 µm). Peptides were separated using a 85 min gradient of mobile phase B 95% (acetonitrile) and mobile phase A (5% containing 0.1 % formic acid). The flow rate was 200 µL/min. Each MS scan range was scanned and acquired in a Xevo G2XS QTof instrument with (100 –1500 *m/z* range) in Q-TOF MS^e mode (Quadripole-time of flight mass spectrometry where E represents collision energy) and Identity E were used in conjunction with LC (capillary liquid chromatography) for robust quantification of a large number of proteins. The maximum ion injection 5 µL. The MS parameters as follows: capillary voltage, 3.0 kV; cone voltage, 30.0 V; source temperature, 150 ºC; desolvation temperature, 500 ºC; desolvation gas, 1000 L/h; and cone gas, 150 L/h. Argon was used as a collision gas and the collision energy was set at 15 eV.

3.3.7 Data Analysis

3.3.7.1 LC-MS/MS data analysis

LC-MS/MS data were processed using MassLynx™ software (Waters Corporation, UK) and Progenesis QIP software (https://www.nonlinear.com/progenesis/qi-for-proteomics). The protein cut off used ≤ 0.05. In addition, Panther software (http://www.pantherdb.org) and Reactome pathway database software (https://reactome.org) were used to assign protein functional classes.

3.4 Results and Discussion

The main purpose of developing skin models is to obtain models able to mimic the structure and function of *in vivo* skin, such as gene and protein expression of Phase I and Phase II XMEs (Kazem *et al*., 2019). The aim of this study was to detect and measure the levels of the protein expression of Phase I and Phase II XMEs in the 3D skin models and to characterise them as a suitable surrogate for native human skin for metabolism assays by liquid chromatography-tandem mass spectrometry (LC-MS/MS). Extracted proteins from human skin and skin models samples were measured by the BCA assay as standard shown in Figure 3.1. This assay is relatively easy to perform and sensitive at 20 ng level. The BCA assay was applied to determine relative concentrations protein in homogenate supernatants and pellets of Labskin and human skin tissues as described by Smith *et al*., (1985).

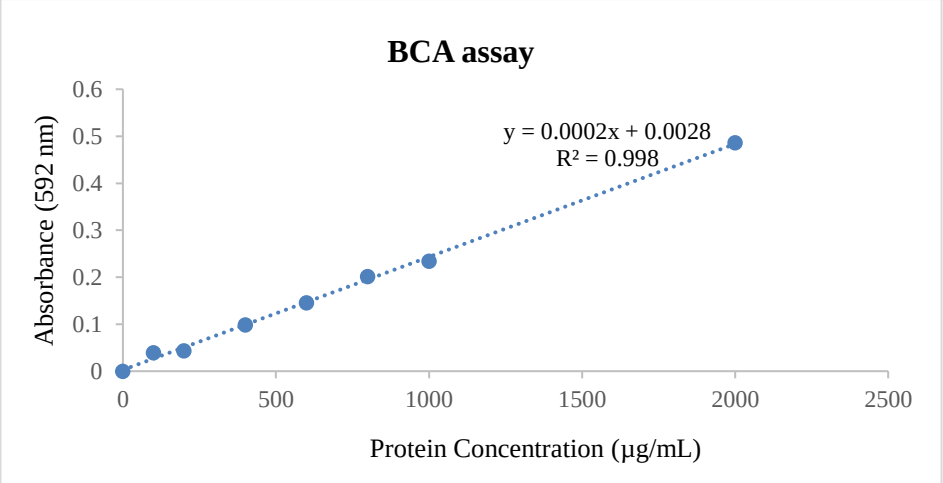

Figure 3.1: A simple protein standard curve is created with dilutions of BCA. Each standard dilution in triplicate absorbance (562 nm) was plotted on protein concentration (µg/mL).

Total protein concentration was found to be between 1500-2000 µg/ml.

Several of the xenobiotic metabolising enzymes (XMEs) in skin were expressed and induced at the RNA level have also expressed in this study at the protein level. From the LC/MS/MS data set enzymes detected include alcohol dehydrogenase class beta (ADH beta), alcohol dehydrogenase class III (ADHIII), aldehyde dehydrogenase 1A1 (ALDH 1A1), aldehyde dehydrogenase 9A1 (ALDH9A1), epoxide hydrolase (EPHX 2), cytochreome P 450 (CYPs: CYP1B1, CYP3A6, CYP11B2, CYP152A1, and CYP78A3) and peroxiredoxin-1 (PRDX1) of Phase I XME proteins and glutathione S-transferase (GSTs: GSTP1, GSTO1) and acetyl-CoA acetyltransferase 1 (ACAT1) of Phase II XME proteins expression were overall detected in Labskin models as well as similar in native human skin. However, these expression of enzymes were found to be at low levels in 3D skin models control. From the total data set, the data for Phase I and Phae II XME were extracted and are shown below.

In a previous study, almost all of XME proteins observed in Labskin models and native human skin were detected as proteins and genes in skin by Oesch *et al*., (2018). Support for the abundance of Phase I and II XMEs: alcohol/aldehyde dehydrogenase, epoxide hydrolase, peroxiredoxin glutathione S-transferase and acetyl-CoA acetyltransferase comes from a report by Couto *et al*., (2021), who first time used a proteomics approach to study Labskin and human skin, but here none of the CYPs proteins were detected.

In order to determine whether CYPs could be detected and induced in 3D skin model, induction experiments were carried out using βNF, RA, PB inducers. LC-MS/MS was performed separately on both microsomal and cytosol fractions and the data combined in the Progenesis QIP software. All identified proteins were classified based on protein ontology (GO). About 327 function hits of 313 total proteins were significant, discovering the functional protein relationships of the XMEs. These were classified into 7 clusters as seen in Figure 3.2.

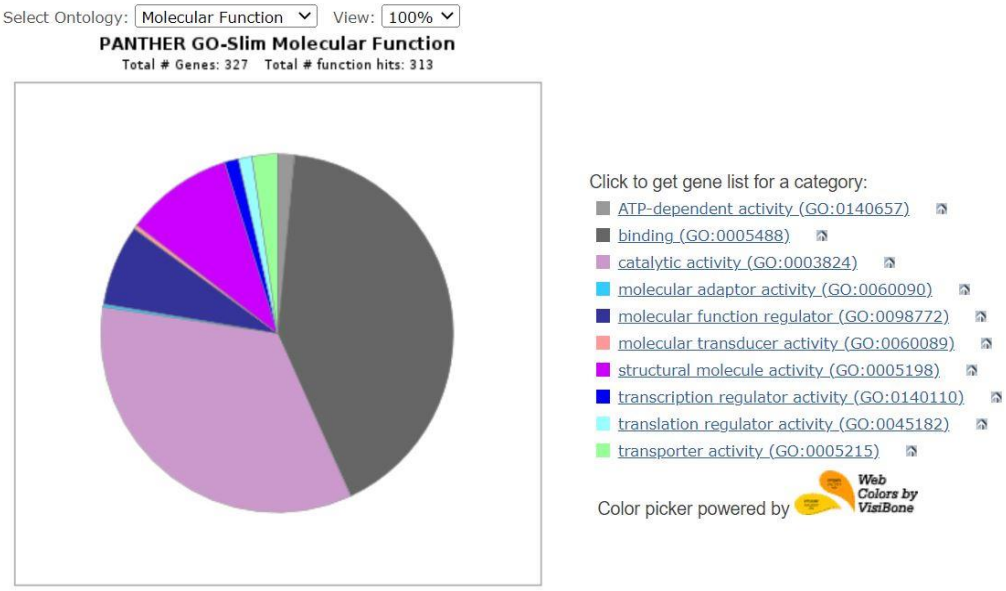

Figure 3.2: Pie chart illustrating the panther software results of molecular functions characterised in the list XMEs of protein families in 3D skin model control Vs Induced 3D skin microsomal and cytosolic fraction using LC-MS/MS. A total of 327 of protein and 313 total function hits were initially included in the exprements analysis. The percentage of function hits is: Binding GO:0005488 and catalytic activity GO:0003824 percentage were similar representing ~130 and ~107 proteins abundance of the function hits. ~23 molecular function regulator hits GO:0098772 and ~1 molecular tranducer activity GO:0060089. The structure molecule activity GO:0005198 acount for ~31 of the function hits. The remaining ~11 function hits are contained of translator regulator activity GO:0045182 and transporter activity GO:0005215.

The majority of Phase I and Phase II XME (including the CYPs and GSTs) were classified in the binding and catalytic activity groups. These represent about ~130 and ~107 proteins abundance of the function hits of the total protein detected and are shown in Figure 3.2. However, the quantiitative proteomics data (preformed by nonlabeld peak intensity measurments) indicated that there was a significant difference at the level of CYPs and GSTs protein in 3D skin control and induced 3D skin compared with native skin. This was in agreement with the previously reported relative levels of CYP and GST protein expression in 3D skin models and human skin (Oesch *et al*., 2007; Oesch *et al*., 2014; Oesch *et al*., 2018). These reports indicated that both Phase I and Phase II XME were expressed at low levels in skin models. In addtion, 4 *in vitro* human skin models (both 2D and 3D) were invistgated and compared with a surrogate of the liver and native human skin (Wiegand *et al*., 2014).

In the work reported here, the proteomics data acquired indicated that chemical induction of Phase I and Phase II XME in the Labskin model produced a model that reflected the *in vivo* skin more realistically. The reactome analysis (Figure 3.3 a, b, c) based on the

differential UniProt-protein obtained from progenesis QI software data was showed XME pathways. The protein and peptides score can be facilitated initial filtering of database search results to provide a useful measure of certain proteins identified.

Table 3.1: Detection of Phase I and Phase II XMEs in a 3D Skin Model Control Vs Normal human skin (FHS) microsomal and cytosolic fractions by LC-MS/MS.

Accession	Description	Peptides	Score	Fold Change FHS/LSE Control
P00325	ADH class beta	9(3)	74.81	32.16
P93629	ADH class III	2(2)	11.01	1.77
P00352	ALDH1A1	3(2)	14.76	2.37
P49189	ALDH9A1	7(4)	37.87	1.00
P34914	EPHX2	4(2)	26.62	4.07
Q16678	CYP1B1	1(1)	3.84	0.42
P11707	CYP3A6	5(3)	26.63	0.92
P15539	CYP11B2	3(1)	13.65	0.71
O31440	CYP152A1	5(4)	30.39	0.70
O48927	CYP78A3	2(1)	10.16	0.03
Q06830	PRDX1	7(4)	47.23	1.80
P32119	PRDX2	3(3)	18.57	2.16
P09211	GSTP1	14(6)	161.11	1.39
P78417	GSTO1	5(5)	33.44	1.03
P24752	ACAT1	2(1)	14.28	4.36

Table 3.2: Detection of Phase I and II (CYP1B1 and GST) XMEs in a 3D Skin Model Control Vs induced with βNF, RA and PB microsomal and cytosolic fractions by LC-MS/MS.

Accession	Description	Peptides	Score	Fold Change LSE βNF/LSE Control	Fold Change LSE RA/LSE Control	Fold Change LSE PB/LSE Control
P00325	ADH class beta	9(3)	74.81	1.30	0.96	1.16
P93629	ADH class III	2(2)	11.01	4.61	6.60	4.14
P00352	ALDH1A1	3(2)	14.76	2.73	2.15	3.17
P49189	ALDH9A1	7(4)	37.87	1.85	1.70	2.91
P34914	EPHX2	4(2)	26.62	3.99	5.19	6.44
Q16678	CYP1B1	1(1)	3.84	2.19	2.63	2.89
P11707	CYP3A6	5(3)	26.63	1.03	0.95	0.99
P15539	CYP11B2	3(1)	13.65	1.35	1.03	1.57
O31440	CYP152A1	5(4)	30.39	2.28	1.91	2.29
O48927	CYP78A3	2(1)	10.16	1.57	1.43	1.35
Q06830	PRDX1	7(4)	47.23	2.16	2.23	2.40
P32119	PRDX2	3(3)	18.57	1.77	1.78	2.28
P09211	GSTP1	14(6)	161.11	2.78	2.65	3.10
P78417	GSTO1	5(5)	33.44	1.35	1.17	1.47
P24752	ACAT1	2(1)	14.28	1.19	1.38	5.00

Table 3.3: Detection of Phase I and II (CYP1B1 and GST) XMEs in Human skin (FHS) Vs induced with βNF microsomal and cytosolic fraction by LC-MS/MS.

Accession	Description	Peptides	Score	Fold Change LES βNF/FHS	Fold Change LSE RA/FHS	Fold Change LSE PB/FHS
P00325	ADH class beta	9(3)	74.81	0.04	0.02	0.04
P93629	ADH class III	2(2)	11.01	2.60	3.72	2.33
P00352	ALDH 1A1	3(2)	14.76	1.15	0.91	1.34
P49189	ALDH 9A1	7(4)	37.87	1.85	1.69	2.19
P34914	EPHX2	4(2)	26.62	0.98	1.27	1.58
Q16678	CYP1B1	1(1)	3.84	5.12	6.15	6.75
P11707	CYP3A6	5(3)	26.63	1.12	1.04	1.08
P15539	CYP11B2	3(1)	13.65	1.89	1.46	2.20
O31440	CYP152A1	5(4)	30.39	3.24	2.72	3.26
O48927	CYP78A3	2(1)	10.16	50.61	46.27	43.50
Q06830	PRDX1	7(4)	47.23	1.10	1.24	1.33
P32119	PRDX2	3(3)	18.57	0.82	0.82	1.05
P09211	GSTP1	14(6)	161.11	2.00	1.91	2.23
P78417	GSTO1	5(5)	33.44	1.31	1.14	1.43
P24752	ACAT1	2(1)	14.28	0.27	0.32	1.15

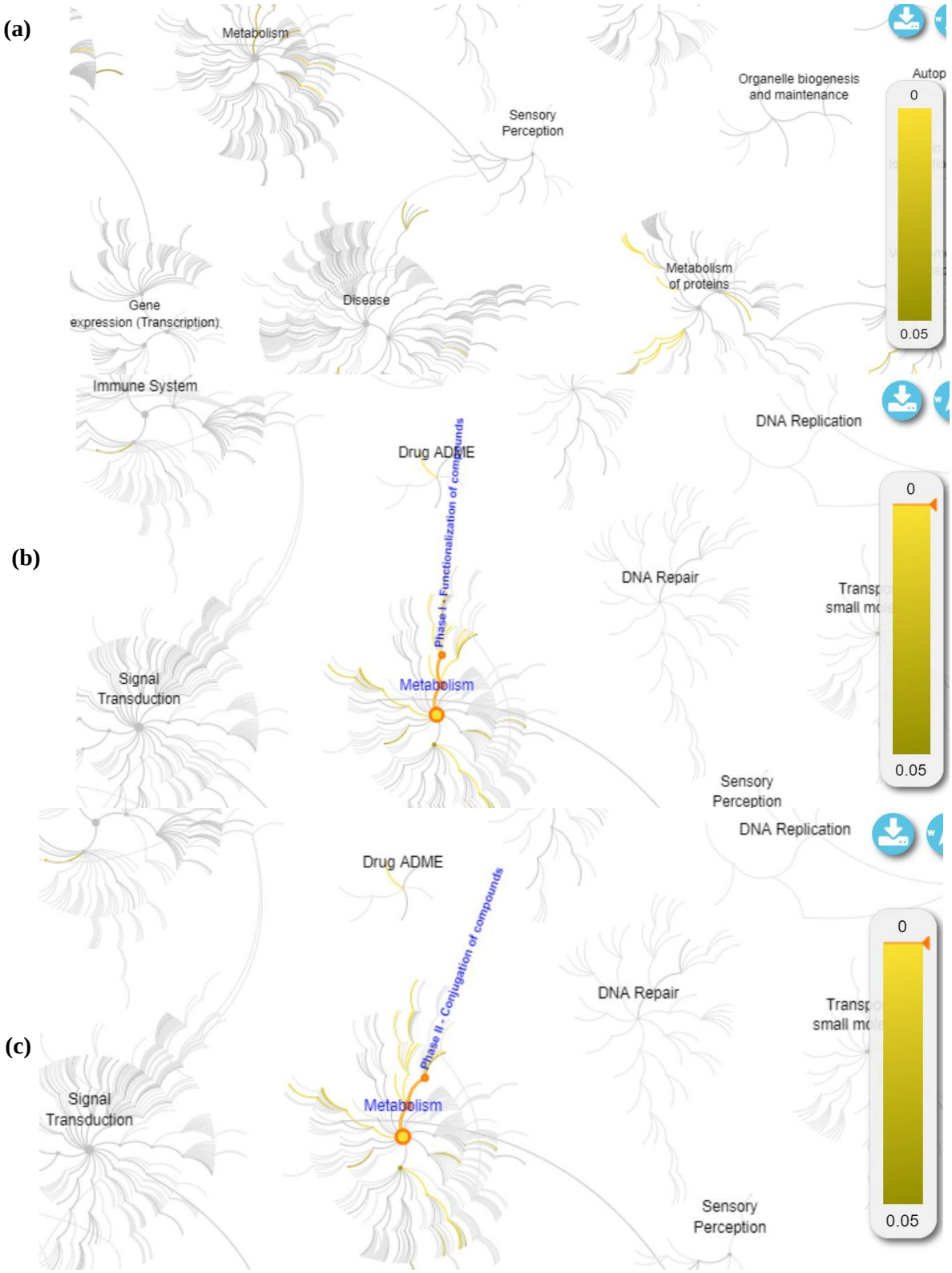

Figure 3.3: Schematic representation **(a)** of reactome pathway analysis of metabolising proteins detection of Phase I and II XMEs in a 3D skin model control (Labskin) and induced βNF, RA, PB of 3D Labskin microsomal and cytosolic fraction by using LC-MS/MS. The yellow color code representation of that pathway in your input dataset. Yellow color is signifies pathways which are indicated as significantly different $P \leq 0.05$. The expression of proteins were identfied of Phase I XMEs **(b)** include CYPs and Phase II **(c)** include conjugation reactions (GST).

The application of RT-qPCR to detect total RNA in the induced models is described in Chapter 2. This is a very sensitive technique, and the data reported here appears to confirm the findings made. However, the relationship of low RNA level to the CYPs and GSTs protein levels is still uncertain (Harris *et al*., 2002; Ahmad & Mukhtar, 2004). Only van Eijl *et al*. (2012) has studied that the levels of CYPs and GSTs protein expression in 3D skin model and human skin compared to liver by using a proteomic approach. The induction of the Phase I XME (CYP1B1 and Phase II of GSTP1 and GSTO1) were also demonstrated in this study.

Our skin model was used to understand the comparative levels of XMEs in respect of protein level as well as their inducibility of enzymes in 3D skin compared with human skin. LC-MS/MS data indicated that CYP1B1, GSTP1 and GSTO1 protein expression of XMEs in the control (untreated) 3D model were at low level compared with human skin. These data were in an agreement with studies of other 3D epidermal models (EpiDerm, EpiSkin^{TM}, SkinEthic^{TM} RHE, ORS-RHE), full thickness skin models (Skin^{TM} FTM, Phenion FTM, Skin^{TM} FTM) (Kazem, *et al*., 2019). Phase I XME levels in the 3D skin model were mostly lower by about 4-10-fold than that found in human liver indicating they do not play an important role in skin (van Eijl *et al*., 2012). However, some Phase II enzymes were observable in skin (Gelardi *et al*., 2001; Wiegand *et al*., 2014).

A clear evidence of XMEs in the 3D Labskin models were detected earlier. Our LC-MS/MS showed a full spectrum of the Phase I and Phase II XMEs in a 3D skin model control (Labskin) and induced βNF, RA, PB of 3D Labskin by using LC-MS/MS (Figure 3.4 a, b and c).

Figure 3.4: Validation of full spectrum of the Phase I and II XMEs in a 3D skin model control (Labskin) and induced βNF, RA, PB of 3D Labskin by using LC-MS/MS.

a)

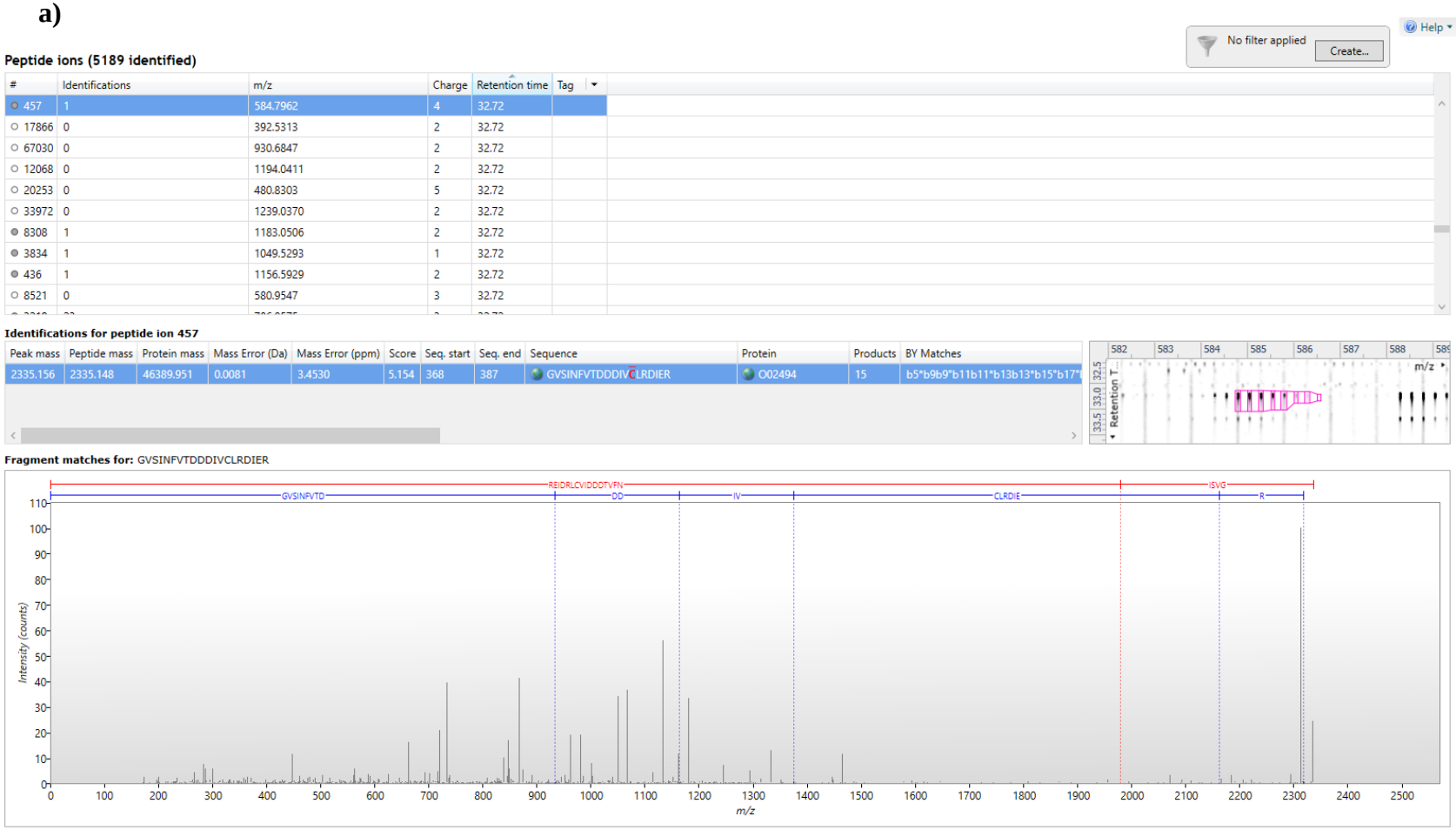

b)

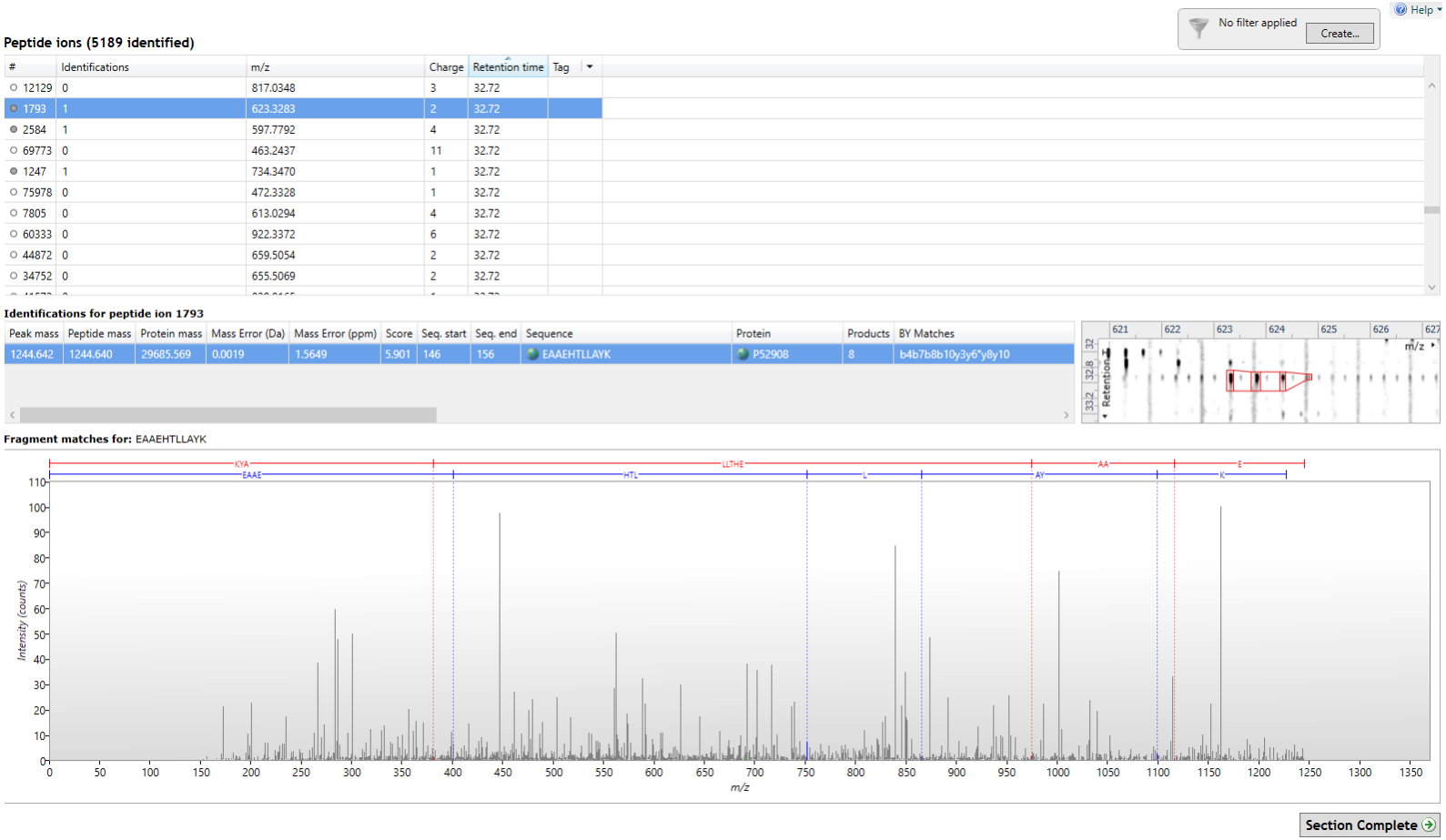
No filter applied
Create...
Help
Peptide ions (5189 identified)
| Identifications | m/z | Charge | Retention time | Tag
12129 | 0 | 817.0348 | 3 | 32.72
1793 | 1 | 623.3283 | 2 | 32.72
2584 | 1 | 597.7792 | 4 | 32.72
69773 | 0 | 463.2437 | 11 | 32.72
1247 | 1 | 734.3470 | 1 | 32.72
75978 | 0 | 472.3328 | 1 | 32.72
7805 | 0 | 613.0294 | 4 | 32.72
60333 | 0 | 922.3372 | 6 | 32.72
44872 | 0 | 659.5054 | 2 | 32.72
34752 | 0 | 655.5069 | 2 | 32.72
Identifications for peptide ion 1793
Peak mass | Peptide mass | Protein mass | Mass Error (Da) | Mass Error (ppm) | Score | Seq. start | Seq. end | Sequence | Protein | Products | BY Matches
1244.642 | 1244.640 | 29685.569 | 0.0019 | 1.5649 | 5.901 | 146 | 156 | EAAEHTLLAYK | P52908 | 8 | b4b7b8b10y3y6*y8y10
621 622 623 624 625 626 627
m/z
Retention
32
32.8
33.2
Fragment matches for: EAAEHTLLAYK
KYA LLTHE AA E
EAAE HTL L AY K
Intensity (counts)
m/z
Section Complete

c)

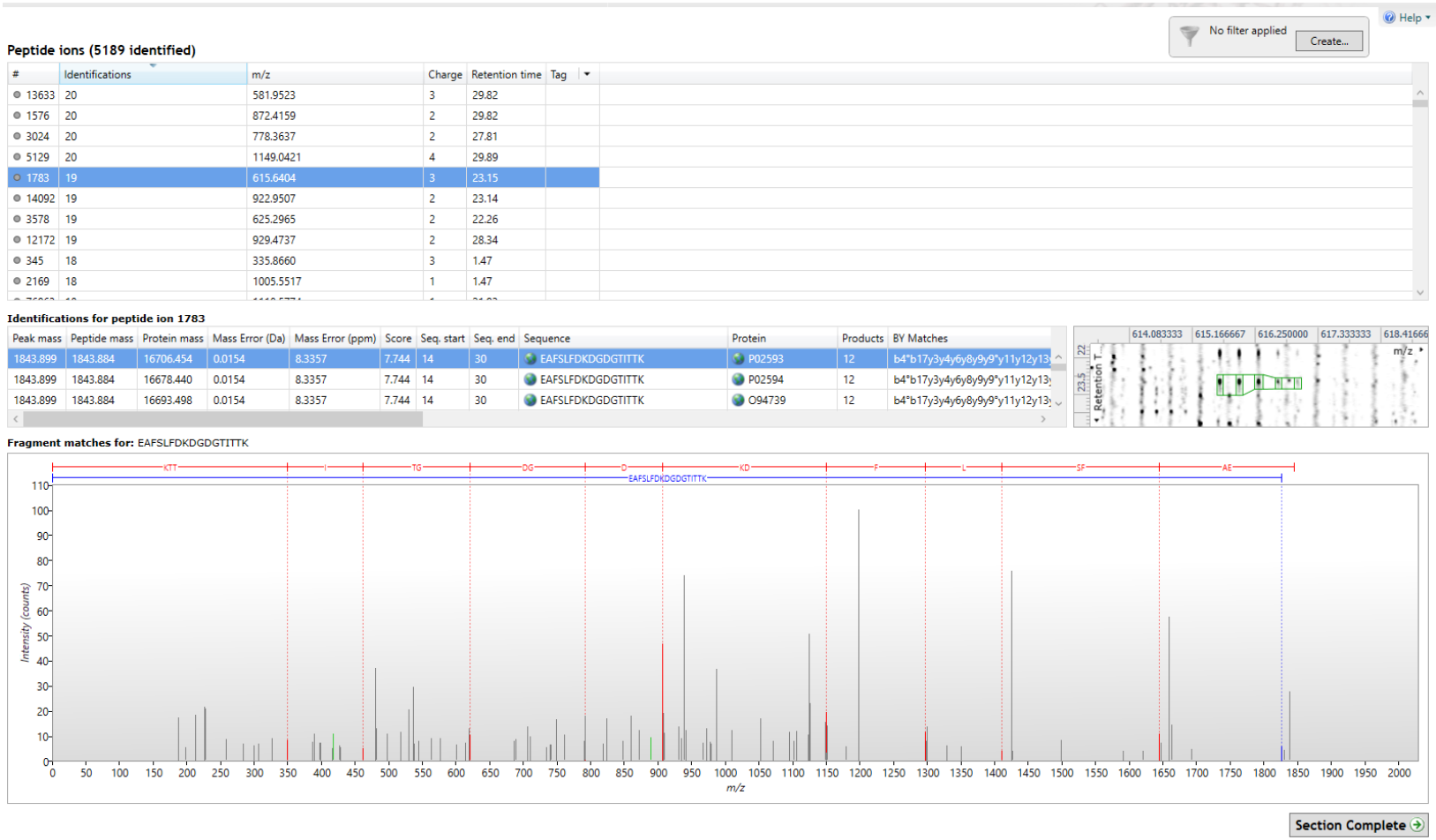
Help
No filter applied
Create...
Peptide ions (5189 identified)
| Identifications | m/z | Charge | Retention time | Tag
13633 | 20 | 581.9523 | 3 | 29.82
1576 | 20 | 872.4159 | 2 | 29.82
3024 | 20 | 778.3637 | 2 | 27.81
5129 | 20 | 1149.0421 | 4 | 29.89
1783 | 19 | 615.6404 | 3 | 23.15
14092 | 19 | 922.9507 | 2 | 23.14
3578 | 19 | 625.2965 | 2 | 22.26
12172 | 19 | 929.4737 | 2 | 28.34
345 | 18 | 335.8660 | 3 | 1.47
2169 | 18 | 1005.5517 | 1 | 1.47
Identifications for peptide ion 1783
Peak mass | Peptide mass | Protein mass | Mass Error (Da) | Mass Error (ppm) | Score | Seq. start | Seq. end | Sequence | Protein | Products | BY Matches
1843.899 | 1843.884 | 16706.454 | 0.0154 | 8.3357 | 7.744 | 14 | 30 | EAFSLFDKDGDGTITTK | P02593 | 12
1843.899 | 1843.884 | 16678.440 | 0.0154 | 8.3357 | 7.744 | 14 | 30 | EAFSLFDKDGDGTITTK | P02594 | 12
1843.899 | 1843.884 | 16693.498 | 0.0154 | 8.3357 | 7.744 | 14 | 30 | EAFSLFDKDGDGTITTK | O94739 | 12
614.083333
615.166667
616.250000
617.333333
618.41666
m/z
Retention T...
Fragment matches for: EAFSLFDKDGDGTITTK
EAFSLFDKDGDGTITTK
Intensity (counts)
m/z
Section Complete

3.4.1 Comparison of basal protein expression of Phase I and Phase II XMEs in a 3D living skin equivalent model (3D LabSkin) control (DMSO treated) with that in human skin

The data obtained from the control sample of Labskin tissue treated with DMSO (final concentration 0.2% v/v) showed no difference from non-treated Labskin. This application of DMSO was very similar to that application used in ORS-RHEs model (Bacqueville *et al*., 2017), suggesting that neither the concentration of the DMSO solvent and the method of application impacted on XMEs protein expression. Proteomic analysis was performed separately on microsomal and cytosolic fraction in both 3D skin model and human skin and the data combined. In general, XME were more abundant in the microsomal rather than cytosolic fraction.

Our LC-MS/MS data are expressed as fold-change of the protein expression as shown in Table 3.1. Overall, about 15 proteins of XMEs profiles are similar in Labskin model as well as human skin but with different levels. The Phase I and II XME expression of ADH beta, ADHIII, ALDH1A1, ALDH9A1, EPHX2, CYP1B1, CYP3A6, CYP11B2, CYP152A1, CYP78A3, PRDX1, PRDX2, GSTP1, GSTO1 and ACAT1 were measured by LC-MS/MS in 3D Labskin model. However, the XME were expressed at lower levels in the 3D skin model control compared with fresh human skin. These confirm earlier work on other skin models reported by (van Eijl *et al*., 2012; Oesch *et al*., 2014).

Interestingly, only CYP1B1 protein was detected in both skin samples but at low level. The expression of skin Phase I XME of down-regulated in the Labskin control, compared to human skin, as shown in Table 3.1. Many CYPs important in drug metabolsim were absent in both 3D skin and human skin, with only few detected in skin model and slightly more in human skin (van Eijl *et al*., 2012). CYPs are mainly expressed in human liver and in higher levels than skin (van Eijl *et al*., 2012; El-Khateeb *et al*., 2019). The absence of detection of CYP1B1 in skin models by proteomics data is surprising (van Eijl *et al*., 2012), although this is consistent with the levels of CYP1B1 RNA which have been reported to be at low level in 3D skin and human skin (Gelardi *et al*., 2001; Ahmad & Mukhtar, 2004; Schober *et al*., 2006; Wiegand *et al*., 2014).

Luu-The *et al*., (2009) and Hu *et al*., (2010) reported that the CYP1B1 gene is detectable in native skin which is supported by our data. Moreover, western blot analysis indicated that CYP1B1 protein is a major CYP in the epidermal layer of native human skin that has a clear function in chemical biotransformation (Katiyar *et al*., 2000); Oesch *et al*., 2014).

However, large variations in the levels of this isoform protein expression were observed from different donors. Baron *et al*., (2001) had earlier reported that the CYP1B1 proteins were of low abundance in the microsomal fraction of human skin keratinocytes. On the other hand, Van Eijl *et al*., (2012) reported that CYP1B1 was absent in both skin and liver microsomal fraction in a LC-MS/MS based study. These data combination of all of these studies and our own data does suggest extensive genetic polymorphism in the level of this protein. In addition, the others of CYP3A6, CYP11B2, CYP152A1, and CYP78A3 were also expressed in the 3D models, but they were found at low levels compared with human skin (Table 3.1).

A number of Phase II XMEs were selected to compare the metabolic capacity of 3D skin model with that of a human skin. GSTs was observed in the 3D models, and its activity there was at 2-fold higher compared with human liver model (van Eijl *et al*., 2012). GSTs proteins found at the RNA level in Labskin (See Chapter 2) have also been detected at the protein level. Both GSTP1 and GSTO1 have been identified in the 3D skin model and human skin and are the predominant form. Overall, GSTs protein were expressed between 0.2-1.5-fold change in the untreated 3D skin model "Labskin"compared with native skin. GSTP1 and GSTO1 were the major isoforms expressed in the 3D skin model "Labskin" but were detected at low levels compared with native human skin. These proteins in the were measured at level (1.39-fold and 1.03-fold) respectively. The levels of these proteins in microsomal and cytosolic fraction were in the control 3D skin models, are in agreement with the proteomics data that was obtained from Labskin (Couto *et al*., 2021).

Similarly, transferase enzymes were identified in the majority of Labskin samples and were present at levels similar or slightly lower to those found in previous work (van Eijl *et al*., 2012), (interestingly GSTs proteins were also reported to be present in both the skin model studied and human skin in this study).

3.4.2 Comparison of basal protein expression of Phase I and Phase II XMEs in the control 3D living skin equivalent model control (DMSO treated) with that 3D skin models subjected to chemical induction

The Phase I and Phase II XME in skin (Labskin and human skin) play a major role in the metabolism of a wide range of many substrates. Due to the low level of XMEs of Phase I and Phase II proteins in Labskin control (treated with DMSO), the expression of ADH class III, ALDH1A1, ALDH9A1, EPHX2, CYP1B1, CYP3A6, CYP11B2, CYP152A1, and CYP78A3, PRDX1, PRDX2 and GSTP1 and GSTO1 and ACAT1of XMEs were

treated with a series of known inducers βNF, RA and PB overall induced after 72 h at high level than Labskin control. Form LC-MS/MS data of the Phase I of CYP1B1 and Phase II of GSTP1 and GSTO1 were detected significant, indicating protein was induced in 3D skin model cultures compared to human skin (NHS). These induced of Phase I and Phase II were significantly ($P \leq 0.05$) up-regulated in the 3D model after 72 h exposure to βNF, RA and PB compared with the LES control (Table 3.2).

CYPs are enzymes associated with the endoplasmic reticulum and mitochondria. In human, they are predominantly observed in the liver. CYP1B1 is an important enzyme in the Phase I metabolism of a wide range of substrates. It is detectable in human skin and Labskin as the CYP1B1 gene as reported in Chapter 2.3 and increased levels of the gene were induced in the skin model compared with human skin. These data were confirmed at the protein level here. Low CYP1B1 protein levels were detected in untreated 3D skin as shown in Table 3.1. Significant induction of this protein was induced after 72 h by 50 μM βNF in the 3D skin tissues compared with untreated skin model. The CYP1B1 expression was upregulated (2.19-fold) in induced 3D skin model Table 3.2. These data are in agreement with previous findings that levels of Phase I XME were very low in the Phenion FT Skin and OS-REp models and in monolayers of NHEKs. However, it was found to be easily inducible in OS-REp model by βNF after 72 h systemic application (Bacqueville *et al*., 2017).

The induction of CYP1B1 in 3D skin models has previously been reported at the gene and enzyme activity level (Hewitt *et al*., 2013; Bacqueville *et al*., 2017). It was found that the induction level was very similar or slightly higher by using of RA than by βNF as the inducing agent. This could be due to a higher affinity of RA for AhR, although the lower dose of RA (10 μM) compared with 50 μM βNF. The level CYP1B1 protein in Labskin models were increased significantly (2.63-fold) by systemic application of 20 μM RA 72 h incubations (Table 3.2). An interesting finding is that CYP1B1 was more highly induced by PB compared to RA and βNF. There was a 2.89-fold increase in CYP1B1 in the 3D skin model induced with phenobarbital (2 mM) compared with control LSE. This is the first study where CYP1B1 has been detected in the Lasbskin model.

The CYP1B1 induction response of Labskin to β-naphthoflavone and *all trans* retinoic acid found here was also observed induced in a full thickness skin model and *in vitro* human epidermal keratinocytes (Du *et al*., 2006; Smith *et al*., 2006). The induction of CYP1B1 using non-ultraviolet-B (UVB) at the same time point using western blot

analysis has been studied. In this work, it appeared that CYP1B1 protein could be detected in epidermal layer of human skin, although most CYPs of other Phase I enzymes levels of other P450s were unaffected by UVB mostly in the human skin (Katiyar *et al*., 2000).

Overall, it can be seen that levels of the CYP1B1 protein are lower in Labskin than native human, however much more comparable than that those in rat and pig skin (Ahmad & Mukhtar, 2004; Schober *et al*., 2006). Benzo[a]pyrene a substrate was metabolised by CYP1B1 to hydroxy, diol, catechol and dione metabol in ORS-RHE model (Hvastkovs *et al*., 2007; Oesch & Arand, 1999).

A number of Phase II XMEs GSTs protein, including GSTP1 and GSTO1 that play a major role in XM in human liver have been identified in our untreated 3D skin model, but in much lower levels than in human skin by using LC-MS/MS. Despite the detection of GSTs gene expression reported in Chapter 2 of the 84 genes expressed in the 3D skin model and human skin (summarizes of GSTs genes showed as heat map in the Chapter 2), GSTs proteins expression was detected in fresh human skin and 3D skin equivalent model.

The determination of Phase II XME levels in skin by LC-MS/MS has not been widely reported. From the glutathione S transferase family, GSTP1 is the major Phase II enzyme expressed in both Labskin and human skin as shown in Table 3.2 and Table 3.3, followed by GSTO1. These GSTs proteins were induced in Labskin, with different levels of increase, using all of the inducers studied here *i.e.* 50 µM βNF, 20 µM RA and 2 mM PB. GSTP1 and GSTO1 proteins catalyze the conjugation of reduced glutathione to a large number of exogenous and endogenous hydrophobic electrophiles (Kazem *et al*., 2019). Its detection and ready induction suggest that GSTs is the main elimination XME in the human skin and skin models.

GSTP1 was induced at level at 2.78-fold by βNF compared with LSE model control (1.39-fold). GSTP1 was also induced and increased after 72 h incubation with 20 µM RA (2.65-fold) and 2 mM PB (3.10-fold) compared with the 3D skin control (treated with DMSO, 0.2%). This increase level is the maximum induction possible without causing any effect on the skin cells (Du *et al*., 2006; Wiegand *et al*., 2014). PB has a great influence on GSTP1 level compared with RA and βNF. This protein has therefore ben confirmed to be the most widely distributed and most abundant enzyme of the GST family in skin tissues.

Additionally, βNF and RA inducers activated the AhR of 3D skin models, leading to induction of GSTO1. This enzyme was induced at 1.35-fold by 50 µM βNF and 1.17-fold by 20 µM RA in the microsomal and cytosolic 3D skin model compared 1.03-fold with untreated 3D skin model. Hence, 50 µM βNF has more impact on XME levels than 20 µM RA. After 72 h with 2 mM PB, GSTO1 was also induced higher at 1.47-fold in as shown in Table 3.2. This is comparable with the level of increase observed of about 40% in primary cell cultures after 48 h induction with PB (Hirel *et al*., 1995; Gelardi *et al*., 2001).

Hirel *et al*., (1995) and Gelardi *et al*., (2001) reported that GSTs are mainly found in the microsomal and cytosolic of in primary cultured keratinocytes and were shown to play significant role in catalysing the conjugation of electrophilic of CDNB. GSTs have previously been detected in a 3D skin model (van Eijl *et al*., 2012). Here, we have been able to extend this work by showing that , CYP1B1 of the Phase I protein and GSTP1 and GSTO1 of Phase II protein could be induced in a 3D model by βNF, RA, and PB.

3.4.3 Comparison of expression of Phase I and Phase II XME in 3D living skin equivalent model (3D Labskin) induced with βNF, RA, PB of with levels in fresh native human skin

The untargetted proteomic experiments performed gave about 327 proteins identified in total. Analysis of function using Panther software (http://www.pantherdb.org) indicated that as discussed in Table 3.3 the expression levels of the Phase I and II XMEs were up-regulated in the 3D skin model after 72 h exposure to the 50 µM βNF, 20 µM RA and 2 mM PB compared with the control model. The comparison of the induced in "Labskin" and human skin have showed that there was a clear variability of Phase I and Phase II XMEs regards to protein expression as shown in Table 3.3. The majority of these proteins were identified in the epidermis. The expression of all investigated enzymes (ADHIII, ALDH1A1, ALDH9A1, EPHX2, CYP1B1, CYP3A6, CYP11B2, CYP152A1, and CYP78A3, PRDX1, PRDX2 and GSTP1 and GSTO1 and ACAT1 in the microsomal and cytosolic fraction of Labskin models induced with βNF, RA, PB were measured at high level.

The levels of these activties reached in induced 3D skin models can be different dependent on donors (Oesch *et al*., 2018).

The levels of mRNA of CYPs genes was consistent in RHS models (T-SkinTM FTM and EpiSkin™ FTM) and RHE models (EpiSkin™, SkinEthic™ RHE, ORS-RHE) compared with those that found in human skin (Hu *et al*., 2010; Neis *et al*., 2010; Eilstein *et al*., 2015; Luu-The *et al*., 2005; Luu-The *et al*., 2009; Bacqueville *et al*., 2017), the LC-MS/MS study in Labskin models showed that the CYPs *e.g*. CYP1B1 protein was also measured in microsomal and cytosolic fraction in the induced "Labskin" model compared with native human skin, indicating the presence of CYP1B1 are similar pathways and function. Notably, the level of CYP1B1 protein was expressed higher in Labskin models induced with βNF, RA, PB iducers. The responses of βNF, RA and PB in Labskin model for CYP1B1 protein were increased higher after systemic application 72 h of 5.12-fold, 6.15-fold and 6.75-fold respectively than those present in native human skin (Table 3.3). This was showed a high level of CYP1B1 in the induced 3D skin model by βNF, RA and PB compared to those found in the epidermis of fresh human skin. This CYP1B1induction is supported by a recent finding in induced ORS-RHE model after treatment of βNF (Bacqueville *et al*., 2017).

GST is widely distributed enzymes in skin which are essential for conjugation reactions. A number of isoforms of GSTs of Phase II include GSTP1 and GSTO1 activity have been found in skin, which is encoded by this GSTs gene, is the main enzyme in the human skin (Raza *et al.*,1991). In our study of Labskin GSTs expression, GSTP1 protein was induced after 50 µM βNF, 20 µM RA and 2 mM PB of 2.00-fold and 1.91-fold and 2.23-fold respectively as shown in Table 3.3. This expression of Phase II enzymes was found in the induced Labskin is greater than those that present in human skin, which is in accordance with Luu-The *et al*., (2009), who has observed that the GSTP1 activity in 3D epidermal models were smiliar or higher than the GSTs activity in the native human skin.

A further increase by βNF and RA was similar induced level for the expression of GSTO1 protein between 1.31-1.14-fold change in induced 3D model (Table 3.3). The level of this enzyme was a significant increase of the PB response during an incubation time of 72 h compared with βNF and RA 72 h induction. GSTO1 was also induced at 1.43-fold in 3D skin model than fresh native human skin.

Therefore, GSTP1 and GSTO1 expression level were found at the most abundant (high level) in 3D skin model induced with treatment of βNF, RA and PB than native human

skin samples according to LC-MS/MS data. These data in the induced 3D skin model and human of GSTP1and GSTO1 protein of Phase II level provide further support for the XMEs in skin as a protective barrier of topical treatments (Oesch *et al*., 2018). In this study, GSTs activities has reported to be reasonably close in 3D skin models include, Episkin™ FTM, EpiDerm™, Episkin™, SkinEthik™ RHE and OS-Rep skin models compared with native skin. Also, Bacqueville *et al*., (2017) has reported strong expression of GSTs was induced higher in ORS-RHE model than in human skin. Overall, significant increase in the expression of GSTs gene was observed and strongly induced in 3D skin model than those presented in human skin. In this study, XMEs level of both GSTP1 and GSTO1 proteins expression were found to be at the high level in the Labskin models compared to GSTs that expressed in native human skin. Other non-human Phase I and II were detected in Labskin model, this could be due to the contamination of experiments during the culture incubation (data not shown). As noted above LC-MS/MS data, existing non-human XME protein identification methods can be related to miss identification include digesting proteins into peptides. In addition, the enzyme sequencing approach can also exclude the correct peptides from the database search space and lead to erroneous identifications.

The LC-MS/MS raw data of this chapter has been attached in the appendix VI link page (223).

3.5 Conclusion

The data obtained in this study provide further support for the concept that XMEs expressed in the skin may contribute to the role of skin as protective barrier by detoxifying XBs following topical exposure. This is an important consideration in safety assessment of topically applied chemicals. The *in vitro* skin model was shown to express many important XMEs, which could be induced in response with βNF, RA and PB inducers. The LC-MS/MS result indicated that the comparison of level of CYP1B1, GSTP1 and GSTO1 protein were expressed low in 3D skin model compared with those that presented in native human skin. However, the responses of drug inducers after systemic application for protein level of the CYPs and GSTs in the 3D skin model were expressed higher than in 3D skin control (untreated 3D skin model) which can be functionally significant. Despite of the relatively low RNA level in the induced 3D skin model, the CYP1B1, GSTP1 and GSTO1 protein of Phase I and Phase II were measured similar or higher in the induced skin model with βNF, RA and PB microsomal and cytosolic fraction than normal human skin by LC-MS/MS.

3.6 References

Ahmad, N., & Mukhtar, H. (2004). Cytochrome p450: A target for drug development for skin diseases. *Journal of Investigative Dermatology, **123***(3), 417-425.

Bacqueville, D., Jacques, C., Duprat, L., Jamin, E. L., Guiraud, B., Perdu, E., Duplan, H. (2017). Characterization of xenobiotic metabolizing enzymes of a reconstructed human epidermal model from adult hair follicles. *Toxicology and Applied Pharmacology, 329*, 190-201.

Baron, J. M., Wiederholt, T., Heise, R., Merk, H. F., & Bickers, D. R. (2008). Expression and function of cytochrome p450-dependent enzymes in human skin cells. *Current Medicinal Chemistry, **15***(22), 2258-2264.

Baron, J. M., HoÈller, D., Schiffer, R., Frankenberg, S., Neis, M., Merk, H. F., & Jugert, F. K. (2001). Expression of multiple cytochrome p450 enzymes and multidrug resistance-associated transport proteins in human skin keratinocytes. *Journal of Investigative Dermatology, **116***(4), 541-548.

Boobis, A. R., Brodie, M. J., Kahn, G. C., Fletcher, D. R., Saunders, J. H., & Davies, D. S. (1980). Monooxygenase activity of human liver in microsomal fractions of needle biopsy specimens. *British Journal of Clinical Pharmacology, **9***(1), 11-19.

Couto, N., Newton, J. R., Russo, C., Karunakaran, E., Achour, B., Al-Majdoub, Z. M., Barber, J. (2021). Label-free quantitative proteomics and substrate-based mass spectrometry imaging of xenobiotic metabolizing enzymes in ex vivo human skin and a human living skin equivalent model. *Drug Metabolism and Disposition, **49***(1), 39-52.

Du, L., Neis, M. M., Ladd, P. A., & Keeney, D. S. (2006). Differentiation-specific factors modulate epidermal CYP1–4 gene expression in human skin in response to retinoic acid and classic aryl hydrocarbon receptor ligands. *Journal of Pharmacology and Experimental Therapeutics, **319***(3), 1162-1171.

Du, L., Neis, M. M., Ladd, P. A., Lanza, D. L., Yost, G. S., & Keeney, D. S. (2006). Effects of the differentiated keratinocyte phenotype on expression levels of CYP1–

4 family genes in human skin cells. *Toxicology and Applied Pharmacology*, ***213***(2), 135-144.

Eilstein, J., Léreaux, G., Arbey, E., Daronnat, E., Wilkinson, S., & Duché, D. (2015). Xenobiotic metabolizing enzymes in human skin and SkinEthic reconstructed human skin models. *Experimental Dermatology*, ***24***(7), 547-549.

El-Khateeb, E., Vasilogianni, A., Alrubia, S., Al-Majdoub, Z. M., Couto, N., Howard, M., Achour, B. (2019). Quantitative mass spectrometry-based proteomics in the era of model-informed drug development: Applications in translational pharmacology and recommendations for best practice. *Pharmacology & Therapeutics*, *203*, 107397.

Gelardi, A., Morini, F., Dusatti, F., Penco, S., & Ferro, M. (2001). Induction by xenobiotics of phase I and phase II enzyme activities in the human keratinocyte cell line NCTC 2544. *Toxicology in Vitro*, ***15***(6), 701-711.

Gibbs, S., van de Sandt, Johannes JM, Merk, H. F., Lockley, D. J., Pendlington, R. U., & Pease, C. K. (2007). Xenobiotic metabolism in human skin and 3D human skin reconstructs: A review. *Current Drug Metabolism*, ***8***(8), 758-772.

Harris, I. R., Siefken, W., Beck-Oldach, K., Brandt, M., Wittern, K., & Pollet, D. (2002). Comparison of activities dependent on glutathione S-transferase and cytochrome P-450 IA1 in cultured keratinocytes and reconstructed epidermal models. *Skin Pharmacology and Physiology*, ***15***(Suppl. 1), 59-67.

Hewitt, N. J., Edwards, R. J., Fritsche, E., Goebel, C., Aeby, P., Scheel, J., Eilstein, J. (2013). Use of human in vitro skin models for accurate and ethical risk assessment: Metabolic considerations. *Toxicological Sciences*, ***133***(2), 209-217.

Hirel, B., Chesne, C., Pailheret, J. P., & Guillouzo, A. (1995). In vitro expression of drug metabolizing enzyme activities in human adult keratinocytes under various culture conditions and their response to inducers. *Toxicology in Vitro*, ***9***(1), 49-56.

Hu, T., Khambatta, Z. S., Hayden, P. J., Bolmarcich, J., Binder, R. L., Robinson, M. K., Osborne, R. (2010). Xenobiotic metabolism gene expression in the EpiDerm™ in

vitro 3D human epidermis model compared to human skin. *Toxicology in Vitro, **24***(5), 1450-1463.

Hvastkovs, E. G., So, M., Krishnan, S., Bajrami, B., Tarun, M., Jansson, I., Rusling, J. F. (2007). Electrochemiluminescent arrays for cytochrome P450-activated genotoxicity screening. DNA damage from benzo [a] pyrene metabolites. *Analytical Chemistry, **79***(5), 1897-1906.

Jugert, F. K., Agarwal, R., Kuhn, A., Bickers, D. R., Merk, H. F., & Mukhtar, H. (1994). Multiple cytochrome P450 isozymes in murine skin: Induction of P450 1A, 2B, 2E, and 3A by dexamethasone. *Journal of Investigative Dermatology*, ***102***(6), 970-975.

Katiyar, S. K., Mukhtar, H., & Matsui, M. S. (2000). Ultraviolet-B exposure of human skin induces cytochromes P450 1A1 and 1B1. *Journal of Investigative Dermatology, **114***(2), 328-333.

Kazem, S., Linssen, E. C., & Gibbs, S. (2019). Skin metabolism phase I and phase II enzymes in native and reconstructed human skin: A short review. *Drug Discovery Today*, ***24***(9), 1899-1910.

Luu-The, V., Duche, D., Ferraris, C., Meunier, J., Leclaire, J., & Labrie, F. (2009). Expression profiles of phases 1 and 2 metabolizing enzymes in human skin and the reconstructed skin models episkin™ and full thickness model from episkin™. *The Journal of Steroid Biochemistry and Molecular Biology*, ***116***(3-5), 178-186.

Luu-The, V., Paquet, N., Calvo, E., & Cumps, J. (2005). Improved real-time RT-PCR method for high-throughput measurements using second derivative calculation and double correction. *BioTechniques*, ***38***(2), 287-293.

Neis, M. M., Wendel, A., Wiederholt, T., Marquardt, Y., Joussen, S., Baron, J. M., & Merk, H. F. (2010). Expression and induction of cytochrome p450 isoenzymes in human skin equivalents. *Skin Pharmacology and Physiology, **23***(1), 29-39.

Oesch, F., Fabian, E., Guth, K., & Landsiedel, R. (2014). Xenobiotic-metabolizing enzymes in the skin of rat, mouse, pig, guinea pig, man, and in human skin models. *Archives of Toxicology*, ***88***(12), 2135-2190.

Oesch, F., Fabian, E., & Landsiedel, R. (2018). Xenobiotica-metabolizing enzymes in the skin of rat, mouse, pig, guinea pig, man, and in human skin models. *Archives of Toxicology*, ***92***(8), 2411-2456.

Oesch, F., & Arand, M. (1999). Role of individual enzymes in the control of genotoxic metabolites. *Molecular and applied aspects of oxidative drug metabolizing enzymes* (pp. 211-220) Springer.

Oesch, F., Fabian, E., Oesch-Bartlomowicz, B., Werner, C., & Landsiedel, R. (2007). Drug-metabolizing enzymes in the skin of man, rat, and pig. *Drug Metabolism Reviews*, ***39***(4), 659-698.

Raza, H., Awasthi, Y. C., Zaim, M. T., Eckert, R. L., & Mukhtar, H. (1991). Glutathione S-transferases in human and rodent skin: Multiple forms and species-specific expression. *Journal of Investigative Dermatology*, ***96***(4), 463-467.

Schober, W., Luch, A., Soballa, V. J., Raab, G., Stegeman, J. J., Doehmer, J., Seidel, A. (2006). On the species-specific biotransformation of dibenzo [a, l] pyrene. *Chemico-Biological Interactions*, ***161***(1), 37-48.

Smith, G., Ibbotson, S. H., Comrie, M. M., Dawe, R. S., Bryden, A., Ferguson, J., & Wolf, C. R. (2006). Regulation of cutaneous drug-metabolizing enzymes and cytoprotective gene expression by topical drugs in human skin in vivo. *British Journal of Dermatology*, ***155***(2), 275-281.

Smith, P. e., Krohn, R. I., Hermanson, G. T., Mallia, A. K., Gartner, F. H., Provenzano, M., Klenk, D. C. (1985). Measurement of protein using bicinchoninic acid. *Analytical Biochemistry*, ***150***(1), 76-85.

van Eijl, S., Zhu, Z., Cupitt, J., Gierula, M., Götz, C., Fritsche, E., & Edwards, R. J. (2012). Elucidation of xenobiotic metabolism pathways in human skin and human skin models by proteomic profiling. *PloS One*, ***7***(7), e41721.

Wiegand, C., Hewitt, N. J., Merk, H. F., & Reisinger, K. (2014). Dermal xenobiotic metabolism: A comparison between native human skin, four in vitro skin test systems and a liver system. *Skin Pharmacology and Physiology*, ***27***(5), 263-275.

Wiśniewski, J. R., Vildhede, A., Norén, A., & Artursson, P. (2016). In-depth quantitative analysis and comparison of the human hepatocyte and hepatoma cell line HepG2 proteomes. *Journal of Proteomics, 136,* 234-247.

Chapter 4

Abundance and Induction of Xenobiotic Metabolising Enzymes in a 3D Skin Model studied by using NanoLC-MS/MS.

4.1 Introduction

Information on xenobiotic metabolism (XM) in the skin has become important, especially since the use of animal skin, such as pig and rat is banned for testing cosmetics. Attempts have also been made to eliminate the use of animals for cosmetics and drugs which are used in genotoxicity in *in vivo* assays (Neis *et al*., 2010). To develop alternative tools to excised human skin and animal skin, several type of 3D skin models (See Table 1.2 3D skin models in Chapter 1) have been established and developed to study the functional activities of Phase I and II XME on foreign chemicals "xenobiotics" reviewed by Oesch *et al*., (2018) and Kazem *et al*., (2019). However, there are very few a systematic proteomics studies for 3D skin models of XME abundance and comparison of these to native human skin.

A few publications have investigated the protein presence of XME in native human skin, Labskin model, and human liver by quantitative proteomics based on mass spectrometry (van Eijl *et al*., 2012; Couto *et al*., 2019; El-Khateeb *et al*., 2019; Couto *et al*., 2021). A lack of information on skin can lead to issues in drug and cosmetic development., Hence the main purpose of this project to further develop the 3D Labskin model is to obtain a 3D skin model able to mimic the enzymatic action of native human skin.

A comprehensive analysis of the abundance of Phase I and II XMEs particularly, CYPs and UGTs microsomal fractions of human liver responsible for drug metabolism was conducted using a label-free quantitative method by Couto et al (Couto *et al*., 2019). They have recently reported a similar study of XME in the Labskin model and compared the levels found with human skin (Couto *et al*., 2021). XME were detected, including alcohol dehydrogenase and cytochrome P450s (CYPs) and carboxylesterase (CES), of Phase I XME and glutathione S-transferase (GSTs) and UDP-glucuronosyltransferases (UGTs) of Phase II XME were found to be expressed at low levels in both the *in vitro* model and native skin, much lower than those previously found in human liver (Couto *et al*., 2019).

This study also indicated that levels of certain XME in Labskin were lower than those in human skin. Here, we investigate chemicals inducibility of cytochrome P450s (CYPs), carboxylesterase (CES), and glutathione S-transferase (GSTs) in 3D Labskin model and compare the induced levels to native human skin using label-free proteomics technique and nano-LC-MS/MS. The use of nano-LC-MS/MS was expected to yield better coverage and sensitivity over similar study conducted using mLC/MS/MS reported in Chapter 3.

4.2 Aims of the Chapter

In the following Chapter, we aimed to develop a suitable method to identify and quantify a wide range of CYPs, CES and GSTs xenobiotic metabolizing enzymes (XME) and their inducibility in 3D skin model (Labskin) compared with native skin using nanoLC-MS/MS. This study represents the most comprehensive analysis of the abundance (protein) of enzymes especially, CYPs, CES and GSTs in the 3D skin (Labskin) model conducted to date.

4.3 Material and Methods

4.3.1 Ethical statement

Native human skin tissues, from two male donors was obtained from volunteers with their informed consent from University of Bradford Ethical Tissue REC reference17/YH/0086 (Bradford, UK) as described in Chapter 2.3.1.

4.3.2 Enzyme induction

The commercial 3D skin model "Labskin product" was obtained and cultured as described previously in Chapter 1.4.2.

Induction performed through the addition of β-naphthoflavone (βNF) dissolved in DMSO (0.2%) was selected on the basis method as described in Chapter 2.3.4.

4.3.3 Label free quantification of Labskin andhuman skin sample preparation

Regardless of which methdology for label free quantification of human skin and Labskin is applied, they all include the following steps: skin sample preparation including protein extraction, reduction, alkylation, and trypsin digestion as described in Chapter 3.3.5. 3D skin model and fresh human skin were isolated with PBS at 65 °C for 2 min and extracted in potassium phosphate buffer (250 mM K_2HPO_4, 150 mM KCl and 1 mM EDTA, pH 7.25) as described in Chapter 3.3.4. Both human skin and 3D tissues were also separated by the difference centrifugation as described previously (van Eijl *et al*., 2012). The protein was measured by bichinchonic acid protein assay as standard according to BCA protocol as decriped previously in Chapter 3.3.4.

The digestion of the 3D skin model and human skin samples were performed according to the manufacturer's instructions (In-Solution Tryptic Digestion) protocol in Chapter 3.3.5. Milipore ZipTip C18 (Size P10; Zip Tips) was then performed to clean-up peptides.

4.3.4 Instrumentation

4.3.4.1 Nano-LC-MS/MS

All experiments were performed using a nano-LC-MS/MS with FAIMS Pro™ (Thermo Fisher Scientific, U.K.) set to EASY-Spray source in positive mode. The separation was performed on nanoLC column: 50 cm x 75 um C18 PepMap Acclaim EASY-Spray). The mobile phase consisted of nanoLC solvent A (water containing 0.1 % FA) and nanoLC solvent B (80/20 CAN/water containing 0.1% FA) with 120 min run time. Loading solvent (98/2 water/CAN containing 0.05% TFA). The flow rate was set as 0.3 µL/min^{-1}. The MS parmeters were as follows: Orbitrap Exploris™ MS resolution 15000; Scan range 380-1500; Isolation window, 1.2; HCD Collision energy was set at 30 EV, source temperature 150 ºC; Oven temperature 40 °C. A 5.0 µL of each sample was loaded, in triplicate.

4.3.5 Data processing for label-free quantification of proteins

Data files were analysed by nanoLC-MS/MS using data dependent acquisition on the Exploris 480. All proteins expression were identified and quantified by searched against reference human proteome database (Proteome Discoverer 2.5. Spectra software). To assess the different level in XME in Labskin compared with human skin, the protein databases were an interpreted according to Gene Ontology (GO), UniProt and fold change. The quantiitative data (preformed by nonlabeld peak intensity measurments) indicated that was a significant difference at the level of proteins in 3D skin control and induced 3D skin compared with native skin.

Moreover, the Panther Software (http://www.pantherdb.org) was applied to assign protein function using UniProt databases. Statistical analyses were performed using Microsoft Excel 2010 and GraphPad Prism v7.03 (La Jolla, CA).

4.4 Results and Discussion

Protein expression and its function were studied in samples of native human skin (HS), Labskin control (LS) and Labskin treated with βNF (LS_ βNF). Label-free proteomics analysis was performed on both the microsomal and cytosol fractions. From the nanoLC-MS/MS data, in about 3351 functional hits of 4374 of total proteins based on protein ontology (GO) as defines classes of protein were detected and quantified. These proteins were classified into 8 groups using the GO molecular function annotation as shown in Figure 4.1.

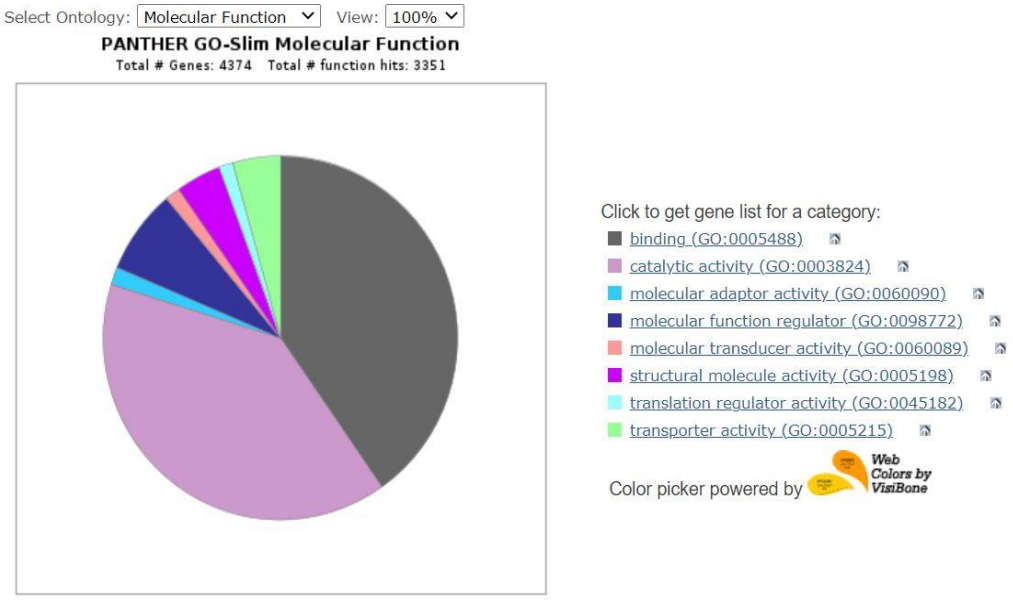

Figure 4.1: GO molecular function distribution of the detected proteins in replicates of Labskin supernatant. According to the molecular function of abundance proteins, approximately 3351 proteins were identified in Labskin model using nanoLC-MS/MS. The most localization and functional assignment of list XMEs in skin detected significantly in binding GO:0005488 and catalytic activity GO:0003824: The proteins were clustered into 8 groups. Binding (GO:0005488) and catalytic activity (GO:0003824) of the function hits were ~1350 and ~1325 protein expression encoding XMEs. Molecular function regulator hits (GO:0098772) ~ 252 and ~ 46 molecular tranducer activity (GO:0060089). The structure molecule activity (GO:0005198) acount for ~138 of function hits. The remaining ~43 function hits contained of translator regulator activity (GO:0045182), ~145 transporter activity (GO:0005215) and ~ 52 molecular adaptor activity (GO:0060090).

The majority of Phase I and Phase II XME (including the CYPs, CES and GSTs) were classified in the binding and catalytic activity groups. Approximately 1350 in the binding and 1325 catalytic activity were identified in Labskin and human skin, as illustrated in Figure 4.1. However, there was different at the protein level of CYPs, CES and GSTs in Labskin control (LS_DMSO) and induced Labskin (LS_βNF) compared to those detected in native skin. This is in good agreement with with the previously reported proteomics data based on protein ontology (GO human) and protein abundance in native human skin and Labskin model using LC-MS/MS (Couto *et al*., 2021). Gene expression and protein levels of CYP, CES and GST in 3D Labskin model and human skin compared with liver has also been reported (Wiegand *et al*., 2014; Oesch *et al*., 2018). These previous studies showed the CYP, CES and GST expression were overall detected at low levels in several

3D skin models. In the work reported here, it was hoped to show that β-naphthoflavone induction of Phase I and II XME in Labskin model produced a good model reflecting the levels of XME in *in vivo* skin more realistically.

4.4.1 Assessment of molecular function of protein and peptides in human skin (HS), 3D Labskin model (LS) and LabSkin model treated with βNF (LS_βNF) using nano-LC-MS/MS

For a more detailed analysis of protein expression in skin, Venn diagrams were generated showing selected significant peptides representing proteins encoding to XME relevant to skin for each of the samples: both human skin (HS), 3D skin model control (LS_DMSO) as well as 3D skin model treated with βNF (LS_βNF). These are shown in Figures 4.2 b. The combined nano-LC-MS/MS data indicated that 92 % proteins and 82 % peptides were detected consistently between human skin and Labskin model.

In total 19262 peptides and 2644 proteins were quantified in HS as shown in Figure 4.2 a and b. Although a large variety of proteins were measured in human skin, some interindividual variability was found in the presence and abundance of these proteins through the three samples of human skin used in our study (Figure 4.2 b). These groups showed a variability 64 in F11, 44 in F12 and 48 in F13 between the three individuals of human skin samples.

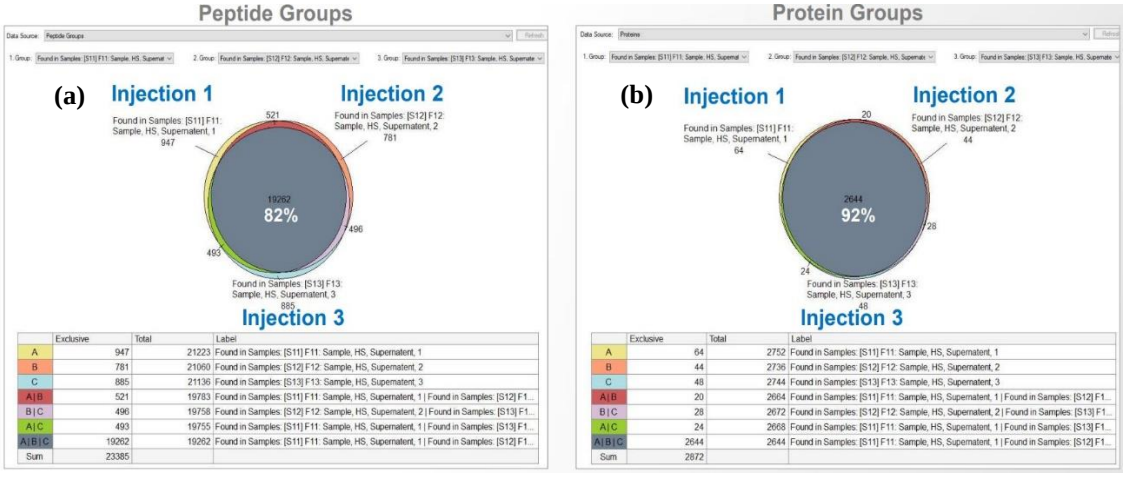

Figure 4.2: Venn diagrams illustrating the distribution of protein and peptide identification groups from duplicate experiments of HS. Of all observed proteins and peptides, 92 % and 82 % were found by enzyme digestion approach. The diagrams represent the overlap of the lists of proteins and peptides variability quantified in HS (S11, S12 and S13) 2644 and 19262 respectively using nanoLC-MS/MS experiments.

These data shows a similar pattern to that earlier reported in human skin and Labskin models (Couto *et al*., 2021). Of note is that a high-level of variability of Phase I and Phase II XME abundance has this also been reported in human liver using label-free proteomics

method (Couto *et al*., 2019). Therefore, this suggest that a larger study requiring larger number of different donors of human skin samples will allow a better understanding of the sources of variability in skin.

The nanoLC–MS/MS methodology detected more unique peptides and proteins in HS compared with the LS_DMSO and LS_βNF samples. This is shown in Figure 4.3. Of the peptides and proteins detected about 14943 peptides and 1426 proteins identification were detected across the supernatant of skin samples including the LS_DMSO, LS_βNF as well as HS samples. However, a clear varibility of proteins between the microsomal and cytosolic fractions of Labskin compared with native skin was observed as shown in Figure 4.3 and 4.4. The total of proteins detected in native human skin was higher than in the Labskin samples. This was as expected due to the greater complexity (more cell types) of human skin compared to Labskin. There were about 235 proteins unique to HS and 30 proteins unique to LS_DMSO (Figure 4.3 b).

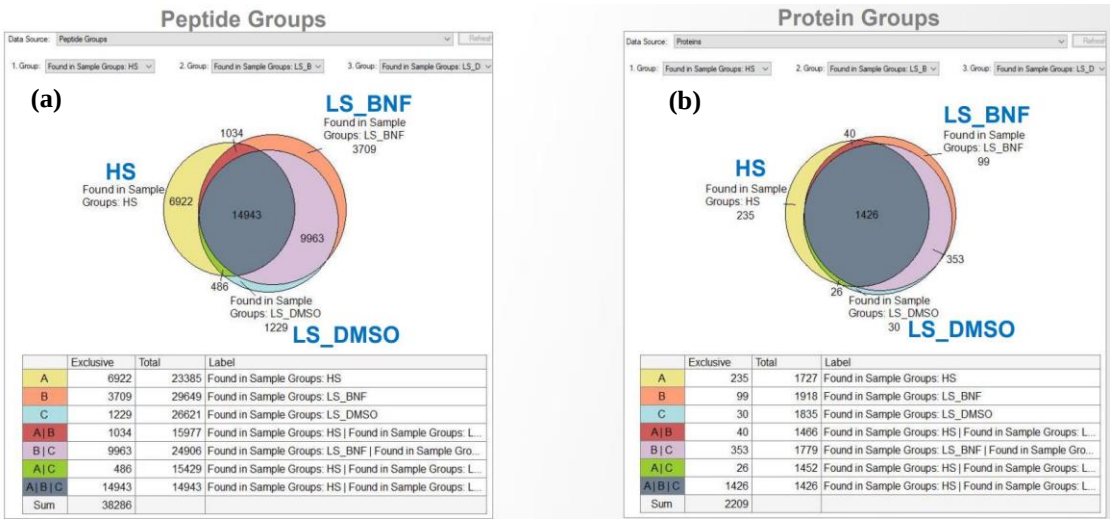

	Exclusive	Total	Label
A	6922	23385	Found in Sample Groups: HS
B	3709	29649	Found in Sample Groups: LS_BNF
C	1229	26621	Found in Sample Groups: LS_DMSO
A | B	1034	15977	Found in Sample Groups: HS | Found in Sample Groups: L...
B | C	9963	24906	Found in Sample Groups: LS_BNF | Found in Sample Gro...
A | C	486	15429	Found in Sample Groups: HS | Found in Sample Groups: L...
A | B | C	14943	14943	Found in Sample Groups: HS | Found in Sample Groups: L...
Sum	38286		

	Exclusive	Total	Label
A	235	1727	Found in Sample Groups: HS
B	99	1918	Found in Sample Groups: LS_BNF
C	30	1835	Found in Sample Groups: LS_DMSO
A | B	40	1466	Found in Sample Groups: HS | Found in Sample Groups: L...
B | C	353	1779	Found in Sample Groups: LS_BNF | Found in Sample Gro...
A | C	26	1452	Found in Sample Groups: HS | Found in Sample Groups: L...
A | B | C	1426	1426	Found in Sample Groups: HS | Found in Sample Groups: L...
Sum	2209		

Figure 4.3: Comparison of proteins and peptides identification representative set of replicate injections between supernatant LS_DMSO, LS_βNF and HS samples. Overall, Venn diagram showing distribution of more unique proteins and peptides identified and quantified in HS compared with LS_DMSO, LS_βNF.

In the Labskin model induced with βNF, many were detected and quantified compared to the control. These yielded an increase of 99 proteins identified (See Figure 3.4 b). This indicated that βNF after 72 h incubation was inducing and increasing XMEs abundance. However the overall expression of proteins groups in LS_βNF was still lower compared to that in HS. These are similar results to those obtained in a previous study of gene expression in the EpiDerm™ model (Hu *et al*., 2010).

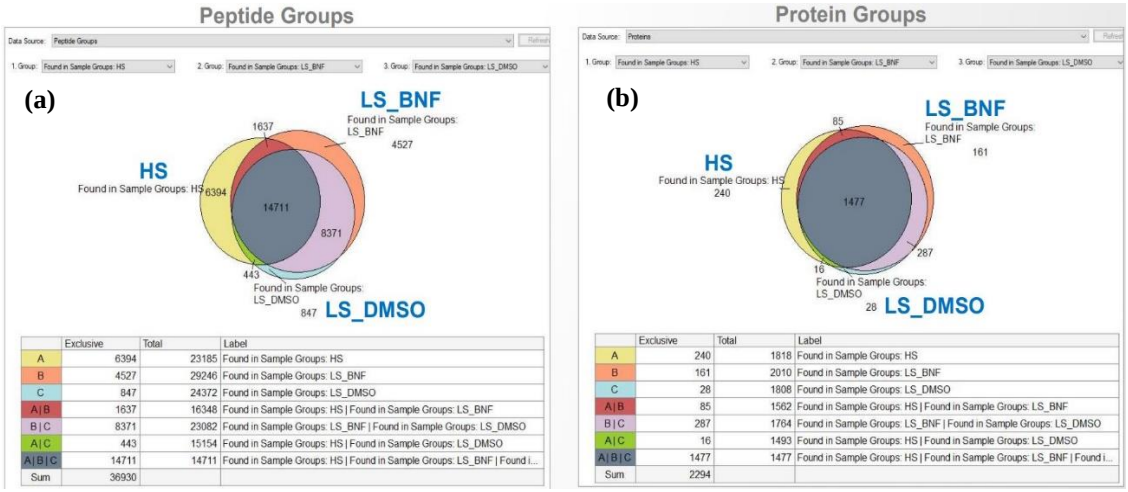

Figure 4.4: Assessment of proteins and peptides identification reflected differences among pellet LS_DMSO, LS_βNF and HS samples. Overall, numbers of peptides of three injections per sample were identified (14711) and these peptides groups corresponds to a total of 1477 proteins. Venn diagram show distribution of unique proteins and peptides three injections per sample in HS, LS_DMSO, and LS_βNF samples.

In order to compare the expression of peptides and proteins in pellet LS_DMSO, LS_βNF and HS as shown in Figure 4.4 a, there are about 14711 peptides identifications corresponding to 1477 total proteins (Figure 4.4 b) which overlapped in HS, LS_DMSO, and LS_βNF samples.

There are 240 unique protein in HS samples and 28 unique proteins were observed in LS_DMSO. The total number of peptides and proteins was increased after induction with βNF and 161 unique proteins were detected in the LS_βNF. The number of these proteins are still lower compared with human skin as illustrated in Venn diagram Figure 4.4 b. Although mRNA and protein level of Phase I and II XME have been measured lower in 3D skin models than human skin (Wiegand *et al*., 2014; van Eijl *et al*., 2012; Couto *et al*., 2021). The results of label-free proteomic analysis overall led to an extension of the Phase I and II XME data obtained by LC-MS/MS, in Chapter 3. These results increase number of phase I and II proteins expression belonging to whole XME in Figure 4.5 as being detected in human skin and Labskin tissues according to nanoLC-MS/MS data.

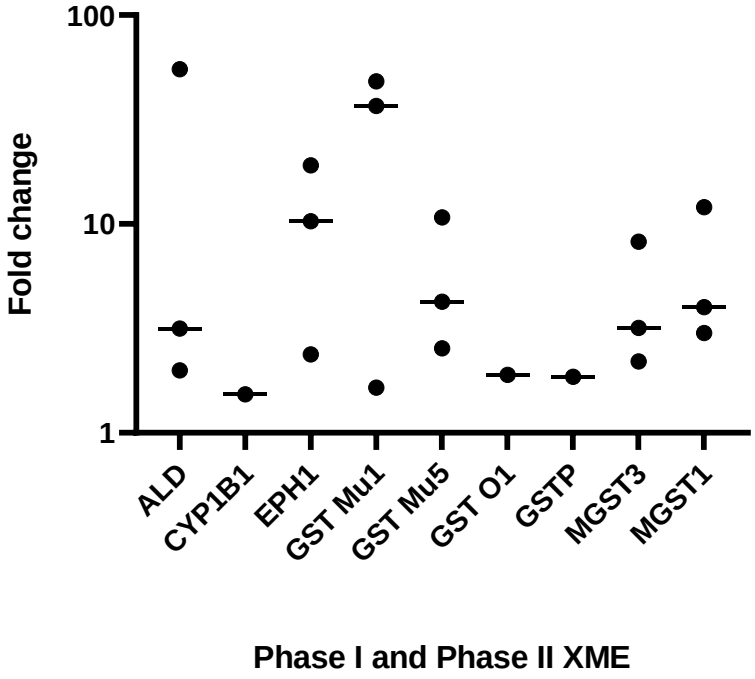

Figure 4.5: Relative expression levels of the Phase I and II of the proteins corresponding to the xenobiotic metabolising enzymes induced 3D skin mode Vs native human skin. The Phase I and Phase II levels overall expressed were much lower in the 3D skin model. Aldehyde dehydrogenase (ALD), Cytochrome P450 1B1 (CYP1B1), Epoxide hydrolase 1 (EPH1), Glutathione S-transferase Mu 5 (GST Mu 5), Glutathione S-transferase omega 1 (GSTO1),), Glutathione S-transferase P (GSTP), Microsomal glutathione S-transferase 3 (MGST 3) and Microsomal glutathione S-transferase 1 (MGST1).

From the total data set, the data for Phase I and Phsae II XME were extracted and are shown in more details below in Table 4.1 and Table 4.2.

4.4.2 Evaluation of the abundance of Phase I and Phase II XME expression in 3D Labskin and human skin

Since mRNA gene expression may not be relative to functional activity, further detailed studies at the protein level are required. In order to understand the occurrence of certain important XME for drug metabolism *i.e.* CYPs and CES of Phase I and GST of Phase II XME of human skin and 3D skin models a detailed investigation of their protein profiles in native human skin and 3D skin models was undertaken. Here, we have compared the levels of these Phase I and II enzymes in the Labskin model and fresh human skin. Both Table 4.1 and Table 4.2 summarize the proteins presence and their abundance level in LS_DMSO, LS_βNF as well as HS samples of 2 different donors. The abundance ratio of Phase I and Phase II XMEs were calculated for HS vs LS_DMSO, vs LS_DMSO vs LS_βNF and HS vs LS_βNF. >1900 protein ratios were quantified with log2 fold change

>1. The list of proteins are provided in excel files for further interrogation of xenobiotics metabolising enzymes as shown in Appendix III. A number of Phase I and II XMEs were selected to compare the level of each protein across all microsomal and cytosolic fractions of the *in vitro* labskin models, *i.e* LS_DMSO and LS_βNF with that of HS. These levels of XMEs expression were assigned according to the fold change.

Using nanoLC-MS/MS in this study has allowed the quantification of over 3351 proteins in the microsomes and cytosol of 3D skin model and native skin, including 25 proteins involved in the metabolism of xenobiotics. These were: alcohol dehydrogenase, aldehyde dehydrogenase, aldehyde oxidase, carboxylesterase, cytochrome P450, NADPH--cytochrome P450 reductase, quinone oxidoreductase, NADH-ubiquinone oxidoreductase, carbonyl reductase, amine oxidase, glutathione S-transferase, sulfotransferase, glutathione hydrolase, glutathione peroxidase, glutathione reductase, sulfotransferase, acetyl-CoA acetyltransferase, aldo-keto reductase, epoxide hydrolase, glutamine gamma-glutamyltransferase, succinate dehydrogenase flavoprotein, sulfide, quinone oxidoreductase, peroxiredoxin, flavin reductase (NADPH), nicotinamide N-methyltransferase, prostacyclin synthase, and short-chain dehydrogenase/reductase. The present data indicated that nanoLC-MS/MS is more sensitive almost 25 times than micro LC-MS/MS (as used in Chapter 3).

These expressed enzymes in the above have been previously reported in the epiderm-200 models, and human skin and compared with human liver using LC-MS/MS (van Eijl *et al*., 2012). However, the Phase I and Phase II levels overall expressed were much lower in the 3D skin model. Comparison of levels of Phase I and Phase II XME in 3D skin "LabSkin" has previously been reported (Couto *et al*., 2021). In the study reported her additional investigations into the induction of Phase I and Phase II XME by chemical inducers such as βNF have been performed. The relative expression of CYPs and CES of Phase I and GSTs of Phase II XME levels, which are the main focus in this study, in microsomal and cytosolic fractions of Labskin control and induced with βNF in comparison with native skin were evaluated further and are discussed below.

4.4.2.1 Phase I XMEs (CYPs and CES) abundance

Cytochrome P450 (CYP) is the most important family of enzymes responsible for the metabolism of several xenobiotics. The data from the label-free quantitative proteomics experiment performed here indicates that the cytochrome P450 enzymes were almost absent in native skin and labskin model samples. Only a small number of isoforms:

CYP1B1, CYP7B1, CYP20A1 and CYP4F22 were identified and quantified as shown in Table 4.1. These data on the expression of CYP are in agreement with those published by Kazem *et al*., (2019) at mRNA or protein level in the Episkin™ FTM, Episkin™, SkinEthik™ RHE, Phenion® FT (PFT) and ORS-RHE EpiDerm™ models.

Interestingly, CYP1B1 was the most predominant CYPs in both the 3D skin model and native human skin. It was down-regulated (0.89-fold change) in the 3D skin model control (LS_DMSO). This is in agreement with published data, where the levels of CYP1B1 RNA have been reported to down-regulated in 3D skin model compared to human skin (Gelardi *et al*., 2001; Ahmad & Mukhtar, 2004; Schober *et al*., 2006; Wiegand *et al*., 2014).

Table 4.1: Detection levels of Phase I XMEs in microsomal and cytosolic fractions of Labskin control and induced with βNF compared with human skin by nano-LC-MS/MS. Protein abundance was based on the presence of at least two different tryptic peptides. The corresponding accession are indicated for all related proteins. The level of protein abundance is represented by fold change.

Accession	Description	Score	Unique Peptides	Fraction	Fold Change HS/LS_DMSO	Fold Change LS_DMSO/LS_BNF	Fold Change HS/LS_BNF
P11766	Alcohol dehydrogenase class-3	131.885	16	microsome	3.54	1.932	1.907
P47895	Aldehyde dehydrogenase 1A3	168.494	24	microsome	1.195	3.491	0.238
P30837	Aldehyde dehydrogenase X	35.363	8	microsome	1.533	1.533	0.958
P30838	Aldehyde dehydrogenase	54.576	11	microsome	14.992	2.112	8.183
P05091	Aldehyde dehydrogenase	139.859	20	microsome	5.098	1.987	3.157
Q06278	Aldehyde oxidase	193.836	31	microsome	-	1.8	8.147
P11766	Alcohol dehydrogenase class-3	51.126	11	cytosol	2.208	2.453	0.947
P30837	Aldehyde dehydrogenase X	50.894	14	cytosol	0.805	1.569	0.595
P47895	Aldehyde dehydrogenase 1A3	145.526	27	cytosol	0.38	2.908	0.139
Q8IZ83	Aldehyde dehydrogenase 16A1	135.959	23	cytosol	0.93	2.416	0.415

P05091	Aldehyde dehydrogenase	119.369	24	cytosol	2.551	2.006	1.319
P51648	Aldehyde dehydrogenase 3A2	55.555	11	cytosol	3.905	2.515	1.47
P30837	Aldehyde dehydrogenase X	50.894	14	cytosol	0.805	1.569	0.595
P28331	NADH-ubiquinone oxidoreductase	104.156	20	cytosol	2.036	2.023	1.096
P34913	Epoxide hydrolase 2	34.316	9	microsome	2.8	1.72	2.092
P07099	Epoxide hydrolase 1	82.436	18	cytosol	19.105	2.374	10.296
P23141	Carboxylesterase 1	145.486	24	microsome	2.45	2.27	1.93
P16435	NADPH--cytochrome P450 reductase	106.428	22	cytosol	1.246	2.221	0.574
P14854	Cytochrome c oxidase subunit 6B1	29.001	5	cytosol	2.552	2.096	0.927
Q6UW02	Cytochrome P450 20A1	12.676	4	cytosol	1.09	1.77	0.61
O75881	Cytochrome P450 7B1	4.439	2	cytosol	1.421	1.97	0.719
Q16678	Cytochrome P450 1B1	2.903	8	cytosol	0.89	1.53	0.58
Q6NT55	Cytochrome P450 4F22	2.586	2	cytosol	1.34	1.69	0.79
P16435	NADPH--cytochrome P450 reductase	106.428	22	cytosol	1.246	2.221	0.574
P30043	Flavin reductase (NADPH)	103.399	9	microsome	10.461	2.138	3.607
Q08257	Quinone oxidoreductase	150.792	19	microsome	0.852	2.002	0.393

Q53FA7	Quinone oxidoreductase	123.493	15	microsome	0.13	1.897	0.066
O95825	Quinone oxidoreductase 1	4.455	1	microsome	0.01	1.63	0.01
P07203	Glutathione peroxidase 1	40.388	9	microsome	3.959	1.446	2.883
P14550	Aldo-keto reductase 1A1	130.335	18	microsome	4.551	2.047	1.951
P15121	Aldo-keto reductase 1B1	139.014	17	microsome	4.298	1.855	2.035
O60218	Aldo-keto reductase 1B10	155.664	20	microsome	0.045	1.682	0.033
P52895	Aldo-keto reductase 1C2	158.204	5	microsome	3.689	1.918	1.87
P42330	Aldo-keto reductase 1C3	148.985	10	microsome	2.758	1.793	1.537
O60218	Aldo-keto reductase 1B10	88.684	15	cytosol	0.01	2.362	0.01
P14550	Aldo-keto reductase 1A1	61.42	13	cytosol	1.17	1.951	0.575
Q16853	Membrane primary amine oxidase	72.442	18	cytosol	9.667	10.972	0.912
P27338	Amine oxidase [flavin-containing] B	68.599	16	cytosol	0.0	0.0	11.104
P21397	Amine oxidase [flavin-containing] A	55.438	13	cytosol	1.069	2.356	0.442
P16152	Carbonyl reductase [NADPH] 1	160.362	15	microsome	3.024	1.732	1.637
O75828	Carbonyl reductase [NADPH] 3	86.97	11	microsome	32.414	1.904	13.004
P16152	Carbonyl reductase [NADPH] 1	105.576	16	cytosol	1.812	2.044	0.897

P28331	NADH-ubiquinone oxidoreductase	104.156	20	cytosol	2.036	2.023	1.096
P34913	Epoxide hydrolase 2	34.316	9	microsome	2.8	1.72	2.092
P07099	Epoxide hydrolase 1	82.436	18	cytosol	19.105	2.374	10.296
P31040	Succinate dehydrogenase flavoprotein	117.611	20	cytosol	3.143	1.99	1.415
Q9Y6N5	Sulfide:quinone oxidoreductase	197.657	29	cytosol	0.331	2.357	0.144
P40261	Nicotinamide N-methyltransferase	29.535	7	cytosol	2.916	2.611	1.147

Table 4.2: Detection levels of Phase II XMEs in microsomal and cytosolic fraction of Labskin control and induced with βNF compared with human skin by nano-LC-MS/MS. Protein abundance was based on the presence of at least two different tryptic peptides. The corresponding accession are indicated for all related proteins. The level of protein abundance is represented by fold change.

Accession	Description	Score	Unique Peptides	Fraction	Fold Change HS/LS_DMSO	Fold Change LS_DMSO/LS_BNF	Fold Change HS/LS_BNF
O15217	Glutathione S-transferase A4	10.495	4	microsome	0.879	1.633	0.532
Q9Y2Q3	Glutathione S-transferase kappa 1	63.526	7	microsome	0.623	1.634	0.384
O43813	Glutathione S-transferase LANCL1	102.976	13	microsome	1.564	1.714	0.901
P09488	Glutathione S-transferase Mu 1	66.725	5	microsome	48.194	1.646	36.773
P46439	Glutathione S-transferase Mu 5	48.639	6	microsome	10.763	2.540	4.238
P78417	Glutathione S-transferase omega-1	103.869	18	microsome	0.99	1.896	0.52
P09211	Glutathione S-transferase P	297.191	15	microsome	0.578	1.853	0.283
P30711	Glutathione S-transferase theta-1	40.215	7	microsome	9.693	1.72	5.571
P09211	Glutathione S-transferase P1	204.632	15	cytosol	0.284	2.242	0.119
Q9Y2Q3	Glutathione S-transferase kappa 1	66.177	8	cytosol	0.553	2.058	0.275

O14880	Microsomal glutathione S-transferase 3	50.028	6	cytosol	8.234	3.176	2.195
P78417	Glutathione S-transferase omega-1	35.459	9	cytosol	1.079	2.212	0.448
O43813	Glutathione S-transferase LANCL1	31.673	7	cytosol	1.272	2.268	0.457
P00390	Glutathione reductase	18.289	4	cytosol	5.393	0.01	0.0
P10620	Microsomal glutathione S-transferase 1	18.204	4	cytosol	12.038	3.008	4.002
Q99735	Microsomal glutathione S-transferase 2	5.623	1	cytosol	1.291	2.569	0.47
O00204	Sulfotransferase 2B1	118.244	16	microsome	0.772	2.144	0.346
O00204	Sulfotransferase 2B1	120.997	16	cytosol	0.282	2.199	0.1
Q9BWD1	Acetyl-CoA acetyltransferase, cytosolic	145.932	15	microsome	0.379	1.843	0.209
P24752	Acetyl-CoA acetyltransferase	79.807	14	microsome	3.06	1.741	1.661
Q06830	Peroxiredoxin-1	149.343	14	microsome	1.362	2.097	0.599
P32119	Peroxiredoxin-2	128.251	13	microsome	2.138	1.698	1.151
Q13162	Peroxiredoxin-4	91.338	11	microsome	4.658	1.657	2.38
P30044	Peroxiredoxin-5	106.321	12	microsome	1.355	1.602	0.829
P30041	Peroxiredoxin-6	151.553	20	microsome	2.303	1.733	1.32
Q06830	Peroxiredoxin-1	135.958	15	cytosol	0.672	2.574	0.278

P30041	Peroxiredoxin-6	104.13	17	cytosol	1.16	2.336	0.514
Q13162	Peroxiredoxin-4	101.473	13	cytosol	2.849	2.089	1.507
P32119	Peroxiredoxin-2	86.717	13	cytosol	1.154	2.404	0.518
P30044	Peroxiredoxin-5	78.247	12	cytosol	0.586	2.082	0.256
Q9BRX8	Peroxiredoxin-like 2A	35.585	7	cytosol	2.713	2.173	1.239
Q8NEX9	Short-chain dehydrogenase/reductase 9C 7	53.895	13	cytosol	0.363	2.683	0.12
P21980	Gamma-glutamyltransferase 2	126.127	23	microsome	0.01	1.892	0.01
Q08188	Gamma-glutamyltransferase E	167.618	25	microsome	6.422	2.077	2.993
P22735	Gamma-glutamyltransferase K	81.021	18	microsome	0.225	1.869	0.131
P22735	Gamma-glutamyltransferase K	278.064	38	cytosol	0.169	2.709	0.062
P21980	Gamma-glutamyltransferase 2	110.565	24	cytosol	0.202	2.481	0.081
Q08188	Gamma-glutamyltransferase E	39.63	11	cytosol	3.545	1.917	1.582
Q96PF1	Gamma-glutamyltransferase Z	1.451	1	cytosol	0.01	3.974	0.01

Western blot analysis also previously been used to show that CYP1B1 protein expression (Luu-The *et al*., 2005) is detected from different donors in human skin. Baron *et al*., (2001) had earlier confirmed the presence of the CYP1B1 protein in a LC-MS/MS based analysis at low abundance in the microsomal fraction of human skin keratinocytes which is also supports the nanoLC-MS/MS data presented here. CYP1B1 was demonstrated to be present in HS samples. In contrast, this protein isoform was not reported to be present in epiderm-200 model, native human skin, and human liver by van Eijl and co workers (van Eijl *et al*., 2012). The data from all studies, combined with this study, suggests that there is extensive genetic polymorphism in the level of CYP1B1. Luu-The *et al*., (2009) and Hu *et al*., (2010) showed that the CYP1B1 gene is evident at low level in EpiSkin™, EpiskinTMF™, and EpiDerm™ models which are in agreement with our data of RT-qPCR. This level was induced at high level (increased about 1.53-fold change) after 72 h with βNF as systemic treatment in the cytosol fraction of Labskin model (LS_βNF). The CYP1B1 Phase I XME is first time as further evidence for the induction of CYP1B1 at protein and RNA level as the most abundant in labskin model. CYP1B1 was detected at low level and induced in labskin at the RNA level by RT-qPCR and the protein level by LC-MS/MS as shown in both Chapter 2 and 3. Moreover, the induction of CYP1B1 gene expression in the ORS-RHE model was also induced at the RNA level by βNF after 72 h systemic application (Bacqueville *et al*., 2017). Hence, the possibility to induce the CYP1B1 protein to create a more "human skin like" model has been demonstrated.

With respect to other CYPs isoforms including CYP7B1, CYP20A1 and CYP4F22 in fresh excised human skin and labskin model, very little new information has became available (see Tables 4.1). These CYPs proteins were expressed lower in the microsomal fraction of LS_DMSO than LS_βNF samples using nano-LC-MS/MS. The activities were induced by βNF inducer. The effect of βNF on CYP7B1 was detected in Labskin, with increasing (1.97-fold change) higher observed compared with Labskin control samples that was at 1.421-fold change. The data also indicated CYP7B1 can also be confirmed at the protein level, which was also reported by label-free quantitative proteomics in the microsomal and cytosolic fractions of Labskin and huamn skin (Couto *et al*., 2021). In contrast, these CYPs were undetectable in the EPI-200 model as well as normal skin due to the variability between donors (van Eijl *et al*., 2012).

CYP20A1 and CYP4F22 at 1.09-fold and 1.34-fold respectively were also detected first time in labskin tissues, a significant increased of this protein were increased about 1.77-fold and 1.69-fold respectively after 72 h by 50 μM βNF in Labskin model compared with

untreated model. However, this levels of proteins were detected much lower in human skin at 0.61-fold and 0.79-fold change. Differences among these abundances in HS and LS were generated by label-free methods as shown in Table 4.1. The majority of CYPs protein abundance were overall detected relatively low activity in native skin. Our data suggest that the protein level are similar to those reported earlier in Chapter 3. In addition to these, the fold difference in CYP20A1 and CYP4F22 mRNA were only evaluated in either EpiDerm™ and human skin (Hu *et al*., 2010), to determine how well Labskin model represents native human skin. It has been reported by Couto *et al*., (2019) that enzyme levels in human skin and 3D skin model can be impacted by culture conditions as well as variability between batches and the skin tissue obtained from donors. These factors are known to decrease enzyme activity. However, the variations in the relative abundance in 3D skin compared to those in native human skin could be owing, in part, to chemicals exposure *i.e.* some suppression in the human samples has taken place. This might explain why in our findings, CYP proteins were more abundant in the 3D model.

Carboxyesterase 1 and 2 (CES1/2) are enzymes that play a significant role in the hydrolysis of xenobiotics (reviewed by Oesch *et al*., (2018) and Kazem *et al*., (2019)). CES1 protein is the most important hydrolase in human liver, as discussed by Berry *et al*., (2009) and Oesch *et al*., (2014), CES 1 expression XME was observed at good levels in the microsomal fraction of the 3D model and HS as illustrated in Table 4.1. This level was smilar in LS_DMSO control (2.45-fold change) compared with LS_βNF (2.27-fold change). Therefore is shown for the first time as being inducible by 50 µM βNF inducer. Additionally it was detected in slightly lower abundance at 1.93-fold compared with both in LS_DMSO and LS_βNF in human skin. The data was in good agreement with earlier studies, CES 1 was readily detected at low level in the *in vitro* model, CES 1 protein in the epiderm-200 model and CES 1 gene in ORS-RHE models (van Eijl *et al*., 2012; Bacqueville *et al*., 2017). In addition, Hu *et al*., (2010) also showed a similar level to those reported here in 3D skin model and human skin. This enzyme was confirmed more recently with methylphenidate hydrochloride as a substrate in Labskin using MALDI-MSI (Couto *et al*., 2021). The Labskin model therefore has the capability for establishing the metabolism of substrates for CES1.

4.4.2.2 Phase II XMEs (GSTs) abundance

Among Phase II XMEs, glutathione transferase (GSTs) are widely distributed in the skin and are essential for several conjugation reactions. Many GSTs isoforms were identified and quantified at significant levels in the Labskin model and native human skin (Table

4.2). Of the GSTs enzymes investigated, the GSTP1 and GSTO1 expression which catalyze the conjugation of reduced glutathione to various exogenous and endogenous hydrophobic electrophiles, are the most abundant isoforms expressed at the protein levels in Labskin models as well as human skin samples (Table 4.2). The Phase II of GSTP1 and GSTO1 were detected in both the cytosolic and microsomal fractions of skin and the model as shown in Table 4.2. These proteins were induced by treatment with βNF inducer in our model. A label free proteomics study was previously used to study the expression levels of GST proteins in Labskin (Couto *et al*., 2021). However, the development of nano-LC high resolution mass spectrometery methodology for such studies as reported here, has improved the sensitivity such that a greater coverage of Phase I and Phase II XME was obtained.

The Phase II enzymes, glutathione S-transferases P1 and glutathione S-transferases omega1 proteins were easily detectable in *in vitro* skin models "LS_DMSO and LS_βNF" at high levels compared to those measured in native human skin. From all Phase II XMEs identified, GSTP1 was detected as the most abundant protein in the fractions of Labskin. The level in microsomal and cytosolic fractions were induced with βNF induction, which were increased about 1.853-fold and 2.242-fold respectively after 72 h. In contrast, these enzymes activity were not induced further by 3-methylcholanthrene (Hu *et al*., 2010). In human skin cytosolic and microsomal fractions, GSTP1 expression was also present, however, lower at 0.119-fold and 0.283-fold respectively than in both LS_DMSO control and LS_βNF. Moreover, GSTP1 has been reported to be highly expressed at the mRNA and their activity in the EpiDerm cytosol than in the epidermal of human skin (Harris et al., 2002; Luu-The *et al*., 2009; Wiegand *et al*., 2014; Götz *et al*., 2012). This expression was verified by RT-qPCR as gene to be functional in the EpiDerm™ using 1-chloro-2,4-dinitrobenzene (CDNB) substrate, and clearly confirmed at protein level in the epiderm-200 model with CDNB as a substrate by LC-MS/MS (van Eijl *et al*., 2012).

Glutathione S-transferase omega-1 (GSTO1) of Phase II was also detected in skin and the skin models as shown in Table 4.2. With respect to these observations of GSTO1 by Hewitt *et al*., (2013), the protein levels seen to be expressed at a comparable level in Labskin model control compared to those in native skin. GSTO1 was quantified at 0.99-fold in microsomal fraction and 1.07-fold in cytosolic fraction of LS_DMSO model. Furthermore, GSTO1 expression was detected at the protein level in native human skin. This is in an agreement with a previous study (Couto *et al*., 2021), GSTO1 was the second most abundant Phase II enzyme. The relative protein expression of GSTO1 in Labskin

model was induced at the highest level. The response of βNF in both the cytosolic and the microsomal fraction of LS_βNF was increased about 1.896-fold and 2.212-fold respectively. This induction was increased after 72 h in 3D induced model. Our results on inducibility of GSTO1 expression is consistent with those of Harris *et al*., (2002) as further investigation for protein expression in the epiderm-200 model and it has been confirmed using GST substrate (van Eijl *et al*., 2012).

The label-free approach also showed treatment with βNF caused significant increase of glutathione S-transferase in the microsomal and cytosolic fractions of 3D skin model. The protein levels were reported at the high level compared with human skin in Table 4.2. However, only glutathione S-transferase Mu 5 and Glutathione S-transferase theta-1 were observed to be significantly higher in human skin compared to the 3D model. In addition, these GSTs isoforms, were not induced after 72 h in LS_βNF. Conflicting observations among the protein levels in native human skin and 3D skin models, the abundance and proteomics analyses could be because the enzymes are preferentially expressed in particular human anatomical sites or because the levels of proteins are controlled as well as varibility of donors.

Although the abundance of CYPs and CES enzymes were described at gene and protein level to be low in comparison with other Phase I enzymes (Bacqueville *et al*., 2017; van Eijl *et al*., 2012), CYP1B1 and CES1 could be identified in our 3D skin model and native human skin. In accordance with other studies, the levels of Phase II were commonly presented higher in this study than those of Phase I XMEs, the highest abundance was quntified for GSTs protein (notably GSTP1 and GSTO1). The comparison of GSTP1 and GSTO1 are in agreement with the findings in native skin (Hu *et al*., 2010).

The proteomics raw data of this chapter has been attached in the appendix III link page (220).

4.5 Conclusion

The use of nanoLC-MS/MS in this study allowed for a study of abundance ratio of XMEs present in Labskin models and native human skin as well as more in depth investigations of certain Phase I and II proteins levels. Clearly, low level of CYPs, CES of Phase I and GSTs of Phase II XMEs in native skin were also reflected in Labskin models. However, our data set showed that βNF induced the production of CYP1B1, CES, GSTP1 and

GSTO1 were detected at the measurable protein level. Even though low RNA level of CYP1B1, CES1, GSTP1 and GSTO1 in the Labskin model induced with βNF were found (as reported in Chapter 2), the proteins levels could be quantified using nanoLC-MS/MS based proteomics. A comparison of Phase I and Phase II XMEs indicated that the Phase II enzymes are much more abundant than Phase I enzymes.

4.6 References

Aebersold, R., Burlingame, A. L., & Bradshaw, R. A. (2013). Western blots versus selected reaction monitoring assays: time to turn the tables? *Molecular & Cellular Proteomics, **12***(9), 2381-2382.

Ahmad, N., & Mukhtar, H. (2004). Cytochrome p450: a target for drug development for skin diseases. *Journal of Investigative Dermatology, **123***(3), 417-425.

Bacqueville, D., Jacques, C., Duprat, L., Jamin, E. L., Guiraud, B., Perdu, E., Bessou-Touya, S., Zalko, D., & Duplan, H. (2017). Characterization of xenobiotic metabolizing enzymes of a reconstructed human epidermal model from adult hair follicles. *Toxicology and Applied Pharmacology, 329*, 190-201.

Baron, J. M., HoÈller, D., Schiffer, R., Frankenberg, S., Neis, M., Merk, H. F., & Jugert, F. K. (2001). Expression of multiple cytochrome p450 enzymes and multidrug resistance-associated transport proteins in human skin keratinocytes. *Journal of Investigative Dermatology, **116***(4), 541-548.

Berry, L. M., Wollenberg, L., & Zhao, Z. (2009). Esterase activities in the blood, liver and intestine of several preclinical species and humans. *Drug Metabolism Letters, **3***(2), 70-77.

Couto, N., Al-Majdoub, Z. M., Achour, B., Wright, P. C., Rostami-Hodjegan, A., & Barber, J. (2019). Quantification of proteins involved in drug metabolism and disposition in the human liver using label-free global proteomics. *Molecular Pharmaceutics, **16***(2), 632-647.

Couto, N., Newton, J. R., Russo, C., Karunakaran, E., Achour, B., Al-Majdoub, Z. M., Sidaway, J., Rostami-Hodjegan, A., Clench, M. R., & Barber, J. (2021). Label-free quantitative proteomics and substrate-based mass spectrometry imaging of xenobiotic metabolizing enzymes in ex vivo human skin and a human living skin equivalent model. *Drug Metabolism and Disposition, **49***(1), 39-52.

El-Khateeb, E., Vasilogianni, A., Alrubia, S., Al-Majdoub, Z. M., Couto, N., Howard, M., Barber, J., Rostami-Hodjegan, A., & Achour, B. (2019). Quantitative mass spectrometry-based proteomics in the era of model-informed drug development:

applications in translational pharmacology and recommendations for best practice. *Pharmacology & Therapeutics, 203*, 107397.

Gelardi, A., Morini, F., Dusatti, F., Penco, S., & Ferro, M. (2001). Induction by xenobiotics of phase I and phase II enzyme activities in the human keratinocyte cell line NCTC 2544. *Toxicology in Vitro, **15***(6), 701-711.

Götz, C., Pfeiffer, R., Tigges, J., Ruwiedel, K., Hübenthal, U., Merk, H. F., Krutmann, J., Edwards, R. J., Abel, J., & Pease, C. (2012). Xenobiotic metabolism capacities of human skin in comparison with a 3D-epidermis model and keratinocyte-based cell culture as in vitro alternatives for chemical testing: phase II enzymes. *Experimental Dermatology, **21***(5), 364-369.

Harris, I. R., Siefken, W., Beck-Oldach, K., Brandt, M., Wittern, K., & Pollet, D. (2002). Comparison of activities dependent on glutathione S-transferase and cytochrome P-450 IA1 in cultured keratinocytes and reconstructed epidermal models. *Skin Pharmacology and Physiology, **15***(Suppl. 1), 59-67.

Hewitt, N. J., Edwards, R. J., Fritsche, E., Goebel, C., Aeby, P., Scheel, J., Reisinger, K., Ouédraogo, G., Duche, D., & Eilstein, J. (2013). Use of human in vitro skin models for accurate and ethical risk assessment: metabolic considerations. *Toxicological Sciences, **133***(2), 209-217.

Hu, T., Khambatta, Z. S., Hayden, P. J., Bolmarcich, J., Binder, R. L., Robinson, M. K., Carr, G. J., Tiesman, J. P., Jarrold, B. B., & Osborne, R. (2010). Xenobiotic metabolism gene expression in the EpiDerm™ in vitro 3D human epidermis model compared to human skin. *Toxicology in Vitro, **24***(5), 1450-1463.

Kazem, S., Linssen, E. C., & Gibbs, S. (2019). Skin metabolism phase I and phase II enzymes in native and reconstructed human skin: a short review. *Drug Discovery Today,*

Luu-The, V., Duche, D., Ferraris, C., Meunier, J., Leclaire, J., & Labrie, F. (2009). Expression profiles of phases 1 and 2 metabolizing enzymes in human skin and the reconstructed skin models Episkin™ and full thickness model from Episkin™. *The Journal of Steroid Biochemistry and Molecular Biology, **116***(3-5), 178-186.

Luu-The, V., Paquet, N., Calvo, E., & Cumps, J. (2005). Improved real-time RT-PCR method for high-throughput measurements using second derivative calculation and double correction. *BioTechniques*, ***38***(2), 287-293.

Neis, M. M., Wendel, A., Wiederholt, T., Marquardt, Y., Joussen, S., Baron, J. M., & Merk, H. F. (2010). Expression and induction of cytochrome p450 isoenzymes in human skin equivalents. *Skin Pharmacology and Physiology*, ***23***(1), 29-39.

Oesch, F., Fabian, E., Guth, K., & Landsiedel, R. (2014). Xenobiotic-metabolizing enzymes in the skin of rat, mouse, pig, guinea pig, man, and in human skin models. *Archives of Toxicology*, ***88***(12), 2135-2190.

Oesch, F., Fabian, E., & Landsiedel, R. (2018). Xenobiotica-metabolizing enzymes in the skin of rat, mouse, pig, guinea pig, man, and in human skin models. *Archives of Toxicology*, ***92***(8), 2411-2456.

Oesch, F., Fabian, E., Oesch-Bartlomowicz, B., Werner, C., & Landsiedel, R. (2007). Drug-metabolizing enzymes in the skin of man, rat, and pig. *Drug Metabolism Reviews*, ***39***(4), 659-698.

Schober, W., Luch, A., Soballa, V. J., Raab, G., Stegeman, J. J., Doehmer, J., Jacob, J., & Seidel, A. (2006). On the species-specific biotransformation of dibenzo [a, l] pyrene. *Chemico-Biological Interactions*, ***161***(1), 37-48.

van Eijl, S., Zhu, Z., Cupitt, J., Gierula, M., Götz, C., Fritsche, E., & Edwards, R. J. (2012). Elucidation of xenobiotic metabolism pathways in human skin and human skin models by proteomic profiling. *PloS One*, ***7***(7), e41721.

Wiegand, C., Hewitt, N. J., Merk, H. F., & Reisinger, K. (2014). Dermal xenobiotic metabolism: a comparison between native human skin, four in vitro skin test systems and a liver system. *Skin Pharmacology and Physiology*, ***27***(5), 263-275.

Chapter 5

Demonstration of the Metabolic Pathway Responsible for Benzydamine metabolism in 3D Skin Model studied by using MSI and LC-MS/MS.

5.1 Introduction

The skin is utilized as a route of drug administration for topical and systemic treatments where the first pass effect must be avoided. Since there are difficulties in obtaining representative human skin for preclinical studies because of issues such as race, age, gender, and genetic polymorphisms, there is a pressing need to develop an alternative *in vitro* model of human skin that can be used (Russo *et al*., 2018). To this end, the use of 3D skin tissue models such as "Labskin" (Innovenn (U.K.) Ltd. York U.K.) has been proposed for drug absorption and biotransformation studies. In recent reviews by Oesch, *et al*., (2018) and Kazem *et al*., (2019), several *in vitro* skin models including reconstructed human epidermis (RHE), 3D differentiated epidermis cultures derived from human keratinocytes (EpiSkin and EpiDerm) and full thickness living skin equivalents (LSEs), such as EpiDermFT, Episkin, and Labskin models in drug absorption and metabolism have been described. These avalibale 3D living skin equivalents (LSEs) are proposed as replacements for animal models which are able to provide useful data.

The use of matrix-assisted laser desorption mass spectrometry imaging (MALDI-MSI) in 3D *in vitro* models of human skin is a valid method for investigation both drug absorption or drug metabolism in skin. A study by Avery *et al*., (2011) reported the first combination of MSI with a comercially available 3D model in an investigation of the absorption of imipramine. The imipramine absorption was clearly detected in the skin epidermal model "Straticell" but no clear evidence of metabolism of imipramine was obsereved. In more recent report by Harvey *et al*., (2016), MALDI-MSI was used to study a Labskin model chemically induced to represent psoriasis disease (Harvey *et al*., 2016). Further work conducted on the Labskin model studied the low levels of Phase I and II enzymes (Russo *et al*., 2018).

The study by Russo *et al*., (2018) demonstrated that the determination of terbinafine absorption as topical delivery treatment and its fragment ions in the epidermal region of Labskin tissues sections by both MALDI-MSI and LC-MS/MS approach. This model has been comprehensively applied for MSI owing to its great physical strength and ease of crysectioning. However, no clear evidence of drug biotransformation in the 3D Labskin models were detected earlier. In fact, there is no consensus agreement on the variety and distribution of metabolizing enzymes present in the epidermal layer of skin (Oesch *et al*., 2014). Additional investigation of Phase I and Phase II XME in skin are required in order to study the reasons for the apparent low levels detected in LSE models.

In a recent review by Oesch *et al*., (2018) and Kazem *et al*., (2019), FMO and CYPs of Phase I and GSTs of Phase II activities in human skin and 3D skin models were reported to be detected. The presence of low levels FMOs and CYPs, and supports the idea that N-methylation and oxidation in skin are mainly catalyzed by CYPs and non-CYP (FMO1/3) mediated. The nonsteroidal anti-inflammatory drug benzydamine (BZD) is a specific substrate used as a topical treatment for characterization of enzyme activity of FMOs and CYPs (Figure 5.1).

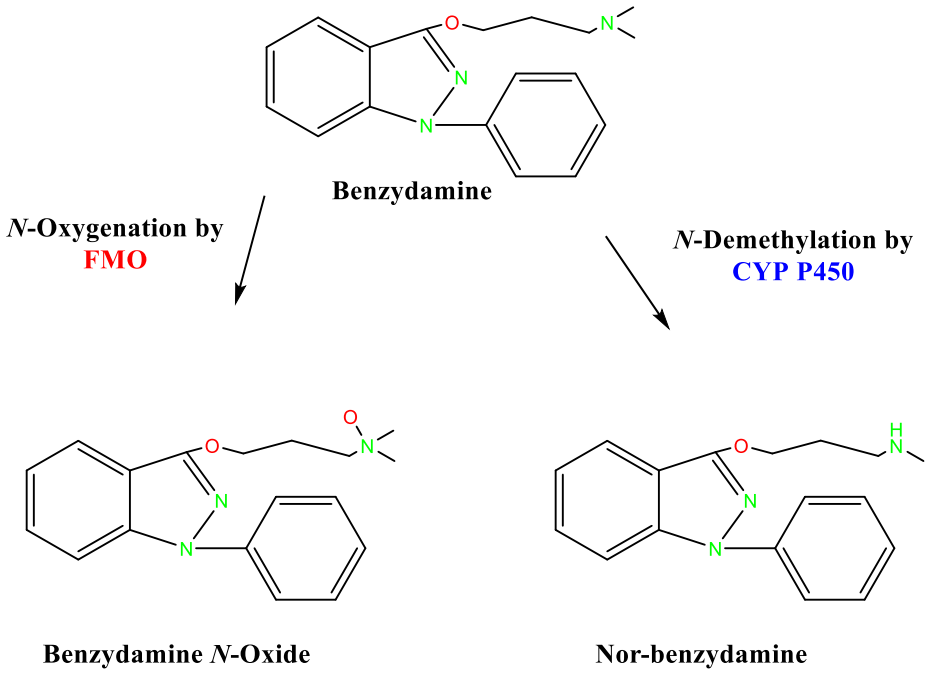

Figure 5.1: Biotransformation pathways and the reactive metabolites of benzydamine substrate.

The drug of benzydamine (BZD) has been reported to be used to measure the activities of FMO1/3 and CYPs in human liver and it is metabolised through N-oxygenation pathways mediated by FMOs to benzydamine *N*-oxide and *N*-demethylation pathways mediated by CYPs as shown in Figure 5.1 (Störmer *et al*., 2000). Störmer *et al*., (2000) and Taniguchi-Takizawa *et al*., (2015) studied the N-oxygenation and N-demethylation activities of these enzymes as marker reactions for FMO1, FMO3 and CYP2D6 in human liver. For the first time, FMOs and CYPs activities were demonstrated for human reconstructed skin models, such as EpiDerm™ and the PhenionFT (Jäckh *et al*., 2011). FMO1/3 in EpiDerm™ model indicated that BZD-*N*-oxidation capacity compared with PhenionFT as shown in systemic substrate incubation. The comparision of BZD oxidation in the two Labskin models could be supported by the BZD as substrate which was showed to be more metabolised detected by FMO1/3 and CYPs (Störmer *et al*., 2000).

5.2 Aims of the Chapter

In this Chapter, an investigation of the detection and localisation of benzydamine (BZD) and its metabolites in commercially available 3D skin model (Labskin) using LC-MS/MS, and MSI, DESI-MS techniques is reported. Here, we reported data supporting the activities of Phase I XMEs (FMO1/3) in 3D skin control and induced 3D Labskin model with β-naphthoflavone (βNF), phenobarbital (PB) and *all-trans* retinoic acid (RA) used as inducers to evaluate the relative contributions of these enzymes in the metabolism study of BZD drug as marker reactions for the enzymes levels.

5.3 Experimental section

5.3.1 Materials

Alpha cyano-4-hydroxycinnamic acid (α CHCA), benzydamine (MW 310.0), and ethanol (EtOH), were purchased from Sigma-Aldrich (Manchester,UK). LC-grade methanol (MeOH) and LC-grade acetonitrile (ACN) and 0.1% formic acid were obtained from Fisher Scientific (Thermofisher.com). Labskin living skin equivalent (LSE) samples were provided by Innovenn (U.K.) Ltd. (York, England).

5.3.2 Enzyme induction

After delivery LSE samples, the skin tissue was activated for 24 h at 37 °C and 5% CO_2 in Labskin maintenance media (4.5 mL per well). The LSE induction experiments were conducted and treated in Labskin maintenance media by systematic treatment with 50 µM β-naphthoflavone (βNF), 2 mM phenobarbital (PB) and 10 µM *all-trans* retinoic acid (RA) for 72 h as described in Chapter 2.3.4. Induction was performed through the addition of inducers dissolved in DMSO. The medium was replaced every 24 h.

5.3.3 LSE Sample Treatment

After 72 h of LSE induction experiments, 20 µL of 300 µg BZD benzydamine (BZD) was treated on each LSE tissue and spread out on an area of 2 cm^2 of the Labskin surface and incubated for 48 h at 37 °C and 5 % CO_2 in fresh Labskin maintenance media. The BZD substrate was dissolved in an mixture made up of water/olive oil (80:20 v/v). LSE control samples were treated with 20 µL of the mixture water/olive oil (80:20 v/v) and incubated for 48 h. After removed LSE from the well insert, all LSEs samples washed with LC-grade MeOH to eliminate excess formulation and, snap-frozen with liquid nitrogen cooled isopentane (2-5 min) and then, stored at −80 °C.

After directly following drug treatment, the 30 µm frozen LSEs tissue sections using a Leica 200 UV cryostat (Leica 200 UV, Leica Microsystems, Milton Keynes, U.K.) were cryosectioned and freeze-thaw mounted onto "polycat" microscope slides (SLS, Hessle, UK) and stored at −80 °C as described by Russo *et al*., (2018).

5.3.4 Sublimation and Recrystallisation

For MALDI-MSI, α CHCA matrix as sublimation method was used for Labskin tissues sections. α-CHCA (300 mg) was spread at the bottom of the sublimation apparatus (Sigma-Aldrich). ITO-coated glass slides containing untrated and treated Labskin tissues were attached to the flat top of the chamber using double-sided tape. The top of the chamber was then attached to the bottom using an O-ring seal and the vacuum was applied. When a stable vacuum of 2.5 x 10^{-2} Torr was reached, the top was filled with cold water (5 °C) and the temperature was set to 180 °C. The process was carried around 20 minutes.

After sublimation process was performed, a glass Petri dish was used to carry out the recrystallisation on sublimated Labskin tissues sections. The ITO glass slide was attached to the underside of a petri dish lid using standard double-sided tape. Solution of 1 mL deionised water and 50 µL LC grade MeOH was pipetted onto filter paper placed at the bottom of the petri dish. Then, the lid was placed on the rest of the dish and placed in the oven for 2 minutes at 180 °C. After that, ITO slide was returned to the oven to dry for a further 2 minutes.

In contrast, no matrix application was used for LSEs tissue sections analysis using both DESI-MS Synapt XS and DESI-MS MRT techniques.

5.3.5 DESI-MS Mass Spectrometry Imaging

All LSEs sample tissues were imaged using Synapt XS and MRT mass spectrometer (Waters, Manchester, U.K.). The DESI solvent used was 95 % of MeOH containing 5 % MQ H20 and 0.5 mL of formic acid. The flow rate injection was 2 µL/min. Multiple images were run in Masslynx^{TM}. All LES samples were analysed in positive ion mode using a scan range of m/z 100-1200 Da, resolution 20,000 FWHM) at spatial resolution of 75 µm x 75µm. Scan time was 45 min. The calibration of instrument was performed by using liver tissue. The ion mobility function was not enabled. Capillary 0.75 kv.

For MALDI-MSI, Labskin experiments were performed using an Autoflex III (Bruker Daltonik GmbH, Germany) equipped with a 200-Hz Smartbeam^{TM} laser. For MALDI-

MSI were acquired in positive mode with mass range of m/z 100-1500, resolution 10,000 FWHM at pixel size of 50 μm × 50 μm, and with laser energy set to 250 arbitrary units.

5.3.6 Skin Extraction

For LC−MS/MS experiments, the LSEs control and treated LSEs tissues were placed for 2 min in 1× PBS preheated at 60 °C. The dermal and epidermal layers from the 3D skin models were isolated by incubation in phosphate-buffered saline (PBS) at 65 °C for 2 min prior by using forceps; then homogenization with a manual homogeniser (Ultra-Turrax, Germany) in 0.5 % of MeOH (Capolongo *et al*., 2010). The homogenate samples were then centrifuged at 13000 rpm at 4 °C for 10 min (Centrifugation, Micro Star17R Microcentrifuge, Germany). The LSE samples stored at -80 °C and ready for LC-MS/MS analysis.

5.3.7 Labskin model with LC−MS/MS

LC−MS/MS were applied using a Xevo G2-XS QToF (Waters Coorporation, Manchester, U.K.) with ionization mode ESI^+ ionization mode. The LC separation was performed using an Acquity UPLC® peptide GSHTM-C18 Column (WatersTM, UK) microbore column (2.1 mm x 100 mm, 1.7 μm) using a 20 min gradient of mobile phase B 80% (acetonitrile) and mobile phase A (20% containing 0.1 % formic acid). The gradient eluition was conducted as follows: 0.0−2.0 min (A, 80%; B, 20%), 2.0−12.0 min (A, 20%; B, 80%), 12.0−18.0 min (A, 20%; B, 80%), 18.0 − 20.0 min (A, 80%; B, 20%). The flow rate was 0.2 mL/min. The injection volume 5 μL. The MS parameters applied: capillary voltage, 3.0 Kv, cone voltage, 40.0 V, source temperature 150 °C, desolvation temperature 500 °C, desolvation gas 1000 L/ h, and cone gas 150 L/h. Argon was utilized as a collision gas and the collision energy was set at 20 eV. The retention time was ∼10.0 min.

5.3.8 Data Analysis

For LC−MS/MS data files, the data of chromatograms peaks for benzydamine (BZD) and its metabolites were also integrated and processed using Mass Lynx software (Waters Corporation, U.K.). Three replicate measurements of each sample were applied.

The DESI-MS imaging on SYNAPT XS and MRT data were set out and and processed using the HDI 1.4 software (Waters Corporation, UK). DESI-MS spectra was processed using MassLynx software. Three replicate images of each epidermal skin section were applied.

5.4 Results and discussion

In a similar way to the detailed study of drug absorption in the Labskin model (Russo *et al*., 2018), it is crucial to investigate drug biotransformation in order to evaluate the toxic effects of chemicals and cosmetics. “Labskin” was used to examine of Phase I activity include cytochrome P450 (CYPs) and non-cytochromes such as flavin-containing monooxygenase (FMO) enzymes activities. The activity of these XME plays an important role in metabolism studies. Since as reported in Chapter 2 and 3, the low levels of FMO1/3 and CYPs gene/protein were expressed in Labskin, chemicals inducer were used in this study for induction of Phase I and II enzymes. The inducers used were β-naphthoflavone (βNF), *all-trans* retinoic acid (RA), and phenobarbital (PB).

Benzydamine (BZD) was used in a “substrate-based mass spectrometry imaging” experiment to detect the presence of Phase I XME in 3D skin tissue. Here, the surface of a commercially available 3D skin model was treated with the BZD for 48h after 72 h induction with one of 50 µM βNF, 10 µM RA and 2 mM PB at 37 °C and 5% CO_2 in fresh Labskin media. The aim of this study was to study the effects of the inducers by detection of the resulting metabolites of BZD substrate based on LC-MS/MS as well as DESI-MS on Synapt XS and MRT were employed. The use of MS here with its high sensitivity and specificity allowed the localisation of the metabolites to the epidermal region for the first time. These data suggest that the analysis of Labskin (LS) could be developed further for a range of drug experiments.

Labskin treated with in water/olive oil (80:20) for 48 hours was used as a blank (Figure 5.2). The mass chromatograms of LC-MS/MS corresponding to the $[M+H]^+$ ions for BZD and its metabolities were integrated and processed.

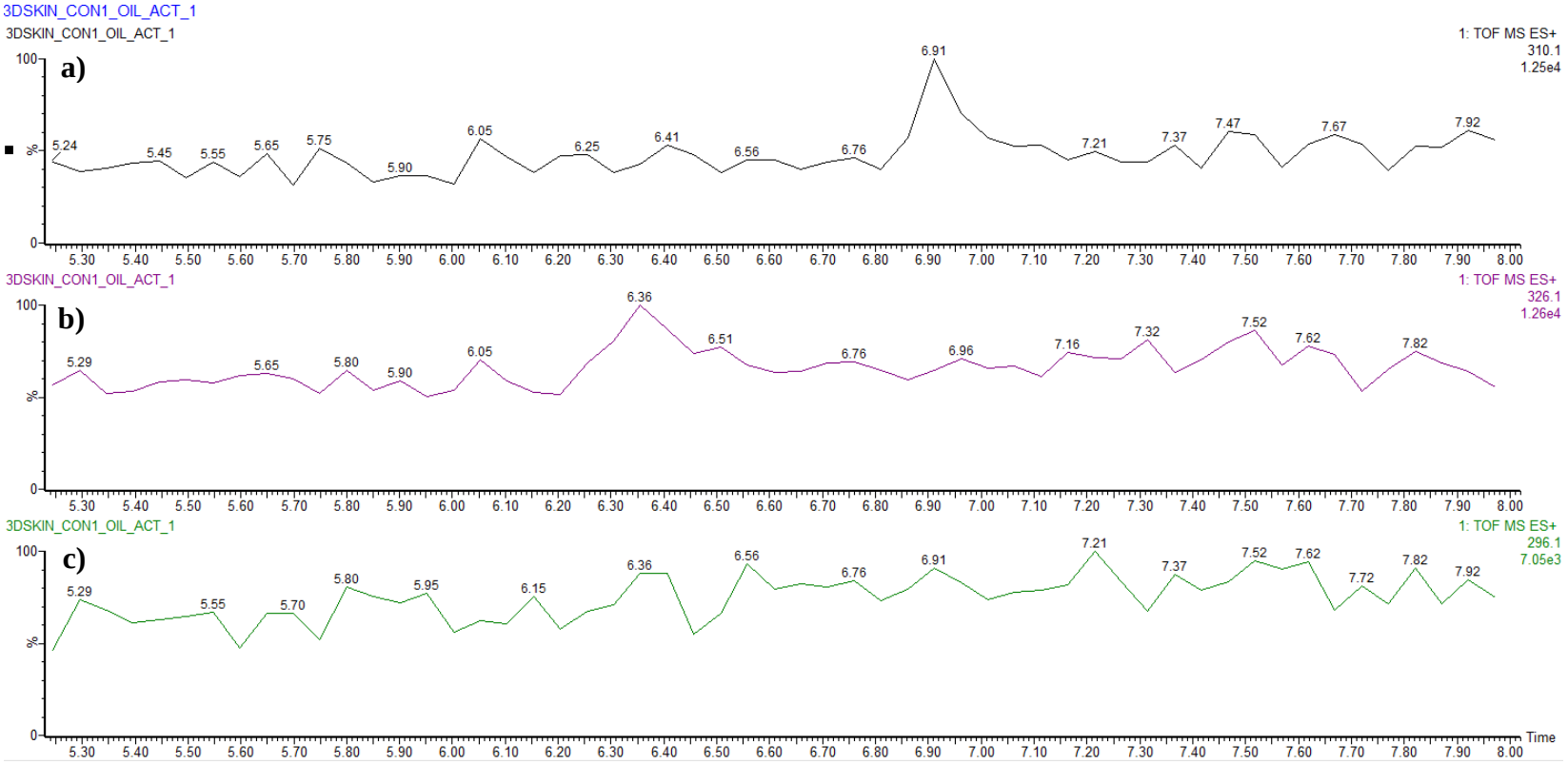

Figure 5.2: Representative mass chromatograms of the LS model non-treated with BZD as topical treatment. LC-MS/MS chromatographic separations of Labskin section treated with in water/olive oil (80:20) for 48 hours were selected as blank Labskin section control in epidermis layer (untreated BZD on the Labskin surface). **(a)** No BZD *m/z* 310.18 at 6.71 min and its metbolities: **(b)** *m/z* 326.17 (7.01 min) BZD-*N*-Oxide and **(c)** *m/z* 296.16 (6.56 min) nor-benzydamine).

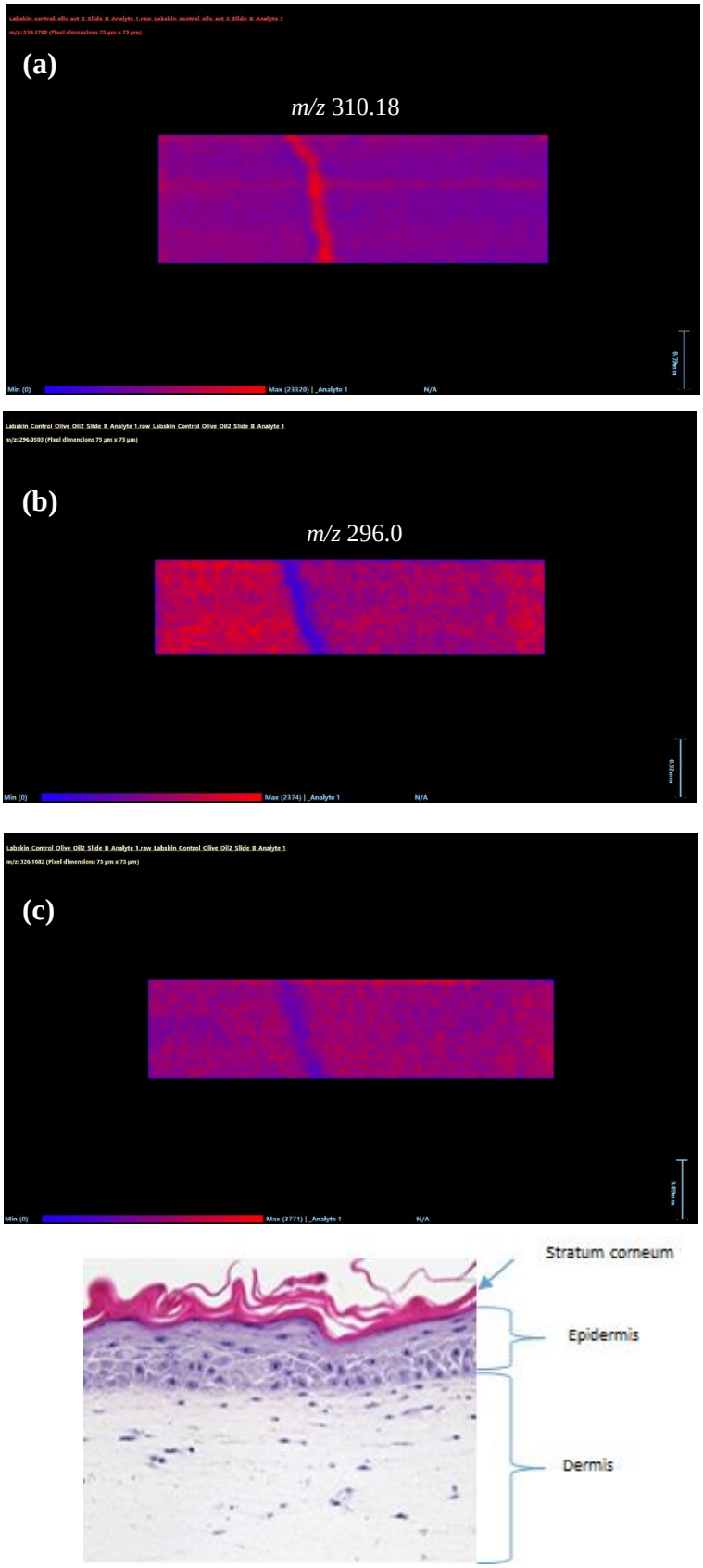

Figure 5.3: DESI-MSI images of non BZD treated (untreated) Labskin model as control: **(a)** *m/z* 310.17 BZD **(b)** *m/z* 296.0 demethyl-BZD and **(c)** *m/z* 326.16 BZD-*N*-Oxide **(D)** the structure of the skin. *Resolution* image = 75 µm. TIC normalisation. The mass value in the scale bar was shown in the top (310.18 *m/z* and 326.16 *m/z* and 296.0 *m/z* in white).

In order to study the distribution of BZD and its metabolities in the epidermis, DESI-MSI was used. MS images clearly showed the epidermis for each Labskin section, and thus these data are very important for the definition of region of interest and extraction of peaks intensity. Figure 5.3 supports the LC-MS/MS data showing that neither BZD nor its major metabolites were detected in the epidermal layer for the control.

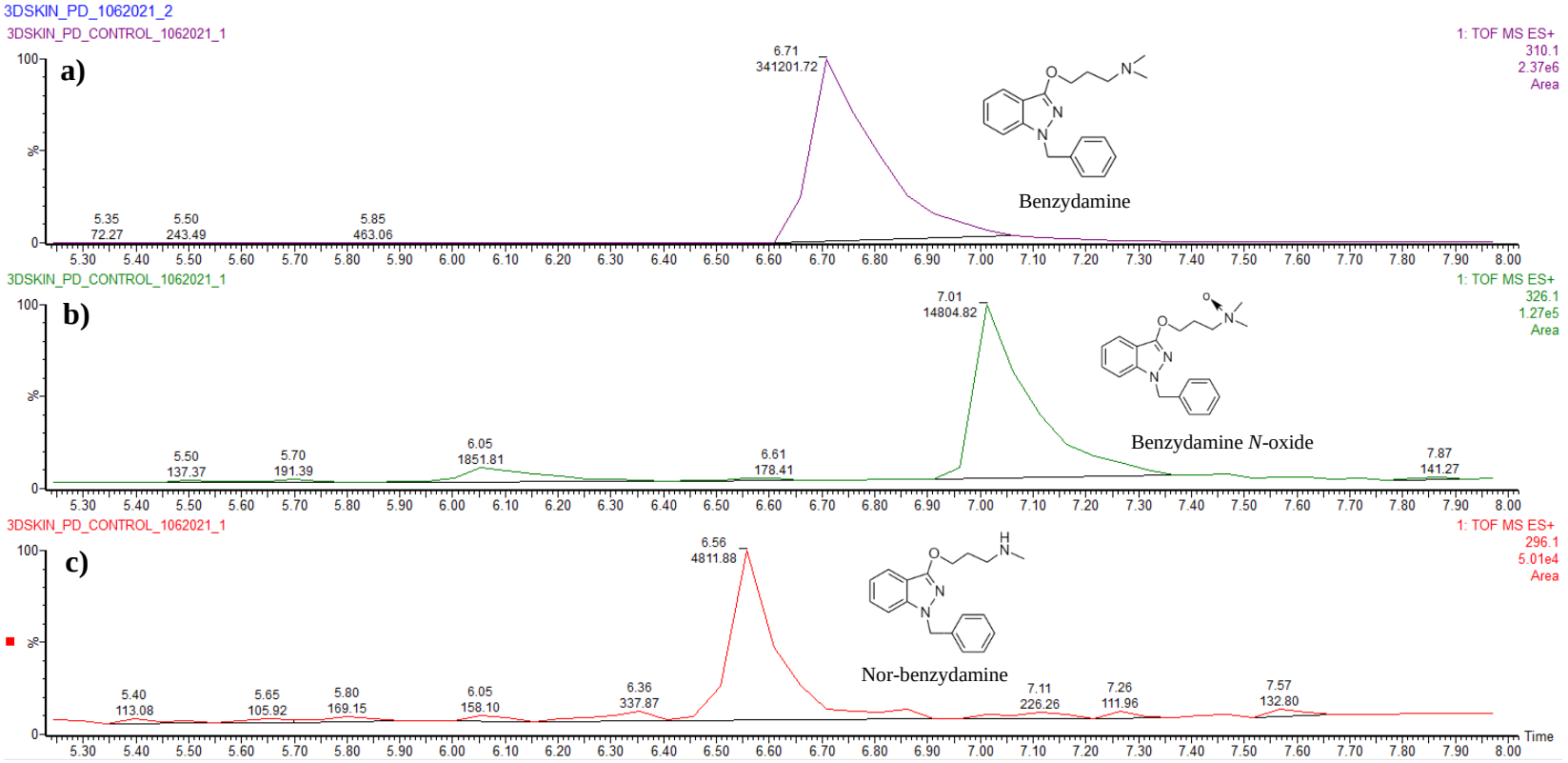

Figure 5.4: Representative of an extracted ion chromatograms of the 3D skin model treated with BZD (LS_BZD) non-induced Labskin with βNF, RA and PB inducers. FMO1/3 and CYPs activities were measured by generated fragments ions of BZD metbolities. **(a)** *m/z* 310.18 (6.71 min) BZD and its metbolities **(b)** *m/z* 326.18 (7.01 min) BZD-N-Oxide and **(c)** *m/z* 296.17 (6.56 min) nor-benzydamine. The peak ratio of the BZD metbolities were used to evaluate the statistical significance of non-induced 3D skin model and induced 3D skin model in terms of precision and accuracy LC/MS/MS.

As shown in the LC/MS data (Figure 5.4 a) , following treatment of a non-induced section BZD substrate was detectable in the epidermal layer at *m/z* 310.18 (6.71 min) along with the *N*-oxide *m/z* 326.17 (7.01 mins) and desmethyl BZD *m/z* m/z 296.17 (6.56 mins). The ratios of the peak areas for BZD and its metabolites were examined as an measure for FMO1/3 and CYPs activities in the Labskin model. To assess the degree of activity the peak areas of the *N*-oxide and desmethyl metabolites were expressed as a % of the peeak area of the parent drug (Table 5.1). This compartison of peak area detected in non-induced LS_BZD control (treated only with BZD), compared with the inducers indicates the chemical effect of βNF, RA and PB. The peak area in LC-MS/MS of LS_BZD control (non-induced) was significantly different about 3.84 ± 0.77 in BZD-*N*-Oxide and 1.89 ± 0.64 desmethyl-BZD corresponding to BZD substrate (See Table 5.1). The peak ratio of BZD elimination by Labskin model were calculated based on these metabolites. In this model, benzydamine *N*-oxide were slightly higher than those of demethyl benzydamine due to the low levels of CYPs genes/proteins as shown in RT-qPCR and proteomics data (Chapters 3 and 4). Almost all of Phase I XME genes/proteins observed low in human skin compared with human liver (van Eijl *et al*., 2012; Wiegand *et al*., 2014; Oesch *et al*., 2018). These reports indicated that the levels in the 3D skin model were mostly lower by about 4-10-fold than that found in liver.

Table 5.1: Validation of BZD absorbtion and metabolism in 3D Labskin model was performed according to percentage of the peak area in non-induced LS_BZD control compared with those that in the induced LS_BZD with βNF, RA and PB.

Labskin Samples	**Peak Area BZD**	**Peak Area Desmethyl BZD**	**Peak Area BZD-*N*-Oxide**	**%Desmethyl**	**%*N*-Oxide**
Control	298807	5197	12077	1.89 ± 0.64	3.84 ± 0.77
βNF	266300	3413	10572	1.51 ± 0.32	4.06 ± 1.33
RA	229483	5197	12077	2.06 ± 0.13	2.85 ± 0.14
PB	151078	2046	6733	1.52 ± 0.16	3.50 ± 0.41

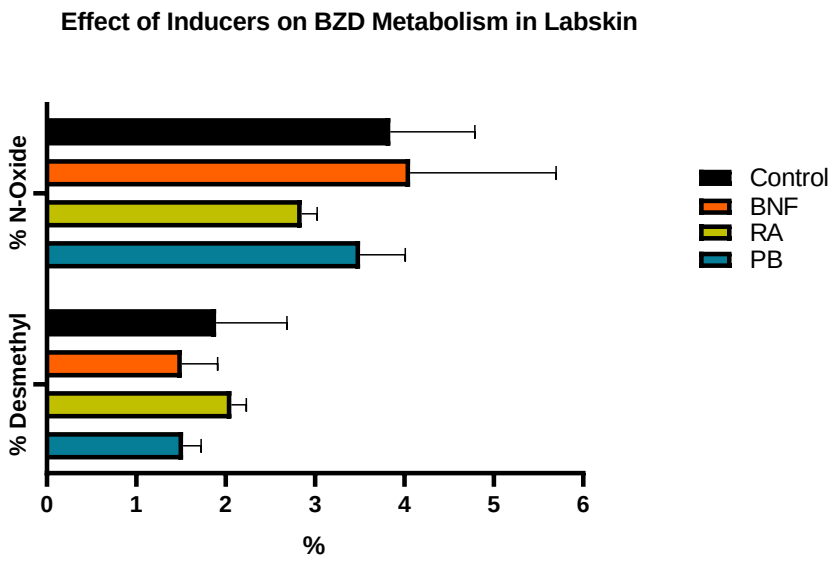

Figure 5.5: Effect of chemical induction on metabolism of the test compound benzydamine (BZD). BZD is metabolised to benzydamine-*N*-oxide by FMO1/3 expression activity and nor-benzydamine by P450 in induction 3D Labskin with βNF yielded surprising results, no increase in P450 activity was observed but an apparent increase in FMO activity (n =3).

It is clear from the data obtained from the non-induced sample that the low levels of Phase I enzyme have potentially been found in the epidermal layer of Labskin models. However, these routes of drug metabolism are likely to be more limited in skin compared with those that occur in human liver. Evidence for metabolities of BZD was also reported in the liver microsome from rat and human by LC-MS/MS (Taniguchi-Takizawa *et al*., 2015).

In agreement with proteomics evidence for FOM1/3 and CYP P450 of XME activity were demonstrated in full thickness 3D skin model, the idea of BZD substrate based mass spectrometry was developed as images for detection BZD-*N*-Oxide and desmethyl-BZD of FMO1/3 and CYPs activities of XMEs using MALDI-MSI and DESI-MS as shown in Figure 5.6 and 5.7. This is the first time we have been able to confirm the presence of BZD and its metabolites in Labskin model. Russo *et al* studied of drug metabolism in Labskin tissue, ritalinic acid metabolite was detected by MALDI-MSI and LC-MS/MS (Russo *et al*., 2018). This indicates that the esterase enzyme activity is potentially located in epidermis tissue.

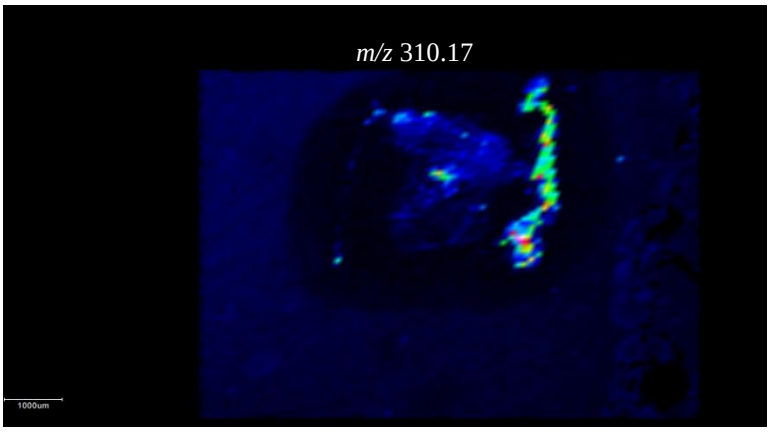

Figure 5.6: MALDI-MSI Image of BZD substrate (*m/z* 310.17 in green) was observed in the non induced section (50 µm pixel size). The Labskin tissue coated with CHCA matrix. No metabolities of the *N*-oxide-BZD and desmethyl-BZD was detected using sublimation method. Resolution image = 75 µm. TIC normalisation. The skin model control (untreated) structure was shown above.

Figure 5.6 shows a MALDI-MSI image of a Labskin sample treated with BZD for 48 h, MALDI images of control and treated LSE showed the distribution of the BZD $[M+H]^+$ ionat *m/z* 310.17 at a pixel size of 50 µm. However using MALDI-MSI, no successful images of BZD-*N*-Oxide and nor-benzydamine metabolities were achieved in both non-induced or induced LSE model as seen in Figure 5.6. Lack of BZD-*N*-Oxide and nor-benzydamine metabolities signal could be an insufficient α CHCA matrix coverage of Labskin tissue section by sublimation method, but to date, no successful MALDI-MSI images of the metabolites have been obtained. In contrast, these metabolities of BZD were imaged by DESI-MSI as presented in Figure 5.7.

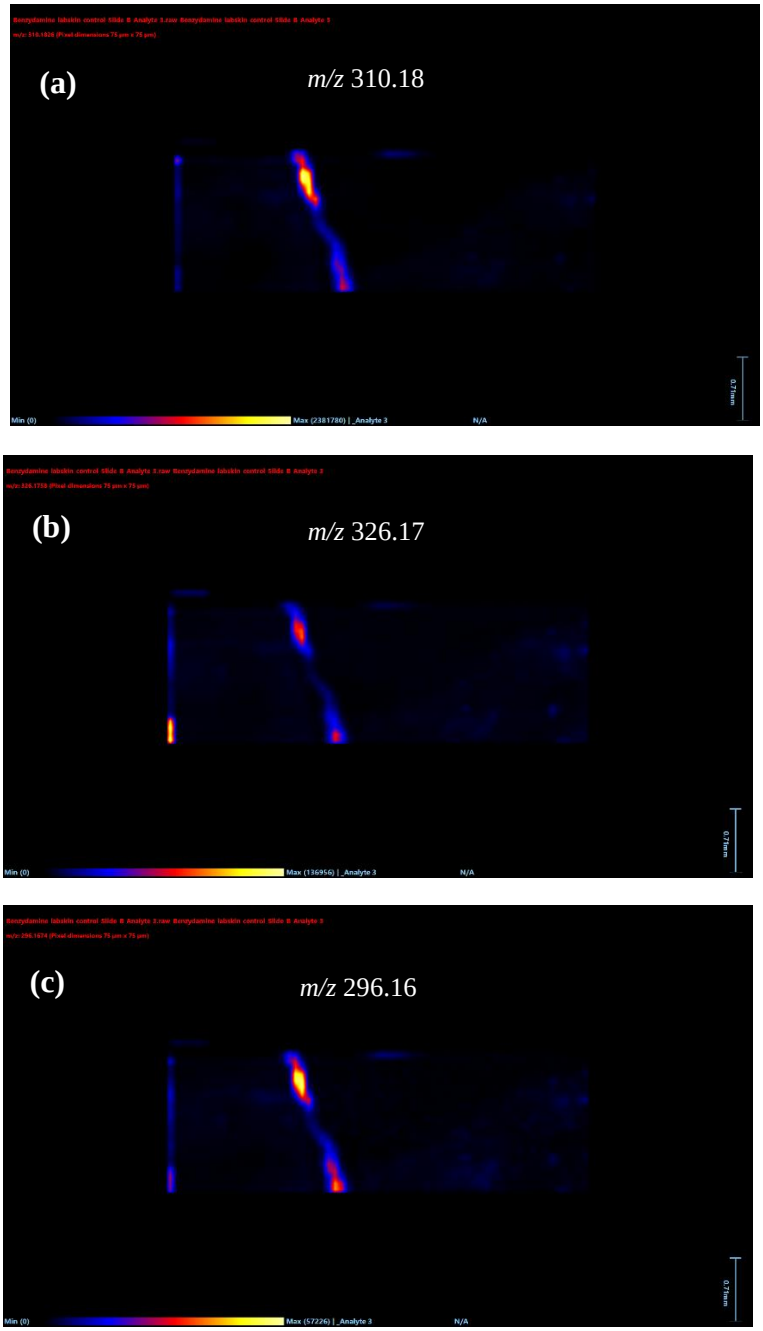

Figure 5.7: DESI-MS Images of BZD metabolism in non-induced 3D Labskin model with βNF, RA and PB ”trated with BZD” recorded at 210,000 mass resolution and 50 mm pixel size. The high mass resolution introduces specificity into the images allowing the individual metabolites to be imaged. Resolution image = 75 µm. TIC normalisation. The mass value in the scale bar was shown in the top (310.18 *m/z* and 326.17 *m/z* and 296.16 *m/z* in white).

After 48 h of the BZD incubation, BZD-*N*-oxide and desmethyl-BZD were observable. The BZD and metabolite signals appear to be localized in epidermal layer. This method clearly gives improved sensitivity for BZD and its metabolites. Figure 5.7 shows the images of BZD *m/z* 310.18 in red (a) and its major metabolites BZD-N-Oxide *m/z* 326.17 in red (b) and desmethyl-BZD *m/z* 296.16 in red (c). This is the first time we have been

able to confirm the presence of the norbenzydamine metabolites by DESI-MSI, thus gave additional evidence for the FMO1/3 and CYPs activities found in the LC-MS/MS study. However, the abundant of these enzymes was relatively low according to the peak area in LSE treated with BZD as control samples (Table 5.1).

Due to the low level of Phase I XME of FMO1/3 and CYPs genes/proteis in LS_BZD control, the XME levels of commercial skin model were induced at significant level by 72 h treatment with a series of known XME inducers as systemic application, 50 μM β-naphthoflavone (βNF), 20 μM *all-trans* retinoic acid (RA) and 2 mM phenobarbital (PB). The β-naphthoflavone, *all-trans* retinoic acid and phenobarbital induction of FMO1/3 and CYPs in 3D skin models has been reported at the gene and enzyme activity level (Hewitt *et al*., 2013; Bacqueville *et al*., 2017). It was found that after induction was similar or slightly higher by βNF, RA and PB. An interesting finding is that βNF compared was appeared to lead to greater induction of FMO than RA or PB (See Figure 5.8 and Table 5.1).

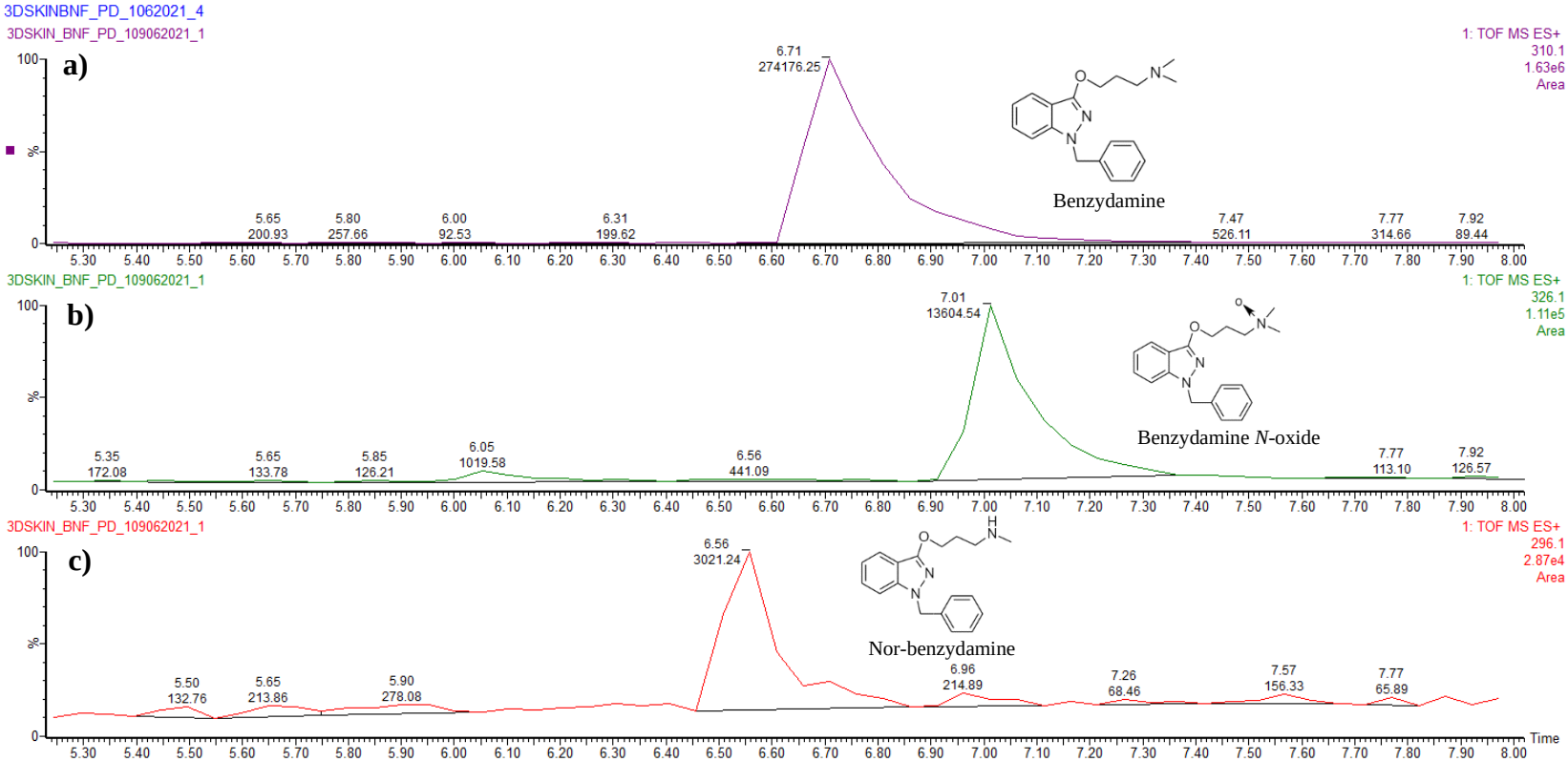
3DSKINBNF_PD_1062021_4
3DSKIN_BNF_PD_10962021_1
a)
1: TOF MS ES+
310.1
1.63e6
Area
6.71
274176.25
Benzydamine
5.65
200.93
5.80
257.66
6.00
92.53
6.31
199.62
7.47
526.11
7.77
314.66
7.92
89.44
3DSKIN_BNF_PD_10962021_1
b)
1: TOF MS ES+
326.1
1.11e5
Area
7.01
13604.54
Benzydamine N-oxide
5.35
172.08
5.65
133.78
5.85
126.21
6.05
1019.58
6.56
441.09
7.77
113.10
7.92
126.57
3DSKIN_BNF_PD_10962021_1
c)
1: TOF MS ES+
296.1
2.87e4
Area
6.56
3021.24
Nor-benzydamine
5.50
132.76
5.65
213.86
5.90
278.08
6.96
214.89
7.26
68.46
7.57
156.33
7.77
65.89
%
Time

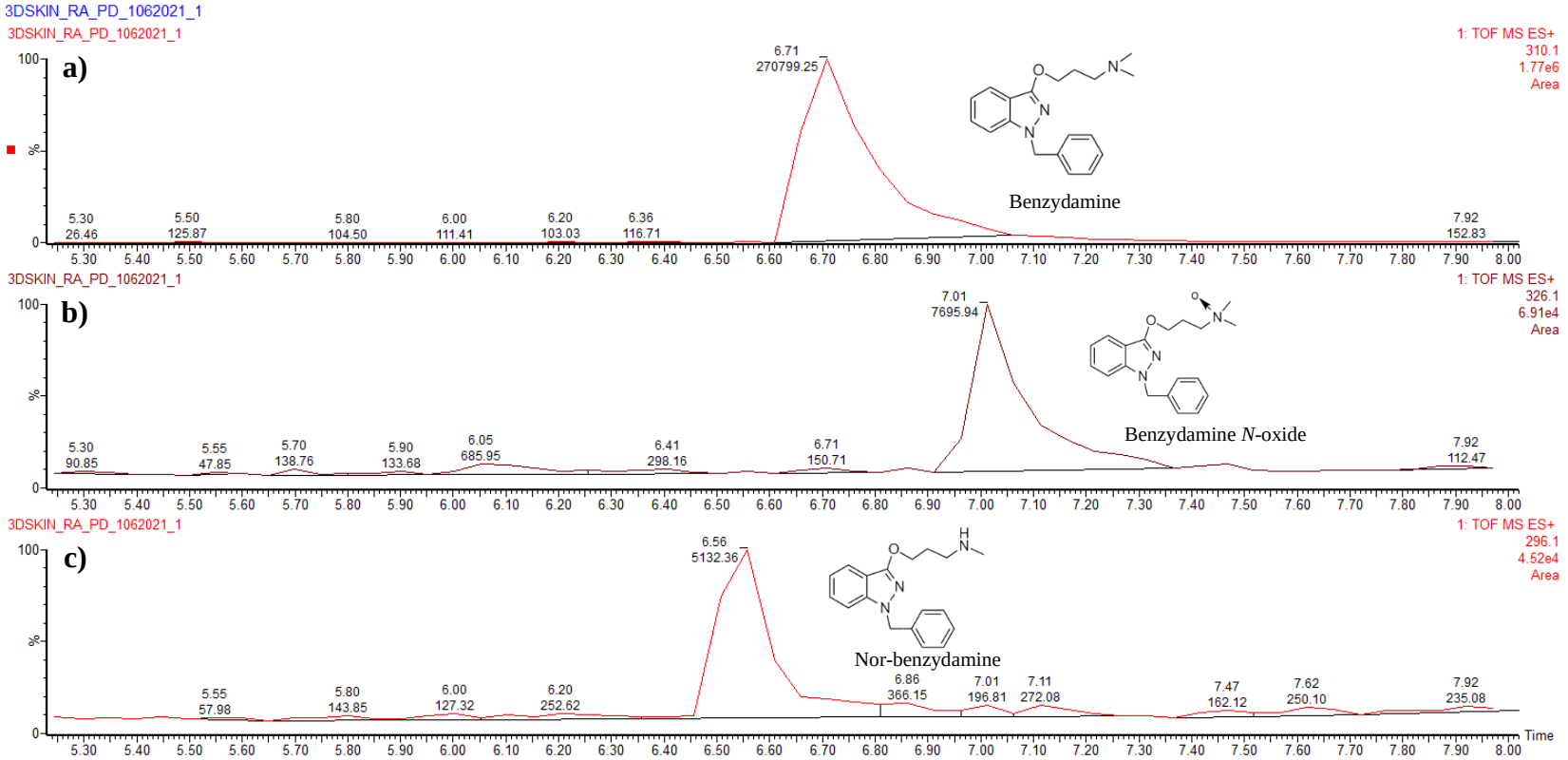
3DSKIN_RA_PD_1062021_1
3DSKIN_RA_PD_1062021_1
1: TOF MS ES+
310.1
1.77e6
Area
a)
6.71
270799.25
Benzydamine
5.30
26.46
5.50
125.87
5.80
104.50
6.00
111.41
6.20
103.03
6.36
116.71
7.92
152.83
3DSKIN_RA_PD_1062021_1
1: TOF MS ES+
326.1
6.91e4
Area
b)
7.01
7695.94
Benzydamine N-oxide
5.30
90.85
5.55
47.85
5.70
138.76
5.90
133.68
6.05
685.95
6.41
298.16
6.71
150.71
7.92
112.47
3DSKIN_RA_PD_1062021_1
1: TOF MS ES+
296.1
4.52e4
Area
c)
6.56
5132.36
Nor-benzydamine
5.55
57.98
5.80
143.85
6.00
127.32
6.20
252.62
6.86
366.15
7.01
196.81
7.11
272.08
7.47
162.12
7.62
250.10
7.92
235.08
%
Time

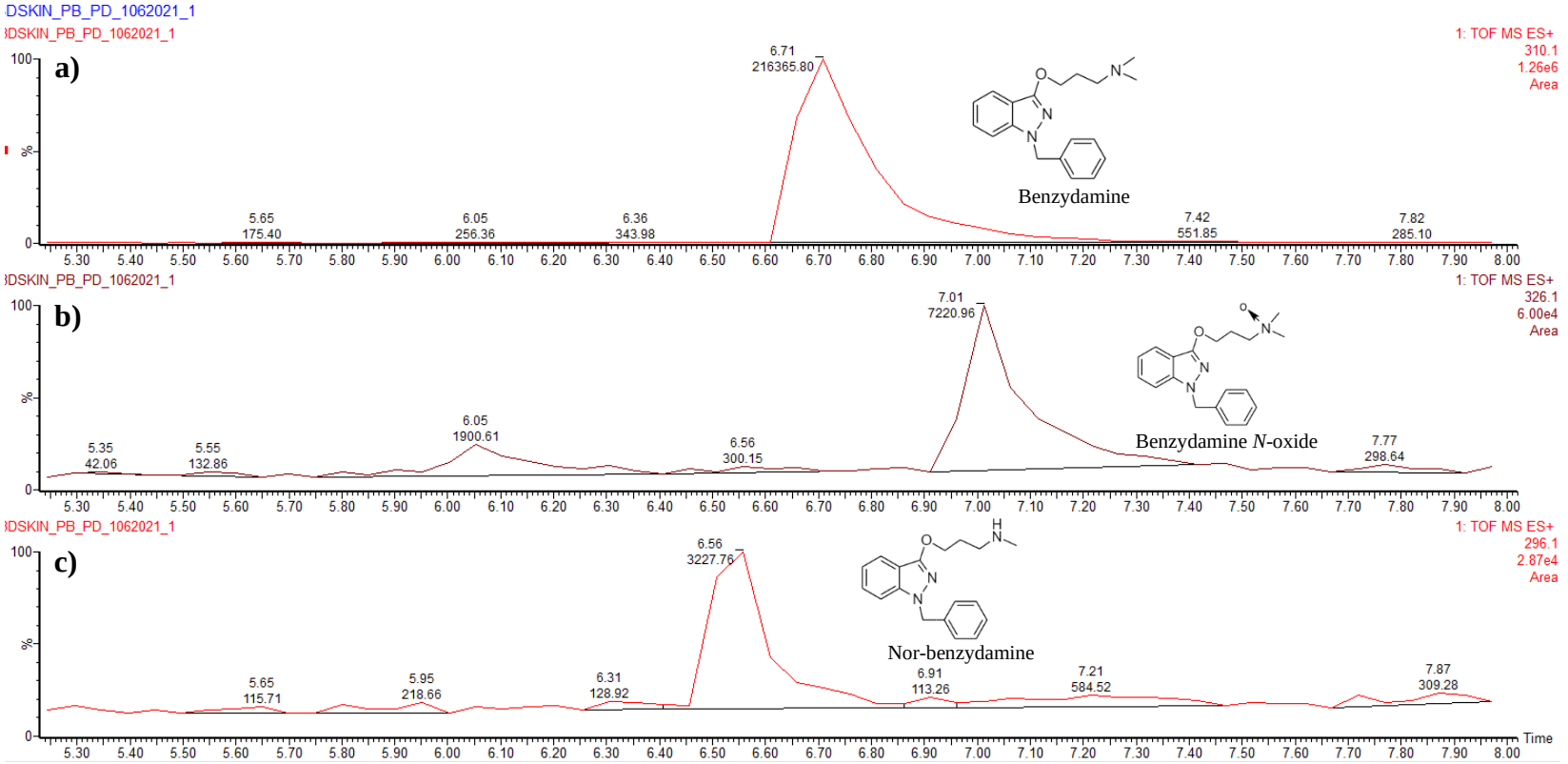

Figure 5.8: LC–MS/MS profile (chromatogram) of the LS model treated with BZD **(a)** at *m/z* 326.17 after induced as systematic treatment with 50 µM β-naphthoflavone (βNF), 20 µM *all-trans* retinoic acid (RA) and 2mM phenobarbital (PB) to increase the level of Phase I enzymes. FMO1/3 activity was the most induced by βNF and verified by benzydamine-*N*-oxide **(b)** at *m/z* 326.17 in 3D skin model while CYPs activity appears to have low catalytic activity which can detect the nor-benzydamine **(c)** at *m/z* 296.1.

It can be seen that our data from a study of the induction of metabolising enzymes in the LSE showed that the abundant Phase I genes/proteins as shown previously (in Chapters 2, 3 and 4) was made different relative contributions on the metabolism. The effect of chemical induction on the metabolism of the test BZD were high metabolised to BZD-*N*-oxide by FMO1/3 and norbenzydamine by CYP2D6 (Figure 5.8). The induction with βNF yielded surprising results, no increase in P450 activity was observed but an apparent slightly increase in FMO1/3 of BZD-*N*-oxide (Table 5.1). This induction of FMO1/3 might be due to the aryl hydrocarbon receptor (AhR) as transcription factor of substrate that can regulates gene or protein expression. In addition, AhR is the main function as sensor of xenobiotics or chemicals for the regulator of enzymes such as cytochrome P450s or FMO1/3 that metabolise these drug. This is in agreement with the low *m/z* 326.17 and *m/z* 296.16 or non detectable levels of CYPs genes/proteins in Labskin model as well as in human skin samples (Chapter 2 and Chapter 3). Thu, FMO1/3 level were more efficient catalysis of BZD test drug. This very similar data obtained using LS tissue from different donors (Couto *et al*., 2021). It has also been reported that expression of CYPs was very low in the ORS-RHE, but this was dramatically induced by βNF inducer (Bacqueville *et al*., 2017). In addition, treatment with βNF resulted strong increase in EROD activities determined in the epidermal compartment of Phenion FT skin (Wiegand *et al*., 2014).

In the present study Labskin treated with *all-trans* retinoic acid and phenobarbital showed only a slight increase in XME activity in skin. It can be seen after 48 h topical treatment on the Labskin surface, the BZD substrate were delivered and metabolised higher to benzydamine-*N*-oxide at *m/z* 326.17 with 7.01 min retention time by FMO1/3 (Figure 5.8 b) than LS control and nor-BZD at *m/z* 296.16 with 6.56 min retintion time by P450 (Figure 5.8 c).

The biotransformation by CYP2D6 (shown in Figure 5.8 c) is clearly identified in the epidermal layer, thus suggesting *m/z* 296.1 norbenzydamine. The norbenzydamine of CYPs activity in the comparative LS_BZD of the RA and PB with control were almost smillar between 1-2 % of the BZD. Despite the the low level of enzymes activity in this model, however, BZD and its metabolities are clearly observable in the DESI-MSI images (Figure 5.9).

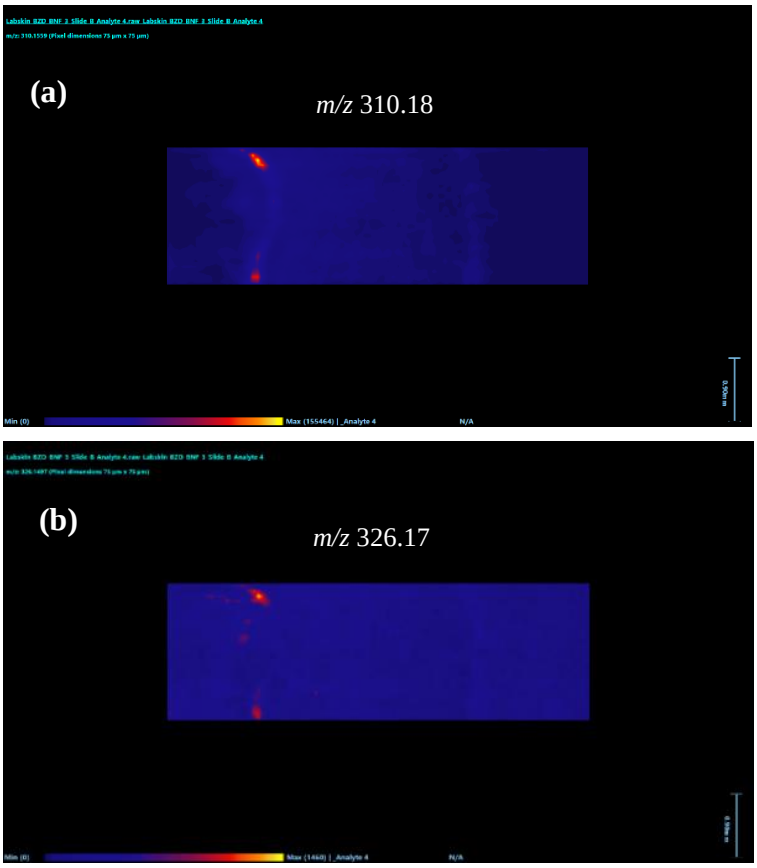

Figure 5.9: Synapt XS DESI-MSI images of induced (beta-naphthoflavone) Labskin model treated as topical treatment of benzydamine recorded at 210,000 mass resolution and 75 µm pixel size. The high mass resolution introduces specificity into the images allowing the individual metabolites to be imaged. Only BZD-*N*-oxide (*m/z* 326.17 in red) possible evidence of FMO1/3 activity. But, no evidence of desmethyl-BZD formation was imaged. The mass value in the scale bar was shown in the top (310.18 *m/z* and 326.17 *m/z* in white)

DESI-MSI experiments were also perfomed on both Waters Synapt-XS and Waters MRT multi-reflecting time of flight mass spectrometer. In the initial DESI-MSI experiments, a blank section of Labskin model as "control" was imaged after treatment with a 20 µL emulsion water/olive oil (80:20) alone as demonstrated in Figure 5.4. DESI-MS images of BZD metabolism in non-induced Labskin with βNF, RA and PB "treated with 300 µg BZD" were recorded at *m/z* 310.18, 210,000 mass resolution and 75 µm pixel size on the MRT. The high mass resolution introduces specificity into images allowing the individual metabolites to be imaged (Figure 5.9). Very similar results were obtained with DESI-MSI on the Synapt-XS to those on the MRT for detection of the presence of BZD-*N*-Oxide and induced activity of the FMO1/3 by βNF inducer in 3D model. Treatment with βNF resulted in an increase of BZD-*N*-oxide determined in epidermal layer of skin suggesting induction of FMO1/3 (Figure 5.9 b). DESI-MS imaging on Synapt XS indicate successful

detection of BZD (*m/z* 310.18 in red as shown in Figure 5.9 a) which is also metabolised to BZD-*N*-oxide (*m/z* 326.17 in red) which is the key metabolite in this study.

In contrast, desmethyl-BZD was not detected in the DESI-MSI experiments conducted using the Synapt XS. This is explained by the low levels of CYPs and the greater sensitivity of the MRT. This was in agreement with the previously reported relative levels of CYP protein expression in 3D skin models and human skin (Oesch *et al*., 2007; Oesch *et al*., 2018). Notable, the RA and PB induction were activated the AhR of microsomal and cytosolic 3D skin models, leading to induction of CYPs and FMO1/3 compared with untreated 3D skin model as shown in Chapter 4.

In the study reported in this chapter further improvement and validation of MSI technique has been performed in order to study the biotransformation of BZD substrate in the epidermal layer of Labskin model. DESI-MS images recorded using the Waters MRT give new confidence in the data produced as mass spectra and images routinely obtain ppb mass accuracy. This approach has been used for the first time to confirm the presence of the BZD and its metabolites. Although DESI-MSI on the Synapt XS did not detected the localisation of the desmethyl metabolite in the epidermal layer of Labskin tissue, the MRT did (See Figure 5.10 and 5.11). Therefore, this confirms the significant advantages of providing high sensitivity and ultra-high resolution of intact molecular species and allowed the confident detection and clear localisation of BZD and its metabolites in skin tissue. As BZD absorved in epidermis of Labskin model (See Figure 5.10 a image and Figure 5.11 spectra), evidence of low detection of the desmethyl-BZD by P450 activity in the LSE model (Figure 5.10 c). This is in agrmeent with the LC-MS/MS data in previous data in Chapter 2 and 3 at the low protein level. Nevertheless, FMO1/3 activity was demonstrated for BZD-*N*-oxide (Figure 5.10 b). This is a very sensitive technique, and the data reported here appears to confrim the findings of high level of Phase I drug metabolizing enzyme genes of FMOs activity in RT-PCR data (Chapter 2). However, the relationship of low RNA level to the CYPs protein levels is still uncertain (Harris *et al*., 2002; Ahmad & Mukhtar, 2004).

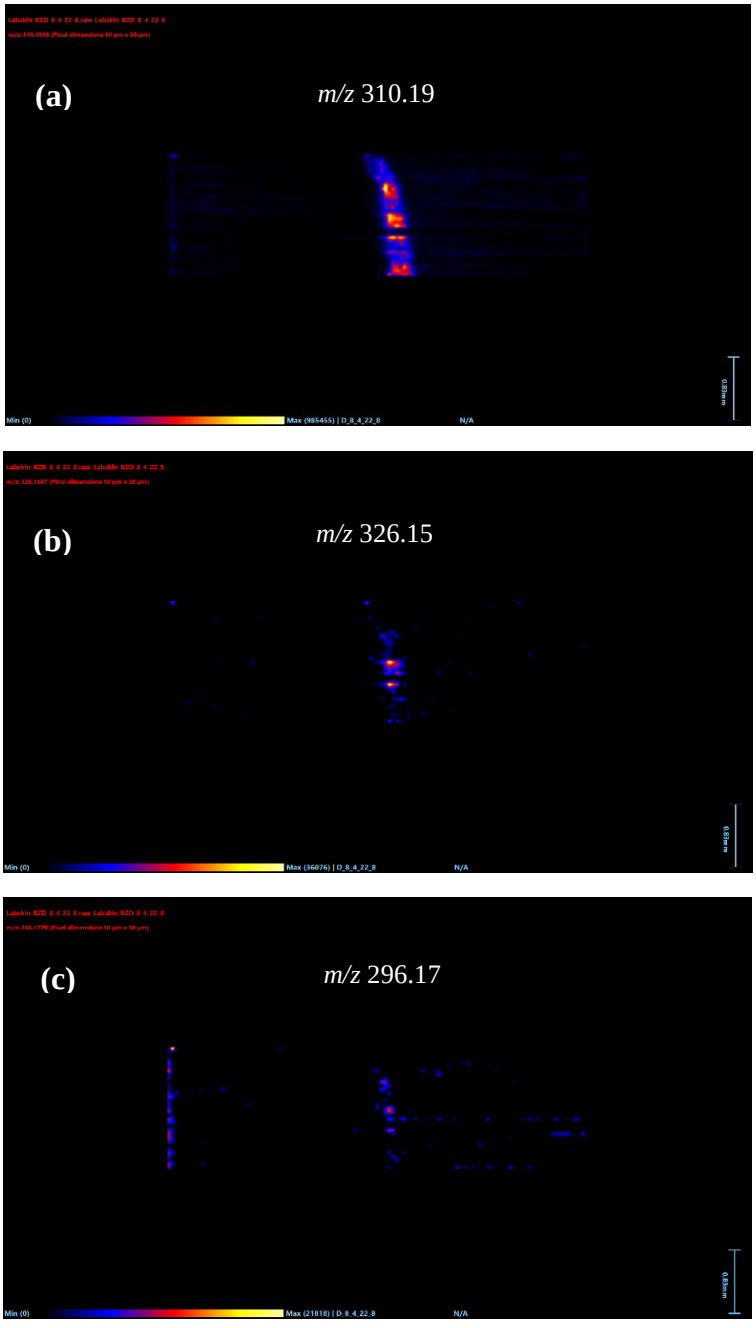

Figure 5.10: DESI-MS Images of BZD metabolism in βNF induced Labskin recorded at 210,000 mass resolution and 75 µm pixel size. The high mass resolution introduces specificity into the images allowing the individual metabolites to be imaged. This is the first time we have been able to confirm the presence of BZD-*N*-oxide and desmethyl-BZD metabolite. **(b)** BZD-*N*-oxide (*m/z* 326.15) and **(c)** desmethyl-BZD (*m/z* 296.16) formation in red possible evidence of FMO1/3 and CYP2D6 activity repectively. The mass value in the scale bar was shown in the top (310.19 *m/z* and 326.15 *m/z* and 296.17 *m/z* in white).

Data from MRT full spectra of the BZD substrate and its metabolities BZD-*N*-oxide and nor BZD generated *m/z* 310.19, 296.17 m/z and *m/z* 326.15 fragment ion in the epidermis section of Labskin was clearly detected in the induced model with βNF (Figure 5.11). The differential ions detected were verified to be consistent with the results from LC-MS/MS.

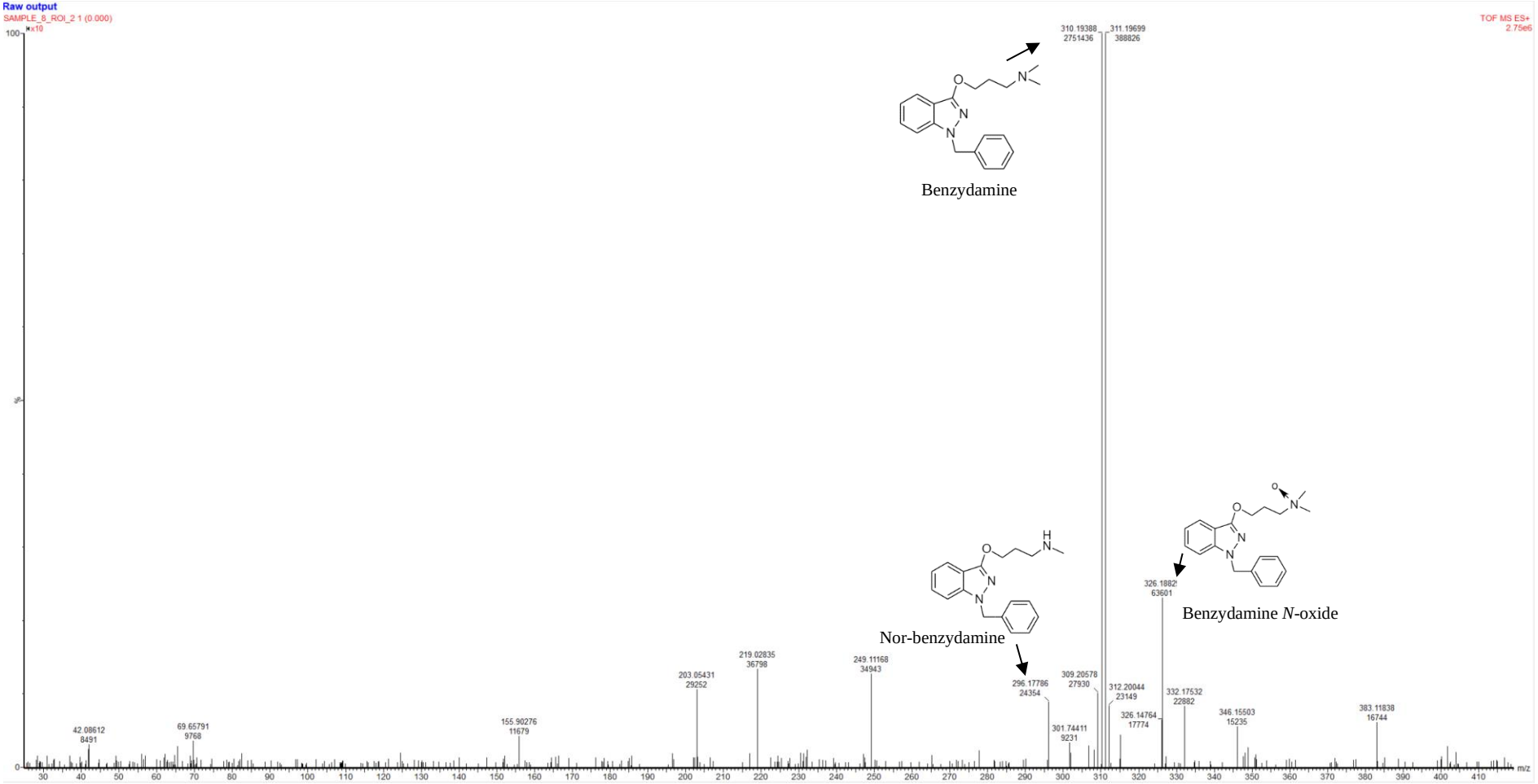

Figure 5.11: MALDI-MRT full spectrum of the BZD substrate and its metabolities *N*-oxide-BZD and desmethyl-BZD generated fragment ion (*m/z* 310.19 , *m/z* 296.17 and *m/z* 326.15 in the epidermis of Labskin model induced with βNF. Resolution image = 60 µm. TIC normalisation.

By compared of mass spectrometry data imaging, the oxidation to BZD-*N*-oxide and the de-methylation to desmethyl-BZD appears to be the highest metabolised in the induced 3D Labskin model by βNF as shown in Figure 5.11.

Validation genes of Phase I and II activity by RT-qPCR (Wiegand *et al*., 2014), BZD is metabolised to benzydamine-*N*-oxide by FMO1/3 and norbenzydamine by CYP2D6 using LC-MS/MS as shown in MRT spectra above. In these data, the biotransformed BZD were detected in the epidermis layer, thus indicating a high impact of chemical inducers on metabolism of the test compound benzydamine. It is interesting to note that the induction with βNF, yielded surprising results, no increase in P450 activity was observed but an apparent increase in FMO activity was higher than RA and PB. The data shown here gave initial results for the levels of chemical induction on the metabolism in 3D Labskin tissue treated with BZD as topical treatment based on mass spectrometry.

5.5 Conclusion

In this chapter, a novel approach for relative quantitation of benzydamine substrate and its metabolites in the epidermal region of a full thickness living skin equivalent model has been presented. The study shown an innovative method to evaluate the performance of the penetration and metabolism of BZD by FOM1/3 and P450. The LC-MS/MS data set of homogenates of isolated epidermal of skin tissue, indicated that the comparison of level of these enzymes in biotranformation study were low in 3D skin control. However, the responses of βNF, RA and PB inducers after 72 h as systemic application for FMO1/3 and CYPs gene or protein in the 3D skin model were expressed higher than those in 3D skin model control which can be functionally significant to be clearly metabolised of BZD to benzydamine-*N*-oxide by FMO1/3 and nor-benzydamine by P450. This abundant FMO1/3 had high rates of *N*-oxygenation of benzydamine in Labskin model. In contrast, the lack of nor-benzydamine detection by P450 is consistent with the levels of mRNA or protein which have been found to be low or undetectable in epidermis layer of skin model compared with native human skin. DESI-MS is a softer ionisation technique for drug imaging compared with MALDI-MSI for the analysis of drug distribution within 3D cell cultures models, such as skin. In this study, DESI-MS data provided further support for the concept that Phase I XME expressed in the 3D skin which may contribute to the role of localised BZD drug and BZD-*N*-oxide and desmthyl metabolites within the in the epidermal layer of the skin models.

5.6 References

Ahmad, N., & Mukhtar, H. (2004). Cytochrome p450: a target for drug development for skin diseases. *Journal of Investigative Dermatology*, ***123***(3), 417-425.

Avery, J. L., McEwen, A., Flinders, B., Francese, S., & Clench, M. R. (2011). Matrix-assisted laser desorption mass spectrometry imaging for the examination of imipramine absorption by Straticell-RHE-EPI/001 an artificial model of the human epidermis. *Xenobiotica*, ***41***(8), 735-742.

Bacqueville, D., Jacques, C., Duprat, L., Jamin, E. L., Guiraud, B., Perdu, E., Bessou-Touya, S., Zalko, D., & Duplan, H. (2017). Characterization of xenobiotic metabolizing enzymes of a reconstructed human epidermal model from adult hair follicles. *Toxicology and Applied Pharmacology*, *329*, 190-201.

Capolongo, F., Santi, A., Anfossi, P., & Montesissa, C. (2010). Benzydamine as a useful substrate of hepatic flavin-containing monooxygenase activity in veterinary species. *Journal of Veterinary Pharmacology and Therapeutics*, ***33***(4), 341-346.

Chen, J., Mannargudi, B. M., Xu, L., & Uetrecht, J. (2008). Demonstration of the metabolic pathway responsible for nevirapine-induced skin rash. *Chemical Research in Toxicology*, ***21***(9), 1862-1870.

Couto, N., Newton, J. R., Russo, C., Karunakaran, E., Achour, B., Al-Majdoub, Z. M., Sidaway, J., Rostami-Hodjegan, A., Clench, M. R., & Barber, J. (2021). Label-free quantitative proteomics and substrate-based mass spectrometry imaging of xenobiotic metabolizing enzymes in ex vivo human skin and a human living skin equivalent model. *Drug Metabolism and Disposition*, ***49***(1), 39-52.

Harris, I. R., Siefken, W., Beck-Oldach, K., Brandt, M., Wittern, K., & Pollet, D. (2002). Comparison of activities dependent on glutathione S-transferase and cytochrome P-450 IA1 in cultured keratinocytes and reconstructed epidermal models. *Skin Pharmacology and Physiology, **15***(Suppl. 1), 59-67.

Harvey, A., Cole, L. M., Day, R., Bartlett, M., Warwick, J., Bojar, R., Smith, D., Cross, N., & Clench, M. R. (2016). MALDI-MSI for the analysis of a 3D tissue-engineered psoriatic skin model. *Proteomics, **16***(11-12), 1718-1725.

Hewitt, N. J., Edwards, R. J., Fritsche, E., Goebel, C., Aeby, P., Scheel, J., Reisinger, K., Ouédraogo, G., Duche, D., & Eilstein, J. (2013). Use of human in vitro skin models for accurate and ethical risk assessment: metabolic considerations. *Toxicological Sciences, **133***(2), 209-217.

Jäckh, C., Blatz, V., Fabian, E., Guth, K., van Ravenzwaay, B., Reisinger, K., & Landsiedel, R. (2011). Characterization of enzyme activities of Cytochrome P450 enzymes, Flavin-dependent monooxygenases, N-acetyltransferases and UDP-glucuronyltransferases in human reconstructed epidermis and full-thickness skin models. *Toxicology in Vitro, **25***(6), 1209-1214.

Kazem, S., Linssen, E. C., & Gibbs, S. (2019). Skin metabolism phase I and phase II enzymes in native and reconstructed human skin: a short review. *Drug Discovery Today,*

Lewis, E., Barrett, M., Freeman-Parry, L., Bojar, R. A., & Clench, M. R. (2018). Examination of the skin barrier repair/wound healing process using a living skin equivalent model and matrix-assisted laser desorption-ionization-mass spectrometry imaging. *International Journal of Cosmetic Science, **40***(2), 148-156.

Oesch, F., Fabian, E., Guth, K., & Landsiedel, R. (2014). Xenobiotic-metabolizing enzymes in the skin of rat, mouse, pig, guinea pig, man, and in human skin models. *Archives of Toxicology*, ***88***(12), 2135-2190.

Oesch, F., Fabian, E., & Landsiedel, R. (2018). Xenobiotica-metabolizing enzymes in the skin of rat, mouse, pig, guinea pig, man, and in human skin models. *Archives of Toxicology*, ***92***(8), 2411-2456.

Oesch, F., Fabian, E., Oesch-Bartlomowicz, B., Werner, C., & Landsiedel, R. (2007). Drug-metabolizing enzymes in the skin of man, rat, and pig. *Drug Metabolism Reviews*, ***39***(4), 659-698.

Russo, C., Brickelbank, N., Duckett, C., Mellor, S., Rumbelow, S., & Clench, M. R. (2018). Quantitative investigation of terbinafine hydrochloride absorption into a living skin equivalent model by MALDI-MSI. *Analytical Chemistry*, ***90***(16), 10031-10038.

Russo, C., Lewis, E. E., Flint, L., & Clench, M. R. (2018). Mass spectrometry imaging of 3D tissue models. *Proteomics*, ***18***(14), 1700462.

Störmer, E., Roots, I., & Brockmöller, J. (2000). Benzydamine N-oxidation as an index reaction reflecting FMO activity in human liver microsomes and impact of FMO3 polymorphisms on enzyme activity. *British Journal of Clinical Pharmacology*, ***50***(6), 553-561.

Taniguchi-Takizawa, T., Shimizu, M., Kume, T., & Yamazaki, H. (2015). Benzydamine N-oxygenation as an index for flavin-containing monooxygenase activity and benzydamine N-demethylation by cytochrome P450 enzymes in liver microsomes

from rats, dogs, monkeys, and humans. *Drug Metabolism and Pharmacokinetics, **30***(1), 64-69.

Uno, Y., Shimizu, M., & Yamazaki, H. (2013). Molecular and functional characterization of flavin-containing monooxygenases in cynomolgus macaque. *Biochemical Pharmacology, **85***(12), 1837-1847.

van Eijl, S., Zhu, Z., Cupitt, J., Gierula, M., Götz, C., Fritsche, E., & Edwards, R. J. (2012). Elucidation of xenobiotic metabolism pathways in human skin and human skin models by proteomic profiling. *PloS One, **7***(7), e41721.

Wiegand, C., Hewitt, N. J., Merk, H. F., & Reisinger, K. (2014). Dermal xenobiotic metabolism: a comparison between native human skin, four in vitro skin test systems and a liver system. *Skin Pharmacology and Physiology, **27***(5), 263-275.

Chapter 6

Conclusion and Future work

6.1 Conclusion

3D *in vitro* tissue models of human skin represent an alternative to monolayer 2D cell culture, *ex-vivo* human and animal skin such as rat and pig to different research. The work described in this thesis is concerned with the optimisation and validation of a human *in vitro* 3D living skin equivalent model "Labskin" for metabolism studies of topically applied xenobiotics. Labskin metabolism of drug through extrahepatic metabolism in the model is compared with human skin.

6.1.1 Investigation of the Induction of gene expression of XME in a 3D Skin Model by RT-qPCR and Western blotting

The overall aim of the current study was to undertaken a comprehensive characterization of the expression level of Phase I XMEs in the commercially available 3D skin "Labskin" model to characterize them so that it could be used as a suitable surrogate for native human skin for metabolism assays. Overall, the *in vitro* 3D skin models showed distinctive profiles at the levels of CYP1A1, CYP3A5, CYP1B1 and FMO2 activity regarding xenobiotic metabolism. A comparison of the expression in the Labskin skin model control, the induced model, and the human skin, showed that the level of gene expression of Phase I XMEs including CYP1A1, CYP3A5, CYP1B1 and FMO2 level were lower in the Labskin compared with that presented in native human skin. Chemical induction increased these levels, but still not to those in native human skin. Understanding the relationship between the levels of XME in 3D skin models and human skin could potentially lead to a model that would be able to predict human skin data from that obtained from 3D models. The data obtained here indicate that the Labskin model could be a valuable, robust *in vitro* tool to help this and address the need for improved non-animal models as alternative methods for evaluation of efficacy, metabolism, and toxicity of cutaneous exposure, but understanding that the levels of XME are lower is required as data is evaluated.

6.1.2 Expression and Induction of XMEs in a 3D Skin Model studied by using LC-MS/MS and Nano-LC-MS/MS

The data obtained in this study provide further support for the concept that XMEs expressed in the skin may contribute to the role of skin as protective barrier by detoxifying xenobiotics following topical exposure. This is an important consideration in safety assessment of topically applied chemicals. The *in vitro* skin model was shown to express many important XMEs, which could be induced in response with βNF, RA and PB inducers. The LC-MS/MS result indicated that the comparison of level of CYP1B1,

GSTP1 and GSTO1 protein were expressed low in 3D skin model compared with those that presented in native skin. However, the responses to drug inducers after systemic application showed that at the protein level of the CYPs and GSTs in the 3D skin model were expressed higher than in 3D Labskin control (untreated 3D skin model). This could be functionally significant. Despite of the relatively low RNA level in the induced 3D skin model, the CYP1B1, GSTP1 and GSTO1 protein were measured similar or higher in the induced skin model with βNF, RA and PB microsomal and cytosolic fractions than normal human skin by LC-MS/MS.

The use of nano-LC-MS/MS in this study allowed for a study abundance ratio of XMEs present in Labskin models and human skin as well as more in-depth investigations of certain Phase I and II proteins levels. About 327 XME proteins were identified in the 3D Labskin model compared with and human skin. The low level of CYPs, CES of Phase I and GSTs of Phase II in native skin were also reflected in Labskin models. However, our data set showed that βNF induced the production of CYP1B1, CES, GSTP1 and GSTO1 proteins. Even though low RNA level of CYP1B1, CES1, GSTP1 and GSTO1 in the Labskin model induced with βNF were found (as reported in Chapter 2), the proteins levels could be quantified using nano-LC-MS/MS based proteomics. A comparison of Phase I and Phase II XMEs indicated that the Phase II enzymes are much more abundant than Phase I enzymes.

6.1.3 Demonstration of the Metabolic Pathway Responsible for Benzydamine in a 3D Skin Model studied by using MALDI-MSI and LC-MS/MS

Overall, human skin and skin model contains many metabolizing enzymes that facilitate a wide range of biotransformation reactions. A novel approach for the detection of these enzymes using benzydamine as a substrate has been demonstrated. Our study presented an innovative method to evaluate the performance of the penetration and metabolism of benzydamine by FOM1/3 and CYP p450 enzymes. Even though low level of Phase I (FMO1/3 and CYPs activity) in native human skin were reflected in Labskin models, the RT-pPCR and proteomics data have showed that βNF, RA and PB after 72 h were induced the production of Phase I gene/protein level (as reported in previous Chapters) which can be functionally significant to be metabolised of topical BZD substrate. Statistical analyses show changes in detection of XME between the treated and untreated Labskin. The LC-MS/MS results of homogenates of isolated epidermis tissue, indicated that benzydamine N-oxygenation and *N*-demethylation mediated by FMO1/3 and CYP2D6 (and other P450 isoforms). These results suggest that the βNF induction of FMO1/3 is responsible and has

a high impact of the metabolic eliminations of BZD drug in the epidermal layer of skin. However, the low of nor-benzydamine detection in skin by P450 is consistent with the levels of mRNA and protein which have been observed at low level in skin model.

Validation of the MALDI-MSI and DESI-MS data supported LC-MS/MS data suggesting localisation of BZD and its metabolites within the Labskin model. Successful detection and imaging of drug compounds within the skin section have been achieved by DESI-MSI. The oxidation of BZD-*N*-oxide and de-methylation to desmethyl-BZD appears to be enhanced in the induced Labskin model by βNF. In this study, DESI-MS is provided further support for the concept that FMO1/3 and CYP P450 of Phase I XME were expressed and induced localised in the epidermal layer (keratinocytes) of skin and in addition biological changes in response treatment/exposure can be examined. In comparison with liver enzyme expression and activity, skin demonstrates overall low Phase I enzyme expression and activity, thus more investigation and validation of the technology is required. Overall, these data should help in the development of 3D skin model for understanding the expression and induced of Phase I and Phase II in skin.

6.2 Suggestions for Future Work

A commercially available 3D skin model "Labskin" has played a role in biological skin research for many years. Recently, however, these models are becoming more widely used as alternative method to improve and convert *in vitro* to *in vivo* studies for drug metabolism. Further investigation of "Labskin" and comparison with native human skin is still required for Phase I and II XME to evaluate metabolism of chemical exposure. The levels of XME in LSE models needs to be improved. Here using new 3D skin models such as stem cells which make cells attractive for regenerative medicine, tissue repair, gene therapy and cell-based therapy in dermatology is a possibility. They have the possibility to provide *in vitro* models to study epidermal lineage selection and its role in the metabolism process. This would provide information on different cells to those already identified/imaged in this study.

Comparing the metabolising enzymes present in *ex vivo* human skin and commercial 3D skin model, LC-MS/MS and DESI-MS technique have shown the ability of the detection of Phase I and II expression of proteomic after chemicals exposure.

Appendices

The raw data of the all thesis chapters has been attached in the appendix I, II and III link: https://drive.google.com/drive/folders/1kgPO-lVdDpEl8wD0sSdhh83d_XNBlB-b?usp=sharing.

Appendice I: comparison of Phase I gene expression in *in vitro* 3D living skin equivalent model control (DMSO treated) with that in human skin.

Enzymes	Ct mean Human skin	Ct mean Untreated 3D skin Model	Δ Ct Human skin	Δ Ct 3D Skin Model	Fold-Change
CYP1A1	35	33.00	6.8	10.16	-10.26
CYP3A5	30.26	28.14	2.06	5.14	-8.45
CYP1B1	29.94	26.59	4.41	11.26	-115.56
FMO2	31.88	28.01	5.58	9.81	-18.76

Appendix II: Comparison of Phase I gene expression in the control 3D living skin equivalent model l (DMSO treated) with that following chemical induction of Labskin model.

Enzymes	Ct mean Untreated 3D Skin model	Ct mean Treated 3D Skin model	ΔCt Untreated 3D Skin model	Δ Ct Treated 3D Skin model	Fold-Change	Inducers
CYP1A1	30.75	28.63	11.15	8.93	4.65	25uM βNF
CYP1A1	32.21	27.86	12.61	8.16	21.85	50uM βNF
CYP3A5	25.73	24.72	6.13	5.02	2.15	2mM PB
CYP1B1	31.54	26.59	11.26	7.56	12.99	20 µM RA
FMO2	32.57	28.01	12.57	9.81	6.77	20 µM RA

Appendix III: Full WS of phase I (CYP1A1, CYP3A5 and FOM2 protein expression) in all skin. The proteins of phase I were detected as band representative as 3D skin model induced with βNF, RA and PB by Western blot. In addition, these proteins were detected in human skin representative as native (fresh) human skin tissues. No CYP1A1 was detected in all skin (both 3D skin model and human skin).

CYP 1A1

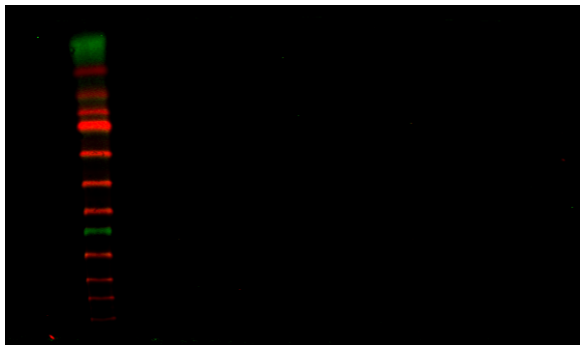

CYP3A5

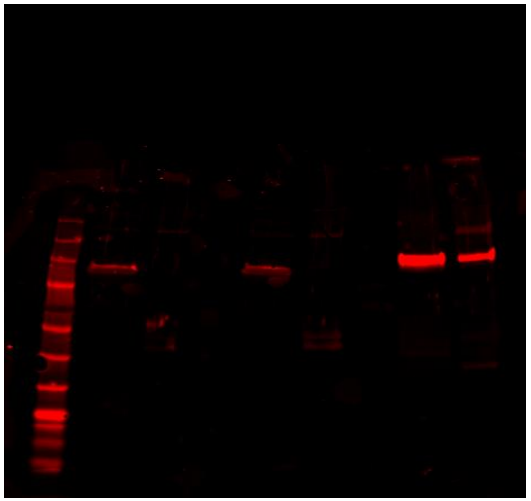

FMO2

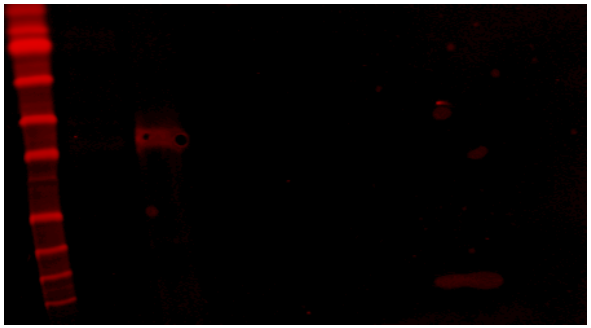

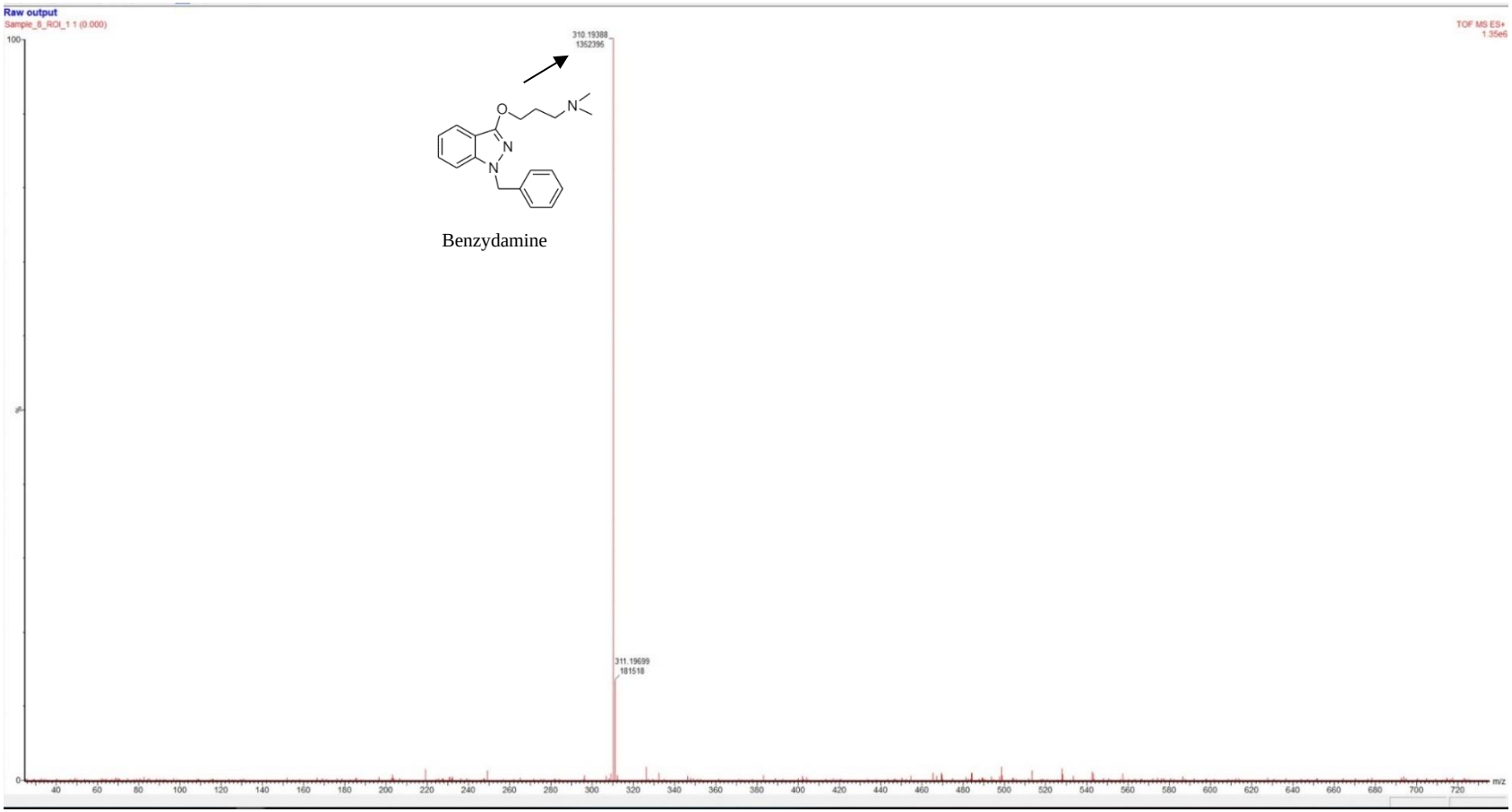

Appendix IV: DESI-MS spectra acquired in positive mode of BZD substrate (300 µg) using the DESI-MS on MRT instrument. It was detected at high intensity *m/z* 310.17 in 3D skin (Labskin) model.

Conference Presentations

Posters Conferences and Mass Spectrometry Courses

- Short Course of introduction pf mass spectrometry at Churchill College, University of Cambridge, UK (2018)
- Presentation of drug metabolism of XMEs in 3D skin model compared with native human skin at Sheffield Hallam University (2018)
- Poster Publication for (Examination of Metabolising Enzymes in a Living Skin Equivalent Model by GeLC-MS at British mass spectrometry society (BMSS conference) at university of Cambridge, UK (2018).
- 18th East Midlands Proteomics Workshop of Optimization and Validation of 3D skin model as alternative to human skin for Xenobiotics study at Sheffield Hallam University (2018)
- 6th SIG Mass spectrometry Imaging Symposium Sheffield Hallam University 2019
- Presented poster of the induction of XMEs level in 3D skin model compared with native human skin at the university of Manchester (2019)
- Attending short course of introduction mass spectrometry, American Society 2020, Taxes USA: Peptides and proteins in Mass Spectrometry
- Investigation of the Induction of gene expression of XMES in a 3D Skin Model and human skin by RT-qPCR and Western blotting in Cosmetic Science: Bridging Established Methods and Novel Technologies, December (2019, France.
- Proteomics Investigation of the Induction of Xenobiotic Metabolising Enzymes in a 3D Skin Model and human skin using LC-MS/MS and Western blotting. Online: American Society for Mass Spectrometry 2020, Taxes USA
- DESI-MS Imaging of a Living Skin Equivalent Model using a Multi-Reflecting Time of Flight Mass Spectrometer 2022, Minneapolis USA.

Papers Publication ready to submit in Citable Scientific Journals

- A review paper: Xenobiotic Metabolising Enzymes of Phase I and Phase II in native human skin, commercially available human skin cell Culture and 3D skin models.
- Investigation of the Induction of Xenobiotic Metabolising Enzymes in a 3D Skin Model and human skin by RT-qPCR and Western blotting.